MALADIES DES MOTONEURONES: Etude des mécanismes de dégénérescence dans la SLA

Gilbert Baillat

Aix-Marseille Université

Mémoire présenté en vue de l'obtention de l'habilitation à diriger des recherches

Discipline : Neurosciences

MALADIES DES MOTONEURONES

Etude des mécanismes de dégénérescence dans la SLA

Gilbert BAILLAT

Membres du jury :

Dr Frédérique Rene, UMR S118, Strasbourg

Pr Francois Valette, IRS, Nantes

Pr Maxime Lehmann, UMR7213, Strasbourg

Pr Jean Louis Mege, président du comité scientifique

Pr Alain Enjalbert, CRN2M, Marseille

Dr Frédéric Brocard, INT, Marseille

24 février 2016

Salle de thèse 2, faculté de Médecine

TABLE DES MATIERES

CURRICULUM VITAE 3

PUBLICATIONS 4

AVANT PROPOS 6

TRAVAUX ANTERIEURS 7

Thématique Striatin, neurosciences (1988-2001) 7

Thématique apoptose, cancérologie (2001-2005) 11

Thématique adhésion cellulaire, cancérologie (2005-2008) 14

Thématique VIH, virologie (2009-2012) 19

Thématique motoneurone, neurosciences (depuis 2013) 24

Rôle de la protéine chaperonne des tubulines TBCE dans la fragmentation du Golgi 24

TRAVAUX EN COURS, PERSPECTIVES 32

Mécanismes moléculaires et conséquences cellulaire des mutations de la protéine SOD1 dans la SLA. 32

Recherche de biomarqueurs des neuropathies dégénératives des motoneurones 37

Développement d'une nouvelle méthode de purification par FACS de motoneurones humains issus d'IPS 38

Analyse des altérations génotypiques et moléculaires de motoneurones humains en condition pathologique 40

CONCLUSION 32

REFERENCES 44

ANNEXES 50

CURRICULUM VITAE

BAILLAT Gilbert

Né le 23 février 1958 à Lézignan Corbières (11)

Ingénieur de Recherche CNRS (IR1), recruté le 01/06/1988

Unité d'affectation : Institut de Neurosciences de la Timone (INT, UMR 7289 CNRS)

Aix Marseille Université, Marseille

Email : gilbert.baillat@univ-amu.fr

Diplômes:

1983	Diplôme d'Ingénieur INSA de Toulouse, option Génie Biochimique.
1988	Doctorat Université P. Sabatier, Toulouse, option Pharmacologie.
2012	Expérimentation animale, niveau 1

Emplois successifs au CNRS

De 1988 à 2001	Thématique Striatin, neurosciences UA 1179/UPR 7221/UPR 9013/UPR 9041 (Marseille)
De 2001 à 2008	Thématique apoptose puis adhésion cellulaire, cancérologie UMR 6032/FRE 2737/U911 (Marseille)
De 2009 à 2012	Thématique VIH, virologie ERT 2011 (Marseille)
Depuis 2013	Thématique motoneurones, neurosciences UMR 7289 (Marseille)

Activités transversales:

Codirection de thèse de 2010 à 2013 avec Dr E. Loret :

S. Médiouni : Etude par des anticorps de patients VIH-1 de la protéine TAT extracellulaire et développement thérapeutique

Signataire d'un brevet AMU-CNRS (EP 2581387)

Membre du comité national du CNRS, section 24 et juré de concours ITRF et ITA

Encadrement d'étudiants : thèse, M1 et M2, ESIL, BTS, etc...

PUBLICATIONS (RG score 2017 : 24.7)

Bellouze S, **Baillat G,** Buttigieg D, De La Grange P, Rabouille C and Haase G (2015) Golgi fragmentation in ALS mouse motor neurons is mediated by Stathmin upregulation leading to microtubule loss and Golgi SNARE accumulation. *J. Neurosc.* Soumis.

Toli D, Buttigieg D, Blanchard S, Lemonnier T, Lamotte d'Incamps B, **Baillat G**, Bohl D, Haase G (2015) Modeling Amyotrophic Lateral Sclerosis in Pure Human iPSc-derived Motor Neurons Isolated by a Novel FACS Double Selection Technique. ***Neurobiology of Disease*** 82 : 269-280.

Bellouze S, Schäfer MK, Buttigieg D, **Baillat G**, Rabouille C, Haase G (2014) Golgi fragmentation in pmn mice is due to a defective ARF1/TBCE cross-talk that coordinates COPI vesicle formation and tubulin polymerization. ***Hum Mol Genet.*** 23(22):5961-75.

Mediouni S, Darque A, Ravaux I, **Baillat G**, Devaux C, Loret E(2013) Identification of a highly conserved surface on Tat variants. ***J Biol Chem.*** 288 (26):19072-80.

Mediouni S, Watkins JD, Pierres M, Bole A, Loret EP, **Baillat G** (2012) A Monoclonal Antibody Directed against a Conformational Epitope of the HIV-1 Trans-activator (Tat) Protein Neutralizes Cross-clade. ***J Biol Chem.*** 287(15):11942-950.

Mediouni S, **Baillat G**, Ravaux I, Dhiver C, Tissot-Dupont H, Mokhtari M, Moreau H, Tamalet C, Brunet C, Paul P, Dignat-George F, Stein A, Brouqui P, Spector SA, Campbell GR, Loret EP (2012) Antiretroviral therapy does not block the secretion of the Human Immunodeficiency Virus Tat Protein. ***Infect Disord Drug Targets*** 12(1), 81-6.

Mediouni S, **Baillat G**, Darque A, Ravaux I, Loret E (2011) HIV-1 infected patients have antibodies recognizing folded Tat. ***Infect Disord Drug Targets*** 11(1):57-63.

Baillat G, Siret C, Delamarre E, Luis J (2008) Early adhesion induces interaction of FAK and Fyn in lipid domains and activates raft-dependent Akt signaling in SW480 colon cancer cells. ***Biochimica et Biophysica Acta*** MCR 1783 (12):2323-31.

Haeberle AM, Castets F, Bombarde G, **Baillat G**, Bailly Y (2006) Immunogold localization of phocein in dendritic spines. ***J Comp Neurol*** 495(3) :336-50.

Baillat G, Garrouste F, Remacle-Bonnet M, Marvaldi J, Pommier G (2005) Bcl-xL/Bax ratio is altered by IFNgamma in TNFalpha- but not in TRAIL-induced apoptosis in colon cancer cell line. ***Biochim Biophys Acta*** MCR 1745 (1):101-10.

Remacle-Bonnet M, Garrouste F, **Baillat G**, Andre F, Marvaldi J, Pommier G (2005) Membrane rafts segregate pro- from anti-apoptotic insulin-like growth factor-I receptor signaling in colon carcinoma cells stimulated by members of the tumor necrosis factor superfamily. ***Am J Pathol*** 167 (3):761-73.

Baillat G, Gaillard S, Castets F, Monneron A (2002) Interaction of phocein with Nucleoside-Diphosphate Kinase, Eps15 and Dynamin I. ***J Biol Chem*** 277 (2) :18961-66.

Baillat G, Moqrich A, Castets F, Baude A, Bailly Y, Benmerah A, Monneron A (2001) Molecular cloning and characterization of phocein, a protein found from the Golgi complex to dendritic spines. ***Mol Biol Cell*** 12 (3): 663-73.

Moqrich A, Mattei MG, Bartoli M, Rakitina T, **Baillat G,** Monneron A, Castets F (1998) Cloning of human striatin cDNA (STRN), gene mapping to 2p22-p21, and preferential expression in brain. ***Genomics*** 51 (1):136-9.

Castets F, Bartoli M, Barnier J, **Baillat G,** Salin P, Moqrich A, Bourgeois JP, Denizot F, Rougon G, Calothy G, Monneron A (1996) A novel calmodulin-binding protein, belonging to the WD-repeat family, is localized in dendrites of a subset of CNS neurons. ***J. Cell Biology*** 143:1051-62.

Castets F, **Baillat G,** Mirzoeva S, Mabrouk K, Garin J, d'Alayer J, Monneron A (1994) A brain synaptosomal adenylyl cyclase of high specific activity is photolabeled with azido-ATP. ***Biochemistry*** 33(17):5063-9.

Orlando C, d'Alayer J, **Baillat G,** Castets F, Jeannequin O, Mazié JC, Monneron A (1992) A monoclonal antibody directed against the catalytic site of Bacillus anthracis adenylyl cyclase identifies a novel mammalian brain catalytic subunit. ***Biochemistry*** 31(12):3215-22.

Mollereau C, Pascaud A, **Baillat G,** Mazarguil H, Puget A, Meunier JC (1988) 5'-Guanylylimidodiphosphate decreases affinity for agonists and apparent molecular size of a frog brain opioid receptor in digitonin solution. ***J Biol Chem.*** 263(34):18003-8.

Mollereau C, Pascaud A, **Baillat G,** Mazarguil H, Puget A, Meunier JC (1988) Evidence for a new type of opioid binding site in the brain of the frog Rana ridibunda. ***Eur J Pharmacol.*** 150(1-2):75-84.

Baillat G, Pascaud A, Mollereau C, Puget A, Mazarguil H, Meunier JC (1986) Characterization, solubilization and purification of an opioid receptor from the brain of the frog Rana ridibunda. ***NIDA Res Monogr.***75:5-8.

AVANT PROPOS

Ingénieur Biochimiste de formation (INSAT) et titulaire d'un Doctorat en Microbiologie et Pharmacologie, j'ai été recruté au CNRS en 1988 comme Ingénieur de Recherche. Au cours de ma carrière, j'ai participé à plusieurs sujets dans des thématiques variées et dans différentes unité. En tant qu'ingénieur en biologie, j'ai conduis en spécialiste leurs développements en déterminant l'ensemble cohérent des techniques nécessaires à leurs réalisations expérimentales.

Depuis 2000, je dirige des projets de recherches de manière autonome et mes travaux ont été validés par des publications que j'ai moi-même rédigées (RG score: 24.2). Ainsi, sur 18 publications, j'ai signé 5 articles en 1er auteur, 3 en 2^{ième} auteur et 1 en dernier auteur. Le fil conducteur de ces différents travaux a été d'éclaircir le fonctionnement de certains mécanismes cellulaires en étudiant tout particulièrement les interactions protéine-protéine.

TRAVAUX ANTERIEURS

Dans ce chapitre, je me limiterai à résumer les travaux effectués dans les articles signés en premier ou dernier auteur (Annexes 1 à 6) et dans le plus récent (Annexe 7).

Thématique Striatin, neurosciences (1988-2001)

Dans l'équipe du Dr A. Monneron, j'ai contribué à la découverte d'une famille de protéines neuronales nommée 'Striatin family' (Pfam 08232). J'ai été cosignataire de 4 articles (Orlando et coll., 1992; Castets et coll., 1994 et 1996; Moqrich et coll., 1998) dont un en deuxième position.

A partir de 2000, j'ai eu la responsabilité de rechercher les partenaires protéiques interagissant avec cette famille afin d'éclaircir leurs fonctions. Par la technique du double hybride, j'ai mis en évidence une interaction avec une protéine de 26 kDa (Fig. 1) jusqu'alors inconnue que j'ai nommée Phocein (Baillat et coll., 2001 ; Annexe 1). Cette protéine présente une homologie limitée avec les sous unités ζ du complexe adapteurs de la Clathrine AP2 ainsi qu'avec le domaine de liaison SH3 (Src homologie 3). Cette interaction a été validée par co-immunoprécipitation et par des expériences de 'pull-down' à l'aide des protéines fusion GST que j'ai produites.

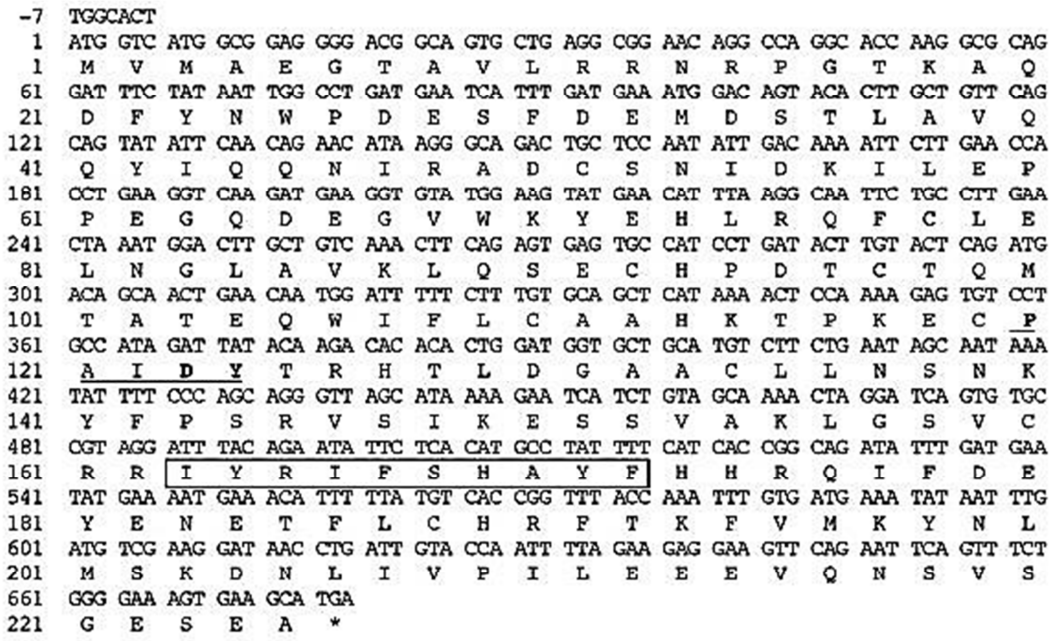

Fig. 1 : Séquences nucléotique (EMBL AJ132008) et protéique de la Phocein. Le domaine de liaison SH3 est souligné, le domaine homologue avec la sous unité ζ d'AP2 est entouré.

La Phocein est exprimée dans la plupart des tissus et chez de nombreuses espèces. Grâce aux anticorps que j'ai produits, elle a été localisée au niveau membranaire et dans le cytosol au sein d'un complexe protéique. Par exemple, elle interagit avec SG2NA, un des membres de la famille Striatin, au niveau du Golgi (Fig. 2).

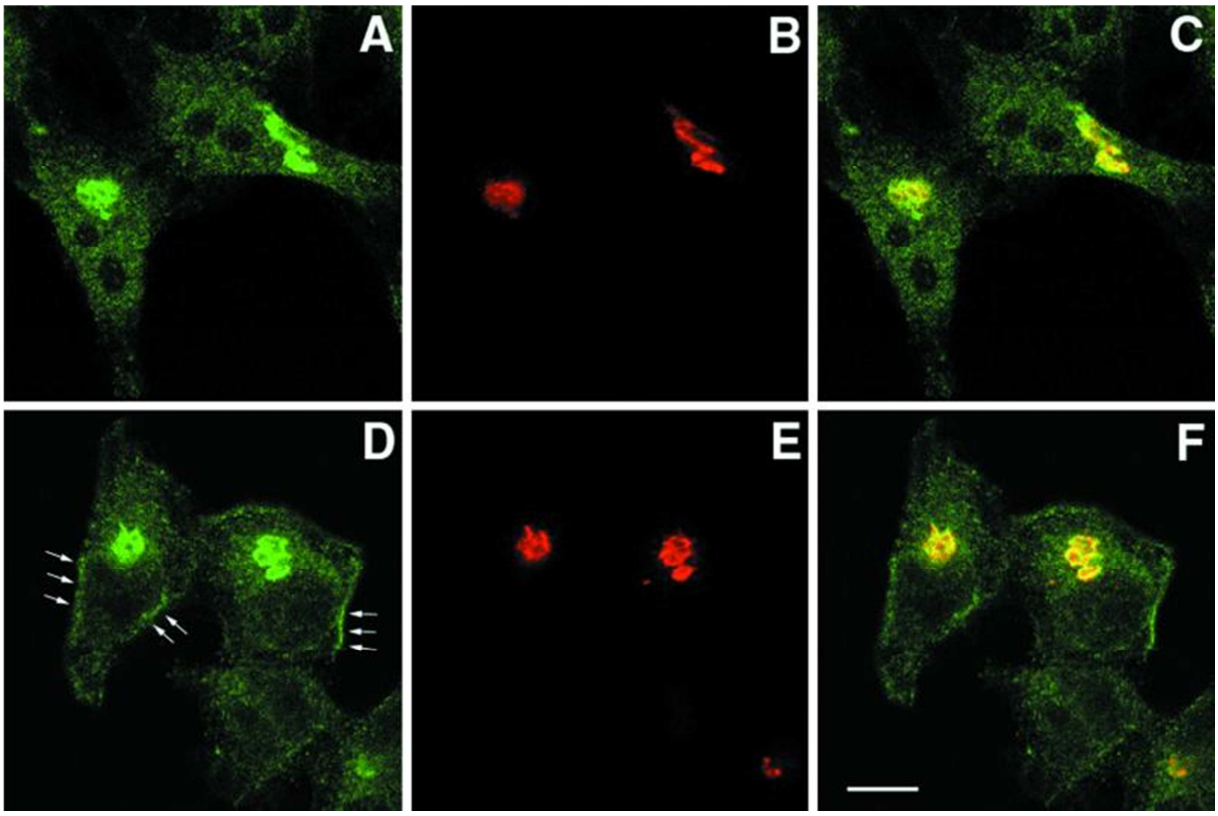

Fig. 2 : Phocein et SG2NA sont localisés à l'appareil de Golgi dans des cellules HELA. Les cellules sont observées en microscopie confocale après marquage par (A) un anticorps anti Phocein, (B et E) un anticorps anti CTR433 spécifique du Golgi et (D) un anticorps anti SG2NA. (C et F) Images composites. (Barre d'échelle =10µm)

La Phocein a aussi été localisée au niveau des épines des cellules de Purkinje du cervelet et des neurones pyramidaux de l'hippocampe (Fig. 3). Cette localisation a été confirmée par microscopie électronique dans un article que j'ai signé en avant dernier auteur (Haeberlé et coll., 2006). Elle est souvent associée à des complexes vésiculaires et son expression postnatale précoce suggère son implication dans le remodelage dendritique au cours du développement.

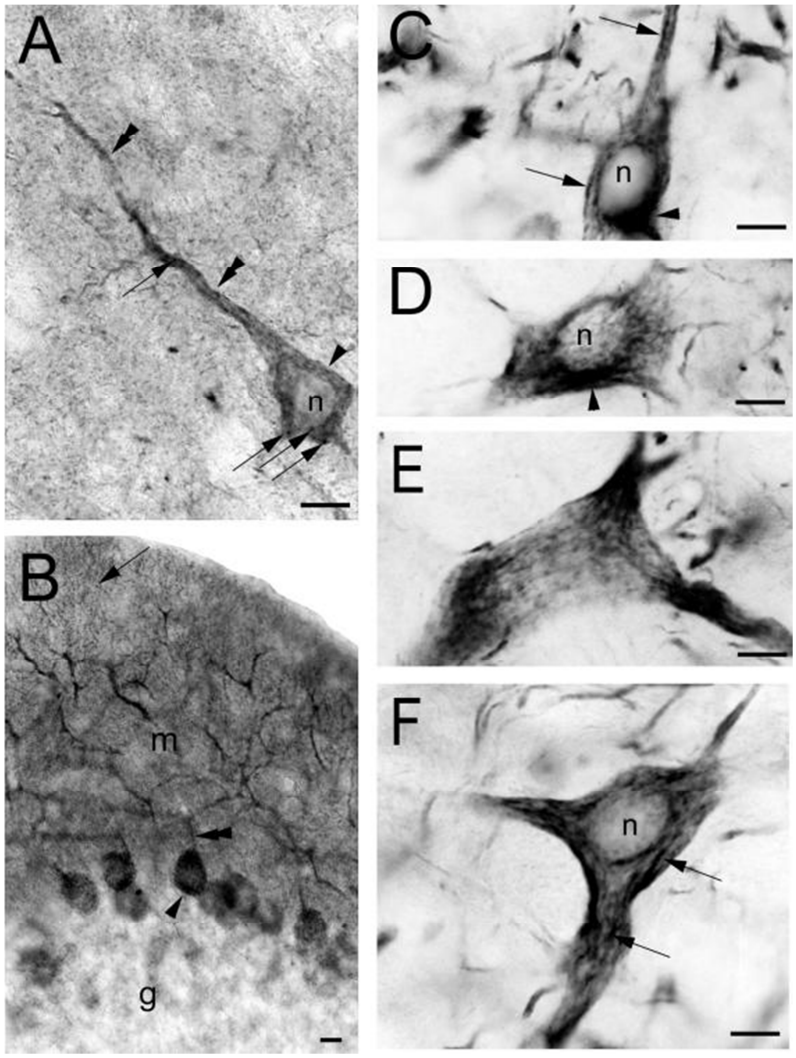

Fig. 3 : Localisation de la Phocein sur coupes de cerveau de rat (A) dans le soma (tête de flèche) et les dendrites (double flèche) des neurones pyramidaux du cortex. Le marquage intra-cytoplasmique se présente sous forme granulaire (flèche). (B) La Phocein est localisée dans le soma (tête de flèche) et dans l'arborisation dendritique des cellules de Purkinje du cervelet, du segment proximal (double flèche) à l'extrémité distale (flèche). (C-F) Un marquage vermiculé (flèche) est observé dans le soma (C, D et F) et dans les dendrites proximales (E). Le marquage proche du noyau semble correspondre au Golgi en C et D. (Barres d'échelle = 10µm)

Dans un deuxième temps, j'ai recherché d'autres membres de ce complexe protéique et ai trouvé des interactions avec NDPK (nucleoside diphosphate kinase), Eps15 et Dynamin I. Ces interactions ont également été confirmées biochimiquement par immunoprécipitation et 'pull-down' et leurs co-localisations démontrées par immunocytochimie sur des neurones embryonnaires d'hippocampe de rat où la Phocein apparait sous forme de spots. La distribution de la Dynamin et de la Phocein se recouvre dans l'appareil de Golgi, à l'émergence des neurites du corps cellulaire et sur toute la longueur des prolongements (Fig. 4).

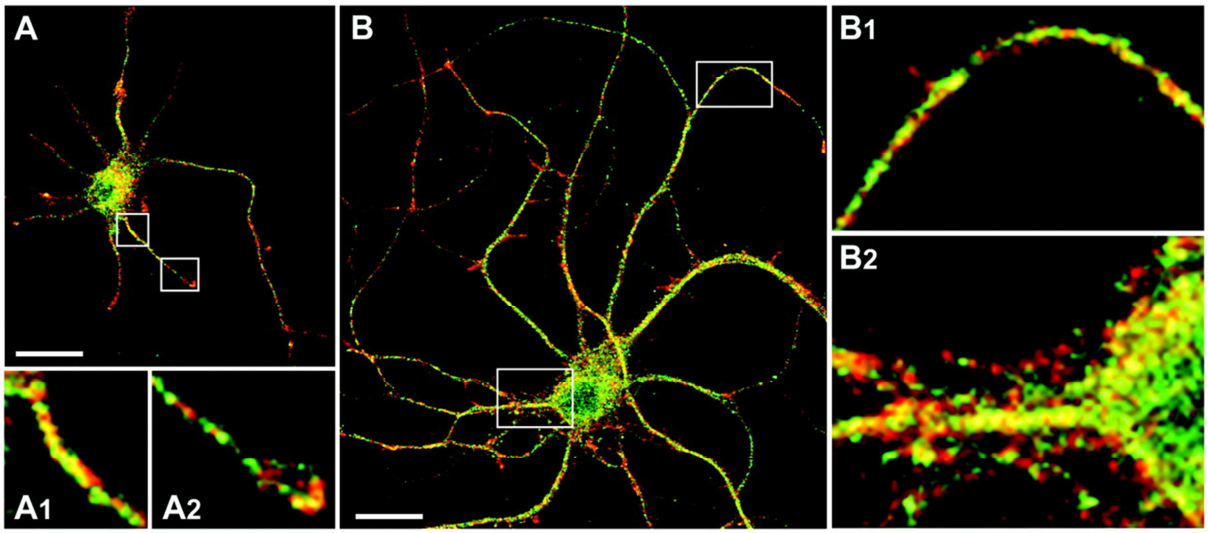

Fig. 4 : Dynamin (en rouge) et Phocein (en vert) sont co-localisées (en jaune) dans des neurones de l'hippocampe (A) au stade 3 et (B) au stade 5. A1, A2, B1 et B2 sont des grossissements (x5) des zones entourées respectives. (Barres d'échelle = 40µm)

NDPK (ou nm23-H1) est une enzyme ubiquitaire qui participe à de nombreux processus et interagit avec de nombreuses GTPases (Kim et coll., 2009). Parmi ces GTPases, la Dynamin joue un rôle essentiel dans le trafic des vésicules à Clathrine (Chappie et Dyda, 2013) et est particulièrement présente dans les neurones. Eps 15 est également impliquée dans le mécanisme endocytose en régulant la fonction d'AP2, le complexe adapteur de la Clathrine (Salcini et coll., 1999). L'interaction de la Phocein avec ces protéines ainsi que sa distribution suggère son implication dans le trafic vésiculaire neuronal comme membre d'un complexe protéique à multiples partenaires. La Striatin et la Zinedin, deux des principaux membres de la famille Striatin avec lesquels interagit la Phocein, semblent d'ailleurs agir comme des protéines d'ancrage multiples par leur domaine WD. Ce complexe joue un rôle dans la signalisation et l'endocytose du système nerveux central (Baillat et coll., 2002; Annexe 2).

Thématique apoptose, cancérologie (2001-2005)

Courant 2001 j'ai intégré l'équipe 'Rôle du microenvironnement cellulaire dans les mécanismes de progression tumorale' dirigée dans un premier temps par le Professeur J. Marvaldi puis par le Professeur J. Luis au sein de l'unité « Interactions entre systèmes protéiques et différenciation dans la cellule tumorale » (UMR 6032). Cette intégration a permis d'amener une expertise en biologie moléculaire et en production de protéines recombinantes. Pour poursuivre un thème de recherche plus personnel, j'ai obtenu du CNRS en juin 2002 une subvention dans le cadre d'une Action Incitative 'Puce à ADN' (n°0693) pour analyser l'expression des gènes régulés par des facteurs d'apoptose de la famille TNF dans des cellules de cancer colique.

L'apoptose est un processus physiologique essentiel qui assure le maintien de l'homéostasie tissulaire en faisant intervenir des facteurs protéiques extracellulaires déclencheurs, tels TNFα et TRAIL (Gaur et Aggarwal , 2003). En cancérologie, la résistance à l'apoptose est un problème majeur qui facilite l'expansion d'un clone néoplasique génétiquement altéré. Sa régulation est un processus complexe qui implique des réseaux en équilibre de médiateurs anti- et pro-apoptotiques, notamment les caspases et les protéines de la famille Bcl2 (comme BCL-xL, Bax ou Bak). Les cellules HT29 D4, un modèle cellulaire de carcinome de colon, sont résistantes à l'apoptose induite par le TNFα mais pas à celle induite TRAIL. Toutefois, un prétraitement par l'interféron γ (IFNγ), une cytokine naturellement produite par les cellules immunitaires, permet de restaurer la sensibilité au TNFα.

Afin de comprendre cette régulation, les profils transcriptionnels induits par TNFα et TRAIL et leurs régulations par l'IFNγ (Tables 1 et 2) ont été comparés par une méthode de cDNA array que j'ai développée au laboratoire. Seuls 10 gènes sont significativement régulés par TNFα ou TRAIL (en gris, Table 1). Ces gènes sont impliqués soit dans la régulation de la voie NFKB, soit dans l'apoptose. En particulier une augmentation d'un facteur 4 de l'expression de BCL-xL est détectée avec le traitement par TNFα alors qu'elle n'est que de 2,5 avec TRAIL. Une forte différence dans l'expression d'IL-8 a également été relevée.

Gene name	Description	Genebank	TNF	TRAIL
			untreated	untreated
IKBα	Nuclear factor of kappa light polypeptide gene enhancer in B-cells inhibitor, alpha	M69043	3.77 ± 0.37	3.58 ± 0.58
NFKB1	Nuclear factor of kappa light polypeptide gene enhancer in B-cells 1 (p105)	M58603	2.35 ± 0.76	2.31 ± 0.41
IL-8	Interleukin 8	M17017	2.66 ± 0.19	1.12 ± 0.05
MMP-7	Matrix metalloproteinase 7	X07819	2.92 ± 0.64	2.08 ± 0.59
BCL-xL	BCL2-like 1	Z23115	3.94 ± 0.24	2.54 ± 0.41
HRK	Harakiri, BCL2-interacting protein	NM_003806	4.42 ± 0.54	4.03 ± 0.42
FADD	Fas associated via death domain	NM_003824	2.39 ± 0.43	1.53 ± 0.21
DFFA	DNA fragment factor-45	NM_004401	2.91 ± 0.23	2.28 ± 0.18
RIP-2	Receptor-interacting serine-threonine kinase 2	AF078530	2.48 ± 0.16	1.40 ± 0.11
FASN	Fatty acid synthase	U26644	5.42 ± 0.50	6.45 ± 1.31

Table 1 : Taux d'expression des gènes de cellules traitées TNF ou TRAIL.

La sensibilisation par IFNγ induit une régulation pour 9 gènes avec TNFα mais pour seulement 3 avec TRAIL (en gris, Table 2). En particulier une baisse de plus de 90% du taux d'expression de BCL-xL est observée avec le TNFα mais pas avec TRAIL ou l'IFNγ seul. L'expression de cette protéine anti apoptotique fortement augmentée par TNFα seul est presque totalement réprimée par la sensibilisation à l'IFNγ.

Gene name	Description	Genebank	IFN+TNF	IFN+TRAIL	IFN
			TNF	TRAIL	untreated
IKBα	Nuclear factor of kappa light polypeptide gene enhancer in B-cells inhibitor, alpha	M69043	1.51 ± 0.25	0.70 ± 0.41	1.79 ± 0.32
IL-8	Interleukin 8	M17017	1.72 ± 0.18	1.36 ± 0.28	1.98 ± 0.25
BCL-xL	BCL2-like 1	Z23115	0.32 ± 0.19	1.16 ± 0.15	0.99 ± 0.12
HRK	Harakiri, BCL2-interacting protein	NM_003806	0.58 ± 0.20	0.49 ± 042	0.67 ± 0.21
FASN	Fatty acid synthase	U26644	2.12 ± 0.12	0.87 ± 0.20	1.85 ± 0.19
MIG	Monokine induced by gamma interferon	NM_002416	5.00 ± 0.46	3.31 ± 0.72	5.65 ± 0.81
ICAM-1	Intercellular adhesion molecule 1 (CD54) human rhinovirus receptor	NM_000201	3.30 ± 0.71	1.92 ± 0.27	2.87 ± 0.45
Cyclin D1	Epidermal growth factor receptor	X00588	2.35 ± 0.38	1.24 ± 0.18	1.99 ± 0.20
EGFR	Cyclin D1 (PRAD1)	M64349	2.12 ± 0.38	1.09 ± 0.23	2.30 ± 0.41

Table 2 : Taux d'expression des gènes de cellules sensibilisées par IFN puis traitées TNF ou TRAIL.

Ces modulations d'expression ont été confirmées par RT-PCR comparative (Fig. 5). De plus, les taux d'expression des protéines pro-apoptotiques Bax et Bak, qui n'avait pas été détectées sur cDNA array, ont pu être mis en évidence en RT-PCR. Ainsi, l'expression du gène Bax est augmentée d'un facteur 3 en présence de TNFα et TRAIL mais n'est pas affectée par le prétraitement à l'IFNγ.

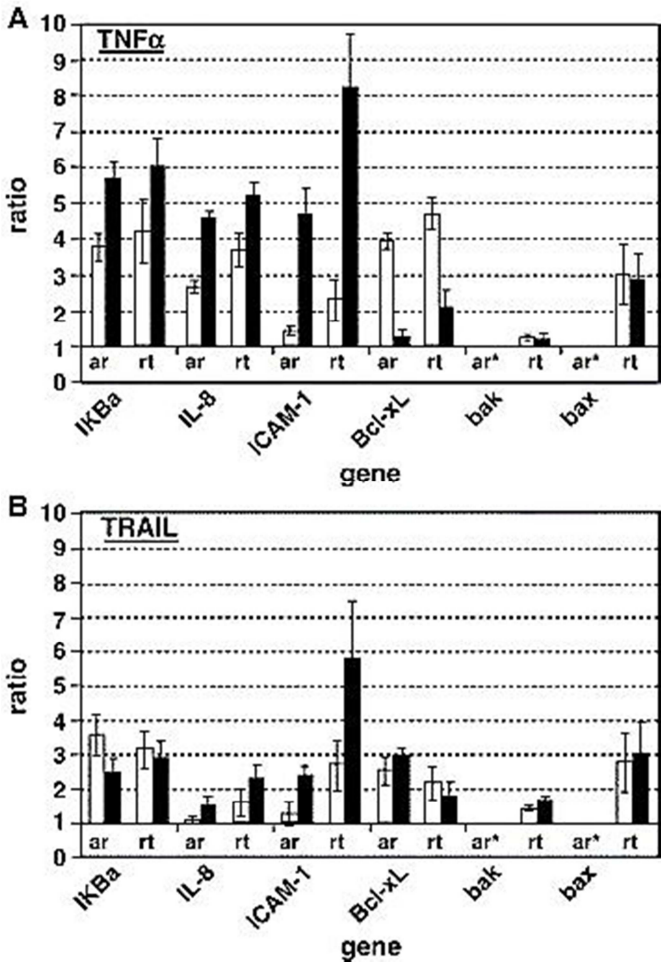

Fig. 5 : Comparaison des profils d'expression des gènes obtenus par cDNA array (ar) ou RT-PCR (rt) dans les cellules HT29 stimulées par (A) TNFα ou (B) TRAIL avec (en noir) ou sans (en blanc) sensibilisation par IFNγ.

L'augmentation de l'expression de Bax déclenchée par les facteurs de mort est contrebalancée par l'augmentation de l'expression de BCL-xL dans le cas du TNFα. Cette surexpression est réprimée en présence d'interferon. Dans les cellules HT29, la mort cellulaire déclenchée par les facteurs de mort de la famille du TNF est donc régulée par le ratio entre les protéines Bax (pro-apoptotique) et BCL-xL (anti-apoptotique) et emprunte la voie mitochondriale.

Ces résultats sur l'association de l'IFNγ et des facteurs de la famille du TNF pourraient fournir une approche thérapeutique intéressante dans le traitement de certains cancers (Baillat et coll., 2005; Annexe 3). Une méthodologie de recherche identique a été appliquée pour analyser l'effet anti-apoptotique de l'IGF-1 sur cette lignée cellulaire et a abouti à une publication (Remacle-Bonnet et coll., 2005). Ce projet de recherche m'a permis d'acquérir une bonne expertise dans l'analyse de l'expression des gènes et une bonne connaissance des voies de transduction impliquées dans la survie et la croissance cellulaire.

Thématique adhésion cellulaire, cancérologie (2005-2008)

Les thèmes du laboratoire ayant été recentrés lors du renouvellement de l'unité, j'ai pris en charge une problématique portant sur le mécanisme d'initiation de la signalisation par les intégrines et la formation du complexe d'adhésion.

Pour permettre la dissémination hématogène des tumeurs, les cellules cancéreuses doivent acquérir des capacités d'adhésion et de migration impliquant des molécules telles que les intégrines qui relient les composants de la matrice extracellulaire aux protéines du cytosquelette. L'assemblage successif des diverses molécules d'adhésion forme une structure appelée complexe d'adhésion, siège de nombreuses interactions protéine-protéine et de signalisations diverses, en particulier des phosphorylations. Une des premières phosphorylations qui suit l'adhésion des intégrines est celle de la FAK (Focal Adhesion Kinase), qui initie la cascade de signalisation intracellulaire (Parsons, 2003). Les protéines kinase de la famille Src (SFKs) sont souvent mises en évidence dans la progression des cancers du côlon. En étant à la fois substrat de phosphorylation et kinase spécifique de la FAK, elles régulent et amplifient la transmission des signaux déclenchés par l'adhésion cellulaire. Cependant les SFKs, au contraire de FAK, sont largement décrites comme localisées dans des structures membranaires particulières appelées microdomaines lipidiques ou rafts (Liang, 2001).

Afin de préciser le mécanisme précoce de l'adhésion et le rôle des rafts, j'ai analysé la cinétique de phosphorylation de FAK et des SFKs, leurs localisations ainsi que l'activation résultante des voies de signalisation des Map kinases et de la PI3 kinase dans des cellules de cancer du côlon SW480 en train d'adhérer. Durant la première heure de l'adhésion, l'engagement des intégrines déclenche l'autophosphorylation de FAK sur la tyrosine en position 397. J'ai montré qu'une fraction non négligeable de cette FAK phosphorylée est localisée transitoirement dans les microdomaines lipidiques lorsque les SFKs sont inhibées (Fig. 6).

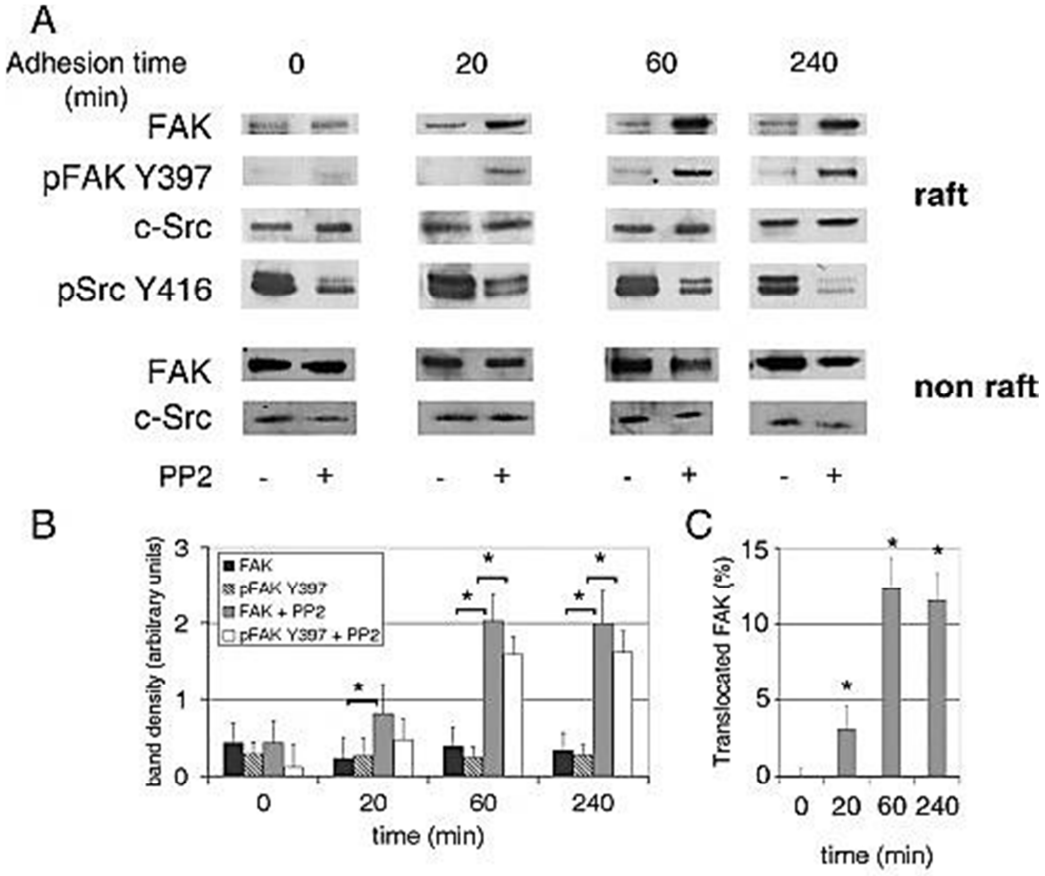

Fig. 6 : (A) Cinétique de distribution de la FAK et de la fraction de FAK phosphorylée sur Y397 (p FAK Y397) dans les compartiments raft et non-raft en présence ou non de PP2, un inhibiteur des SFKs. (B) Quantification de la distribution FAK et p FAK Y397 et (C) de la proportion de FAK présente dans les rafts sur 4 expériences indépendantes. Src est utilisé comme référence (* statistiquement significatif).

Dans ces conditions, la quantité de FAK dans les rafts atteint son maximum (12%) au bout d'1h et reste ensuite constante. Cette localisation est donc régulée par des phosphorylations induites par des SFKs. La phosphorylation des tyrosines 861 et 925 déclenche la translocation hors des domaines rafts comme le démontre des transfections avec des plasmides exprimant différentes variants FAK portant des mutations sur les sites de phosphorylation (non muté ou wt, F397Y, F861Y et F925Y) fusionnés avec un marqueur HA,. En effet, les mutants non phosphorylables sur les tyrosines 861 et 925 bloquent FAK dans les rafts (Fig. 7). De plus, l'utilisation du variant F397Y confirme qu'il est nécessaire que ce site soit phosphorylable pour permettre la localisation dans les domaines lipidiques.

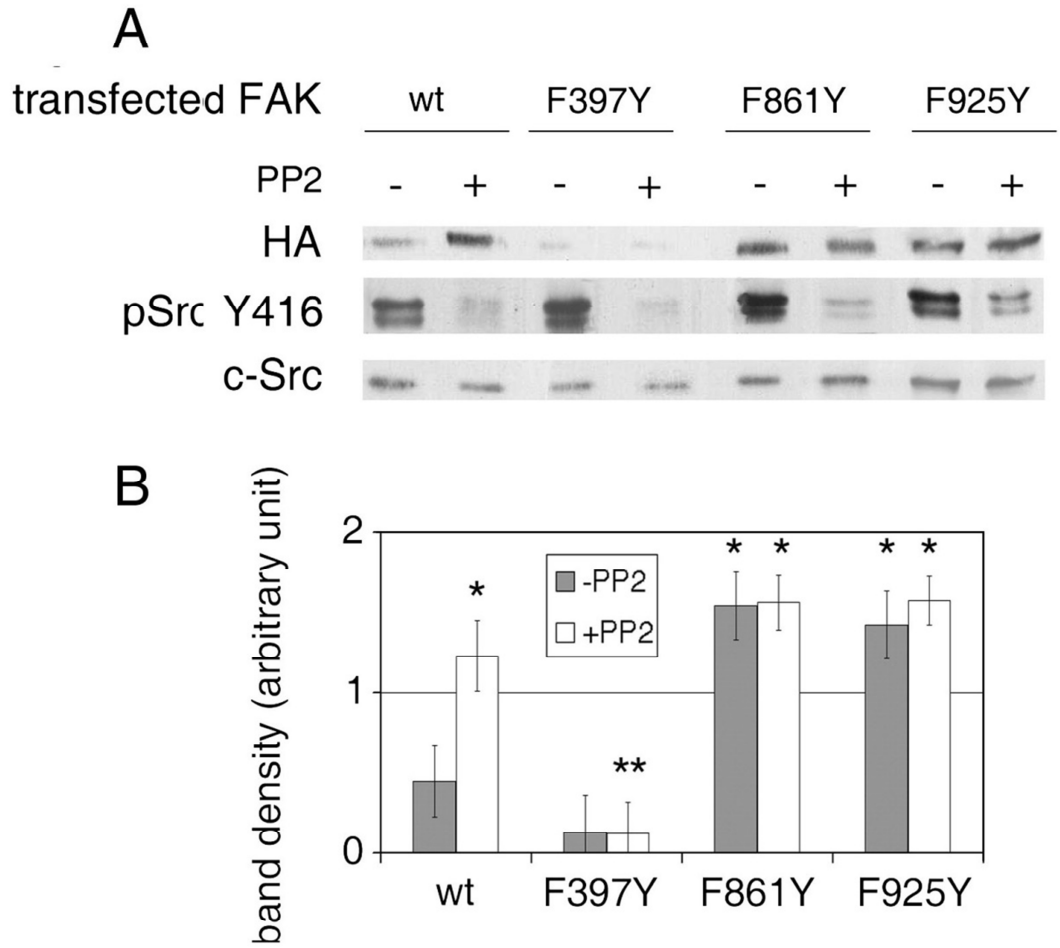

Fig. 7 : (A) Distribution des constructions FAK marqués par un tag HA dans les domaines lipidiques après transfection et 1h d'adhésion en présence ou non de PP2. (B) Quantification d'après 8 expériences indépendantes. Src est utilisé comme référence (* statistiquement significatif par rapport à wt sans PP2).

Dans les domaines lipidiques, FAK interagit uniquement avec Fyn, un des membres de la famille Src, comme le démontre des expériences de co-immunoprécipitation (Fig. 8). Dans ce compartiment, Fyn est donc la SFK responsable de la phoshorylation de FAK et de sa translocation. En revanche, FAK interagit aussi avec c-Src dans les autres fractions.

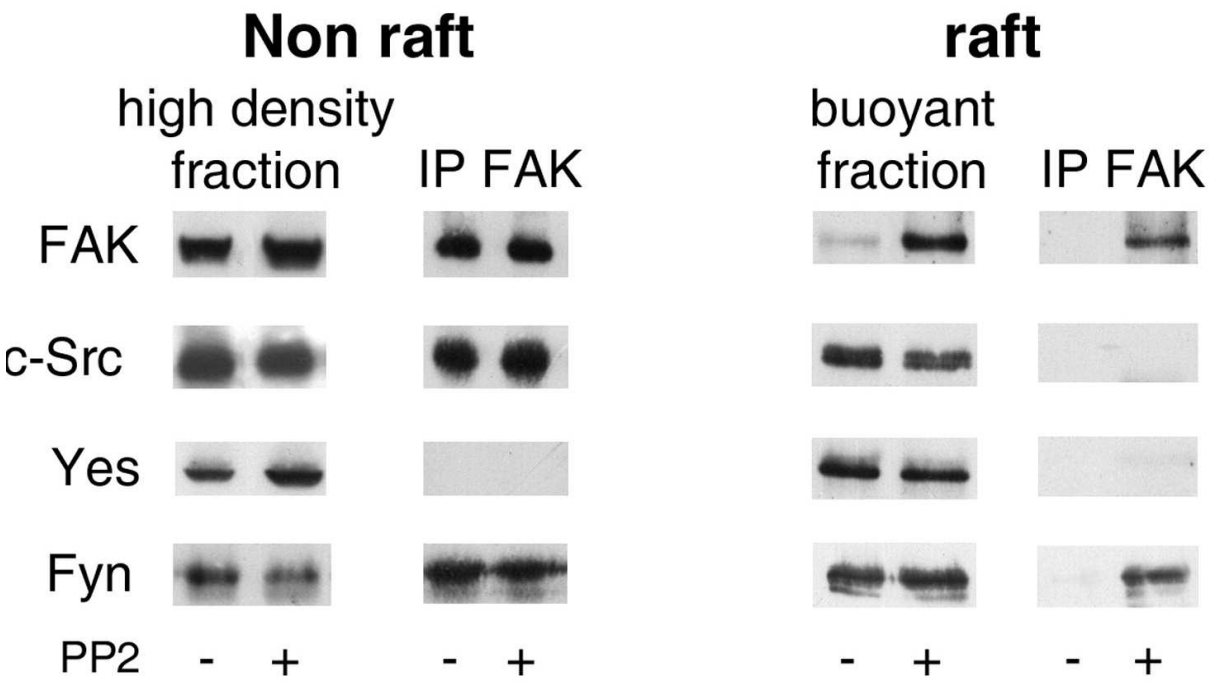

Fig. 8 : Co-immunoprécipitations de FAK avec c-Src, Yes and Fyn dans les compartiments raft and non-raft en présence ou non de PP2.

Durant cette première heure d'adhésion, la voie PI3K/Akt atteint son maximum d'activation et est dépendante de l'intégrité des domaines lipidiques. Au contraire, l'activation de la voie MAPK/Erk continue à augmenter pendant au moins 4 heures et est indépendante des domaines rafts/caveolés. Ainsi, pour la première fois, une interaction de FAK et Fyn dans les microdomaines lipidiques durant les temps précoces de l'adhésion a été démontrée (Baillat et coll., 2008; Annexe 4). Cette interaction provoque l'activation rapide de la voie PI3K/Akt. Une signalisation spécifique de la survie et de la prolifération intervient donc dans les domaines rafts/caveolés lorsqu'une cellule cancéreuse établit ses premiers contacts avec la matrice extracellulaire de son nouvel environnement (Fig. 9).

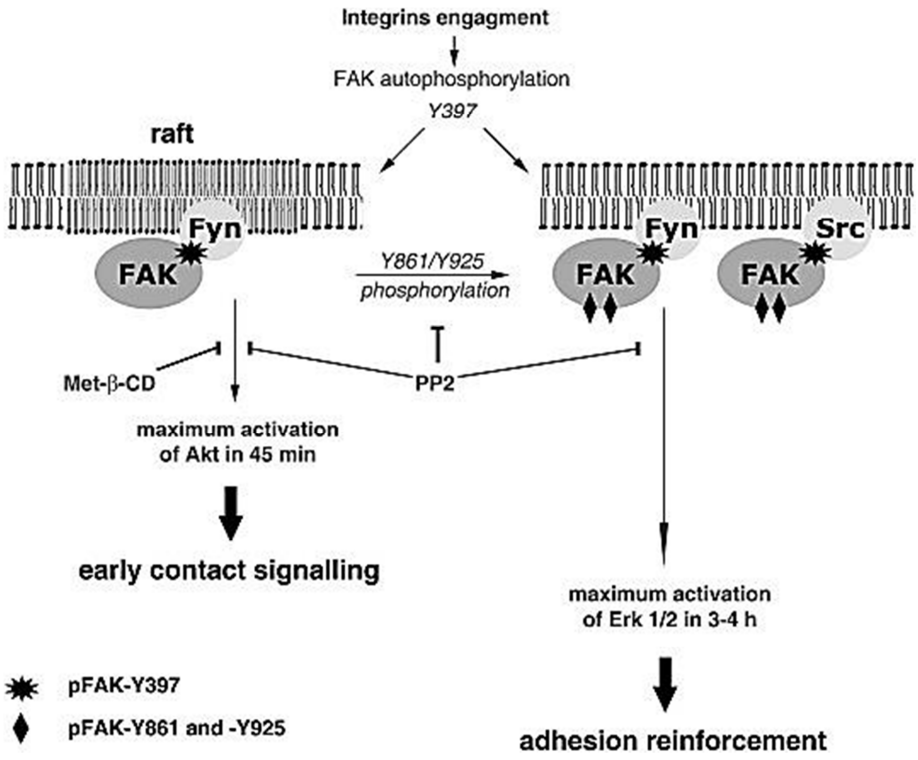

Fig. 9 : Schéma du modèle d'activation d'une voie spécifique de l'adhésion passant par les microdomaines lipidiques.

Thématique VIH, virologie (2009-2012)

Au 1er janvier 2009, le Dr E. Loret et moi-même avons sollicité la création d'une équipe de recherche technologique (ERT) afin de concevoir des outils thérapeutiques contre le Sida. L'ERT 2011 a vu le jour en mai 2009 sous la dénomination ETRAV pour « Equipe Technologique de Recherche Appliquée au VIH » avec l'appui de la direction du CNRS et de l'Université de la Méditerranée Aix- Marseille 2. La conception d'un vaccin contre le virus humain de l'immunodéficience de type 1 (VIH-1) est rendue difficile par sa grande variabilité génétique. En effet, pour chaque nouveau variant, les protéines du VIH-1 que sont gp120, Nef, Vif, Vpr, Vpu et Tat montrent des caractéristiques différentes au niveau moléculaire et biologique et sont donc difficiles à cibler. La première protéine synthétisée par la cellule infectée est la protéine Tat (Trans-Activator of Transcription). Tat est une protéine régulatrice de 11.9 kDa, qui est essentielle pour la transcription et la production des autres protéines du VIH-1. Son rôle principal est d'activer l'expression des gènes viraux dans les cellules infectées mais Tat est également secrétée comme le prouve sa détection dans le sérum de patients. Cette Tat exogène est capable d'entrer dans des cellules non infectées comme les lymphocytes T, induisant ainsi leur apoptose, ou d'activer la transcription virale dans des cellules infectées de manière latente,. Tat joue donc un rôle non seulement de protéine essentielle pour la réplication du VIH-1, mais aussi de toxine extracellulaire (Campbell et Loret, 2009). Il est donc important de comprendre les relations structure-fonction liées aux différents rôles de Tat pour le développement de nouveaux vaccins contre le SIDA inhibant cette protéine.

La fonctionnalité de différents variants de la protéine Tat synthétisés dans l'équipe a été vérifiée par des tests biologiques et leurs caractéristiques conformationnelles ont été étudiées dans différents milieux. Bien que précédemment décrite comme une protéine sans structure 3D stable, nous avons démontré que Tat doit posséder une conformation pour avoir une activité biologique. Cette structure nécessite des conditions de tampons et de pH se rapprochant des conditions physiologiques et est suffisamment stable pour se reformer après une dénaturation partielle (Fig. 10).

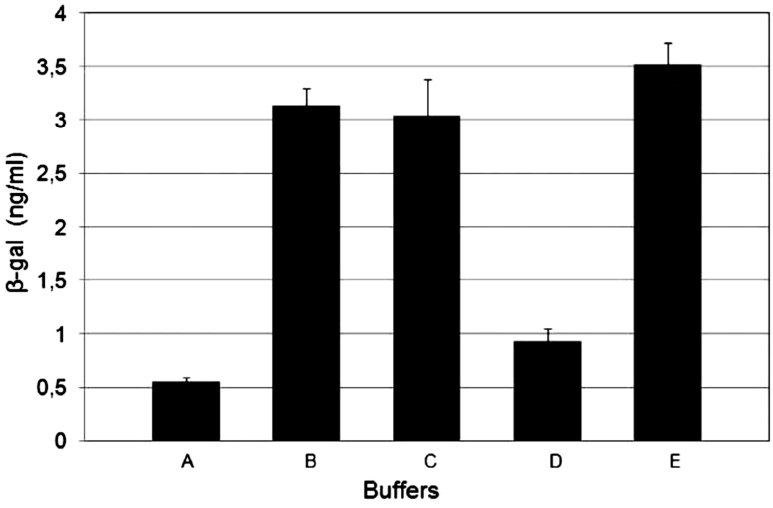

Fig. 10 : Taux de transactivation de la Tat HXB2 mesuré par l'activation de l'expression du gène *lac Z* dans des cellules HeLa-P4 : (A) contrôle sans Tat ; (B) avec Tat ; (C) avec Tat chauffée à 90° ; (D) avec Tat chauffée à 90° en présence d'urée ; (E) avec Tat en présence d'urée.

Nous avons également montré que 8 patients séropositifs sur les 40 testés possèdent des anticorps reconnaissant spécifiquement cette conformation 3D de Tat. Ce travail a donné lieu à un article que j'ai signé en deuxième auteur (Médiouni et coll., 2011; Annexe 5).

A l'aide de variants Tat représentant les 5 sous-types principaux, les caractéristiques de reconnaissance des anticorps anti-Tat ont été analysées durant 12 mois chez une cohorte de 50 patients séropositifs sous trithérapie. Nous avons mis en évidence que, même sous traitement, de la Tat circulante existe chez 86% des patients (Fig. 11). De façon surprenante, ce taux d'anticorps varie fortement au cours du temps chez un même sujet suggérant une sécrétion intermittente mais constante de Tat (Médiouni et coll., 2012).

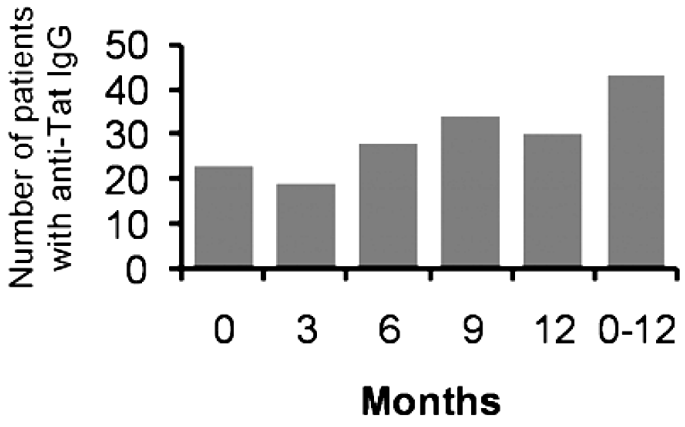

Fig. 11 : Nombre de patients possédant des anticorps contre au moins un sous type de Tat à différents temps et sur 1 an (0-12).

Ce résultat suggère que, bien que la virémie soit contrôlée par le traitement, des cellules infectées sont encore présentes soit sous forme latente soit dans des sanctuaires où elles continuent à produire des protéines virales de manière épisodique. La trithérapie n'est donc pas suffisante pour guérir les patients et d'autres moyens thérapeutiques doivent être élaborés pour éradiquer la maladie.

Dans ce but, un anticorps monoclonal nommé 7G12 reconnaissant différents sous-types de la protéine Tat avec des affinités identiques a été produit. Cet anticorps reconnait un épitope tridimensionnel commun comme le montre des expériences de dénaturation et est capable de neutraliser la transactivation de ces sous-types (Fig. 12). Les anticorps 27A8 et 6E7 reconnaissant respectivement les domaines linéaires terminaux C et N sont utilisés aux mêmes concentrations comme contrôle négatifs.

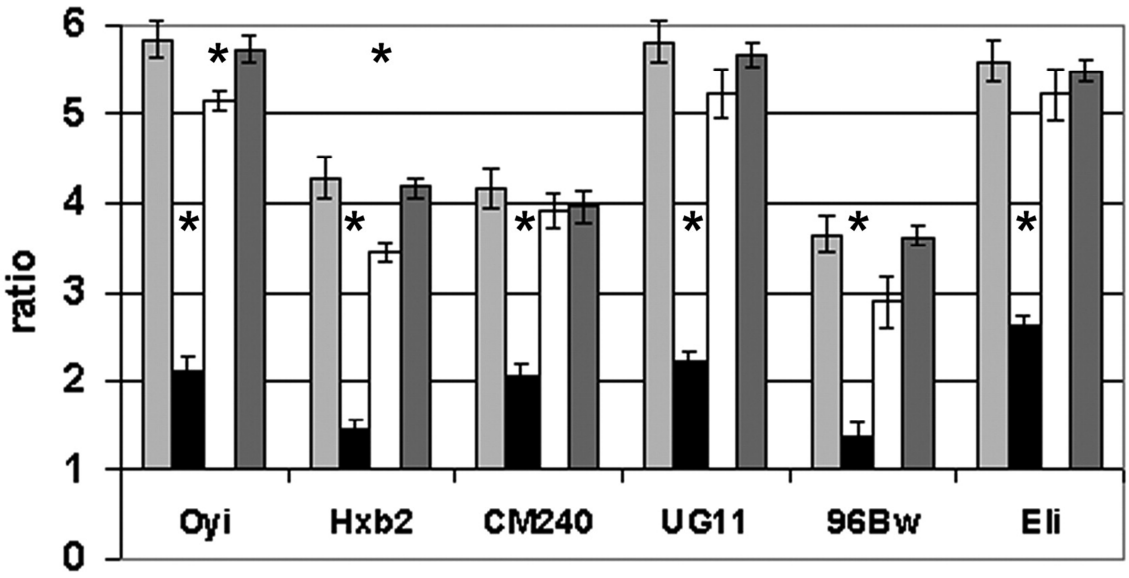

Fig. 12 : Neutralisation de l'activité de transactivation de différents variants Tat en absence (en gris clair) ou en présence de 7G12 (en noir), d'anticorps anti Tat contrôle 27A8 (en blanc), and 6E7 (en gris foncé) (* statistiquement significatif).

Cet anticorps bloque la capacité de Tat à pénétrer une cellule (Fig. 13), l'empêchant ainsi de jouer son rôle de toxine extracellulaire envers le système immunitaire des patients.

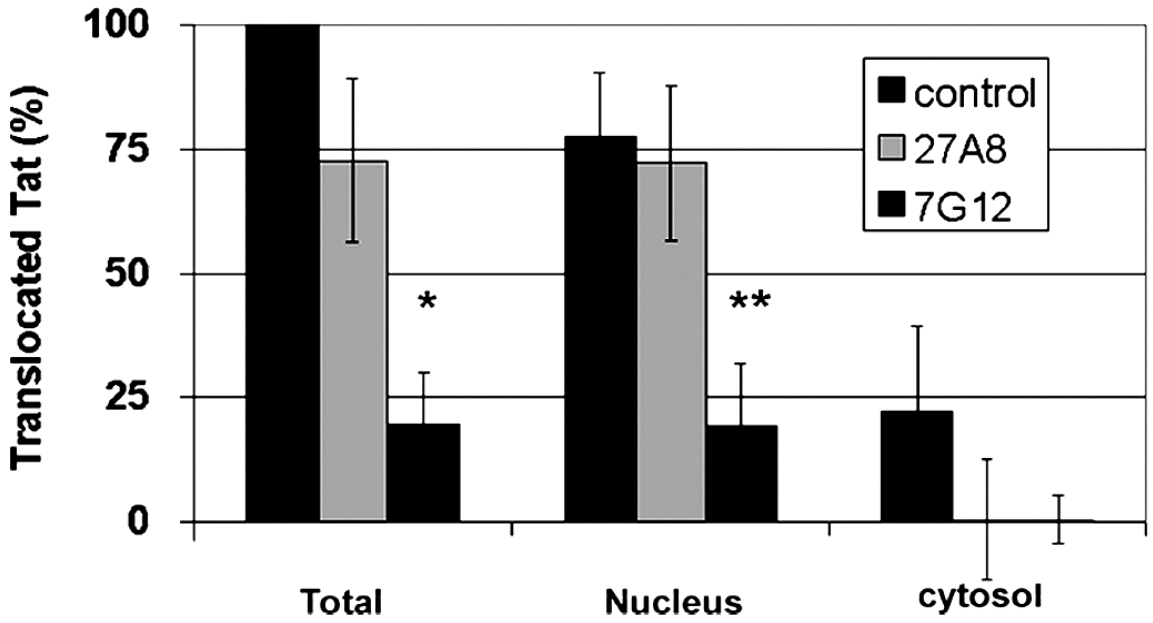

Fig. 13 : Blocage de l'internalisation de Tat par l'anticorps 7G12. Analyse densitométrique de 3 Western blots analysant la présence de Tat dans le cytosol et le noyau de cellules Jurkat après préincubation avec ou sans anticorps (control). L'Annexin I et la P-Ac-Histone sont utilisés respectivement comme marqueurs des fractions cytosolique et nucléaire. L'anticorps 27A8 reconnaissant le domaine C terminal de Tat est utilisé comme contrôle négatif (* et ** statistiquement significatif).

Après humanisation, cet anticorps pourrait donc représenter un candidat intéressant pour une immunisation thérapeutique passive. Ces résultats ont abouti au dépôt d'un brevet (EP2581387 A1) dont je suis cosignataire ainsi que d'un article dont je suis dernier auteur (Médiouni et coll., 2012 ; Annexe 6).

Cet anticorps a également permis de définir l'épitope conformationnel commun aux différents variants Tat, étape importante dans la perspective de créer un vaccin commun contre différentes souches virales. A partir de cet épitope, un peptide de 56 acides aminés, appelé MIMOOX, a été modélisé à partir de Tat Oyi dans le but de produire un agent de vaccination de moindre coût. Après sa synthèse, une oxydation établit un pont disulfure entre des cystéines placées à des positions permettant de recréer la structure 3D recherchée. La similarité de conformation entre Tat Oyi et MIMOOX a été vérifiée par dichroïsme circulaire. L'anticorps 7G12 reconnait MIMOOX avec une affinité à peine 2 fois plus basse que pour Tat Oyi et cette reconnaissance est complétement abolie en présence d'agents dénaturant le pont disulfure. MIMOOX possède donc l'épitope conformationnel commun des Tats. Des anticorps produits contre MIMOOX ont été capables de reconnaitre différents variants de Tat avec une bonne affinité (Fig. 14) confirmant l'intérêt du peptide dans une approche vaccinale (Médiouni et coll., 2013).

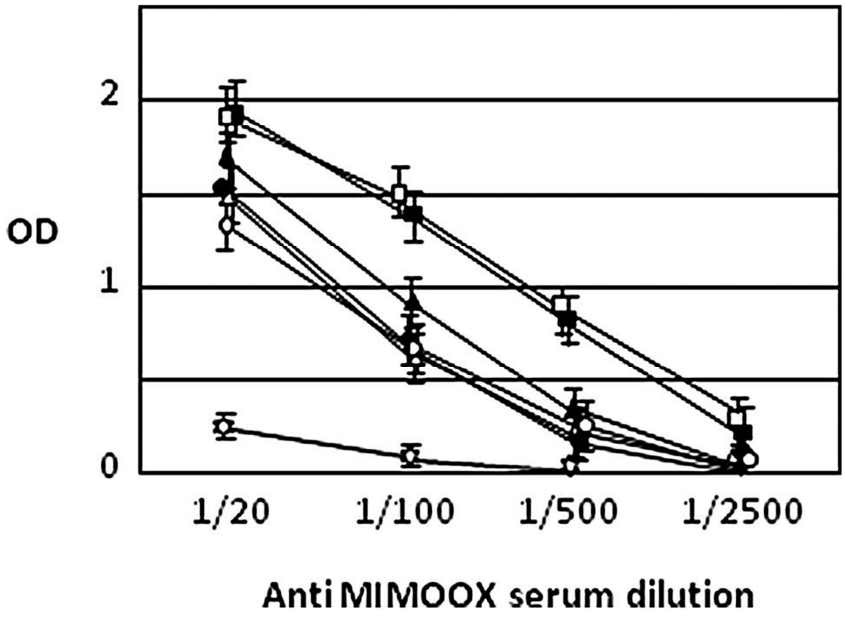

Fig. 14 : Reconnaissance par ELISA de MIMOOX (■) et des Tats Oyi (□), UG11RP (Δ), 96BW (○), Eli (●), CM240 (▲) par le sérum anti-MIMOOX. Un mélange de peptides couvrant la séquence d'OYI est utilisé comme contrôle négatif (☼).

Lors de mon implication dans les travaux de cette ERT, j'ai apporté une expertise dans le domaine biologique indispensable pour ses activités de recherche et codirigé une étudiante en thèse (Mlle Médiouni). J'ai également acquis une certaine connaissance du milieu hospitalier et des processus de transfert et de valorisation des résultats scientifiques. Les structures de type ERT et IFR ayant disparu lors du dernier plan quadriennal, j'ai rejoint l'UMR 7289 (INT) afin de renforcer ses activités de biologie.

Thématique motoneurone, neurosciences (depuis 2013)

Mon activité de recherche se réalise dans l'équipe MoMoThe (Maladies des Motoneurones : Modélisation et Thérapies), en collaboration avec le Dr Haase, sur un sujet concernant la Sclérose Latérale Amyotrophique (SLA). Dans ce manuscrit, je me limiterais à exposer nos derniers résultats sur cette thématique et à en développer les perspectives. Toutefois, j'apporte aussi mon expertise en biologie dans la réalisation des projets scientifiques de l'ensemble de l'unité.

Egalement appelée maladie de Charcot, la SLA est une maladie sévère et fatale des motoneurones de l'adulte. Elle est caractérisée par la dégénérescence sélective et progressive des neurones moteurs de la moelle épinière, du tronc cérébral et du cortex cérébral. Elle provoque une paralysie progressive de l'ensemble de la musculature squelettique des membres, du tronc (y compris les muscles respiratoires) et de l'extrémité céphalique. Elle touche les deux sexes avec une incidence annuelle d'environ 2,5 cas / 100 000. Cette maladie apparait de manière sporadique dans 90 à 95% des cas et aucune cause n'a pu être retenue avec suffisamment de certitude jusqu'à présent. Parmi les cas ayant une cause génétique familiale (5 à 10%), plus de 25 gènes ont été impliqués tels que SOD1, Alsin/ALS2, Senataxin, VAP-B, Dynactin, Tau, FUS, TDP43. Récemment, des répétitions multiples de l'hexanucléotide GGGGCC dans le gène C9ORF72 ont été identifiées dans des cas de SLA sporadique et familiale (DeJesus-Hernandez et coll., 2012; Renton et coll., 2012) mais les mécanismes aboutissant à la maladie restent à éclaircir.

Les neurones moteurs qui dégénèrent dans la SLA montrent de nombreux changements structuraux tels que la présence d'agrégats intracellulaires, une désorganisation du cytosquelette et des anomalies des organelles intracellulaires. La fragmentation de l'appareil de Golgi survient précocement au cours de la pathologie, bien avant l'apparition d'autres anomalies pathologiques dans les neurones moteurs de patients. Ces anomalies ont été pour la première fois rapportées en 1990 (Mourelatos et coll., 1990), puis confirmées ultérieurement (Gonatas et coll., 1992). A l'heure actuelle, le mécanisme à l'origine de la fragmentation de l'appareil de Golgi n'est toujours pas identifié que ce soit dans des modèles murins ou chez les patients atteints de SLA.

Rôle de la protéine chaperonne des tubulines TBCE dans la fragmentation du Golgi

Des souris *pmn* (*progressive motor neuropathy*) ont été utilisées comme modèle de maladie du neurone. Ces souris homozygotes pour la mutation *pmn* présentent une atrophie

musculaire associée à un retard de croissance staturo-pondéral (Schmalbruch et coll., 1991). Une paralysie progressive des membres postérieurs s'installe dès le 15ème jour de vie postnatale. La paralysie se généralise ensuite et touche l'ensemble des muscles d'innervation volontaire : les muscles des membres, du tronc et les muscles respiratoires. Les souris meurent par asphyxie consécutive à la paralysie des muscles respiratoires vers le 35ème jour de vie postnatale (Kennel et coll., 1996). Des études histologiques ont mis en évidence une atrophie des muscles squelettiques suite à une dégénérescence rétrograde des axones des nerfs périphériques. Cette dégénérescence est liée à une mutation faux sens d'une protéine localisée au niveau du Golgi, la chaperonne des tubulines TBCE (Tubulin Binding Cofactor E) qui participe à l'assemblage des tubulines, au trafic cellulaire, à la transduction de signaux et à la migration cellulaire. Cette mutation consiste en la substitution d'une thymine par une guanine dans la position 1570 du gène, aboutissant à une substitution d'un tryptophane par une glycine en position 524 (Trp524Gly) qui inactive la protéine (Bommel et coll., 2002; Martin et coll., 2002).

Des souris *pmn* âgées de 25 à 30 jours ont été utilisées pour élucider le rôle de TBCE dans l'apparition des anomalies golgienne. Notre activité de recherche a mis en évidence que cette perte de fonction induit des anomalies importantes du Golgi dans les neurones moteurs lombaires sur des coupes de moelle épinière de souris *pmn* (Fig. 15).

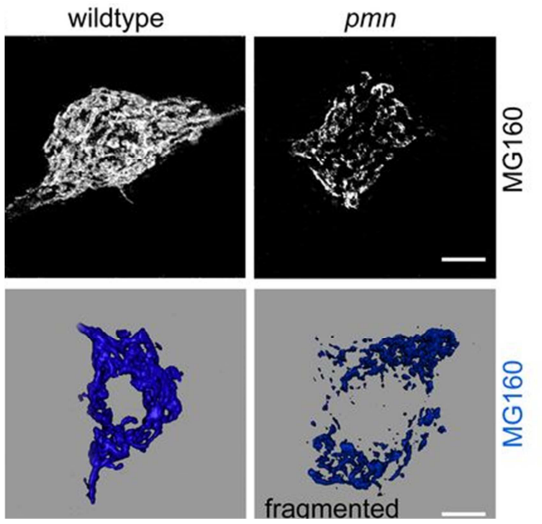

Fig. 15 : Anomalies du Golgi dans les motoneurones des souris *pmn* mises en évidence en microscopie confocale à fluorescence en utilisant un anticorps contre la protéine marqueur du Golgi MG160. Les figures en dessous montrent la modélisation 3D de la surface du Golgi. (Barre d'échelle = 10µm)

La fragmentation et l'atrophie du Golgi ressemblent à celles rapportées dans la SLA et se produisent avec des cinétiques similaires. Ces anomalies ont été observées en microscopie

électronique qui montre que l'empilement des citernes golgiennes est progressivement remplacé par des petites vésicules. Entre l'apparition des premiers symptômes 15 jours après la naissance et la mort de l'animal vers 35 jours, le taux de vésicules augmente de 4 fois, suggérant que l'appareil de Golgi se fragmente par vésiculation progressive.

Afin de démontrer que la mutation sur TBCE est bien responsable des anomalies observées, nous avons utilisé des lignées de souris *pmn* complémentées par transgénèse, soit partiellement (TBCE$^{PA/+}$*pmn*) soit totalement (TBCE$^{PC/+}$*pmn*), avec le gène sauvage TBCE (Martin et coll., 2002). Dans ces lignées, la complémentation, induit la disparition des altérations des nerfs phréniques de souris *pmn* et retarde de plusieurs semaines la létalité. Dans notre étude, le Golgi des motoneurones de ces lignées transgéniques présente une morphologie normale et les protéines retrouvent des taux d'expression identiques à ceux observés dans la lignée sauvage (Fig. 16).

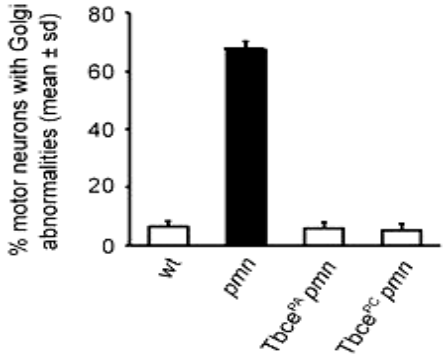

Fig. 16 : Rétablissement d'une morphologie golgienne normale en restaurant l'expression de TBCE dans les motoneurones des souris *pmn*.

Les changements pathologiques sont donc bien dus à la perte d'expression de TBCE dans la lignée *pmn* puisqu'ils peuvent être annulés par l'expression transgénique de la protéine. Ces résultats ont été confirmés en utilisant une lignée de motoneurones, nommée NSC34, dans lesquels le contenu en protéine TBCE endogène peut être appauvri par l'utilisation d'un siRNA TBCE (si TBCE). Un siRNA sans effet sur l'expression des protéines est utilisé comme contrôle négatif (si ctrl). La lignée cellulaire NSC34 est issue d'une fusion de neurones moteurs de moelle épinière de souris et de neuroblastomes. Ces cellules, qui possèdent de nombreuses caractéristiques moléculaires et phénotypiques du neurone moteur (Cashman et coll., 1992), sont donc un bon modèle *in vitro* qui permet de moduler des expressions de protéines par siRNA ou par transfection de plasmides. Le rôle essentiel de TBCE pour la polymérisation des microtubules à partir du Golgi où ce cofacteur est localisé a été précédemment démontré (Schaefer et coll., 2007).

Effectivement, nous avons trouvé que la quantité de microtubules qui contiennent de la tubuline détyrosinée caractéristique du Golgi est très diminuée dans les souris *pmn* et dans les motoneurones appauvris en TBCE (Fig.17).

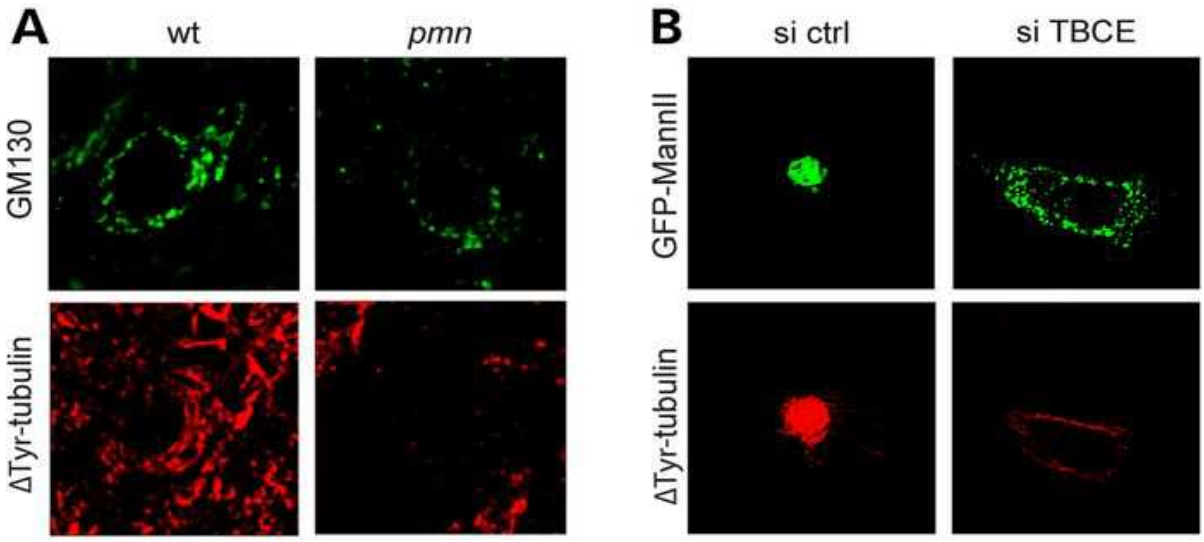

Fig. 17 ; Défauts de polymérisation des microtubules associés au Golgi dans les motoneurones *pmn* (A) et dans les cellules NSC34 appauvries en TBCE (B) révélés par un anticorps anti tubuline détyrosinée (ΔTyr-tubuline). La fragmentation de l'appareil de Golgi est mise en évidence par les marquages GM130 et GFP-Mannosidase II.

L'appauvrissement en TBCE dans les cellules NSC34 induit une diminution de la quantité d'α-tubuline polymérisée qui passe sous forme soluble, ce qui doit affecter le transport des vésicules. L'influence de cette fragmentation sur le trafic vésiculaire golgien a donc été étudiée. Une diminution des protéines β-COP et ε-COP, qui font partie du complexe de transport entre le RE et le Golgi nommé COPI, a été mise en évidence (Fig. 18). Par contre aucune influence sur l'expression des protéines associées aux vésicules de transport COP II ou à Clathrine n'a été observée, suggérant une action spécifique sur COP I.

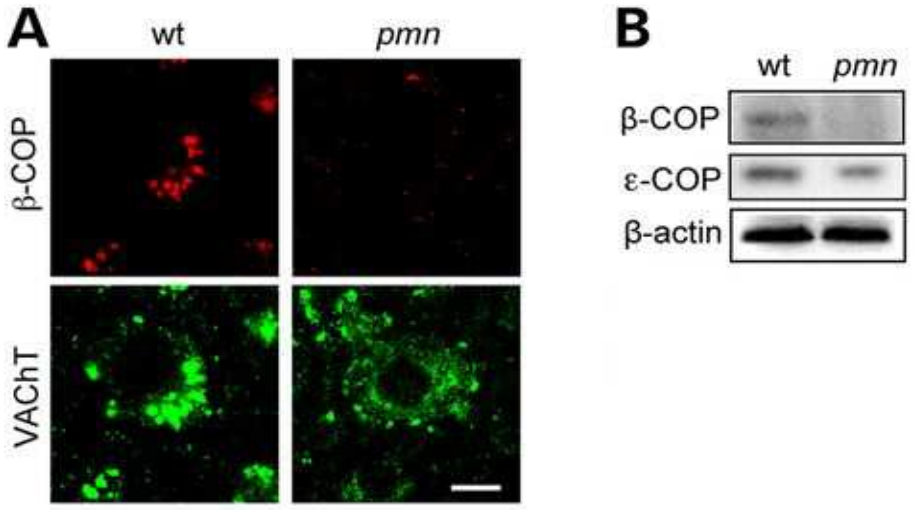

Fig. 18 : Diminution de l'expression de β-COP et ε-COP visualisée (A) par microscopie confocale sur neurone de souris *pmn* de 25 jours versus souris sauvage wt (le transporteur vésiculaire de l'acétylcholine ou VAchT est utilisé comme contrôle) et (B) par Western blot sur des extraits de moelle épinière de souris *pmn* de 25 jours versus souris sauvage wt (β-actine est utilisée comme contrôle). (Barre d'échelle = 10µm)

Les analyses biochimiques révèlent également une redistribution cytosolique du complexe protéique d'amarrage cis-golgienne GM130/p115 spécifique de COPI ainsi qu'une augmentation de l'expression des protéines golgiennes v-SNARE GS15 et GS28 qui sont impliquées dans l'arrimage et la fusion des vésicules (Fig. 19).

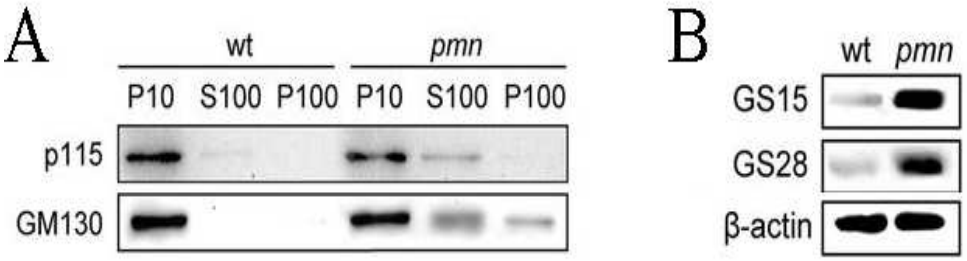

Fig. 19 : (A) Redistribution des protéines GM130 ET p115 des membranes (fraction P10) vers le cytosol (fraction S100) et pour GM130 vers des vésicules (fraction P100) à partir d'extraits de moelle épinière de souris *pmn* versus souris sauvage wt. **(B) Augmentation de l'expression de GS28 et GS15** dans la moelle épinière de souris *pmn* de 25 jours versus souris sauvage (β-actine est utilisée comme contrôle).

La dynamique d'apparition de ces altérations a été étudiée sur des souris *pmn* âgées de 5, 10, 15, 25 et 35 jours. GM130 et GS28 présentent des détections perturbées dans les motoneurones dès le 10^{ième} jour, soit 5 jours avant les premiers signes cliniques et histopathologiques. Dans les lignées de souris TBCE$^{PA/+}$*pmn* et TBCE$^{PC/+}$*pmn*

complémentées par transgénèse les protéines β-COP, GS28 et GS15 retrouvent des taux d'expression identiques à ceux observés dans la lignée sauvage (Fig. 20).

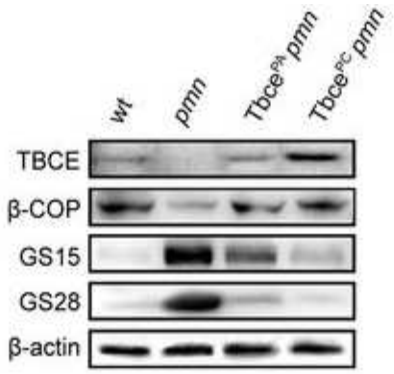

Fig. 20 : Restauration de l'expression de β-COP, GS28 et GS15 dans les motoneurones des souris TBCE$^{PA/+}$*pmn* et TBCE$^{PC/+}$*pmn*.

La distribution des protéines GM130, β-COP, GS28 et GS15 entre le Golgi, les vésicules et le réticulum endoplasmique a été comparée entre des cellules NSC34 normales ou appauvries en TBCE. Dans les cellules traitées par si TBCE, ces protéines qui sont observées dans le Golgi des cellules contrôles, sont déplacées vers des fractions de plus forte densité correspondant au compartiment vésiculaire (Fig. 21).

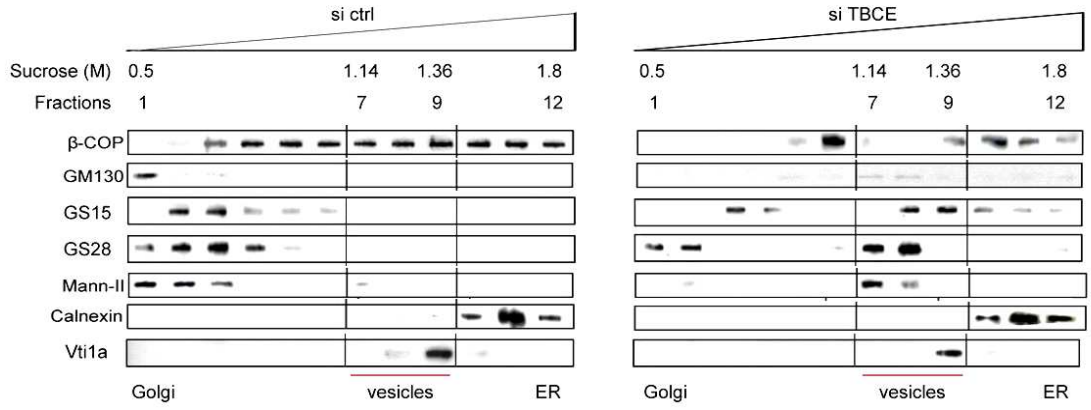

Fig. 21 : Distribution sur gradient de sucrose des protéines étudiées provenant de cellules NSC34 contrôles (si ctrl) ou appauvries en TBCE (si TBCE). Les protéines Mannosidase-II (Mann-II), Calnexin et Vti 1a sont respectivement utilisées comme contrôle des fractions du Golgi, du réticulum endoplasmique (ER) et des vésicules (vesicles).

Ainsi, de façon surprenante, la perte de TBCE entraine un niveau réduit de vésicules COP I, diminue le recrutement des facteurs d'amarrage GM130/p115 et augmente l'expression des protéines golgiennes v-SNARE GS15 et GS28. Ces anomalies moléculaires confirment les

défauts observés dans le trafic vésiculaire avec une accumulation de vésicules qui seraient non revêtues de coatomères, non arrimées et non fusionnées avec les membranes golgiennes. Ces données suggèrent que TBCE maintient la structure du Golgi en ajustant la polymérisation des microtubules associés par la formation des vésicules COP I.

Pour vérifier cette hypothèse, nous avons modulé l'expression d'ARF1, la petite GTPase qui est connue pour contrôler la formation des vésicules COP I (Goldberg, 2000). Des plasmides exprimant soit la forme sauvage d'ARF1 (ARF1 wt) soit sa forme mutée constitutivement active (ARF1 Q71L) permettent de restaurer un Golgi normal, l'expression de β-COP et la polymérisation des microtubules dans des cellules NSC34 appauvries en TBCE (Fig. 22).

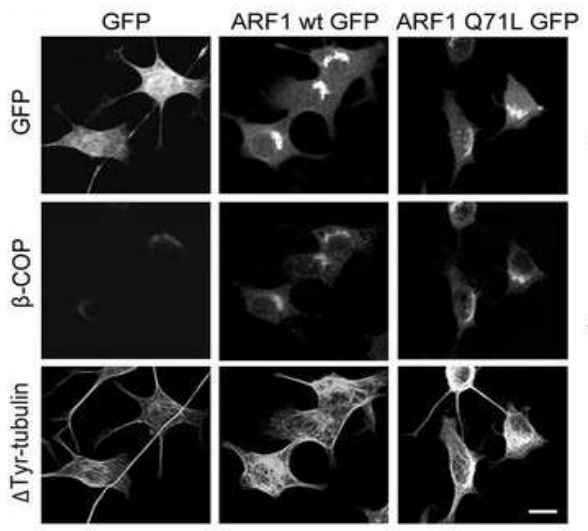

Fig. 22 : Restauration du Golgi normal, de l'expression de β-COP et de la polymérisation des microtubules associées dans des cellules NSC34 appauvries en TBCE, transfectées par la forme sauvage (ARF1 wt GFP) ou constitutivement active (ARF1 Q71L GFP) d'ARF1 marquée par la GFP. Un plasmide GFP vide est utilisé comme contrôle.

Ainsi, ARF1, qui contrôle la formation des vésicules COPI, semble mobiliser les protéines restantes de TBCE à la membrane du Golgi ce qui augmente la polymérisation des microtubules associés et restaure le trafic vésiculaire. Ces données révèlent une interaction jusqu'alors insoupçonnée entre ARF1 et TBCE qui permet de contrôler la polymérisation des microtubules à partir du Golgi et la formation de vésicules COPI. L'ensemble de ces résultats a permis de proposer un scénario impliquant ARF1 et TBCE aboutissant à la fragmentation du Golgi (Fig. 23).

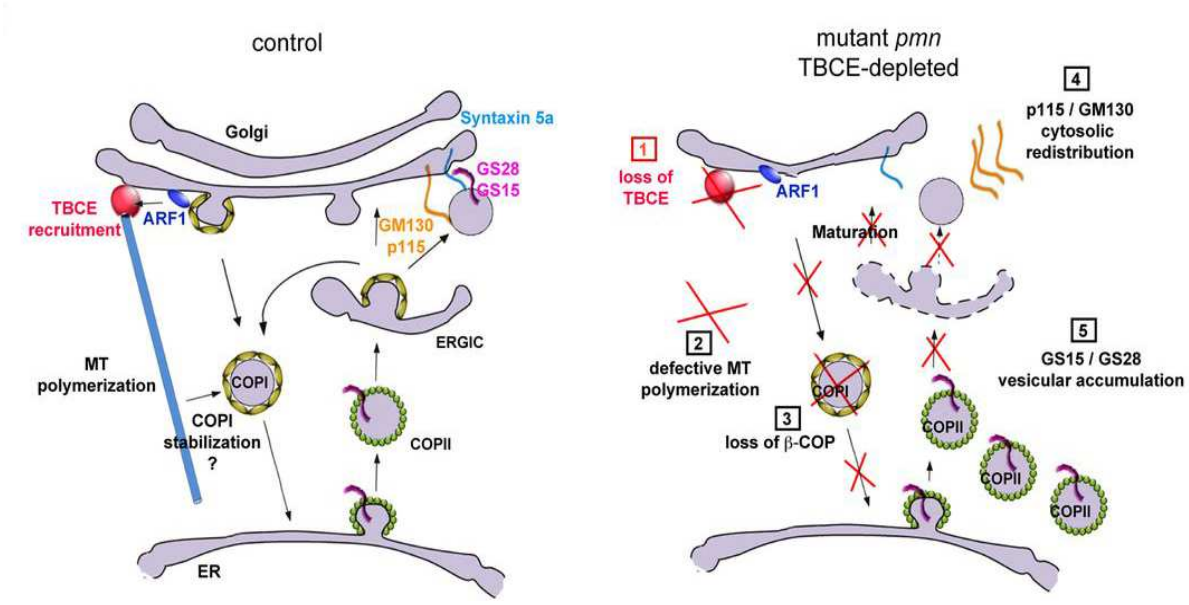

Fig. 23 : Schéma du scénario de fragmentation du Golgi dans les souris *pmn* versus les souris sauvage contrôle.

Ce défaut de coordination entre intégrité du réseau microtubulaire associé au Golgi et amarrage des vésicules COPI permet d'expliquer la fragmentation vésiculaire observée dans la SLA et dans d'autres maladies neurodégénératives. Ces anomalies pathologiques compromettent le transport des constituants axonaux et synaptiques et représenterait une contribution importante à la dégénérescence et aux dysfonctionnements des motoneurones. L'ensemble de ces résultats a été publié dans Human Molecular Genetics (Annexe 7).

TRAVAUX EN COURS, PERSPECTIVES

Mécanismes moléculaires et conséquences cellulaire des mutations de la protéine SOD1 dans la SLA.

L'identification de mutations sur le gène codant pour SOD1 (Super Oxyde Dismutase 1) chez des patients atteints de SLA a engendré la création de lignées de souris transgéniques surexprimant la SOD1 humaine mutée (Gurney et coll., 1994). A l'heure actuelle, 12 mutations humaines différentes ont été exprimées chez la souris (Turner et Talbot, 2008). Tous les animaux exprimant la hSOD1 mutée présentent une fragmentation de l'appareil de Golgi visible très précocement (Mourelatos et coll., 1996). Malgré le développement de ces modèles murins, la compréhension des mécanismes moléculaires de la dégénérescence sélective des motoneurones induite par ces mutations demeure limitée. La neurotoxicité de la SOD1 mutée semble surtout découler de l'acquisition de nouvelles propriétés et il est probable que ce soit le résultat d'une combinaison de plusieurs facteurs. Afin d'éclaircir les mécanismes moléculaires induit par ces mutations, notre équipe a utilisé les deux lignées murines les plus courantes : $SOD1^{G93A}$ et $SOD1^{G85R}$.

Les souris transgénique $SOD1^{G93A}$ utilisées, classiquement répertoriée B6SJL-Tg $(SOD1*G93A)^{dl}$ 1GurJ ou $SOD1G93A^{G1L}$, possèdent 8 copies du gène SOD1 humain avec la mutation G93A et développent un phénotype paralytique entre 6 et 9 mois (Gurney, 1997). Sur le plan histopathologique, différentes anomalies ont été observées dans les neurones moteurs spinaux lombaires dont une fragmentation de l'appareil de Golgi (Mourelatos et coll., 1996).

Comme la protéine $SOD1^{G85R}$ humaine a une demi-vie très courte, son expression dans les souris $SOD1^{G85R}$ est quasi égale à l'expression de la SOD1 murine endogène (Bruijn et coll., 1997; Wang et coll., 2009). L'apparition d'une paralysie des membres postérieurs et d'atrophie musculaire se situe entre 8-10 mois. Deux semaines après l'apparition des premiers symptômes, environ 40% des axones de gros calibre des neurones moteurs dégénèrent. Sur le plan histopathologique, la présence d'agrégats immunoréactifs pour SOD1 est détectée dès le $6^{ième}$ mois de vie postnatale (Bruijn et coll., 1997). Au stade terminal de la pathologie, de larges inclusions riches en SOD1apparaissent aussi bien dans les corps cellulaires que dans la partie proximale de l'axone des neurones moteurs (Bruijn et coll., 1997; Bruijn et coll., 1998). Dans ce modèle, un ralentissement du transport axonal lent dû à un défaut de transport des tubulines est observé précocement au moins 6 mois avant le début des signes cliniques (Williamson and Cleveland, 1999).

Dans notre équipe, les anomalies morphologiques de l'appareil de Golgi précédemment décrites (Gonatas et coll., 2006) ont été confirmées par des marquages immuno-histochimiques sur coupes de moelles épinières lombaires de souris transgéniques $SOD1^{G93A}$ et $SOD1^{G85R}$ (Fig. 24).

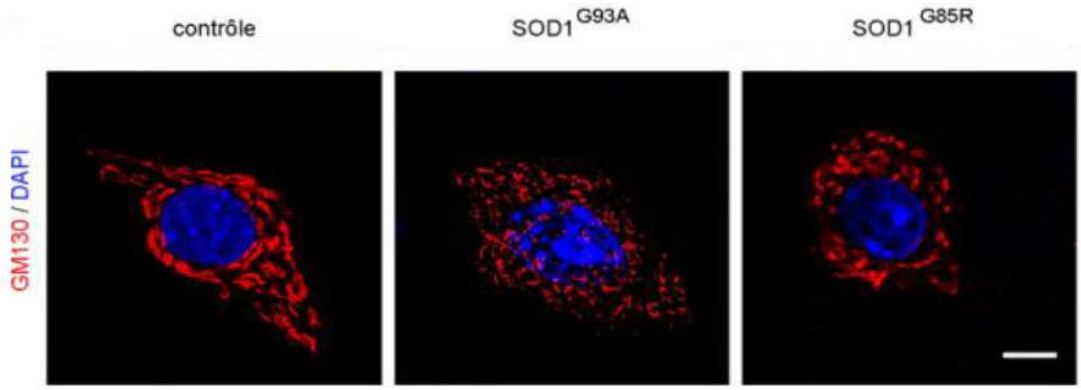

Fig. 24 : Morphologie du Golgi identifié par GM130 (en rouge) dans les neurones moteurs de souris sauvages (contrôle), SOD1G93A et SOD1G85R. Le noyau (en bleu) est identifié grâce au DAPI (Barre d'échelle : 10µm).

Afin de vérifier s'il y avait une transformation vésiculaire de l'appareil Golgi telle que celle précédemment décrite chez les souris mutantes *pmn*, nous avons analysé l'expression de différentes protéines impliquées dans la vésiculation (Fig. 25).

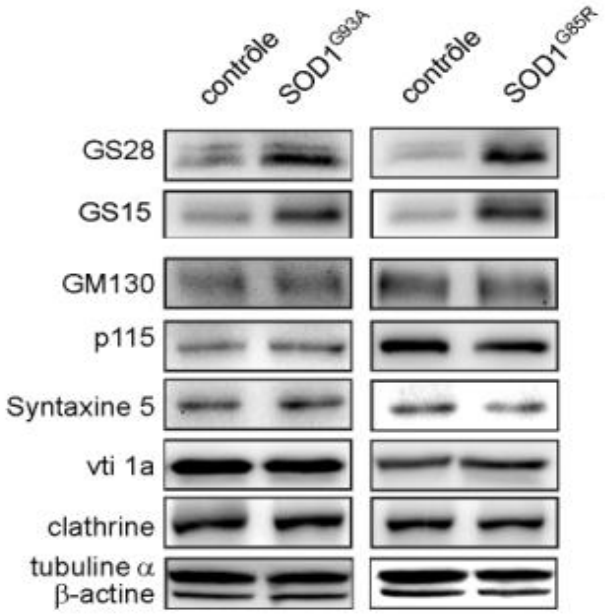

Fig. 25 : Expression de GS28, GS15, GM130, p115, Syntaxine 5, Vti 1A et Clathrine dans les souris SOD1G85R et SOD1G93A versus les souris sauvage (contrôle). La tubuline α et la β-actine sont utilisées comme contrôle de charge.

Des surexpressions de GS28 et de GS15 sont observées dans les souris mutées. En revanche les quantités protéiques sont similaires pour la t-SNARE Syntaxine 5 ainsi que pour les protéines d'amarrage GM130 et p115, pour la t-SNARE endosomale Vti1a et pour la clathrine. Ces résultats indiquent que les anomalies morphologiques golgiennes (fragmentation) dans les neurones moteurs des souris SOD1^{G93A} et SOD1^{G85R} sont associées à des anomalies moléculaires de certaines des protéines régulant le trafic vésiculaire. Une accumulation de structures ponctiformes contenant la protéine GS15 a également été observée dans les motoneurones des souris SOD1^{G93A} et SOD1^{G85R}. Ces résultats indiquent donc que, comme dans les souris *pmn*, la fragmentation du Golgi s'accompagne d'une vésiculation accrue.

Nous avons ensuite vérifié si ces anomalies golgienne et ces altérations vésiculaire dans les neurones moteurs des souris exprimant la SOD1 mutée sont la conséquence d'une dynamique altérée des microtubules (MTs) associés à l'appareil de Golgi (Fig. 26).

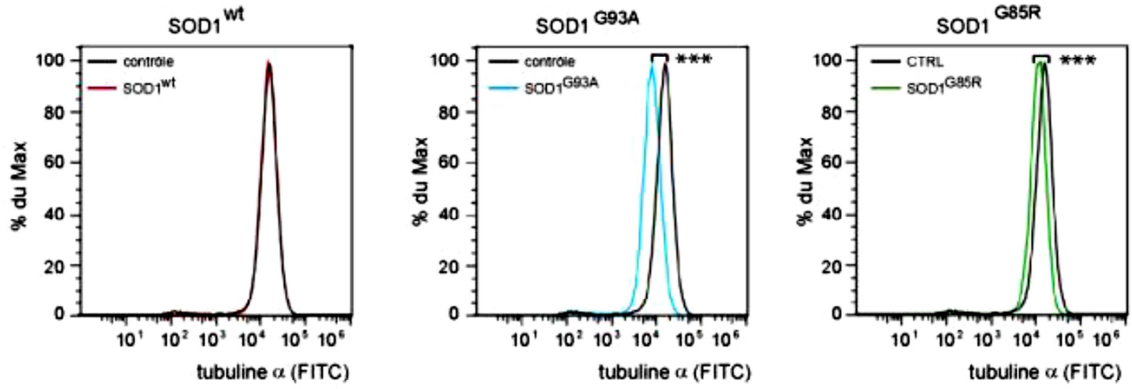

Fig. 26 : Analyse par FACS du contenu en tubuline polymérisées dans les motoneurone NSC34 exprimant la SOD1 humaine sauvage (SOD1wt, en rouge), la SOD1 mutée en position 93 (SOD1^{G93A,} en bleu) ou en position 85 (SOD1^{G85R}, en vert) versus des motoneurones transfectés par un plasmide vide (contrôle, en noir). Les tubulines sont marquées à l'aide d'un anticorps anti tubuline FITC.

Une perte de microtubules est observée dans les neurones moteurs exprimant la SOD1 mutée. Ces altérations des microtubules associées au Golgi ont été confirmées par immunohistochimie sur coupes de moelles épinières de souris SOD1^{G93A} et SOD1^{G85R}. L'expression de SOD1 mutée affecte donc la dynamique des MTs dérivés du Golgi ce qui pourrait être à l'origine de la fragmentation de cette organelle dans la SLA.

Afin de confirmer ces données dans un modèle cellulaire, j'ai transfecté des cellules NSC34 avec des plasmides exprimant les SOD mutées. Des anomalies golgiennes

comparables au modèle murin ainsi que des surexpressions des protéines GS28 et GS15 ont ainsi été mises en évidence (Fig. 27).

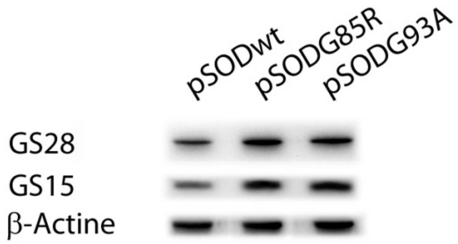

Fig.27 : Augmentation de l'expression de GS28 et GS15 dans des cellules NSC34 transfectées avec des plasmides exprimant la SOD1 mutée en position 93 (pSODG93A) ou en position 85 (pSODG85R) versus un plasmide exprimant SOD1 humaine sauvage (pSODwt). La β-actine est utilisée comme contrôle de charge.

Les travaux de Strey et coll. (2004) ont précédemment montré une augmentation de l'expression de la protéine Stathmine 1 dans les neurones moteurs $SOD1^{G93A}$. La Stathmine 1 fait partie d'une famille de protéine comprenant la protéine SCG10 (Superior cervical Ganglion clone 10) ou Stathmine 2, la protéine SCLIP (SCG10-like protein) ou Stathmine 3 et la protéine RB3 ou Stathmine 4. La Stathmine 1 est exprimée de façon ubiquitaire et cytosolique alors que les autres membres de la famille sont principalement considérés comme spécifique au neurone et localisés au niveau de l'appareil de Golgi et de structures vésiculaires dans le corps cellulaire et les neurites (Bieche et coll., 2003; Stein et coll., 1988 ; Gavet et coll., 2002). Ce sont des phosphoprotéines qui, selon leur état de phosphorylation, induisent la dépolymérisation des MTs *in vitro* et *in vivo* en séquestrant les dimères de tubuline libres. Notre hypothèse est que la surexpression de protéines de la famille des Stathmines pourrait être à l'origine des anomalies golgienne et des altérations vésiculaires.

Nous avons mis en évidence cette surexpression de protéines de la famille des Stathmines dans des motoneurones des souris $SOD1^{G93A}$ et $SOD1^{G85R}$ (Fig. 28).

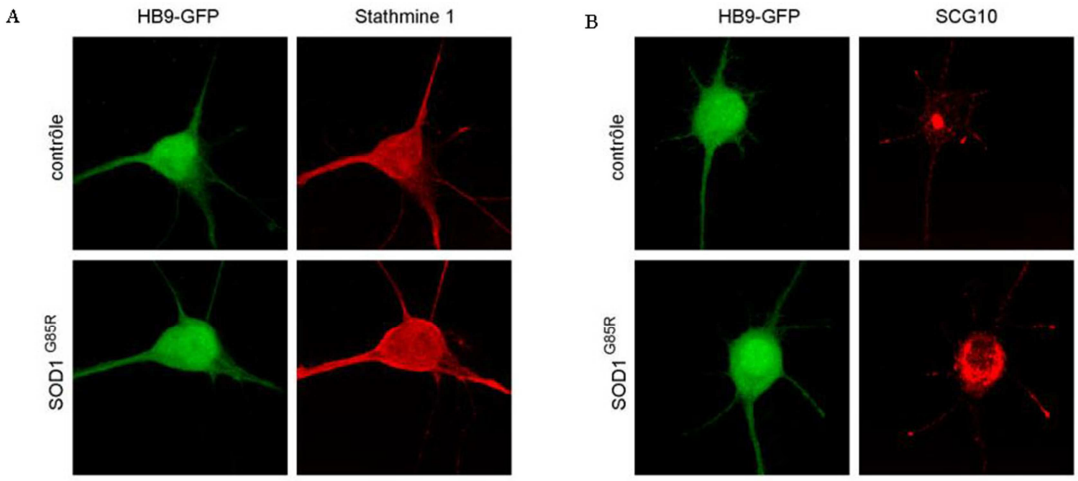

Fig.28 : Images confocales de neurones moteurs (Hb9:GFP positifs) de souris contrôle et SOD1^{G85R}.
L'immunoréactivité de la Stathmine 1(A) et de SCG10 (B) est augmentée chez les souris SOD^{G85R}.

Pour démontrer que l'augmentation de l'expression des protéines de la famille des Stathmines induit les anomalies golgiennes, j'ai transfecté des cellules NSC34 différentiées en neurones avec des plasmides exprimant Stathmine 1 ou SCG10 (Fig. 29).

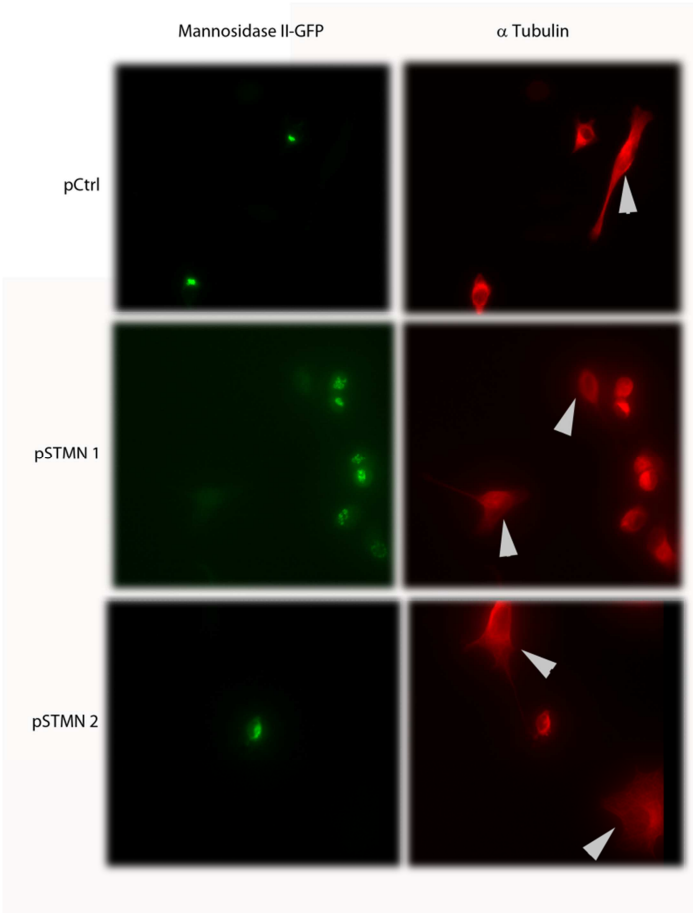

Fig.29 : Anomalies du Golgi (en vert) et des MTs (en rouge) dans des cellules NSC34 transfectées avec des plasmides exprimant Stathmine 1 (pSTMN 1) ou SCG10 (pSTMN 2) versus le plasmide vide (pCtrl).

L'expression de la Mannosidase II taguée par la GFP montre les cellules ayant incorporées les plasmides versus les non transfectées (flèche) mais aussi la stucture du Golgi.

Les cellules transfectées ont effectivement montrées des anomalies du Golgi comparables à celles observées dans les motoneurones de souris SOD^{G85R} et SOD^{G93A} ainsi que des modifications morphologiques dues à des perturbations du réseau microtubulaire. De plus, les taux d'expression de GS28 et GS15 sont augmentés dans les cellules transfectées comme précédemment observé dans les motoneurones des souris mutées (Fig. 30).

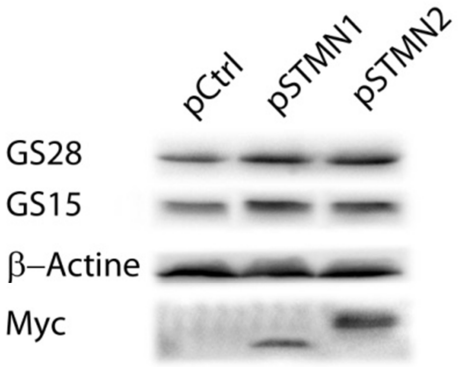

Fig.30 : Augmentation de l'expression de GS28 et GS15 dans des cellules NSC34 transfectées avec des plasmides exprimant Stathmine 1 (pSTMN 1) ou SCG10 (pSTMN 2) taguées par cMyc versus le plasmide vide (pCtrl). La β-actine est utilisée comme contrôle de charge.

Ceci apporte la preuve que la surexpression des Stathmines 1 et 2 induit des anomalies du Golgi et des microtubules et donc un défaut du transport dépendant des MTs. Les vésicules de transport s'accumuleraient dans le corps cellulaire des neurones SOD1 mutées et ne seraient plus acheminées vers la terminaison synaptique ou vers les cônes de croissance entrainant la dégénérescence des motoneurones dans la pathologie. Une publication sur ces résultats est actuellement en cours de rédaction que je signerai en tant que co-1er auteur.

Recherche de biomarqueurs des neuropathies dégénératives des motoneurones

Si de nombreux traitements ont été testés, seul le riluzole (Rilutek®) est capable de ralentir la progression de la maladie de Charcot chez l'homme à condition d'agir le plus tôt possible. Malheureusement, il n'existe actuellement aucun test de dépistage précoce de la SLA et des maladies apparentées. De plus, le diagnostic clinique précoce est difficile en raison de l'hétérogénéité phénotypique de la maladie. Des études précédentes dans le sang ou le liquide céphalo-rachidien ont rapporté des anomalies biologiques concernant des voies

physiopathologiques variées (stress oxydant, inflammation, excitotoxicité…). Toutefois, aucune de ces anomalies n'a une sensibilité ou une spécificité suffisante pour constituer un marqueur de la maladie. Ce retard diagnostique est préjudiciable à la prise en charge de la maladie car il empêche l'institution précoce d'un traitement visant à préserver les motoneurones survivants.

Nos résultats ont mis en évidence une fragmentation du Golgi identique dans les souris transgéniques SOD1 ainsi que dans les souris mutantes pmn, 2 lignées modèles de la maladie. Ces anomalies de l'appareil du Golgi ont également été décrites chez des patients SLA (Gonatas et coll., 2006). Cette fragmentation s'accompagne d'une dérégulation importante des protéines golgiennes, en particulier une surexpression des protéines v-SNARE GS15 et GS28 impliquées dans l'arrimage et la fusion des vésicules COP1. Par ailleurs, des expériences préliminaires ont montré que ces protéines peuvent être détectées dans le liquide céphalo-rachidien et dans le sérum sanguin de patients SLA. Les altérations du Golgi surviennent très tôt dans ce type de pathologie ce qui renforce l'intérêt de ces protéines comme moyen de détection précoce.

Je me propose donc d'évaluer le potentiel de ces protéines comme biomarqueurs de la SLA. En particulier, il faudra comprendre et quantifier le processus de libération de ces protéines golgiennes lors de la dégénérescence des motoneurones dans les lignées murines mimant la pathologie. Nous comptons également rechercher d'autres candidats protéiques potentiels liés à l'appareil de Golgi ou aux MTs afin d'améliorer la spécificité de la réponse. En collaboration avec le centre des maladies neuromusculaires de l'APHM, nous allons comparer dans un deuxième temps les niveaux des marqueurs sélectionnés dans le liquide céphalo-rachidien et le sérum de patients SLA (ou avec des neuropathies apparentées) et de patients sains. Nous espérons que l'utilisation comme biomarqueurs de protéines impliquées dans la fragmentation du Golgi et les anomalies microtubulaires rendra plus précoce et plus précis le diagnostique des maladies dégénératives du motoneurones, permettra le suivi des patients et rendra plus facile le développement de nouvelles thérapies et des essais cliniques.

Développement d'une nouvelle méthode de purification par FACS de motoneurones humains issus d'IPS

La technologie IPSC (induced pluripotent stem cells) utilise des cellules souches pluripotentes induites produites en laboratoire à partir de cellules somatiques (kératinocytes ou de fibroblastes) adultes (Takahashi and Yamanaka, 2006). A partir de ces cellules, il est ensuite possible de générer des neurones moteurs de patients. Ainsi, des cellules IPS ont pu

être différenciées en motoneurones à partir d'une patiente de 82 ans ayant une forme familiale de SLA (Dimos et coll., 2008).

Toutefois, ces techniques génèrent d'autres types cellulaires, en particulier des interneurones, qui peuvent nuire à l'interprétation des anomalies phénotypiques dans la dégénérescence pathologique des motoneurones. Nous avons mis au point une nouvelle méthode de purification par FACS de motoneurones dérivés d'IPS humains, obtenus par une collaboration avec l'Unité Biothérapies pour les Maladies Neurodégénératives de l'Institut Pasteur. Nous avons utilisé pour un premier tri un vecteur rapporteur lentiviral Hb9::RFP couplé à une double sélection basée sur le récepteur de faible affinité des neurotrophines, p75. Hb9 est un facteur de transcription à homéodomaine qui joue un rôle très important dans l'identité motoneuronale. Il agit au stade progéniteur dans la spécification générale des motoneurones en réprimant l'expression des interneurones et au stade post-mitotique dans la consolidation de l'identité des colonnes motrices (Arber et coll., 1999; Lee et coll., 2008; Thaler et coll., 1999). Toutefois, le promoteur Hb9 n'est pas complétement spécifique des motoneurones car il est aussi actif dans certains interneurones comme vérifié par QRT-PCR (Fig. 32). Pour améliorer la pureté, les cellules Hb9 ont été incubées avec un anticorps contre $p75^{NTR}$, un récepteur de basse affinité pour les facteurs neurotrophiques NGF, BDNF, NT4/5 et NT3 (Kaplan et Miller, 2000) très exprimé à la surface des motoneurones. Cet anticorps couplé à la biotine est ensuite révélé avec une streptavidine-FITC et les cellules marquées sont ensuite triées par FACS (Fig. 31).

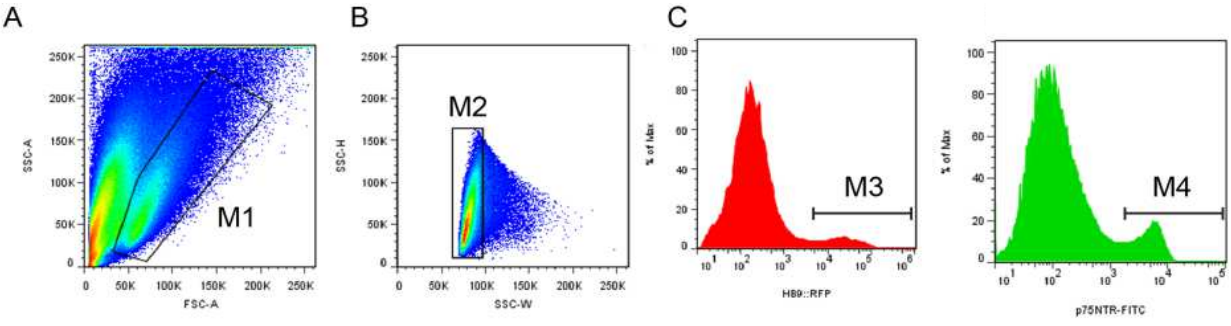

Fig. 31 : Isolation de motoneurones dérivés d'IPS par FACS : (A) exclusion des débris cellulaires; (B) élimination des doublets cellulaires; (C) sélection de la population M3 (HB9::RFP positive) et de la population M4 (fraction de M3 immunoréactive contre $p75^{NTR)}$) .

Cette double sélection permet d'éliminer les interneurones indésirables comme le démontre la baisse de l'expression des marqueurs spécifiques des interneurones parallèlement à l'augmentation de celle des marqueurs des motoneurones (Fig.32).

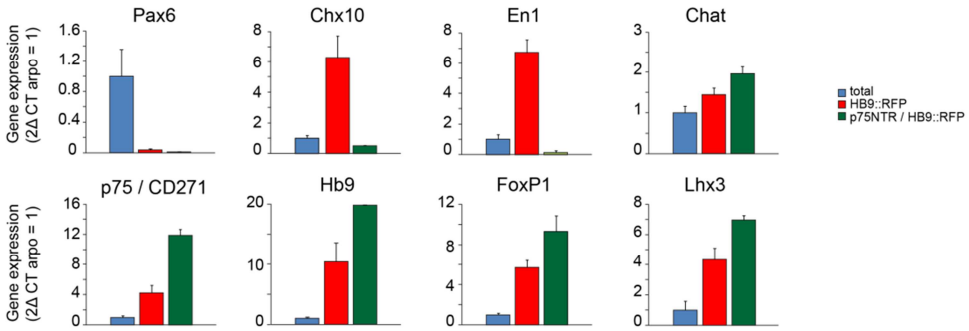

Fig. 32: Caractérisation par QRT-PCR des populations neuronales avant (en bleu) et après simple (en rouge) ou double (en vert) sélection par FACS. Pax6 est un marqueur des précurseurs neuronaux; Chx10 and En1 caractérisent les interneurones; ChAt, Foxp1 and Lhx3 sont des marqueurs des neurones moteur.

L'expression d'En1 est réduite de 48 fois et celle de CHx10 de 13 fois, deux marqueurs des interneurones V1 and V2a respectivement, en comparaison avec les expressions observées dans les cellules simplement triées Hb9, indiquant une élimination quasi-totale de ces types cellulaires. Les précurseurs neuronaux sont aussi éliminés comme l'indique la réduction drastique de l'expression de Pax6.

Les cellules triées mises en culture développent rapidement une morphologie motoneuronale caractéristique telle que de larges corps cellulaires et de longues projections axonales similaires à celles de motoneurones non triés. Le taux de survie après 3 divisions cellulaires de 2 clones isolés est de 21 ± 3.7 % et 45 ± 10.5 % avec un rendement moyen de 1.83 ± 0.75 %. Des expériences en électrophysiologie (patch clamp) ont enregistré des potentiels d'action après dépolarisation qui montrent que ces cellules sont pleinement fonctionnelles.

Ces données démontrent pour la première fois la possibilité d'isoler une population homogène de motoneurones dérives d'IPS à travers une double sélection HB9 et $p75^{NTR}$. Ce modèle cellulaire de neurones moteurs devrait contribuer à améliorer notre compréhension des mécanismes en jeu dans la SLA et d'autres maladies neurologiques affectant cette population. Ces résultats, décrits dans un article dans lequel je suis co-auteur, viennent d'être soumis à publication.

Analyse des altérations génotypiques et moléculaires de motoneurones humains en condition pathologique sur motoneurones issus d'IPS de patients

Alors que plusieurs analyses génomiques ont été menées chez des patients atteints de SLA et divers modèles murins, il n'existe pas à ce jour de méta-analyse publiée sur les changements d'expression de gènes causés par la SLA. Pourtant, ces informations pourraient être un outil utile pour déduire les mécanismes sous-jacents des maladies neurodégénérative car ils fournissent des valeurs pouvant être exploitées non seulement pour un seul gène exprimé de manière aberrante mais aussi pour des voies ou groupes de gènes. Dans ce type d'étude, la population de cellules utilisées est primordiale pour l'interprétation des résultats. Les profils d'expressions publiés présentent des différences importantes non seulement entre les différents modèles murins mais aussi entre le modèle souris et des échantillons de patients. Ces différences, dues à la variabilité entre espèces, aux différences d'environnements cellulaires ou aux fonds génétiques des lignées murines, réduisent l'intérêt des modèles murins dans ce type d'études. Ainsi, dans les neurones moteurs isolés de mutants SOD murins, la réponse transcriptionnelle générale est très pertubée en comparaison de lignées analogues, avec par exemple une hausse de la régulation de gènes du cycle cellulaire, des niveaux réduits d'expression de gènes de la réponse anti-oxydantes mais peu d'augmentation de celle de gènes de mort cellulaire (Kirby et coll., 2005; Perrin et col., 2005; Ferraiuolo et coll., 2007). De plus, le profilage sur des tissus post-mortem humains ne peut donner qu'un aperçu de la phase terminale de la maladie, souvent après des années de dommages inflammatoires et hypoxique. Par conséquent, il est extrêmement difficile avec ces échantillons de séparer la cause et l'effet. En revanche, la technologie IPS permet d'obtenir en abondance des neurones moteurs spécifiques de patient et rend possible de générer des profils d'expression quasi présymptomatiques dans la SLA humaine.

Mon projet est d'utiliser cette technique pour obtenir des populations de motoneurones isolés de patients SLA grâce à notre collaboration avec l'Unité Biothérapies pour les Maladies Neurodégénératives de l'Institut Pasteur. Ces motoneurones dérivés d'IPS présentent l'avantage de permettre d'accéder à plusieurs types de mutations que l'on peut potentiellement trouver chez les patients atteints de SLA, y compris les mutations sporadiques. La purification des motoneurones par FACS que nous avons développée représente une avancée importante pour l'analyse des altérations phénotypiques et moléculaires en conditions pathologiques compte tenu que l'hétérogénéité des types cellulaires issus d'IPS fausse les observations. Ces

neurones ‘SLA’ pourront ensuite être génétiquement et moléculairement analysées et comparées à des populations de motoneurones de personnes non atteintes.

Cependant, la purification par FACS réduit le temps de survie des motoneurones triés à quelques jours rendant les analyses sur le long terme difficile. Je suis donc en train d’optimiser les conditions de culture en testant des cocktails de différents facteurs neurotrophiques afin de rallonger la survie cellulaire. Je compte aussi essayer l’utilisation de milieux conditionnés à partir d’autres types cellulaires connus pour leurs effets trophiques.

Ce modèle cellulaire issu d’IPS ne peut être pertinent que si les populations vulnérables aux maladies neurodégénératives sont bien représentées. Dans la corne ventrale de la moelle épinière, les neurones moteurs sont anatomiquement séparés en sous-groupes qui reflètent à la fois la fonction et l'origine du développement. Tout d'abord, les neurones moteurs sont divisés en "colonnes" qui reflètent les grandes catégories de cibles post-synaptiques en dehors de la moelle épinière. Deuxièmement, les neurones moteurs sont divisés en «pools» plus localisées, qui reflètent les objectifs post-synaptiques spécifiques comme un groupe musculaire particulier. Les quatre grandes colonnes sont: la colonne motrice latérale (LMC), la colonne motrice médiane (MMC), la colonne motrice hypaxial (HMC), et la colonne motrice préganglionnaires (PGC) (Dasen et Jessell, 2009). La LMC, qui innerve la musculature des membres, est la plus précocement endommagée dans la SLA. La MMC, qui innerve la musculature dorsale, et la HMC, qui innerve la musculature intercostale et abdominale, sont ensuite touchées. La proportion de chaque sous type devra donc être déterminée à l’aide de marqueurs spécifiques. Ce projet, qui comporte à la fois un aspect hospitalier et un aspect fondamental, pourrait devenir un bon sujet de thèse dans lequel mon expérience dans le domaine de l’analyse génomique serait un atout (Baillat et coll., 2005).

CONCLUSION

Mes travaux de recherche m'ont permis d'utiliser de nombreuses techniques couvrant les domaines de la biochimie, de la biologie cellulaire et moléculaire. Grâce à elles, j'ai concrétisé plusieurs sujets d'étude qui ont donné lieu à des publications et acquis une expertise dans des thématiques diverses. Au cours de ces années, j'ai encadré de nombreux stagiaires et étudiants thésards, médecins, pharmaciens, de M1, de M2, d'écoles d'ingénieur et de BTS. J'ai également assuré une codirection de thèse.

Affecté depuis le 1er avril 2013 à l'UMR 7289 (INT), je collabore avec l'unique chercheur statutaire de l'équipe MoMoThe sur un sujet qui concerne les maladies des motoneurones et tout particulièrement l'étude de leur dégénérescence dans la SLA, dans lequel j'apporte mes compétences et mon expérience professionnelle. Rapidement intégré aux études commencées, j'ai cosigné une première publication dès 2014. De plus, deux autres articles portant ma signature sont actuellement en cours dont un en tant que co-1er auteur. Cette expertise nouvellement acquise dans cette thématique, en particulier au niveau du tri cellulaire, me permet maintenant d'être autonome pour des sujets plus personnels.

Mon expérience professionnelle, développée sur 27 ans de carrière scientifique, m'apporte la capacité d'assumer des responsabilités plus importantes, comme diriger un étudiant en thèse. Dans ce but, je désire donc obtenir le diplôme d'Habilitation à Diriger les Recherches au sein de l'Université d'Aix-Marseille.

REFERENCES

Arber S, Han B, Mendelsohn M, Smith M, Jessell TM and Sockanathan S. (1999) Requirement for the homeobox gene Hb9 in the consolidation of motor neuron identity. ***Neuron*** 23: 659-74.

Baillat G, Moqrich A, Castets F, Baude A, Bailly Y, Benmerah A, Monneron A. (2001) Molecular cloning and characterization of phocein, a protein found from the Golgi complex to dendritic spines. ***Mol. Biol .Cell*** 12(3):663−73.

Baillat G, Gaillard S, Castets F, Monneron A. (2002) Interactions of phocein with nucleoside-diphosphate kinase, Eps15, and Dynamin I. ***J. Biol. Chem.*** 277(21):18961−6.

Baillat G, Garrouste F, Remacle−Bonnet M, Marvaldi J, Pommier G. (2005) Bcl-xL/Bax ratio is altered by IFNgamma in TNFalpha- but not in TRAIL-induced apoptosis in colon cancer cell line. ***Biochim. Biophys. Acta.*** 1745(1):101−10.

Baillat G, Siret C, Delamarre E, Luis J. (2008) Early adhesion induces interaction of FAK and Fyn in lipid domains and activates raft-dependent Akt signaling in SW480 colon cancer cells. ***Biochim. Biophys. Acta.*** 1783(12):2323−31.

Bellouze S, Schäfer MK, Buttigieg D, Baillat G, Rabouille C, Haase G. (2014) Golgi fragmentation in pmn mice is due to a defective ARF1/TBCE cross-talk that coordinates COPI vesicle formation and tubulin polymerization. ***Hum. Mol. Genet***. 23(22):5961-75.

Bieche I, Maucuer A, Laurendeau I, Lachkar S, Spano AJ, Frankfurter A, Levy P, Manceau V, Sobel A,Vidaud M and Curmi PA. (2003) Expression of stathmin family genes in human tissues: non-neuralrestricted expression for SCLIP. ***Genomics*** 81: 400-10.

Bommel H, Xie G, Rossoll W, Wiese S, Jablonka S, Boehm T, Sendtner M. (2002) Missense mutation in the tubulin-specific chaperone E (Tbce) gene in the mouse mutant progressive motor neuronopathy, a model of human motoneuron disease. ***J. Cell Biol.*** 159(4):563-9.

Bruijn LI, Becher MW, Lee MK, Anderson KL, Jenkins NA, Copeland NG, Sisodia SS, Rothstein JD, Borchelt DR, Price DL and Cleveland DW. (1997) ALS-linked SOD1 mutant G85R mediates damage to astrocytes and promotes rapidly progressive disease with SOD1-containing inclusions. ***Neuron*** 18: 327-338.

Bruijn LI, Houseweart MK, Kato S, Anderson KL, Anderson SD, Ohama E, Reaume AG, Scott RW and Cleveland DW. (1998) Aggregation and motor neuron toxicity of an ALS-linked SOD1 mutant independent from wild-type SOD1. ***Science*** 281: 1851-54.

Campbell GR, Loret EP. (2009) What does the structure-function relationship of the HIV-I Tat protein teach us about developing an AIDS vaccine? ***Retrovirology*** 6: 50-63.

Castets F, Baillat G, Mirzoeva S, Mabrouk K, Garin J, d'Alayer J, Monneron A. (1994) A brain synaptosomal adenylyl cyclase of high specific activity is photolabeled with azido-ATP. ***Biochemistry*** 33(17):5063−9.

Castets F, Bartoli M, Barnier JV, Baillat G, Salin P, Moqrich A, Bourgeois JP, Denizot F, Rougon G, Calothy G, Monneron A. (1996) A novel calmodulin-binding protein, belonging to the WD-repeat family, is localized in dendrites of a subset of CNS neurons. ***J. Cell Biol.*** 134(4):1051−62.

Chappie JS, Dyda F. (2013) Building a fission machine--structural insights into dynamin assembly and activation. ***J. Cell Sci.*** 126:2773-84.

Dasen JS, Jessell TM (2009) Hox networks and the origins of motor neuron diversity. ***Curr Top Dev Biol.*** 88:169-200.

Dejesus-Hernandez M, Rayaprolu S, Soto-Ortolaza AI, Rutherford NJ, Heckman MG, Traynor S, Strongosky A, Graff-Radford N, Van Gerpen J, Uitti RJ, Shih JJ, Lin SC, Wszolek ZK, Rademakers R, Ross OA. (2013) Analysis of the C9orf72 repeat in Parkinson's disease, essential tremor and restless legs syndrome. ***Parkinsonism Relat. Disord.*** 19(2):198-201.

Dimos JT, Rodolfa KT, Niakan KK, Weisenthal LM, Mitsumoto H, Chung W, Croft GF, Saphier G, Leibel R, Goland, R, Wichterle H, Henderson CE and Eggan K. (2008) Induced

pluripotent stem cells generated from patients with ALS can be differentiated into motor neurons. ***Science*** 321:1218-21.

Ferraiuolo L, Heath PR, Holden H, Kasher P, Kirby J, Shaw PJ. (2007) Microarray Analysis of the Cellular Pathways Involved in the Adaptation to and Progression of Motor Neuron Injury in the SOD1 G93A Mouse Model of Familial ALS. ***J. Neurosci.*** 27(34): 9201-19.

Gaur U, Aggarwal BB. (2003) Regulation of proliferation, survival and apoptosis by members of the TNF superfamily. ***Biochem. Pharmacol.*** 66 (8):1403-08.

Gavet O, El Messari S, Ozon S and Sobel A. (2002) Regulation and subcellular localization of the microtubule-destabilizing stathmin family phosphoproteins in cortical neurons. ***J. Neurosci. Res.*** 68: 535-50.

Goldberg J. **(**2000) Decoding of sorting signals by coatomer through a GTPase switch in the COPI coat complex. ***Cell*** 100(6):671-9.

Gonatas NK, Stieber A, Mourelatos Z, Chen Y, Gonatas JO, Appel SH, Hays AP, Hickey WF, Hauw JJ. (1992) Fragmentation of the Golgi apparatus of motor neurons in amyotrophic lateral sclerosis. ***Am. J. Pathol.*** 140:731-7.

Gonatas NK, Stieber A and Gonatas JO. (2006) Fragmentation of the Golgi apparatus in neurodegenerative diseases and cell death. ***J. Neurol. Sci.*** 246: 21-30.

Gurney ME, Cutting FB, Zhai P, Andrus PK, Hall ED. (1996) Pathogenic mechanisms in familial amyotrophic lateral sclerosis due to mutation of Cu, Zn superoxide dismutase. ***Pathol. Biol. (Paris)*** 44(1):51-6.

Gurney ME. (1997) The use of transgenic mouse models of amyotrophic lateral sclerosis in preclinical drug studies. ***J. Neurol. Sci.*** 152 Suppl 1: S67-73.

Haeberlé AM, Castets F, Bombarde G, Baillat G, Bailly Y. (2006) Immunogold localization of phocein in dendritic spines. ***J. Comp. Neurol.*** 495(3):336−50.

Kaplan DR and Miller FD (2000) Neurotrophin signal transduction in the nervous system. ***Curr. Opin. Neurobiol.*** 10: 381-91.

Kennel PF, Fonteneau P, Martin E, Schmidt JM, Azzouz M, Borg J, Guenet JL, Schmalbruch H, Warter JM, Poindron P. (1996) Electromyographical and motor performance studies in the pmn mouse model of neurodegenerative disease. ***Neurobiol. Dis.*** 3(2):137-47.

Kim HD, Youn B, Kim TS, Kim SH, Shin HS, Kim J. (2009) Regulators affecting the metastasis suppressor activity of Nm23-H1. ***Mol. Cell Biochem.*** 329(1-2):167-73.

Kirby J, Halligan E, Baptista MJ, Allen S, Heath PR, Holden H, Barber SC, Loynes CA, Wood-Allum CA, Lunec J, Shaw PJ. (2005) Mutant SOD1 alters the motor neuronal transcriptome: implications for familial ALS. ***Brain*** 128(Pt 7):1686-706

Lee S, Lee B, Joshi K, Pfaff SL, Lee JW and Lee SK. (2008) A regulatory network to segregate the identity of neuronal subtypes. ***Dev. Cell*** 14: 877-89.

Liang X, Nazarian A, Erdjument-Bromage H, Bornmann W, Tempst P, Resh MD. (2001) Heterogeneous fatty acylation of Src family kinases with polyunsaturated fatty acids regulates raft localization and signal transduction. ***J. Biol. Chem.*** 276: 30987–94.

Martin N, Jaubert J, Gounon P, Salido E, Haase G, Szatanik M, Guénet JL. (2002) A missense mutation in Tbce causes progressive motor neuronopathy in mice. ***Nat. Genet.*** 32(3):443-7.

Mediouni S, Baillat G, Darque A, Ravaux I, Loret E. (2011) HIV-1 Infected Patients Have Antibodies Recognizing Folded Tat. ***Infect Disord Drug Targets*** 11(1):57−63.

Mediouni S, Watkins JD, Pierres M, Bole A, Loret EP, Baillat G. (2012) A monoclonal antibody directed against a conformational epitope of the HIV-1 trans-activator (Tat) protein neutralizes cross-clade. ***J. Biol. Chem.*** 287(15):11942−50.

Mediouni S, Darque A, Baillat G, Ravaux I, Dhiver C, Tissot−Dupont H, Mokhtari M, Moreau H, Tamalet C, Brunet C, Paul P, Dignat−George F, Stein A, Brouqui P, Spector SA, Campbell GR, Loret EP. (2012) Antiretroviral therapy does not block the secretion of the human immunodeficiency virus tat protein. ***Infect Disord Drug Targets*** 12(1):81−6.

Mediouni S, Darque A, Ravaux I, Baillat G, Devaux C, Loret EP. (2013) Identification of a highly conserved surface on Tat variants. ***J. Biol. Chem.*** 288(26):19072−80.

Moqrich A, Mattei MG, Bartoli M, Rakitina T, Baillat G, Monneron A, Castets F. (1998) Cloning of human striatin cDNA (STRN), gene mapping to 2p22-p21, and preferential expression in brain. ***Genomics*** 51(1):136−9.

Mourelatos Z, Adler H, Hirano A, Donnenfeld H, Gonatas JO, Gonatas NK.(1990) Fragmentation of the Golgi apparatus of motor neurons in amyotrophic lateral sclerosis revealed by organelle-specific antibodies. ***Proc. Natl. Acad. Sci.USA*** 87:4393-95.

Mourelatos Z, Gonatas NK, Stieber A, Gurney ME and Dal Canto MC. (1996) The Golgi apparatus of spinal cord motor neurons in transgenic mice expressing mutant Cu,Zn superoxide dismutase becomes fragmented in early, preclinical stages of the disease. **Proc. *Natl. Acad. Sci. USA*** 93: 5472-77.

Orlando C, d'Alayer J, Baillat G, Castets F, Jeannequin O, Mazié JC, Monneron A. (1992) A monoclonal antibody directed against the catalytic site of Bacillus anthracis adenylyl cyclase identifies a novel mammalian brain catalytic subunit. ***Biochemistry*** 31(12):3215−22.

Parsons JT. (2003) Focal adhesion kinase: the first ten years. ***J. Cell Sci.*** 116: 1409–16.

Perrin F E, Boisset G, Docquier M, Schaad O, Descombes P, Kato AC. (2005). No widespread induction of cell death genes occurs in pure motoneurons in an amyotrophic lateral sclerosis mouse model. ***Human molecular genetics*** 14(21): 3309-20.

Remacle−Bonnet M, Garrouste F, Baillat G, Andre F, Marvaldi J, Pommier G. (2005) Membrane rafts segregate pro- from anti-apoptotic insulin-like growth factor-I receptor signaling in colon carcinoma cells stimulated by members of the tumor necrosis factor superfamily. ***Am. J. Pathol.*** 167(3):761−73.

Renton AE and all. (2011) A hexanucleotide repeat expansion in C9ORF72 is the cause of chromosome 9p21-linked ALS-FTD. ***Neuron*** 72(2): 257-68.

Salcini AE, Chen H, Iannolo G, De Camilli P, Di Fiore PP. (1999) Epidermal growth factor pathway substrate 15, Eps15. ***Int. J. Biochem. Cell Biol.*** 31(8):805-9.

Schaefer MK, Schmalbruch H, Buhler E, Lopez C, Martin N, Guénet JL, Haase G. (2007) Progressive motor neuronopathy: a critical role of the tubulin chaperone TBCE in axonal tubulin routing from the Golgi apparatus. ***J. Neurosci.*** 27(33):8779-89.

Schmalbruch H, Jensen HJ, Bjaerg M, Kamieniecka Z, Kurland L. (1991) A new mouse mutant with progressive motor neuronopathy. ***J. Neuropathol. Exp. Neurol.*** 50(3):192-204.

Stein R, Mori N, Matthews K, Lo LC and Anderson DJ. (1988) The NGF-inducible SCG10 mRNA encodes a novel membrane-bound protein present in growth cones and abundant in developing neurons. ***Neuron*** 1: 463-76

Strey CW, Spellman D, Stieber A, Gonatas JO, Wang X, Lambris JD and Gonatas NK. (2004) Dysregulation of stathmin, a microtubule-destabilizing protein, and up-regulation of Hsp25, Hsp27, and the antioxidant peroxiredoxin 6 in a mouse model of familial amyotrophic lateral sclerosis. ***Am. J. Pathol.*** 165: 1701-18.

Takahashi K and Yamanaka S. (2006) Induction of pluripotent stem cells from mouse embryonic and adult fibroblast cultures by defined factors. ***Cell*** 126: 663-76.

Thaler J, Harrison K, Sharma K, Lettieri K, Kehrl J and Pfaff SL. (1999) Active suppression of interneuron programs within developing motor neurons revealed by analysis of homeodomain factor HB9. ***Neuron*** 23: 675-87.

Turner BJ and Talbot K. (2008) Transgenics, toxicity and therapeutics in rodent models of mutant SOD1-mediated familial ALS. ***Prog. Neurobiol.*** 85: 94-134.

Wang L, Deng HX, Grisotti G, Zhai H, Siddique T and Roos RP. (2009) Wild-type SOD1 overexpression accelerates disease onset of a G85R SOD1 mouse. ***Hum. Mol. Genet.*** 18: 1642-51.

Williamson TL and Cleveland DW. (1999) Slowing of axonal transport is a very early event in the toxicity of ALS-linked SOD1 mutants to motor neurons. ***Nat. Neurosci.*** 2: 50-6.

ANNEXES

Annexe 1

Molecular Biology of the Cell
Vol. 12, 663–673, March 2001

Molecular Cloning and Characterization of Phocein, a Protein Found from the Golgi Complex to Dendritic Spines

Gilbert Baillat,* Abdelaziz Moqrich,* Francis Castets,* Agnès Baude,† Yannick Bailly,‡ Alexandre Benmerah,§ and Ariane Monneron*‖

*FRE Centre National de la Recherche Scientifique 9041 and †FRE Centre National de la Recherche Scientifique 9024, Centre National de la Recherche Scientifique, 13009 Marseille, France; ‡FRE Centre National de la Recherche Scientifique 2180, 67084 Strasbourg, France; and §Institut National de la Santé et de la Recherche Médicale E9925, Faculté Necker-Enfants Malades, 75730 Paris, France

Submitted July 27, 2000; Revised December 7, 2000; Accepted January 9, 2001
Monitoring Editor: Monty Krieger

Phocein is a widely expressed, highly conserved intracellular protein of 225 amino acids, the sequence of which has limited homology to the σ subunits from clathrin adaptor complexes and contains an additional stretch bearing a putative SH3-binding domain. This sequence is evolutionarily very conserved (80% identity between *Drosophila melanogaster* and human). Phocein was discovered by a yeast two-hybrid screen using striatin as a bait. Striatin, SG2NA, and zinedin, the three mammalian members of the striatin family, are multimodular, WD-repeat, and calmodulin-binding proteins. The interaction of phocein with striatin, SG2NA, and zinedin was validated in vitro by coimmunoprecipitation and pull-down experiments. Fractionation of brain and HeLa cells showed that phocein is associated with membranes, as well as present in the cytosol where it behaves as a protein complex. The molecular interaction between SG2NA and phocein was confirmed by their in vivo colocalization, as observed in HeLa cells where antibodies directed against either phocein or SG2NA immunostained the Golgi complex. A 2-min brefeldin A treatment of HeLa cells induced the redistribution of both proteins. Immunocytochemical studies of adult rat brain sections showed that phocein reactivity, present in many types of neurons, is strictly somato-dendritic and extends down to spines, just as do striatin and SG2NA.

INTRODUCTION

Neurons have unique structural and functional polarity: they extend a single, usually long and thin axon and numerous shorter, thicker dendrites (Dotti *et al.*, 1988; Craig and Banker, 1994). Information gathered and processed by the dendrites flow through the axons to the synapses. The structure and composition of axons and dendrites are quite different, particularly concerning their respective plasma membranes, cytoskeleton (Gunning *et al.*, 1998; Baas, 1999), and proteins involved in vesicular traffic, such as motor proteins (Foletti *et al.*, 1999; Burack *et al.*, 2000). Striatin is a neuronal, intracellular protein strictly expressed in the somato-dendritic compartment, including spines, of subsets of neurons: thus, it can be considered as a marker of neuronal polarity (Castets *et al.*, 1996; Kachidian *et al.*, 1998; Salin *et al.*, 1998). Found in the cytosol as well as associated with membranes, striatin is endowed with protein-protein association modules as diverse as a caveolin-binding motif, a coiled-coil structure, a Ca^{2+}-calmodulin–binding amphiphilic helix, and a WD-repeat domain (Castets *et al.*, 1996; Bartoli *et al.*, 1998, 1999b; Moqrich *et al.*, 1998). Striatin down-regulation in embryonic motoneurons leads to the blockade of dendritic, but not axonal, growth, indicating that it may play a role in the establishment of polarity within developing neurons (Bartoli *et al.*, 1999a). The physiological effect elicited by down-regulating this quantitatively minor cellular component suggests that striatin lies at a signaling crossroad and cannot be bypassed. Owing to these multiple functional domains, we hypothesized that striatin might be a scaffold allowing establishment, in a Ca^{2+}-dependent manner, of multiprotein complexes specific to soma and dendrites.

‖ Corresponding author. E-mail address: monneron@lncf.cnrs-mrs.fr.

Abbreviations used: β-gal, β-galactosidase; aa, amino acid; ADH, alcohol dehydrogenase; AP, adaptor protein complexes; Arf, ADP-ribosylation factor; BFA, brefeldin A; BSA, bovine serum albumin; cat, catalase; DMEM, Eagle's medium modified by Dulbecco; ER, endoplasmic reticulum; GST, glutathione *S*-transferase; kb, kilobases; ORF, open reading frame; PBS, phosphate saline buffer; TBS, Tris saline buffer; TG, thyroglobulin; TSM, Tris saline-Mg^{2+} buffer.

To validate such a hypothesis, we searched for potential interactors of striatin, and by means of the two-hybrid strategy, we identified a novel, intracellular, 26-kDa protein, phocein (named after the Greek founders of the port of Marseille). Because we recently showed that two proteins, SG2NA and zinedin, share with striatin identical protein-protein association modules (Castets *et al.*, 2000), we looked for their possible interaction with phocein, which, indeed, was verified by in vitro experiments.

The sequence of phocein was found to contain stretches of homology with the σ subunits of clathrin adaptor complexes. Clathrin, a coat protein, is linked to different types of vesicles by various sets of adaptor protein complexes (AP), heterotetramers comprising two heavy chains or adaptins and two light chains, a μ and a σ chain (Schmid, 1997; Kirchhausen, 1999). AP-1 occurs on the Golgi complex, whereas AP-2 is found at the plasma membrane. Other clathrin adaptor complexes have been recently discovered, such as AP-3 (Dell'Angelica *et al.*, 1997; Simpson *et al.*, 1997) and AP-4 (Dell'Angelica *et al.*, 1999).

The data presented in this study show that phocein, although mostly present on the Golgi complex in unpolarized HeLa cells, is seen within adult rat brain neurons from the perinuclear area down to the smallest dendritic branches.

MATERIALS AND METHODS

Two-Hybrid Assay

A fusion protein comprising the LexA DNA-binding domain and striatin was used as a bait to search for fusion proteins expressed by a construct containing a rat brain cDNA library (Matchmaker; Clontech, Palo Alto, CA) and the activation domain of Gal4 (Dagher and Filhol-Cochet, 1997). A full-length striatin insert (Castets *et al.*, 1996) was ligated into the pLex 11 vector (a gift from M.C. Dagher, Commissariat à l'Energie Atomique, Grenoble, France) in-frame with the LexA DNA-binding domain, yielding plasmid pLex-stri. L40 yeast strain cells grown in minimal medium were transformed with pLex-stri, using the lithium acetate method (Gietz *et al.*, 1992). The Lex-stri fusion protein was stably expressed in L40 cells, as verified by immunoblotting using anti-striatin antibodies (Castets et al., 1996). L40 cells expressing Lex-stri were transformed with the plasmid library. From 5×10^6 colonies obtained 5 d after cotransfection, 63 colonies were His^+. They were tested for β-galactosidase (β-gal) activity by a color filter assay using the substrate 5-bromo-4-chloro-3-indolyl-D-galactoside. Plasmids from the 58 His^+ Lac Z^+ colonies were prepared according to the method of Kimmel and Berger (1987). After electroporation in *Escherichia coli* HB101 cells of Leu^- phenotype, the selected library plasmids were rescued by complementing the Leu^- phenotype on minimal medium. The 58 selected colonies were accounted for by only two plasmids, encoding inserts of 1.7 and 2.5 kilobases (kb), respectively, named pGAD 10-phocein-1.7 and pGAD 10-phocein-2.5. Inserts were sequenced using the specific primers of pGAD10 and primers designed by a "gene walking" strategy (ESGS, Evry, France). The 1.7-kb sequence was fully included in the 2.5-kb sequence, which contained an open reading frame (ORF) of 678 bp, encoding phocein, preceded by 7 bp and followed by a 3′-noncoding sequence ending by a poly-A stretch (phocein sequence, -7 to $+2506$).

Northern Blots

Total RNA from various rat tissues were purified using TRIZOL (Life Technologies, Grand Island, NY). Each RNA (10 μg) was electrophoresed on 1% agarose-6% formaldehyde gels and transferred on Nytran-plus membranes (Schleicher and Schuell, Keene, NH). A 659-bp phocein probe (nucleotides -7 to $+652$) was obtained by digesting pGAD10-phocein-2.5 with *Eco*RI. Phocein and actin probes were labeled by random priming with [α^{32}P]dCTP. The blots were hybridized overnight at 42°C in the presence of formamide. After hybridization, the membranes were washed several times at 50°C in 0.1× SSC and 0.1% SDS. Membranes were exposed at -70°C with amplifying screens, using Fuji (Tokyo, Japan) films.

Production of a GST-Phocein Fusion Protein and Obtaining Antibodies

A 2-kb *Bam*HI/*Bgl*II fragment of the selected library plasmid was subcloned in a pGEX4T-3 vector (Amersham Pharmacia Biotech, Arlington Heights, IL), yielding pGST-phocein encoding the full-length phocein sequence in-frame with that of glutathione *S*-transferase (GST). *E. coli* JM109 cells were transformed and, upon induction by 0.1 mM isopropyl β-D-thiogalactoside, expressed high levels of GST-phocein (52 kDa). The cells were lysed, and the fusion protein contained in the soluble fraction was purified on glutathione-Sepharose. Two rabbits were immunized with the purified fusion protein according to published procedures (60–120 μg per injection). Antisera were tested on Western blots of purified GST-phocein and rat brain subfractions. Anti-GST-phocein antibodies were affinity purified either on strips of blots of GST-phocein or on a GST-phocein affinity resin (obtained by coupling 3 mg of GST-phocein to 1 ml of CNBr-activated Sepharose 4B (Amersham Pharmacia Biotech). The blots or resin were incubated for a few hours with the anti-phocein serum and washed, and the antibodies were eluted with 0.1 M glycine-HCl buffer, pH 2.5. The antibody solution was adjusted to pH 7.5. It was mixed with 50% glycerol and 0.1% bovine serum albumin (BSA) and kept at -20°C.

Coimmunoprecipitation and Pull-Down Assays

Rat brain homogenates were fractionated, using buffers containing either 0.1 mM Ca^{2+} or 1 mM EDTA, into cytosol and a 100,000 × *g* pellet, containing membranes (the detergent-soluble fraction) and cytoskeleton (the detergent-insoluble fraction) (Bartoli *et al.*, 1998). Protein was determined by the microBCA method (Pierce, Rockford, IL). For immunoprecipitation assays, brain fractions were precleared by incubation at 4°C for at least 1 h with preimmune serum-coated Pansorbin cells (Calbiochem, San Diego, Ca; 1 ml of cell suspension for 10 mg of brain protein).

For coimmunoprecipitation assays, batches of 200 μl of a 10% suspension of washed Pansorbin cells preincubated in 1% BSA-containing Tris saline buffer (TBS buffer; 50 mM Tris-HCl, pH 7.4, and 150 mM NaCl) were incubated with 140 μg of rabbit preimmune immunoglobulins or affinity-purified anti-phocein, anti-striatin, anti-SG2NA, and anti-zinedin antibodies, in the presence of 0.1% BSA (Castets *et al.*, 2000) for at least 4 h at 4°C with gentle agitation. The Pansorbin cells were washed in TBS several times. Precleared brain cytosol (0.5 ml, ~1 mg) or the Lubrol-soluble brain fraction was added and incubated overnight at 4°C with gentle agitation. Pansorbin cells were washed four times (two first washes with 50 mM Tris-HCl, pH 7.4, 500 mM NaCl, 1 mM EDTA, and 0.5% Nonidet P-40; two last washes with 50 mM Tris-HCl, pH 7.4, 150 mM NaCl, 1 mM EDTA, and 0.05% deoxycholate) and boiled for 5 min in Laemmli sample buffer. The solubilized proteins were electrophoresed on 8, 10, or 15% polyacrylamide-SDS gels and transferred onto Protran membranes (Schleicher and Schuell). The antibodies used for revelation were the anti-striatin serum 75 (1:2000; Castets *et al.*, 1996) and affinity-purified anti-phocein, anti-SG2NA, and anti-zinedin antibodies (all at 0.2–0.3 μg/ml). The ECL procedure (Pierce) was used.

For pull-down assays, 2.5 μg GST or purified GST-phocein were incubated with 40 μl of 50% glutathione-sepharose for 2 h at 4° in TBs containing 0.1% BSA. After three washes in TBS, 200 μl (about 400 μg protein) of rat brain cytosol or lubrol-soluble fraction were added to the resin and incubated overnight at 4° with gentle agita-

tion. After extensive washes with TBS, the resin pellets were treated as above.

Immunofluorescence Studies and Fractionation of HeLa cells: Brefeldin A (BFA) Treatment

HeLa and Hep-2 cells (American Type Culture Collection, Manassas, VA) were grown in Eagle's medium modified by Dulbecco (DMEM), supplemented with 10% fetal calf serum, 2 mM L-glutamine, penicillin, and streptomycin (GIBCO-BRL, Grand Island, NY). For treatment with BFA (Sigma, St. Louis, MO), HeLa cells grown on coverslips were incubated for 1, 2, and 10 min at 37°C with 5 μg/ml BFA in DMEM or with a 1:2000 dilution of ethanol in DMEM as a control. Cells were then fixed and processed for immunofluorescence.

For immunofluorescence studies, cells grown on coverslips were washed in phosphate saline buffer (PBS), fixed in a solution containing 3.7% paraformaldehyde and 30 mM sucrose, for 30 min at 4°C. The cells were washed once in PBS and, after quenching for 10 min, were washed in PBS containing 50 mM NH_4Cl and washed again in PBS supplemented with 1 mg/ml BSA. The cells were incubated with primary antibodies in permeabilization buffer A (PBS containing 1 mg/ml BSA and 0.05% saponin or 0.1% Triton X-100) for 45 min at room temperature. After two washes in buffer A, the cells were incubated for 45 min at room temperature in buffer A containing the labeled secondary antibody. After two washes in buffer A and one in PBS, the cells were mounted on microscope slides in 100 mM Tris-HCl buffer, pH 8.5, containing 100 mg/ml Mowiol (Calbiochem) and 25% (vol/vol) glycerol. The antibodies used were a mouse monoclonal antibody CTR433 (a gift of M. Bornens, Institut Curie, Paris, France); a mouse monoclonal antibody raised against clathrin light chains (American Type Culture Collection, CON-1); a mouse monoclonal antibody raised against γ-adaptin (Sigma, A 4200); preimmune rabbit immunoglobulins (Sigma); Texas Red-conjugated goat anti-mouse immunoglobulins and Alexa 488-conjugated goat anti-rabbit immunoglobulins (Molecular Probes, Eugene, OR); Cy5-conjugated goat anti-mouse immunoglobulins (Amersham-Pharmacia-Biotech).

Subcellular fractionation was performed according to the method of Monneron and d'Alayer (1978) with modifications. Briefly, confluent cells from 10 dishes (10 cm in diameter) were washed in TSM (50 mM Tris-HCl, pH 7.4, buffer, containing 150 mM NaCl, 5 mM $MgCl_2$, and inhibitors of proteases), homogenized in 2.3 M sucrose at room temperature with a motor-driven glass-Teflon Potter homogenizer, and adjusted with cold TSM to 40% sucrose using a refractometer. The homogenate was layered above a 1.8-ml 50% sucrose-TSM cushion and overlayered with TSM buffer in 12-ml polyallomer tubes. The gradients were centrifuged at 120,000 $\times$ *g* for 2 h at 4°C. The white membrane fraction termed G obtained at the interface of 40% sucrose-TNM buffer and the yellow fraction termed M obtained at the interface of homogenate-50% sucrose were collected and washed. The nuclear pellet and the cytosol were saved. All fractions were normalized for protein and analyzed on 15 and 7% polyacrylamide-SDS gels, and the proteins were transferred to nitrocellulose.

Immunohistochemical Study of Rat Brain Sections

Adult Wistar rats were deeply anesthetized using a mixture of 0.5 ml of ketamine (50 mg/ml, Rhône-Mérieux, Lyon, France) and 0.37 ml of xylazine (2 mg/kg, Bayer, Elkhart, IN). They were transcardially perfused with 400 ml of 0.1 M phosphate buffer, pH 7.4, containing 4% paraformaldehyde. The brain and adrenal glands were removed and postfixed in the same solution. Vibratome sections, 30–40 μm, were cut and processed for immunocytochemistry at the optical level, using the immunoperoxidase method as described previously (Bernard *et al.*, 1997). Briefly, sections were preincubated in PBS containing 10% normal goat serum and incubated for 15 h at room temperature in a solution containing the primary antibodies. Primary antibodies were affinity-purified anti-phocein antibodies (0.1 to 0.5 μg/ml in PBS containing 1% normal goat serum). Control antibodies were unimmunized rabbit antibodies (Sigma), and solutions of affinity-purified anti-phocein antibodies preadsorbed on the blotted phocein fusion-protein. The sections were washed, incubated for 1.5 h in biotinylated goat anti-rabbit antibodies (1:200; Vector Laboratories, Burlingame, CA), washed, incubated for 1 h in an avidin-biotin-peroxidase solution, and washed. Peroxidase was revealed by using 3,3′-diaminobenzidine in the presence of 0.01% H_20_2, with nickel salt enhancement. Low-magnification light microscopy images were acquired with a light microscope (Nikon, France S.A., Champigny-Sur-Marne, France) coupled to a 3-chip charge-coupled device camera linked to a computer (Power Mac; Macintosh). The acquired image dimensions, 768 $\times$ 576 pixels, were reduced to obtain a final resolution of 300 dots per inch. High-magnification images were obtained from scanned photomicrographs (1200 $\times$ 1200 pixels). An image-editing software (Adobe Photoshop; Adobe Systems, Mountain View, CA) was used to create montages, which were printed on a dye sublimation printer. Only contrast and brightness of images were adjusted digitally.

Miscellaneous

In Vitro Transcription Translation Assay. A phocein-encoding plasmid pcDNA 3-phocein was obtained by inserting the phocein insert contained in pGAD 10-phocein-2.5 into the *Not*I site of plasmid pcDNA 3 (Invitrogen, San Diego, CA). Transcription-translation in vitro assays were performed using the TNT T7 system (Promega, Madison, WI) and pcDNA3-phocein, in the presence of [S^{35}]methionine (1000 Ci/mmol; ICN, Costa Mesa, CA).

Gel Filtration. Brain cytosol (3.7 mg of protein in 3 ml of TBS containing 1 mM EDTA) was performed on a Biogel A 5m column (1.9 $\times$ 85 cm; calibrated as indicated by d'Alayer *et al.*, 1983). Calibrating proteins were porcine thyroglobulin (TG; r = 9.8 nm), β-gal (r = 8.2 nm), catalase (cat; r = 5.2 nm), and alcohol dehydrogenase (ADH; r = 4.6 nm).

Sucrose Gradients. Brain cytosol (400 μl, 0.6 mg of protein) was layered on 11-ml sucrose gradients, 15–45%, and centrifuged for 16 h at 105.000 $\times$ *g* at 4°C. After centrifugation, 21 fractions (450 μl each) were collected, starting from the bottom of the gradient. Calibrating proteins were ADH (7.4 S), cat (11.3 S), apoferritin (17.2 S), and TG (19 S).

RESULTS

Identification of Phocein and Domain Prediction

A yeast two-hybrid screen of a rat brain library conducted with a LexA-striatin fusion protein yielded a clone containing an insert of 2.5 kb encoding a 225-amino acid (aa) ORF. The corresponding protein, of 26 kDa theoretical molecular weight, has been named phocein (Figure 1A). The ATG codon lies within a classical eukaryotic translation start sequence. An in vitro transcription-translation–coupled assay showed that the plasmid encoding phocein directs the synthesis of a protein of 26 kDa, the predicted molecular mass (Figure 2, lane A; in lane B, brain cytosol present on the same blot was revealed by anti-phocein affinity-purified antibodies). Two polyadenylation signals are present in the 3′-untranslated sequence at nucleotides 923 and 2456 (Baillat and Castets, unpublished results). A BLASTN 2 search resulted in several matches (Altschul *et al.*, 1997). One, a mouse cDNA named 2C4D (970 bp, accession number U01138) is 98% identical with phocein cDNA (Temeles *et al.*,

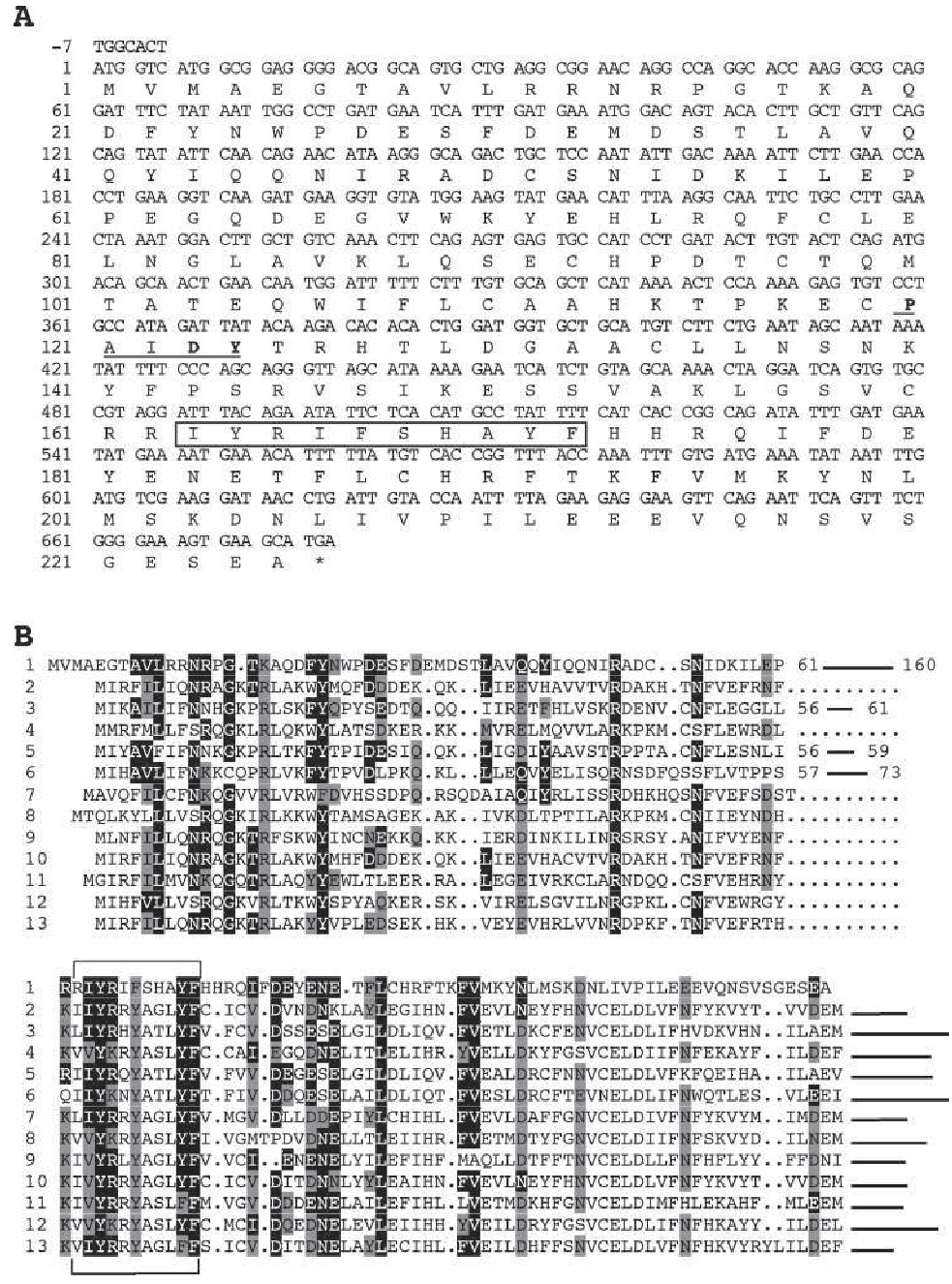

1994). However, a 1-bp frameshift with respect to the phocein sequence, due to a sequencing error, results in a shorter ORF with a different C-terminal deduced protein sequence. Several other matches occurred in human cDNAs and genomic sequences, some of which contain the entire phocein gene, encoding protein sequences 100% identical with the rat sequence. Some of these sequences localize to chromosome 11. Search in expressed sequence tag databases allowed us to predict the correct mouse cDNA sequence, encoding a putative protein of 26 kDa, 100% identical with the rat sequence, and we were able to establish that there are several stop codons upstream of the translation start ATG. The *Drosophila melanogaster* gene encoding phocein is now known (chromosome II; accession number AAF57380) and encodes a protein 223 aa long that is 80% identical to the human sequence. In the worm *Caenorhabditis elegans* chromosome III, a sequence (AAB59173) encodes a predicted protein sequence of 223 aa, which is 67% identical to the human sequence.

In addition to finding orthologues of phocein in different species by a Blast search, a Proscan search (Bairoch *et al.*, 1997) was conducted and revealed an interesting homology

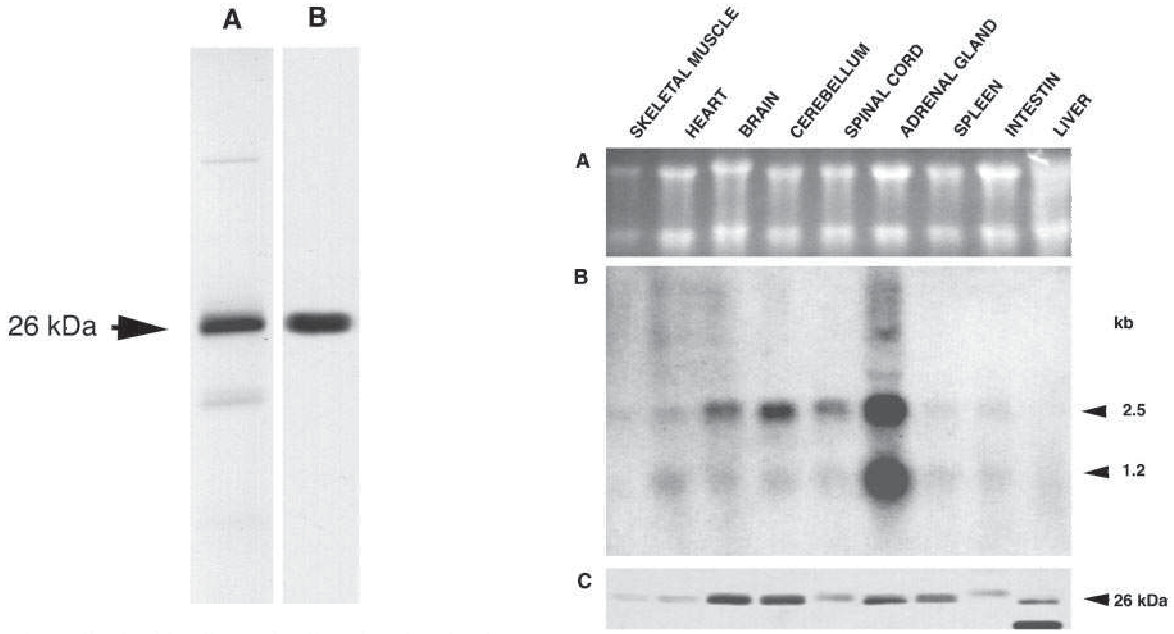

Figure 2. Phocein synthesized in vitro and native phocein migrate at the same apparent molecular mass in SDS-gels. (A) Phocein synthesized in vitro using pcDNA3-phocein and an in vitro transcription-translation assay. Autoradiogram. (B) Western blot of rat brain cytosol revealed by affinity-purified anti-phocein antibodies.

(78% identity) with the "clathrin adaptor complexes small chain signature" of the σ subunits (I, L, V, M) (I, L, V, M)YRxxxxLYF (Prosite PS00989) (Figure 1, boxed). We compared the phocein sequence with the ProDom multialignment of the adaptor complex σ subunits (12 known protein sequences, excluding orthologues) and found several stretches of conserved aa, identically spaced, in the amino- and carboxy-terminal regions of phocein (Figure 1B).

Between the two blocks containing homologous stretches, phocein displays a 100-aa–long stretch (aa 61–160) that has no counterpart in σ subunits and contains a putative SH3-binding domain (aa 120–124, underlined in Figure 1A) of the type PxxDY recently described by Mongiovi *et al.* (1999). Several putative phosphorylation sites exist (four for casein kinase II: aa 29–32, 52–55, 101–104, 115–118; three for protein kinase C: aa 115–117, 138–140, 147–149; one for protein kinase A: aa 149–152). Finally, it may be interesting to note that phocein and the yeast protein mob1 share 22% identity and 47% homology over a stretch of 185 aa (Luca and Winey, 1998). Mob1p is implicated in the onset of septum formation in *Schizosaccharomyces pombe* (Salimova *et al.*, 2000). The aa implied in the identities and homologies seen between phocein and, respectively, the yeast σ subunits and mob1 are not particularly overlapping.

Phocein Is Expressed in Many Tissues

Multitissue rat Northern blots (Figure 3 A) were analyzed with a phocein probe (Figure 3B). Phocein transcripts were prominent in cerebellum, brain, spinal cord, and especially the adrenal gland. Two transcripts of 2.5 and 1.2 kb were present, the 2.5-kb transcript being more abundant. The presence of two transcripts could be explained by the fact that in rat there are two polyadenylation sites. Blots exposed for a longer time also revealed phocein transcripts in muscle, heart, and several other tissues.

Rabbit antibodies were raised against a GST–whole-length phocein fusion protein. They were affinity purified and used to follow phocein expression at the protein level. As shown in Figure 3C, cytosolic phocein was abundant in brain and cerebellum, in agreement with the Northern blot data, and in the adrenal gland. However, the amount of cytosolic phocein in this gland was not as high as would be expected from the abundance of the transcripts; the adrenal gland also contained a sizable amount of particulate phocein, but other tissues did also. In spleen, on the contrary, the amount of protein was larger than expected from the Northern blots. Intestinal phocein migrated with a slightly different apparent molecular mass than in other tissues; furthermore, one additional abundant protein of slightly lower apparent molecular mass was immunolabeled in liver.

Brain Phocein Is Both Cytosolic and Associated with Membranes

Brain fractionation showed that phocein is distributed both in the cytosol (40%) and in the particulate, detergent-soluble fraction (60%). Phocein was wholly solubilized from a 100,000 $\times$ *g* pellet using nonionic detergents such as Lubrol-PX or zwitterionic detergents such as 3-([3-cholamidopropyl]dimethylammonio)-2-hydroxy-1-propanesulfonate. Striatin and the other proteins of its family, zinedin and

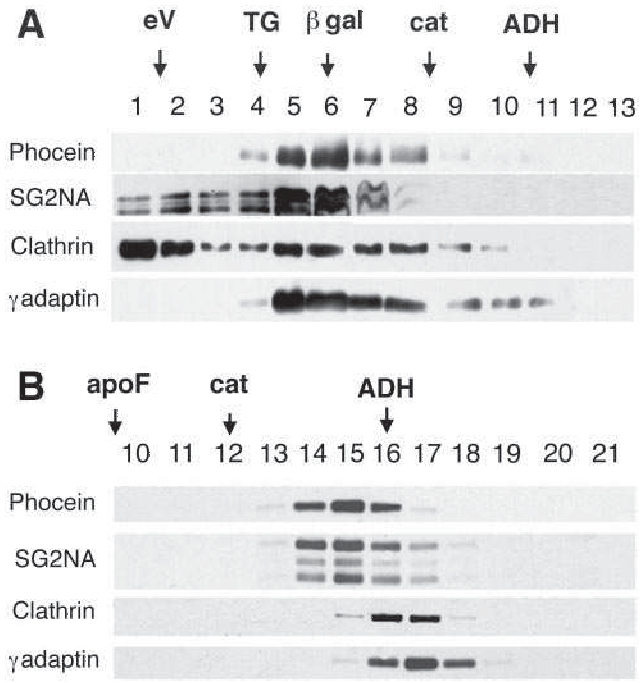

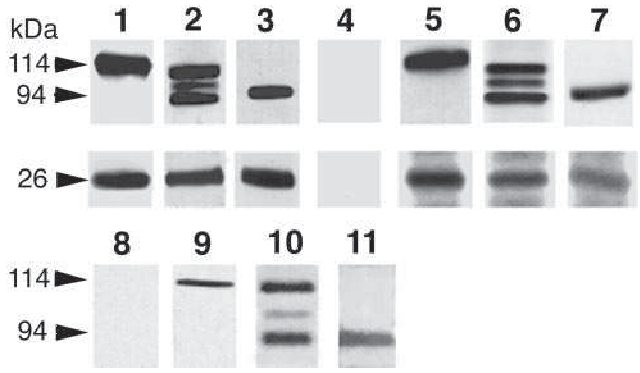

SG2NA, behave in the same way (Castets *et al.*, 1996, 2000; Bartoli *et al.*, 1998).

Data from gel filtration experiments and sucrose gradient centrifugations showed that brain cytosolic phocein was present in fractions corresponding to proteins or protein complexes of larger size than expected for each monomer. Gel filtration showed that, although some cytosolic phocein eluted in fractions compatible with the expected Stokes radius (~4 nm if globular), most of it eluted in fractions of much larger Stoke's radii, 7–10 nm (Figure 4 A), similar, for instance, to values obtained for clathrin adaptor complexes (7.0 for AP-1 and AP-2, 8.5 for AP-3, 6.5 nm for AP-4; Dell'Angelica *et al.*, 1999) (see the γ-adaptin lane in Figure 4A). SG2NA was found in the same fractions. In addition, small amounts of phocein and SG2NA were detected in the excluded volume (Figure 4A, excluded volume eV: fractions 1 and 2), indicating the presence of phocein within bulky complexes. Sucrose gradient experiments again indicated that both phocein and SG2NA were present in fractions containing proteins with an S value of 8.5 ± 0.5 (Figure 4B). Thus, both phocein and SG2NA behaved as protein complexes.

Phocein Interacts with All Members of the Striatin Family

The two-hybrid strategy in yeast demonstrated that phocein directly interacts with striatin. Coimmunoprecipitation and pull-down assays using brain fractions were performed to confirm this interaction in vitro and to see whether phocein also interacts with zinedin and SG2NA, which share the same protein-protein association modules. Striatin (Figure 5, lane 1, top), SG2NA (Figure 5, lane 2, top), and zinedin (Figure 5, lane 3, top) contained in rat brain cytosol were coimmunoprecipitated along with phocein by anti-phocein antibodies (Figure 5, lanes 1–3, bottom) but not by rabbit unimmunized antibodies (Figure 5, lane 4). Coimmunoprecipitation of these proteins also occurred when detergent-solubilized membranes were used (Baillat and Monneron, unpublished results). Conversely, phocein from rat brain cytosol (Figure 5, lanes 5–7, bottom) or from solubilized brain membranes (Baillat and Monneron, unpublished results) was coimmunoprecipitated along with striatin (Figure 5, lane 5, top), SG2NA (Figure 5, lane 6, top), and zinedin (Figure 5, lane 7 top), using the respective affinity-purified antibodies, whereas striatin, SG2NA, and zinedin were not detected when Pansorbin cells coated with control antibodies were used (as in Figure 5, lane 4).

In pull-down experiments, in which glutathione-Sepharose beads saturated with GST-phocein or with GST were

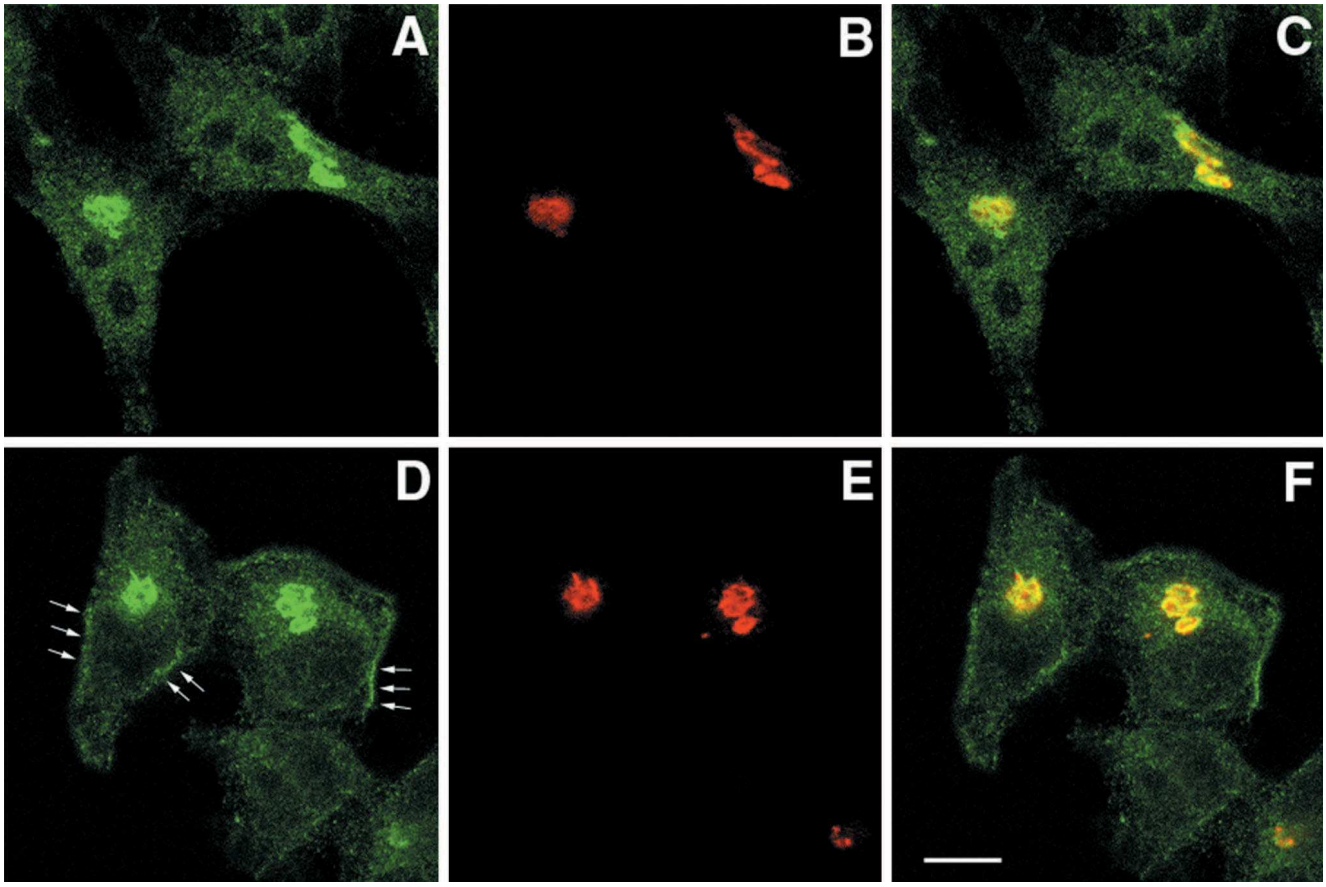

Figure 6. Phocein and SG2NA localize to the Golgi apparatus in HeLa cells. HeLa cells were fixed, permeabilized, and processed for immunofluorescence microscopy using rabbit, affinity-purified anti-phocein (A) and anti-SG2NA antibodies (D) and a mouse monoclonal antibody raised against CTR433 (B and E), revealed by an Alexa 488-labeled antibody raised against rabbit immunoglobulins and a Cy5-labeled antibody raised against mouse immunoglobulins. Cells were observed under a confocal microscope. Medial optical cuts of representative cells are shown (C and F). Areas of colocalization appear yellow in the computer-generated composite image. Bar, 10 μm.

incubated with rat brain cytosol or solubilized membranes, endogenous striatin was retained on GST-phocein–coated beads (Figure 5, lane 9), as well as SG2NA (Figure 5, lane 10) and zinedin (Figure 5, lane 11), but not on GST–coated beads (Figure 5, lane 8).

Phocein and SG2NA Colocalize over the Golgi Area of HeLa Cells

Because subcellular localization of proteins can be conveniently studied in HeLa and Hep-2 cells, which are amenable to treatment with various drugs, we studied the localization of phocein and SG2NA in the two cell lines. SG2NA was expressed in both, whereas striatin was not, a fact consistent with the restricted expression of the latter protein to a few species of neurons (Castets *et al.*, 1996). Because the results obtained with the two cell lines were very similar, only the results obtained with HeLa cells are shown. As shown in Figure 6, antibodies against phocein (A) and SG2NA (D) strongly revealed a seemingly tubular, reticulated, juxtanuclear network that appeared to be the Golgi apparatus. The staining observed with either antibody was considered to be specific because it was not observed with preimmune immunoglobulins or with antibodies raised against striatin or antibodies preincubated with the respective antigens (Baude and Monneron, unpublished results). The presumptive Golgi labeling was confirmed by the use of the CTR433 antibody, which recognizes a medial Golgi resident protein (Figure 6, B and E) (Jasmin *et al.*, 1989). The colocalization of phocein and SG2NA with the CTR433-immunolabeled protein was indicated by classical immunofluorescence (Benmerah, unpublished results) and confirmed by combined confocal images, showing yellow staining of the Golgi apparatus in the combined images (Figure 6, C and F). Phocein and SG2NA only partially colocalized with clathrin and AP-1 (γ-adaptin) at the level of the trans-Golgi network (Benmerah, unpublished results). The use of confocal microscopy showed that, close to some areas of the plasma membrane, bright signals from SG2NA were observed (Figure 6, D, arrows). Such labeling was not seen in the case of phocein.

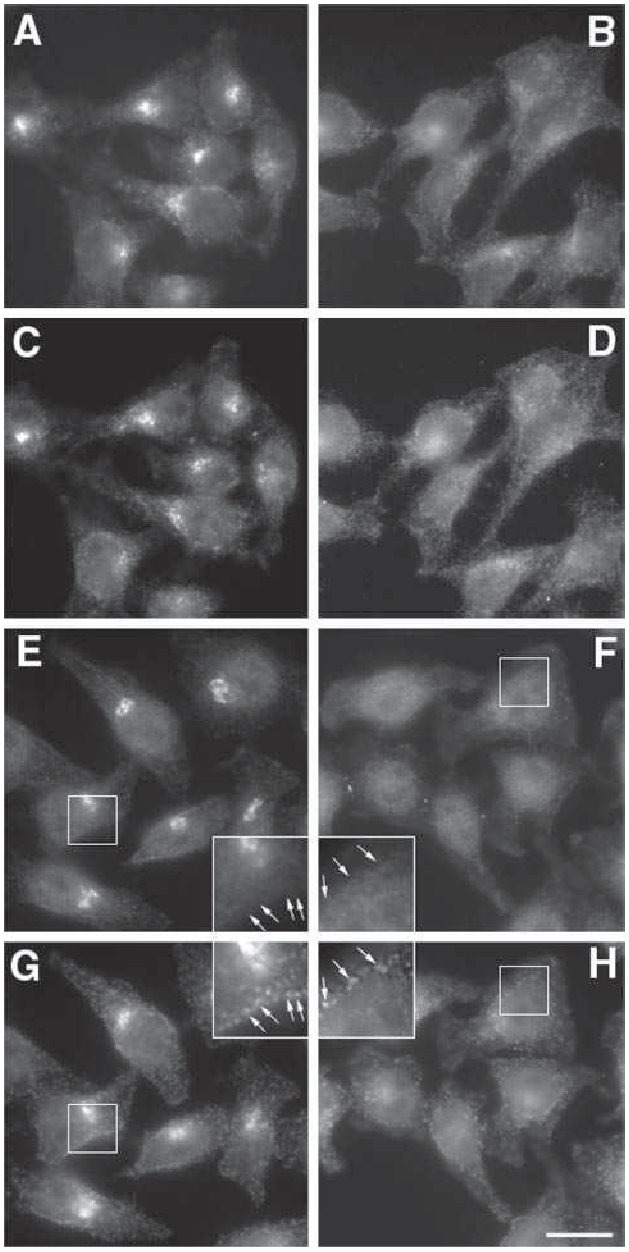

Figure 7. Phocein is mislocalized to cytosol in BFA-treated cells. Ethanol (A, C, E, and G)- and BFA (B, D, F, and H)-treated cells (A–D, 2-min treatment; E–H, 10-min treatment) were fixed and processed for immunofluorescence microscopy using an anti-γ-adaptin monoclonal antibody (100.3; A and B), the polyclonal, affinity-purified anti-phocein antibodies (C–F), and an anti-clathrin monoclonal antibody (CON-1; G and H), revealed by a Texas Red-labeled antibody raised against mouse immunoglobulins and an Alexa 488-labeled antibody raised against rabbit immunoglobulins. Cells were observed under an epifluorescence microscope attached to a cooled charge-coupled device camera. The same field is shown in A and C, in B and D, in E and G, and in F and H. Note that in G clathrin coats are seen over the Golgi area as well as at the plasma membrane, whereas in H, the only clathrin coats left are localized at the plasma membrane. From E to H, insets show a higher magnification (2×) of the portions of cells included in squares. Bar, 15 μm (30 μm in the insets).

Phocein Association with the Golgi Complex Is Sensitive to BFA

Golgi-associated clathrin coats containing the adaptor complex AP-1 are dispersed away from Golgi membranes by BFA, whereas plasma membrane-associated clathrin coats containing the adaptor complex AP-2 are not modified by BFA (Klausner *et al.*, 1992; Robinson and Kreis, 1992). When HeLa cells were treated for 2 min with BFA, AP-1 became dispersed throughout the cell (Figure 7, compare A and B). A shorter time (1 min) lead to little effect on AP-1 localization (Benmerah, unpublished results). Phocein was dispersed in exactly the same way as was AP-1 (Figure 7, 2-min treatment, compare C and D; Benmerah, unpublished results). With respect to the BFA treatment, SG2NA behaved just as did phocein and AP-1 (Benmerah, unpublished results). The effect of BFA was specific of Golgi-associated coats because a 10-min treatment had no effect on plasma membrane-associated clathrin coats, as shown by the fact that the peripheral punctate clathrin staining seen at the plasma membrane was not affected (Figure 7, compare insets in G and H). Phocein was not detected where coated pits were observed (Figure 7, compare insets in F and H).

Next, we investigated whether phocein actually binds membranes in HeLa cells. Subfractionation of lysed HeLa cells on sucrose gradients yielded, in addition to nuclei, three different fractions: 1) floated, light membranes, originating from plasma membrane, smooth endoplasmic reticulum (ER), and Golgi; 2) cytosol; and 3) heavy membranes (mitochondria, some nuclear membranes, lysosomes, and cytoskeleton) (% protein content of the fractions: 5, 30, 65) (Monneron and d'Alayer, 1978). Phocein, present only in the cytosol and the light membrane fraction, was threefold enriched in the latter, because the phocein ratio in the light membrane fraction versus cytosol was approximately 1:2 (Monneron, unpublished results). Because the light, floated membrane fraction had been thoroughly washed before analysis, the enrichment of phocein in this fraction indicated that phocein binds membranes. The light membrane fraction also contained a sizable amount of SG2NA and almost all the caveolin and most of the γ-adaptin (the heavy chain of AP-1) present in the cell lysate.

In the CNS, Phocein Immunoreactivity Occurs in Neurons and Is Somato-dendritic

Immunocytochemistry at the optical level was applied to rat brain, cerebellum, brain stem, and adrenal gland sections using affinity-purified antibodies. Immunoreactivity for phocein was present throughout the rat brain (all cortical layers, including both pyramidal cells, Figure 8A, and non-pyramidal cells; amygdaloid, septal, habenular, and thalamic complexes; hippocampus, all layers; caudate-putamen), cerebellum (essentially molecular layer and Purkinje cell bodies, glomeruli, and some Golgi cells, Figure 8 B; deep cerebellar nuclei), and brainstem. The strongest labeling occurred in the motor nuclei of cranial nerves in the pons and the bulb (Figure 8, C–F).

In all the examined brain structures, immunoreactivity for phocein was present only in neurons, not in glial cells. The labeling was intracytoplasmic, restricted to cell bodies and dendrites (Figure 8, A-F). Importantly, phocein was excluded from axons, just as were striatin and SG2NA. Nuclei

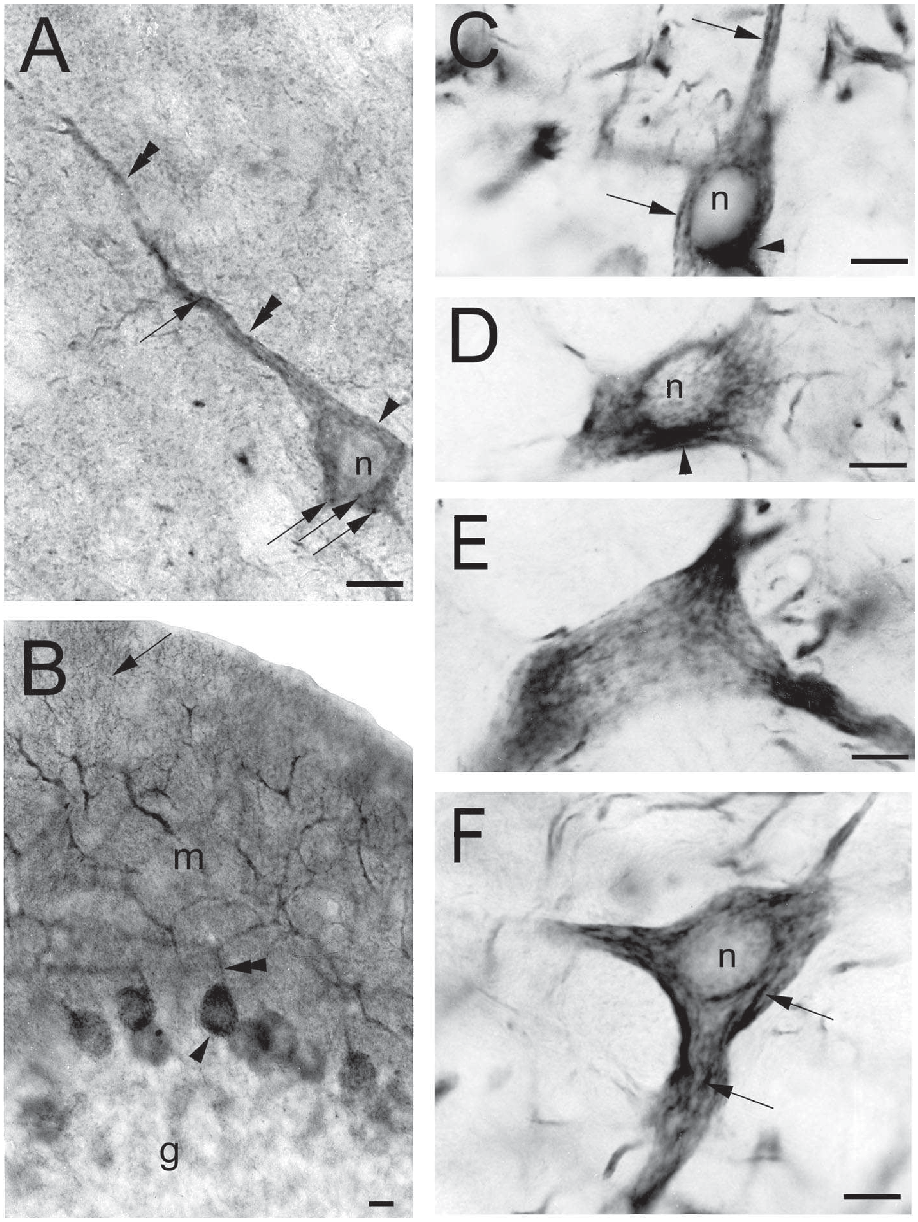

were unlabeled (Figure 8, A–F). In the soma (Figure 8, A–D and F), the labeling was particulate and often reticulated, suggesting staining of the ER. Perinuclear staining was usual, probably due to the staining of the Golgi apparatus (Figure 8, A, C, and D). Labeling was vermiculated all along the dendrites (Figure 9, A and E: proximal dendrites). Preliminary ultrastructural studies of the cerebellum molecular layer indicate that phocein is present within spines, associated with membrane profiles (Y. Bailly, unpublished data).

In addition to brain structures, the adrenal gland was studied. The medulla strongly reacted with anti-phocein antibodies, whereas the cortex was much less stained (Monneron, unpublished results). Phocein and SG2NA distributions in this gland are thus comparable.

Control experiments showed that 1) the omission of anti-phocein antibody resulted in the removal of all staining; 2) no staining was obtained when either preimmune sera or rabbit control immunoglobulins were used as primary antibodies; and 3) preabsorption of the anti-phocein antibodies with blotted GST-phocein resulted in the absence of staining.

DISCUSSION

The rationale to identify the partners of striatin was that major cellular and physiological effects had been observed following striatin down-regulation (Bartoli *et al.*, 1999a). Indeed, striatin, an intracellular, neuronal protein endowed

with multiple protein-protein interaction domains, has a very peculiar localization, being restricted to CNS structures primarily related to locomotor activity (Castets *et al.*, 1996; Bartoli *et al.* 1998, 1999a,b; Moqrich *et al.*, 1998). Furthermore, it displays a polar subcellular distribution, being strictly localized to the somato-dendritic compartment (Castets *et al.*, 1996; Kachidian *et al.*, 1998; Salin *et al.*, 1998;). On the one hand, the transient blockade of striatin synthesis in embryonic motoneurons resulted in the severe impairment of dendritic growth. On the other hand, striatin down-regulation in live rats led to a decrease in locomotor activity that paralleled the decrease of striatin in striata (Bartoli *et al.*, 1998). To define the molecular role of striatin, we used a yeast two-hybrid strategy to search for partners and identified phocein, a 225-aa intracellular protein. Validation of the interaction between phocein and striatin by in vitro experiments was straightforward. The respective interactions of phocein with SG2NA and zinedin, which belong to the striatin family (Castets *et al.*, 2000), were also demonstrated.

Fractionation of brain homogenate shows that phocein is distributed, in approximately equal amounts, in the cytosol, where it behaves as a protein complex, and in the membrane fraction. The proteins belonging to the striatin family are identically distributed (Castets *et al.*, 2000). Because the sequence of phocein lacks a region that could account for a transmembrane segment, as well as properly located motifs required for prenylation and myristoylation, phocein is likely to be associated with membranes through its interaction with striatin, zinedin, and SG2NA. The latter proteins are themselves not transmembrane proteins, but their association with membranes is robust, because it withstands high ionic strength and alkaline treatments (Monneron, unpublished results).

An interesting finding was the sequence homology between the N- and C-terminal domains of phocein and the σ subunits of adaptor proteins, the two homologous phocein domains being separated by an additional, intervening stretch containing a putative SH3-binding motif. The sequence homology between phocein and σ subunits led us to hypothesize that phocein might be a component of a novel coat, quite different from known adaptors. Immunolocalization studies of phocein in cultured cells (HeLa and Hep-2 cells) indeed showed that phocein is conspicuous over the Golgi area, where it colocalizes with SG2NA. To be recruited onto the Golgi complex, AP-1 and AP-3 need the intervention of ADP-ribosylation factors (Arfs), at variance with the AP-2 complex at the plasma membrane. Treatment of cells with BFA, which inhibits the activity of Arf exchange factors, results in the dispersion of Arf-dependent coats and, within minutes, in the fragmentation of the Golgi complex, which is cycled back to the ER (Donaldson *et al.*, 1992; Klausner *et al.*, 1992; Robinson and Kreis, 1992; Dell'Angelica *et al.*, 1997). Noticeably, the various classes of Arf exchange factors display variable sensitivities to BFA (Chardin and McCormick, 1999). We show here that, in HeLa cells, phocein and SG2NA follow the fate of AP-1 upon BFA treatment, an indication that their sensitivity to BFA is comparable to that of known Golgi-associated coat complexes. However, in addition to coats, Arf1 activation also results in the assembly onto Golgi membranes of several cytosolic proteins, such as actin, ankyrin, and the βIΣ* species of spectrin; the recruitement of these proteins is prevented by BFA (De Matteis and Morrow, 1998).

Although the localization of phocein to the Golgi complex in HeLa cells and its sensitivity to BFA are compatible with the hypothesis of a role for phocein in vesicular traffic, at the moment we are lacking functional data to support that idea. The distribution of phocein within polarized cells such as neurons neither confirms nor denies this hypothesis. Within adult brain neurons, phocein is not confined to the Golgi complex. As seen in rat brain sections, phocein immunolabeling, although it filling the soma, is found within dendrites down to the most distal and tenuous branches and spines. Noticeably, the axons are unstained. Striatin, SG2NA, and phocein thus share exactly the same subcellular distribution. Such polar distributions are quite important to stress, because, if the hypothesis of a relationship between phocein and vesicular traffic holds true, no neuronal coats or proteins involved in vesicular traffic have been, to our knowledge, demonstrated to be restricted to either axons or dendrites, with the exception of EEA1 (Wilson *et al.*, 2000).

It is noteworthy to recall that phocein is highly conserved throughout the animal kingdom: the phocein orthologues found in *D. melanogaster* and *C. elegans* are unusually conserved (80% identity between fly and human, 67% between worm and human). Studies of phocein in such species should therefore help determine its function, which appears to be a very conserved cellular process.

ACKNOWLEDGMENTS

The pertinent suggestions and comments from Pietro De Camilli have been very helpful. We also thank Domenica Borgese, Bruno Goud, André LeBivic, and John Bergeron for critical reading of the manuscript. We thank Michel Bornens for supplying the CTR433 antibody, Yann Goureau for expert assistance in confocal microscopy, and Yves Colette for supplying HeLa cells. This work was supported by Centre National de la Recherche Scientifique and by grants from the Association pour la Recherche sur le Cancer (ARC 9318 to A.M. and F.C. and ARC 9679 to A. Benmerah) and Association Française contre les Myopathies (AFM FRN 210/6481). Abdelaziz Moqrich was supported by the Association pour la Recherche sur le Cancer (1999) and by the Lilly Foundation (2000).

REFERENCES

Altschul, S.F., Madden, T.L., Schäffer, A.A., Zhang, J., Zhang, Z., Miller, W., and Lipman, D.J. (1997). Gapped BLAST, and PSI-BLAST. a new generation of protein database search programs. Nucleic Acids Res. *25*, 3389–3402.

Baas, P.W. (1999). Microtubules and neuronal polarity: lessons from mitosis. Neuron *22*, 23–31.

Bairoch, A., Bucher, P., and Hoffmann, K. (1997). The PROSITE database: its status in 1997. Nucleic Acids Res. *25*, 317–322.

Bartoli, M., Gaillard, S., and Monneron, A. (1999b). European Congress of Cell Biology Book of Abstracts, Bologna, Italy: T. Pozan, 136–137.

Bartoli, M., Monneron, A., and Ladant, D. (1998). Interaction of calmodulin with striatin, a WD-repeat protein present in neuronal dendritic spines. J. Biol. Chem. *273*, 22248–22253.

Bartoli, M., Ternaux, J.P., Forni, C., Portalier, P., Salin, P., Amalric, M., and Monneron, A. (1999a). Down-regulation of striatin, a neuronal calmodulin-binding protein, impairs rat locomotor activity. J. Neurobiol. *40*, 234–243.

Bernard, V., Somogyi, P., and Bolam, J.P. (1997). Cellular, subcellular, and subsynaptic distribution of AMPA-type glutamate receptor subunits in the neostriatum of the rat. J. Neurosci. *17*, 819–828.

Burack, M.A., Silverman, M.A., and Banker, G. (2000). The role of selective transport in neuronal protein sorting. Neuron *26*, 465–472.

Castets, F., Bartoli, M., Barnier, J.V., Baillat, G., Salin, P., Moqrich, A., Bourgeois, J.P., Denizot, F., Rougon, G., Calothy, G., and Monneron, A. (1996). A novel calmodulin-binding protein, belonging to the WD-repeat family, is localized in dendrites of a subset of CNS neurons. J. Cell Biol. *134*, 1051–1062.

Castets, F., Rakitina, T., Gaillard, S., Moqrich, A., Mattei, M-G., and Monneron, A. (2000). Zinedin, SG2NA and striatin are calmodulin-binding, WD-repeat proteins principally expressed in brain. J. Biol. Chem. *275*, 19970–19977.

Chardin, P., and McCormick, F. (1999). Brefeldin A: the advantage of being uncompetitive. Cell *97*, 153–155.

Craig, A.M., and Banker, G. (1994). Neuronal polarity. Annu. Rev. Neurosci. *17*, 267–310.

Dagher, M.C., and Filhol-Cochet, O. (1997). Making hybrids of two-hybrid systems. BioTechniques *22*, 916–922.

d'Alayer, J., Berthillier, G., and Monneron, A. (1983) Structure of brain adenylate cyclase: proteolysis-dependent modifications. Biochemistry *22*, 3948–3953.

Dell'Angelica, E.C., Mullins, C., and Bonifacino, J.S. (1999). AP-4, a novel protein complex related to clathrin adaptors. J. Biol. Chem. *274*, 7278–7285.

Dell'Angelica, E.C., Ohno, H., Ooi, C.E., Rabinovich, E., Roche, K.W., and Bonifacino, J.S. (1997). AP-3, an adaptor-like protein complex with ubiquitous expression. EMBO J. *16*, 917–928.

De Matteis, M.A., and Morrow, J.S. (1998). The role of ankyrin and spectrin in membrane transport and domain formation. Curr. Opin. Cell. Biol. *10*, 542–549.

Donaldson, J.G., Finazzi, D., and Klausner, R.D. (1992). Brefeldin A inhibits the Golgi membrane-catalyzed exchange of guanine nucleotide onto ARF protein. Nature *360*, 350–352.

Dotti, C.G., Sullivan, C.A., and Banker, G. (1988). The establishment of polarity by hippocampal neurons in culture. J. Neurosci. *8*, 1454–1468.

Foletti, D.L., Prekeris, R., and Scheller, R.H. (1999). Generation and maintenance of neuronal polarity: mechanisms of transport and targeting. Neuron *23*, 641–644.

Gietz, D., St. Jean, A., Woods, R.A., and Schiestl, R.H. (1992). Improved method for high efficiency transformation of intact yeast cells. Nucleic Acids Res. *20*, 1425.

Gunning, P., Hardeman, E., Jeffrey, P., and Weinberger, R. (1998). Creating intracellular structural domains: spatial segregation of actin and tropomyosin isoforms in neurons. BioEssays, *20*, 892–900.

Jasmin, B.J., Cartaud, J., Bornens, M., and Changeux, J.P. (1989). Golgi apparatus in chick skeletal muscle: changes in its distribution during end-plate development and after denervation. Proc. Natl. Acad. Sci. USA *86*, 7218–7222.

Kachidian, P., Vuillet, J., Bartoli, M., Castets, F., Nieoullon, A., and Kerkerian-Le Goff, L. (1998). Relationships between striatin-containing neurons and cortical or thalamic afferent fibers in the rat striatum: an ultrastructural study by dual labeling. Neuroscience *85*, 111–122.

Kimmel, A.R., and Berger, S.L. (1987). Preparation of cDNA and the generation of cDNA libraries: overview. Methods Enzymol. *152*, 307–316.

Kirchhausen, T. (1999). Adaptors for clathrin-mediated traffic. Annu. Rev. Cell Dev. Biol. *15*, 705–732.

Klausner, R.D., Donaldson, J.G., and Lippincott-Schwartz, J. (1992). Brefeldin A: insights into the control of membrane traffic and organelle structure. J. Cell Biol. *116*, 1071–1080.

Luca, F.C., and Winey, M. (1998). *MOB1*, an essential yeast gene required for completion of mitosis and maintenance of ploidy. Mol. Biol. Cell *9*, 29–46.

Mongiovi, A.M., Romano, P.R., Panni, S., Mendoza, M., Wong, W.T., Musacchio, A., Cesareni, G., and Di Fiore, P.P. (1999). A novel peptide-SH3 interaction. EMBO J. *18*, 5300–5309.

Monneron, A., and d'Alayer, J. (1978). Isolation of plasma and nuclear membranes of thymocytes. I. Enzymatic composition and ultrastructure. J. Cell Biol. *77*, 211–231.

Moqrich, A., Mattei, M.G., Bartoli, M., Rakitina, T., Baillat, G., Monneron, A., and Castets, F. (1998). Cloning of human striatin cDNA (STRN), gene mapping to 2p22–p21, and preferential expression in brain. Genomics *51*, 136–139.

Robinson, M.S., and Kreis, T.E. (1992). Recruitment of coat proteins onto Golgi membranes in intact and permeabilized cells: effects of brefeldin A and G protein activators. Cell *69*, 129–138.

Salimova, E., Sohrmann, M., Fournier, N., and Simanis, V. (2000). The *S. pombe* orthologue of the *S. cerevisiae mob1* gene is essential and functions in signaling the onset of septum formation. J. Cell Sci. *113*, 1695–1704.

Salin, P., Kachidian, P., Bartoli, M., and Castets, F. (1998). Distribution of striatin, a newly identified calmodulin-binding protein in the rat brain: an in situ hybridization and immunocytochemical study. J. Comp. Neurol. *397*, 41–59.

Schmid, S.L. (1997). Clathrin-coated vesicle formation and protein sorting: an integrated process. Annu. Rev. Biochem. *66*, 511–548.

Simpson, F., Peden, A.A., Christopoulou, L., and Robinson, M.S. (1997). Characterization of the adaptor-related protein complex, AP-3. J. Cell Biol. *137*, 835–845.

Temeles, G.L., Ram, P.T., Rothstein, J.L., and Schultz, R.M. (1994). Expression patterns of novel genes during mouse preimplantation embryogenesis. Mol. Reprod. Dev. *37*, 121–129.

Wilson, J.M., de Hoop, M., Zorzi, N., Toh, B., Dotti, C.G., and Parton, R.G. (2000). EEA1, a tethering protein of the early sorting endosome, shows a polarized distribution in hippocampal neurons, epithelial cells and fibroblasts. Mol. Biol. Cell *11*, 2657–2671.

Annexe 2

MEMBRANE TRANSPORT STRUCTURE FUNCTION AND BIOGENESIS:

Interactions of Phocein with Nucleoside-Diphosphate Kinase, Eps15, and Dynamin I

Gilbert Baillat, Stéphane Gaillard, Francis Castets and Ariane Monneron

J. Biol. Chem. 2002, 277:18961-18966.
doi: 10.1074/jbc.M108818200 originally published online February 28, 2002

THE JOURNAL OF BIOLOGICAL CHEMISTRY
Vol. 277, No. 2, Issue of May 24, pp. 18961–18966, 2002
Printed in U.S.A.

Interactions of Phocein with Nucleoside-Diphosphate Kinase, Eps15, and Dynamin I*

Received for publication, September 13, 2001, and in revised form, February 15, 2002
Published, JBC Papers in Press, February 28, 2002, DOI 10.1074/jbc.M108818200

Gilbert Baillat‡, Stéphane Gaillard§, Francis Castets¶, and Ariane Monneron‖

From the INSERM U464, Faculté de Médecine Nord, Bd. Pierre Dramard, 13916 Marseille Cedex 20, France

Phocein, an intracellular protein interacting with striatin, bears a few homologies with the σ-subunits of clathrin adaptor proteins (Baillat, G., Moqrich, A., Castets, F., Baude, A., Bailly, Y., Benmerah, A., and Monneron, A. (2001) *Mol. Biol. Cell* 12, 663–673). Using phocein as a bait in a yeast two-hybrid screen, we identified two novel interacting proteins, nucleoside-diphosphate kinase (NDPK) and Eps15. Immunoprecipitation and pull-down experiments involving native and/or recombinant phocein and, respectively, NDPK and Eps15, biochemically validated their interactions. NDPK and Eps15 were recently shown to be functional neighbors of dynamin. Dynamin I is shown here to directly interact with NDPK through its C-terminal proline-rich domain, whereas recombinant phocein associates with native dynamin I. Immunocytochemical studies of rat embryonic hippocampal neurons demonstrated partial co-localization of phocein and dynamin I. Phocein thus appears to be a component of the complexes involved in some steps of the vesicular traffic machinery.

Phocein, highly conserved throughout the animal kingdom, is a 26-kDa intracellular protein expressed in multiple tissues (1). The sequence of phocein contains within its N- and C-terminal regions several short stretches homologous to the σ-subunits of clathrin adaptor complexes, suggesting a role in vesicular traffic. Subcellular fractionation of HeLa cells and rat brain showed that phocein partitions between the cytosol and the detergent-soluble membrane fractions. In unpolarized cells, phocein is prominent in the Golgi area, whereas in mature neurons, it is found in the perikaryal-dendritic region (1).

Phocein is a direct partner of the members of the striatin family (1). This family includes striatin, SG2NA, and zinedin, which are multimodular, WD repeat, and calmodulin-binding proteins thought to act both as scaffolds and as signaling proteins (2–5). In the adult, such proteins are mostly expressed in neurons, where they localize to the somato-dendritic compartments. Phocein co-localizes with striatin and/or SG2NA (1, 6).

To further investigate the function of phocein, we searched for phocein partners using the two-hybrid screen in yeast. Several partners of phocein were found, including: the β-subunit of nucleoside-diphosphate kinase (NDPK,[1] EC 2.7.4.6) and Eps15. NDPKs are ubiquitous enzymes that exchange γ-phosphates between nucleoside tri- and diphosphates (7). Eps15 is a multidomain protein involved in clathrin-mediated endocytosis (8, 9). Recently, NDPK and Eps15 have been shown by genetic studies to be functional neighbors of dynamin, a GTPase that plays a critical role in endocytosis; NDPK mutations in *Drosophila*, as well as Eps15 mutations in *Caenorhabditis elegans*, enhance the phenotypes of dynamin mutations (10, 11). Altogether, these findings strengthen the hypothesis that phocein participates in membrane traffic and more specifically in membrane budding reactions.

EXPERIMENTAL PROCEDURES

Two-hybrid Assay—Phocein fused to the LexA DNA-binding domain was used as a bait to search for fusion proteins expressed by a rat brain cDNA library encoding the activation domain of Gal4 (plasmid pGAD10, Matchmaker, CLONTECH, Palo Alto, CA) (12). A full-length phocein insert (1) was ligated into the pLex-11 vector (a gift from M.C. Dagher, CEA Grenoble, France) in-frame with the LexA DNA-binding domain, yielding plasmid pLex-pho. L40 yeast strain cells grown in minimal medium were transformed with pLex-pho, using the lithium acetate method (13). The Lex-pho fusion protein was stably expressed in L40 cells, as verified by immunoblotting using anti-phocein antibodies. L40 cells expressing Lex-pho were transformed with the plasmid library. From 8×10^6 colonies obtained 5 days after cotransfection, 100 were His^+. They were tested for β-galactosidase activity by a color filter assay using the substrate 5-bromo-4-chloro-3-indolyl-D-galactoside (X-gal). Plasmids from the 68 $His^+/LacZ^+$ colonies were prepared according to Kimmel and Berger (14). After electroporation in *Escherichia coli* HB101 cells of Leu^- phenotype, the selected library plasmids were rescued by complementing the Leu^- phenotype on minimal medium and subjected to restriction analysis. Selected inserts were sequenced (ESGS, Paris, France).

Antibodies—Anti-phocein antibodies have been described (1). Anti-dynamin goat antibodies (sc-6402, Santa Cruz Biotechnology, Santa Cruz, CA) were directed against the proline-rich, C-terminal domain (PRD) of human dynamin I. A rabbit anti-NDPK A antibody (sc-343) was from Santa Cruz Biotechnology; it cross-reacts with the β-subunit of NDPK. A goat anti-Eps15 antibody (sc-11716) was from Santa Cruz Biotechnology, and a monoclonal anti-Eps15 antibody was a gift from P. Di Fiore. They recognize at least two proteins of 135 and 120 kDa, which are believed to be diversely phosphorylated species of Eps15. For immunocytochemistry, the monoclonal anti-dynamin Hudy-1 antibody was used (Upstate Biotechnology, Lake Placid, NY). Fluorescent secondary antibodies used for confocal microscopy were Alexa-conjugated antibodies from Molecular Probes (Eugene, Oregon).

Brain Fractionation—Adult Wistar rats were deeply anesthetized using a mixture of 0.5 ml of ketamine (50 mg/ml, Rhône-Mérieux) and 0.37 ml of xylazine (2 mg/kg, Bayer). Brain homogenates were prepared

* This work was supported by Center National de la Recherche Scientifique and by Grant ARC 9318 from the Association pour la Recherche sur le Cancer (to F. C. and A. M.) and Grant AFM FRN 210/7961 from the Association Française contre les Myopathies. The costs of publication of this article were defrayed in part by the payment of page charges. This article must therefore be hereby marked "*advertisement*" in accordance with 18 U.S.C. Section 1734 solely to indicate this fact.

‡ Present address: CNRS UMR 6032, Faculté de Pharmacie, 27 Bd. Jean Moulin, 13385 Marseille Cedex 5, France.

§ Supported by a fellowship from Ministere de l'education National, de la Recherche et de la technologie.

¶ To whom correspondence may be addressed. Tel.: 33-491-69-88-58; Fax: 33-491-09-05-06; E-mail: castets.f@jean-roche.univ-urs.fr.

‖ To whom correspondence may be addressed. Tel.: 33-491-59-42-99 and 33-491-69-88-58; Fax: 33-491-09-05-06; E-mail: a.founette@wanadoo.fr and monneron@lncf.cnrs-mrs.fr.

[1] The abbreviations used are: NDPK, nucleoside-diphosphate kinase; GST, glutathione *S*-transferase; PRD, proline-rich domain; PBS, phosphate-buffered saline; NGS, normal goat serum; CHAPS, 3-[(3-cholamidopropyl)-dimethylammonio]-1-propanesulfonate.

in TBS buffer (Tris-HCl 50 mM, pH 7.4, NaCl 150 mM containing inhibitors of proteases, 10-ml final volume for one brain). Cytosol was obtained by centrifuging the homogenate for 1 h at 100,000 × *g*, 4 °C. The pellet was homogenized in TBS-CHAPS buffer (TBS buffer containing 7.5 mM CHAPS and 0.5 M NaCl) and centrifuged for 1 h at 100,000 × *g*. The supernatant was referred to as the CHAPS fraction. Protein was determined using the Schaffner and Weissmann assay (15).

Coimmunoprecipitation Assays—There was no need to overexpress the interacting proteins since they were represented in sufficient amounts in brain extracts. For coimmunoprecipitation assays, 300–600 μl of freshly obtained brain cytosol or CHAPS fraction (250 mM NaCl final concentration) were incubated with 40 μg of affinity-purified rabbit anti-phocein antibodies or 40 μg of affinity-purified rabbit anti-NDPK antibodies or 40 μg of rabbit preimmune immunoglobulins (Sigma) overnight at either 4 or 30 °C with gentle agitation. Batches of 40 μl of Dynabeads (Dynal, Oslo, Norway) washed in TBS containing 0.1% bovine serum albumin were added to the samples and further incubated at the appropriate temperature for 4 h. Dynabeads were washed several times in the appropriate TBS or TBS-CHAPS buffers and boiled for 5 min in Laemmli sample buffer. The solubilized proteins were analyzed on 8 and 15% SDS-polyacrylamide gels and transferred onto Protran membranes (Schleicher and Schuell, Dassel, Germany).

The antibodies used to reveal Western blots were described above and diluted to 0.2–1 μg/ml. Bound antibodies were detected using the ECL procedure (Pierce) or the phosphatase-alkaline procedure (Promega, Madison, WI).

In some cases, the amount of the relevant protein (phocein and Eps15) in the immunoprecipitates (respectively obtained with anti-NDPK and anti-phocein antibodies) was quantified and expressed as the percent of the protein present in the samples of cytosol prior to incubation with the antibody (three separate experiments). Precise quantification was achieved by densitometric analyses of the immunoreactive bands using the NIH Image 1.59 software.

Pull-down Assays—Recombinant rat NDPK was obtained as follows. A 786-bp *Nco*I-*Eco*RI fragment of a plasmid selected from the yeast library, pGAD-NDPK (see below), was subcloned in a modified pGEX-KT vector (Amersham Biosciences) carrying the PreScission Protease site and yielded plasmid pGEX-P-NDPK. This plasmid encodes the full-length NDPK sequence in-frame with glutathione *S*-transferase (GST). *E. coli* DH5 α cells were transformed and, upon induction by 0.1 mM isopropyl-β-D-thiogalactoside, expressed high levels of GST-P-NDPK (43 kDa). The cells were lysed, and the fusion protein contained in the soluble fraction was bound to glutathione-Sepharose 4B (Amersham Biosciences). Recombinant phocein was obtained by subcloning the phocein cDNA in the modified pGEX-KT vector, as described above. pGEX-6P-PRD was obtained by inserting the PRD fragment of dynamin I into pGEX-6P (16). GST-P-NDPK, GST-P-phocein, and GST-P-PRD were eluted from the glutathione-Sepharose resin using reduced glutathione and used as such. Alternatively, NDPK, phocein, and PRD were cleaved from GST using PreScission protease (Amersham Biosciences), as indicated by the supplier. The polyhistidine human dynamin I deletion construct missing the PRD domain (His-dynamin Δ PRD), as well as GST-amphiphysin construct (amino acids 545–695), were described (16). PGEX-5.1 vectors encoding domains I, II, and III of Eps15 were kindly provided by A. Benmerah (8).

From 4 to 6 μg of GST-phocein (1), GST-P-NDPK, GST-P-PRD, or GST were incubated with 40 μl of 80% glutathione-Sepharose for 2 h at 4 °C in phosphate-saline buffer (PBS). After three washes in PBS containing 0.1% bovine serum albumin, beads were incubated with gentle agitation overnight at either 4 or 30 °C with 300 μl of rat brain cytosol or 300 μl of CHAPS fraction or with 150–300 μl of 5 μM solutions of recombinant NDPK or dynamin I PRD fragment or phocein. After extensive washes with PBS containing 7.5 mM CHAPS and 0.1% bovine serum albumin, the beads were boiled in Laemmli sample buffer and treated as above.

Cell Culture, Immunofluorescence, and Confocal Microscopy—Cultures of primary E18 hippocampal neurons were prepared as described (17). Neurons at stages 3 and 5 were fixed for 20 min in 4% paraformaldehyde at room temperature, washed in PBS, and incubated in PBS containing 0.1% Triton X-100 and 10% normal goat serum (NGS) for 15 min at room temperature. After several washes, cells were blocked with PBS containing 10% NGS (PBS/NGS) for 2 h at room temperature and then incubated in PBS/NGS containing 10 μg/ml of either the monoclonal anti-dynamin Hudy-1 or mouse preimmune immunoglobulins (Sigma) and 5 μg/ml of either rabbit anti-phocein antibodies or rabbit preimmune antibodies (Sigma) for 1 h at room temperature. After several washes in PBS, hippocampal neurons were incubated in PBS/NGS containing Alexa 546-conjugated goat anti-mouse (1:800) and Alexa 488-conjugated goat anti-rabbit antibodies (1:400) for 1 h at room temperature followed by several washes in PBS. Coverslips were mounted in Mowiol.

Labeling was viewed with a confocal laser scanning microscope (Leica TCS) equipped with an argon-krypton laser (488-, 568-, and 657-nm excitation lines). For double staining, light emitted from the two fluorophores was detected sequentially. Band-pass filters were chosen to select each emission. Images were reconstructed from a series of optical sections taken in the *x-y* plane from consecutive *z* positions (0.45–0.5 μm apart) using the standard microscope software (Leica Scanware). Original fields were made up of 512 × 512 pixels. Images were processed with Adobe Photoshop.

RESULTS

Isolation of NDPK and Eps15 as Phocein Interactors in a Yeast Two-hybrid Screen—To identify interacting proteins, phocein was used as a bait in a yeast two-hybrid screen of a rat brain cDNA library. Among the 68 positive clones obtained, 5 encoded NDPK, 2 encoded a fragment of Eps15, 26 encoded the ferritin H chain, and 35 contained plasmids of different insert sizes, not further studied. Four positive identical clones encoded an insert of 0.9 kb containing the 456-bp entire sequence of the β-subunit of NDPK (18); a fifth positive clone encoded a 1.3-kb insert encompassing the latter sequence and extending further into the 3′ non-coding sequence. Rat NDPKs consist of homo-hexamers of α or β isoforms, which are 89% identical (18). Both isoforms are found in brain. Two identical positive clones contained a 1.7-kb insert encoding the last 317 C-terminal amino acids of Eps15 and part of the 3′ non-coding sequence. The C-terminal domain of Eps15 contains several Asp-Pro-Phe (DPF) motifs and binds the ear domain of α-adaptin (8).

Biochemical Validation of the Interactions of Phocein with NDPK and Eps15—In vitro biochemical confirmation of the interactions revealed by the yeast two-hybrid screen was achieved by reciprocal coimmunoprecipitation of rat brain proteins and by pull-down experiments. Phocein and NDPK were found in brain cytosol (Fig. 1, *A* and *B*, *lane 1*) as well as in CHAPS-solubilized membrane fractions, abbreviated as CHAPS fractions (Fig. 1, *A* and *B*, *lane 4*). Anti-NDPK antibodies immunoprecipitated NDPK from cytosol (Fig. 1*B*, *lane 2*) or from CHAPS fractions (Fig. 1*B*, *lane 5*). Phocein endogenous to each fraction coimmunoprecipitated with NDPK (Fig. 1*A*, *lanes 2* and *5*). From 5 to 10% of the phocein contained in the cytosol sample was immunoprecipitated by the anti-NDPK antibodies (mean of three experiments). Control immunoprecipitates obtained with preimmune immunoglobulins contained neither phocein nor NDPK (Fig. 1, *A* and *B*, *lanes 3* and *6*). Reciprocally, anti-phocein antibodies incubated with rat brain cytosol fractions coimmunoprecipitated small amounts of NDPK together with phocein (Fig. 1*C*, *lane 2*), whereas control immunoprecipitates contained neither protein (Fig. 1*C*, *lane 3*). Performing the incubations at 30 *versus* 4 °C resulted in slightly enhanced amounts of coimmunoprecipitated protein. Varying the Ca^{2+} concentration of the incubated samples did not affect the latter parameter. We further demonstrated that the interaction between phocein and NDPK is direct using GST pull-down experiments with recombinant proteins. GST-phocein (Fig. 2*A*, *lane 1*) pulled down recombinant NDPK (Fig. 2*B*, *lane 1*), whereas GST did not (Fig. 2*A*, *lane 2*). Reciprocally, GST-P-NDPK (Fig. 2*A*, *lane 3*) pulled down recombinant phocein (Fig. 2*B*, *lane 3*), whereas GST did not (Fig. 2*A*, *lane 4*).

Similarly, *in vitro* biochemical confirmation of the interaction between phocein and Eps15 was obtained. Eps15 contained in endogenous rat brain cytosol (Fig. 3, *lane 1*) was detected in small amounts in immunoprecipitates obtained with antibodies directed against phocein (Fig. 3, *lane 2*), whereas it was absent from immunoprecipitates obtained with preimmune immunoglobulins (Fig. 3, *lane 3*). From 1 to 6% of the Eps15 contained in the cytosol sample was immunoprecipi-

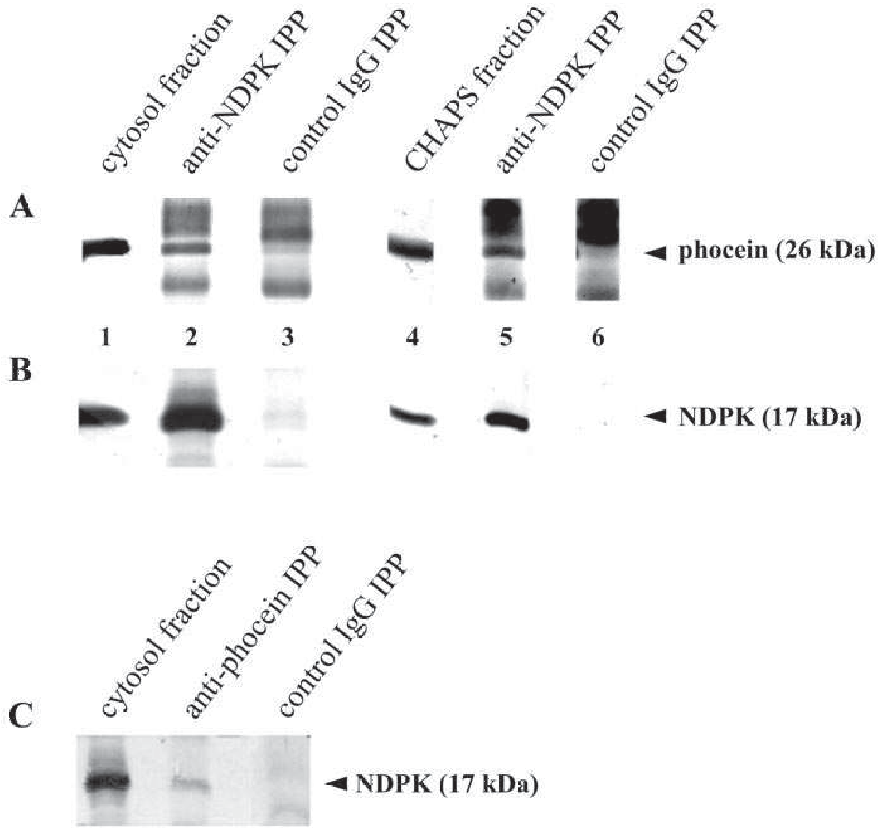

FIG. 1. **Phocein and NDPK coimmunoprecipitate.** Western blots revealed with anti-phocein antibodies (*A*) and anti-NDPK antibodies (*B* and *C*). *A* and *B*, *lane 1*, brain cytosol; *lane 2*, immunoprecipitate (*IPP*) obtained by incubating anti-NDPK antibodies with cytosol; *lane 3*, immunoprecipitate obtained by incubating control antibodies with cytosol; *lane 4*, CHAPS fraction; *lane 5*, immunoprecipitate obtained by incubating a CHAPS fraction with anti-NDPK antibodies; *lane 6*, immunoprecipitate obtained by incubating a CHAPS fraction with control antibodies. *C*, *lane 1*, brain cytosol; *lane 2*, immunoprecipitate obtained by incubating anti-phocein antibodies with cytosol (although the signal obtained is weak, it is present in all experiments); *lane 3*, immunoprecipitate obtained by incubating control antibodies with cytosol.

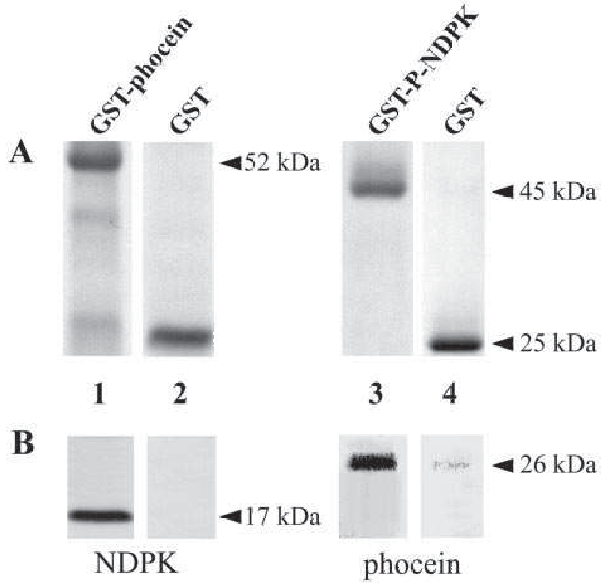

FIG. 2. **GST-phocein and recombinant NDPK physically interact.** *A*, Ponceau red staining of a blot containing GST-phocein (*lane 1*), GST-P-NDPK (*lane 3*), and GST (*lanes 2* and *4*) incubated with recombinant rat NDPK (*lanes 1* and *2*) or recombinant rat phocein (*lanes 3* and *4*). *B*, Western blot, revealed with anti-NDPK antibodies (*lanes 1* and *2*) and anti-phocein antibodies (*lanes 3* and *4*).

tated by anti-phocein antibodies. Pull-down experiments showed that Eps15 contained in rat brain cytosol fractions was pulled down by GST-phocein (Fig. 3, *lane 4*) but not by GST (Fig. 3, *lane 5*). Attempts to express the correctly folded protein GST fused to the C-terminal fragment of Eps is in sufficient amount to study its putative interaction with recombinant phocein were unsuccessful.

Phocein Interacts with Dynamin I—Dynamin has been shown to be a direct partner of Eps15 (11) and a potential partner of NDPK (10). Since phocein was proposed to have a role in vesicular traffic, we investigated whether phocein interacts with dynamin I. As shown in Fig. 4, immunoprecipitates obtained by incubating anti-phocein antibodies with rat brain cytosol (*lane 3*) contained dynamin I. Likewise, pull-down experiments conducted with GST-phocein (Fig. 5*A*, *lanes 1* and *2*) incubated with rat brain cytosol (Fig. 5*A*, *lane 1*) or a CHAPS fraction (Fig. 5*A*, *lane 2*) showed that dynamin was pulled down by GST-phocein (Fig. 5*B*, *lanes 1* and *2*), whereas it was not pulled down by GST (Fig. 5, *A* and *B*, *lane 3*). However, attempts to demonstrate a direct interaction between dynamin and phocein using recombinant proteins (GST-P-PRD, His-dynamin Δ PRD, and phocein) yielded only negative results, although GST-P-PRD was able to pull down recombinant amphiphysin (not shown) (16).

NDPK and Dynamin I Directly Interact in Vitro—Although Eps15 was shown to interact not only genetically but also biochemically with dynamin (11), no physical association of NDPK with dynamin could be demonstrated despite a strong genetic interaction between the two proteins in *Drosophila* (10). We further investigated the interaction between NDPK and dynamin. Dynamin I was present in immunoprecipitates obtained by incubating anti-NDPK antibodies with rat brain cytosol (Fig. 4, *lane 2*) or a CHAPS fraction (Fig. 4, *lane 5*), whereas immunoprecipitates obtained with control antibodies were devoid of dynamin I (Fig. 4, *lanes 4* and *6*). We next incubated the fusion protein GST-P-NDPK with rat brain cytosol (Fig. 6*A*, *lane 1*) or a CHAPS fraction (Fig. 6*A*, *lane 2*); in both cases, GST-P-NDPK pulled down endogenous dynamin I (Fig. 6*B*, *lanes 1* and *2*), whereas GST did not (Fig. 6, *A* and *B*, *lane 3*).

To determine whether the interaction between recombinant dynamin and NDPK is direct, we performed pull-down experiments involving GST-P-NDPK (Fig. 6*A*, *lane 4*) and the recom-

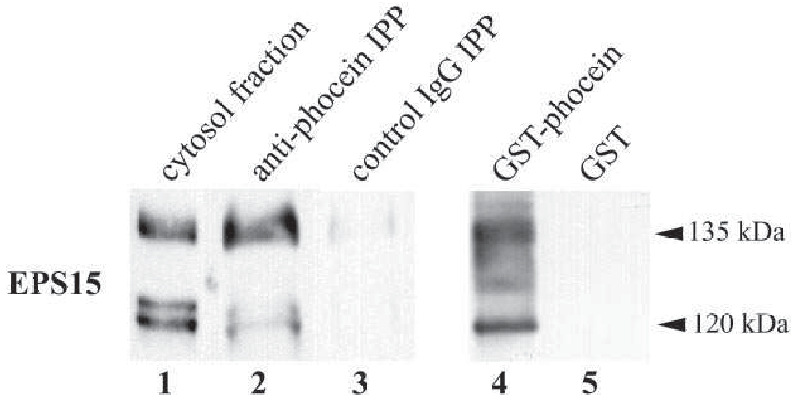

FIG. 3. **Brain Eps15 coimmunoprecipitates along with phocein and is pulled down by GST-phocein.** Western blots revealed with anti-Eps15 antibodies correspond to: *lane 1*, rat brain cytosol; *lanes 2* and *3*, immunoprecipitates obtained by incubating anti-phocein antibodies (*lane 2*) and control antibodies (*lane 3*) with cytosol; *lanes 4* and *5*, GST-phocein (*lanes 4*) and GST (*lane 5*) incubated with cytosol.

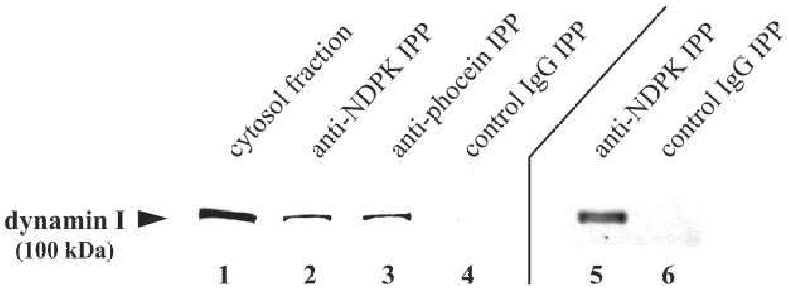

FIG. 4. **NDPK and dynamin coimmunoprecipitate.** Western blot revealed with anti-dynamin I antibodies. *Lane 1*, rat brain cytosol; *lanes 2* and *5*, immunoprecipitates obtained with anti-NDPK antibodies incubated with cytosol (*lane 2*) and CHAPS fractions (*lane 5*); *lane 3*, immunoprecipitate obtained with anti-phocein antibodies incubated with cytosol; *lanes 4* and *6*, immunoprecipitates obtained with control antibodies incubated with cytosol (*lane 4*) and a CHAPS fraction (*lane 6*).

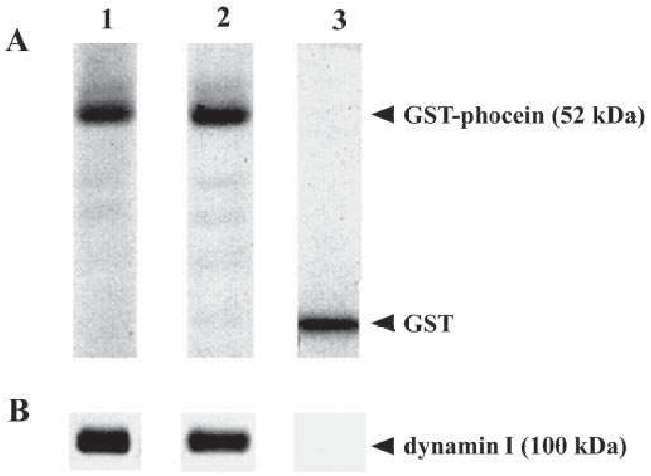

FIG. 5. **Brain dynamin I is pulled down by GST-phocein.** GST-phocein (*lanes 1* and *2*) and GST (*lane 3*) were incubated with rat brain cytosol (*lane 1*) or a CHAPS fraction (*lanes 2* and *3*). *A*, Ponceau red staining of the blotted fusion proteins. *B*, blots revealed with anti-dynamin I antibodies.

binant PRD fragment. GST-P-NDPK pulled down this PRD fragment (Fig. 6*B*, *lane 4*), whereas GST did not (Fig. 6*B*, *lane 5*). GST-P-NDPK did not pull down the fusion protein containing dynamin deleted from the PRD (not shown). Reciprocally, GST-P-PRD (Fig. 6*A*, *lane 6*) pulled down recombinant NDPK (Fig. 6*B*, *lane 6*), whereas GST (Fig. 6*A*, *lane 7*) did not (Fig. 6*B*, *lane 7*).

Compared Localizations of Phocein and Dynamin I—Hippocampal cells from rat E18 embryos, cultured for 3 and 10 days (Banker's stages 3 and 5), extended several branched neurites (Fig. 7, *A* and *B*). Phocein immunoreactivity (green fluorescence) was conspicuous all over the soma, except for nuclei, and involved all neurites. It appeared as small spots in neurites and perikarya; however, the staining was more diffuse in the perinuclear region. Dynamin I immunoreactivity (red fluorescence) also had a spotty appearance and involved all neurites and perikarya. Confocal microscopy showed that the distribution of the two proteins overlapped within several regions: in the Golgi area (Fig. 7*A*) at the emergence of neurites from the cell body, where the dynamin labeling however spread closer to the cell surface than the phocein labeling (Fig. 7, *A1* and *B2*) and within neurites (Fig. 7, *A1*, *B1*, and *B2*). Colocalization was observed at Banker's stage 3 in growth cones (Fig. 7, *A2*). Immunolabeling of NDPK in these neurons revealed the presence of the protein in all subcellular compartments, nucleus, soma and neurites, down to the smallest branches (not shown).

DISCUSSION

Phocein was isolated previously as a partner of the members of the striatin family. Based on its homology to the σ-subunit of adaptor proteins, its subcellular localization, and its sensitivity to brefeldin A, phocein was proposed to be involved in vesicular traffic (1). Here, we have identified two novel binding partners for phocein, NDPK and Eps15. Both proteins have been implicated in membrane traffic, further strengthening a potential role of phocein in membrane dynamics. More specifically, all these proteins appear to be part of a protein network, which also includes dynamin.

As demonstrated both *in vitro* and *in vivo*, phocein directly interacts with NDPK. NDPKs are ubiquitous enzymes that participate in a variety of cell processes and appear to be important in the supply of local pools of GTP (for example, in the cytoplasm near the cell surface, where a large number of GTPases operate (19–22)). Among them, dynamins are GTPases that play an essential role in the fission of clathrin-coated vesicles from the plasma membrane and are also implicated in other steps of intracellular vesicular trafficking (reviewed in Refs. 23–25). Although in the case of most GTPases, GTP binding is controlled by guanyl-nucleotide exchange factors, it appears that for dynamins, GTP loading is primarily dependent upon the local concentration of substrate, thus explaining the dependence of dynamin activity on NDPK. Dynamins are endowed with very low affinity for GTP, yet they have particularly high intrinsic (1–2 min^{-1}) and stimulated (over 100 min^{-1}) rates of GTP hydrolysis (24, 26, 27). Based on copurification experiments, Shpetner and Vallee (28) were the

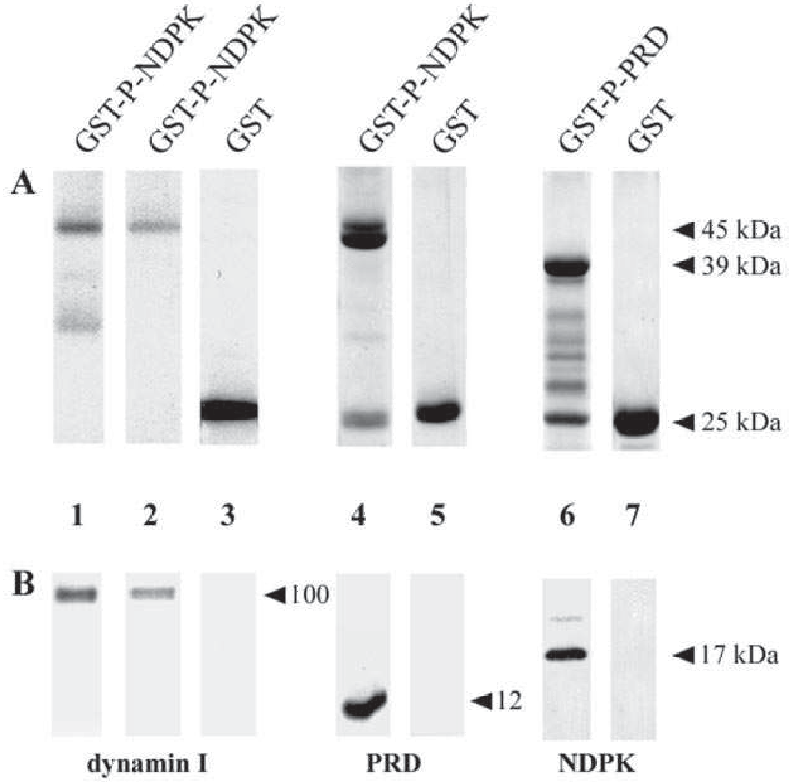

FIG. 6. **NDPK directly interacts with dynamin I *in vitro*.** *A*, Ponceau red staining of blots containing GST-P-NDPK (*lanes 1*, *2*, and *4*), GST-P-PRD (*lane 6*), and GST (*lanes 3*, *5*, and *7*). The fusion proteins had been incubated previously with cytosol (*lane 1*) or CHAPS fractions (*lanes 2* and *3*), the recombinant PRD fragment of dynamin I (*lanes 4* and *5*), and recombinant NDPK (*lanes 6* and *7*). *B*, the lower part of the blots revealed with anti-dynamin I (*lanes 1–5*) and anti-NDPK antibodies (*lanes 6* and *7*).

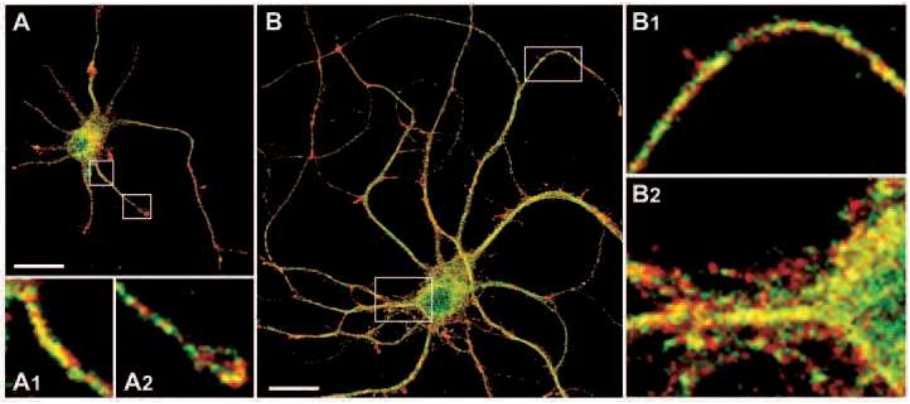

FIG. 7. **Dynamin and phocein partially co-localize in cultured hippocampal neurons.** Stage 3 (*A*) and stage 5 (*B*) neurons were fixed and processed for immunofluorescence microscopy using rabbit anti-phocein (5 μg/ml) (*green*) and mouse anti-dynamin I (10 μg/ml) (*red*) antibodies. Areas of co-localization appear *yellow* in the computer-generated composite image. *A1*, *A2*, *B1*, and *B2* are 5× enlargements of the *boxed* regions in *panels A* and *B*, respectively. In *panels A* and *B*: *scale bar*, 40 μm.

first to consider a possible role for NDPK in dynamin function. Recently, genetic studies conducted in *Drosophila* by Krishnan *et al.* (10) have shown that the activity of NDPK is critically required for the function of dynamin at synapses. They suggested that NDPK 'transiently associates with dynamin, thus being optimally positioned to provide a very high local concentration of soluble GTP.' However, using fly heads and techniques such as coimmunolocalization, coimmunoprecipitation, or pull-down experiments, they did not find physical evidence for such an association. The present study provides a clear indication that mammalian dynamin and NDPK physically interact.

Dynamin is present throughout the cell (29, 30) and is particularly concentrated in nerve terminals (31–33). Phocein, according to our previous immunocytochemical data (1), is found in the perikaryal-dendritic region of neurons, down to the spines, whereas in non-neuronal cells, it localizes predominantly in the Golgi complex. By contrast, within neurons, immunoreactivity for NDPK is diffuse and ubiquitous. NDPK is thus present in the subcellular regions where phocein and dynamin are expressed, in agreement with their partial association in brain extracts. The distributions of phocein and dynamin partially overlap in neurons, as well as in unpolarized cultured cells, in which dynamin isoforms are indeed detected at the level of the Golgi complex (34, 35). Within neurons, phocein may be implicated in only a subset of the reactions assisted by dynamin I, more specifically in reactions that occur in dendrites.

The other phocein partner identified in the yeast two-hybrid assay, Eps15, has been implicated at several steps of the endocytic pathway. Eps15 is a major, regulated binding protein for the clathrin adaptor AP-2. Its enrichment at the neck of clathrin-coated pits, as determined by immunogold cytochemistry, has suggested a function somehow interconnected with the action of dynamin (8, 9, 36–38). Clathrin-dependent endocytosis is selectively blocked when Eps15 function is perturbed by antibody or peptide microinjection or by the expression of constructs that function by dominant negative interference (Ref. 39 and references therein). Interestingly, Salcini *et al.* (11) very recently showed that mammalian Eps15 and dynamin genetically and biochemically interact, both *in vitro* and *in vivo*.

Phocein is thus a part of the multiprotein complexes com-

prising NDPK, Eps15, dynamin, and the proteins of the striatin family (2, 3, 5). That these complexes are bulky has been shown by gel filtration and sucrose gradient centrifugation (1). Blotted immunoprecipitates obtained by antibodies directed against phocein can be sequentially shown to contain all these proteins. However, the analyzed immunoprecipitates are a mixture of complexes; as a result, it is not possible to know whether these proteins all coexist within one given complex at the same time. Nevertheless, even if phocein interacts with these proteins in a sequential manner, such results are clearly in favor of a likely role of phocein in vesicular trafficking, particularly endocytosis. Yet how do these interactions occur? In both its N- and C-terminal domains, phocein has homology to the σ-subunits of AP membrane adaptors and thus might be components of AP complexes. Preliminary experiments indicate that γ- and α-adaptins, respectively, components of the AP1 and AP2 adaptors, coimmunoprecipitate with phocein even in rather harsh conditions. The finding that γ-adaptin coimmunoprecipitates with phocein is consistent with the localization of phocein at the Golgi complex (1). Likewise, coimmunoprecipitation of α-adaptin with phocein is consistent with a role in clathrin-mediated endocytosis. Availability of antibodies directed against various adaptor subunits should help clarify whether phocein could actually be part of stable tetrameric adaptor complexes.

Phocein, however, may exist independently of known AP subunits. Phocein has a central domain containing a putative Src homology 3 (SH3)-binding motif not conserved in σ-subunits. Another protein, stonin 2, which has homology to the μ-subunit of AP adaptors, is not found in tetrameric complexes (40).

Whatever the way through which phocein is inserted within these NDPK, Eps15, dynamin, and striatin-containing complexes, phocein could help localize and/or stabilize their association. Since phocein has been shown to be a substrate of the protein phosphatase 2A, it is likely that some of its interactions are regulated by its phosphorylation state (6).

The multimodular WD repeat-containing and calmodulin-binding proteins that constitute the striatin family are likely to play scaffolding and Ca^{2+}-dependent signaling roles. Phocein, their major interactor, which also interacts with proteins involved in vesicular trafficking, could be involved in the cross-talk between endocytosis and signaling; growing evidence is now documented for this cross-talk (41).

Acknowledgments—We are deeply indebted to Pietro De Camilli for numerous gifts of antibodies and plasmids and especially for kindly discussing and orienting our research. We thank Paolo Di Fiore for the generous gift of monoclonal anti-Eps15 antibodies. We thank Bénédicte Dargent for advice concerning the confocal laser microscope.

REFERENCES

1. Baillat, G., Moqrich, A., Castets, F., Baude, A., Bailly, Y., Benmerah, A., and Monneron, A. (2001) *Mol. Biol. Cell* **12,** 663–673
2. Castets, F., Bartoli, M., Barnier, J.-V., Baillat, G., Salin, P., Moqrich, A., Bourgeois, J.-P., Denizot, F., Rougon, G., Calothy, G., and Monneron, A. (1996) *J. Cell Biol.* **134,** 1051–1062
3. Castets, F., Rakitina, T., Gaillard, S., Moqrich, A., Mattei, M.-G., and Monneron, A. (2000) *J. Biol. Chem.* **275,** 19970–19977
4. Bartoli, M., Monneron, A., and Ladant, D. (1998) *J. Biol. Chem.* **273,** 22248–22253
5. Bartoli, M., Ternaux, J.-P., Forni, C., Portalier, P., Salin, P., Amalric, M., and Monneron, A. (1999) *J. Neurobiol.* **40,** 234–243
6. Moreno, C. S., Lane, W. S., and Pallas, D. C. (2001) *J. Biol. Chem.* **276,** 24253–24260
7. Parks, R. E., and Agarwal, R. P. (1973) in *The Enzymes* (Boyer, P. D., ed) Vol. 8, pp. 307–333, Academic Press, New York
8. Benmerah, A., Begue, B., Dautry-Varsat, A., and Cerf-Bensussan, N. (1996) *J. Biol. Chem.* **271,** 12111–12116
9. Tebar, F., Sorkina, T., Sorkin, A., Ericsson, M., and Kirchhausen, T. (1996) *J. Biol. Chem.* **271,** 28727–28730
10. Krishnan, K. S., Rikhy, R., Rao, S., Shivalkar, M., Mosko, M., Narayanan, R., Etter, P., Estes, P. S., and Ramaswami, M. (2001) *Neuron* **30,** 197–210
11. Salcini, A. E., Hilliard, M. A., Croce, A., Arbucci, S., Luzzi, C., Tacchetti, C., Daniell, L., De Camilli, P., Pelicci, P. G., Di Fiore, P. P., and Bazzicalupo, P. (2001) *Nat. Cell. Bio.* **3,** 755–760
12. Dagher, M.-C., and Filhol-Cochet, O. (1997) *BioTechniques* **22,** 916–922
13. Gietz, D, St. Jean, A., Woods, R. A., and Schiestl, R. H. (1992) *Nucleic Acids Res.* **20,** 1425
14. Kimmel, A. R., and Berger, S. L. (1987) *Methods Enzymol.* **152,** 307–316
15. Schaffner, W., and Weissmann, C. (1973) *Anal. Biochem.* **56,** 502–514
16. Grabs, D., Slepnev, V. I., Songyang, Z., David, C., Lynch, M., Cantley, L. C., and De Camilli, P. (1997) *J. Biol. Chem.* **272,** 13419–13425
17. Banker, G., and Goslin, K. (1998) *Culturing Nerve Cells* 2nd Ed, pp. 339–370, MIT Press, Cambridge, MA
18. Shimada, N., Ishikawa, N., Munakata, Y., Toda, T., Watanabe, K., and Kimura, N. (1993) *J. Biol. Chem.* **268,** 2583–2589
19. Kikkawa, S., Takahashi, K., Takahashi, K.-I., Shimada, N., Ui, M., Kimura, N., and Katada, T. (1990) *J. Biol. Chem.* **265,** 21536–21540
20. Klinker, J. F., and Seifert, R. (1999) *Eur. J. Biochem.* **261,** 72–80
21. Zhu, J., Tseng, Y.-H., Kantor, J. D., Rhodes, C. J., Zetter, B. R., Moyers, J. S., and Kahn, C. R. (1999) *Proc. Natl. Acad. Sci. U. S. A.* **96,** 14911–14918
22. Otsuki, Y., Tanaka, M., Yoshii, S., Kawazoe, N., Nakaya, K., and Sugimura, H. (2001) *Proc. Natl. Acad. Sci. U. S. A.* **98,** 4385–4390
23. Schmid, S. L., McNiven, M. A., and De Camilli, P. (1998) *Curr. Opin. Cell Biol.* **10,** 504–512
24. Hinshaw, J. E. (2000) *Annu. Rev. Cell Dev. Biol.* **16,** 483–519
25. McNiven, M. A., Cao, H., Pitts, K. R., and Yoon, Y. (2000) *Trends Biochem. Sci.* **25,** 115–120
26. Hill, E., van der Kaay, J., Downes, C. P., and Smythe, E. (2001) *J. Cell Biol.* **152,** 309–323
27. Marks, B., Stowell, M. H. B., Vallis, Y., Mills, I. G., Gibson, A., Hopkins, C. R., and McMahon, H. T. (2001) *Nature* **410,** 231–235
28. Shpetner, H. S., and Vallee, R. B. (1992) *Nature* **355,** 733–735
29. Noda, Y., Nakata, T., and Hirokawa, N. (1993) *Neuroscience* **55,** 113–127
30. Powell, K. A., and Robinson, P. J. (1995) *Neuroscience* **64,** 821–833
31. Takei, K., McPherson, P. S., Schmid, S. L., and De Camilli, P. (1995) *Nature* **374,** 186–190
32. McPherson, P. S., Takei, K., Schmid S. L., and De Camilli, P. (1994) *J. Biol. Chem.* **269,** 30132–30139
33. Estes, P. S., Roos, J., van der Bliek, A., Kelly, R. B., Krishnan, K. S., and Ramaswami, M. (1996) *J. Neurosci.* **16,** 5443–5456
34. Jones, S. M., Howell, K. E., Henley, J. R., Cao, H., and McNiven, M. A. (1998) *Science* **279,** 573–577
35. Cao, H., Thompson, H. M., Krueger, E. W., and McNiven, M. A. (2000) *J. Cell Sci.* **113,** 1993–2002
36. Benmerah, A., Bayrou, M., Dautry-Varsat, A., and Cerf-Bensussan, N. (1999) *J. Cell Sci.* **112,** 1303–1311
37. Iannolo, G., Salcini, A. E., Gaidarov, I., Goodman, O. B. Jr., Baulida, J., Carpenter, G., Pelicci, P. G., Di Fiore, P. P., and Keen, J. H.(1997) *Cancer Res.* **57,** 240–245
38. Torrisi, M. R., Lotti, L. V., Belleudi, F., Gradini, R., Salcini, A. E., Confalonieri, S., Pelicci, P. G., and Di Fiore, P. P. (1999) *Mol. Biol. Cell* **10,** 417–434
39. Lamaze, C., Dujeancourt, A., Baba, T., Lo, C. G., Benmerah, A., and Dautry-Varsat, A. (2001) *Mol. Cell* **7,** 661–671
40. Martina, J. A., Bonangelino, C. J., Aguilar, R. C., and Bonifacino, J. S. (2001) *J. Cell Biol.* **153,** 1111–1120
41. Di Fiore, P. P., and De Camilli, P. (2001) *Cell* **106,** 1–4

Annexe 3

Available online at www.sciencedirect.com
SCIENCE DIRECT
Biochimica et Biophysica Acta 1745 (2005) 101–110
BIOCHIMICA ET BIOPHYSICA ACTA
BBA
http://www.elsevier.com/locate/bba

Bcl-xL/Bax ratio is altered by IFNγ in TNFα- but not in TRAIL-induced apoptosis in colon cancer cell line

Gilbert Baillat*, Francoise Garrouste, Maryse Remacle-Bonnet, Jacques Marvaldi, Gilbert Pommier

ISPDCT (IPHM), FRE CNRS 2737, Université de la Méditerranée, Faculté de Pharmacie, 27 Bd. Jean Moulin, 13385 Marseille Cedex 5, France

Received 21 September 2004; received in revised form 1 December 2004; accepted 22 December 2004
Available online 11 January 2005

Abstract

Apoptosis is a crucial mechanism to eliminate harmful cells in which growth factors and cytokines are key regulators. In HT29-D4 cells, a model of human colon carcinoma, IFNγ presensitization is essential to induce an apoptotic response to TNFα whereas it only slightly enhances TRAIL-induced apoptosis. To compare the transcriptional profiles induced by TNFα and TRAIL and their regulation by IFNγ, we optimized a cDNA array analysis on targeted signaling pathways and confirmed the gene expression modulations by comparative RT-PCR. Although the two TNFSF ligands induced a same strong up-expression of pro-apoptotic Bax gene, the expression of anti-apoptotic Bcl-xL gene was more strongly up-regulated in TNFα- than in TRAIL-stimulated cells. Thus, TRAIL but not TNFα induced apoptotic mitochondrial cascade as highlighted by cytochrome *c* release into cytosol. IFNγ presensitization of TRAIL-stimulated cells did not induce any change in cytochrome *c* release, suggesting that the increase of IFNγ/TRAIL-induced apoptosis is independent of this pathway. In contrast, IFNγ pretreatment prevented Bcl-xL gene up-expression in TNFα-stimulated cells and allowed cytochrome *c* release. Thus, we hypothesize that the Bcl-xL/Bax ratio can block the apoptotic response in TNFα-stimulated cells but allows cell death initiation when it is altered by a crosstalk between IFNγ presensitization and TNFα induced signalings.

Keywords: Apoptosis; Colon cancer; Tumor necrosis factor superfamily; IFNγ; Bcl-2 family; cDNA array

1. Introduction

Tumor Necrosis Factor Superfamily (TNFSF) ligands play an essential role in many important biological processes, many of them are implicated in various human diseases, including cancer [1]. At least 19 distinct members exist which bind to different receptors homologous in their extracellular domains. Much remains unknown about the mechanisms by which these ligands transduce signals, sometimes opposite, in cancer cells. For instance, TNF-related apoptosis-inducing ligand (TRAIL) induces apoptosis in the majority of cancer cells, including colon cancer cell lines [2]. By contrast, TNFα induces apoptosis in only some cancer cell lines although TNFα high-affinity receptors (TNFR1 and TNFR2) are expressed in almost all the cell types [3]. In spite of their distinct receptors, all TNFSF ligands share common signaling pathways through mitogen-activated protein kinase (MAPK) cascades and activation of nuclear factor-kappaB (NF-KappaB), a transcription factor involved in both inflammation, migration and cell survival [4]. Thus, many TNFSF members can activate both apoptotic and anti-apoptotic signaling, the resulting effects depending on the cell type and interferences with extracellular signaling molecules. Among them, Interferon gamma (IFNγ) induces the production of different types of anti-tumorigenic and angiostatic proteins [5,6]. Interactions between the growth factor signalings and cytokine loops play also a crucial role in premalignant tissue survival, regulating growth/survival/apoptosis in a complex dance of changing partners and overlapping steps [1,5].

* Corresponding author. Fax: +33 04 91 83 56 53.
E-mail address: gilbert.baillat@pharmacie.univ-mrs.fr (G. Baillat).

0167-4889/$ - see front matter © 2005 Elsevier B.V. All rights reserved.
doi:10.1016/j.bbamcr.2004.12.005

In HT29-D4 cells, a colon carcinoma model, TRAIL was a potent apoptotic inducer while TNFα required cell presensitization by IFNγ to trigger apoptosis. We used a DNA array analysis to clarify how apoptotic response was induced by these TNFSF ligands and regulated by IFNγ.

2. Materials and methods

2.1. Cell culture and induction of apoptosis

HT29-D4 human colon adenocarcinoma cell line was cultured routinely in Dulbecco's modified Eagle medium (DMEM) supplemented with 10% fetal calf serum (FCS) as reported elsewhere [7–9]. For each experiment, HT29-D4 cells were seeded at a density of 2.5×10^5 cells/cm^2 in six-well tissue culture dishes. After 24 h, the cells were washed and further incubated in FCS-free DMEM containing 0.1% BSA for 24 h at 37 °C. After washing, the cells were incubated with or without IFNγ (40 ng/ml) for 15 min at 37 °C and washed twice again. TNFα (50 ng/ml) or TRAIL (100 ng/ml) was added at concentrations inducing an optimal cell death. IFNγ was purchased from Genzyme and TNFα and TRAIL from R & D Systems. All of the experiments were repeated at least four times.

2.2. Apoptosis assay

After a 24 h period of incubation, cells were assayed for apoptosis by using YO-PRO-1 dye (Molecular Probes Inc.) that was added at a final concentration of 4.0 μM and incubated 2 h at 37 °C. Cells were then analyzed on a fluorescent plate reader (Fluoroskan Ascent FL, Labsystems) at excitation and emission wavelengths of 485 and 530 nm, respectively. Untreated cells lysed by 0.1% Triton X-100 were used to measure the 100% cell death. In these experiments, data from triplicate determinations issued from at least four independent experiments were plotted and expressed as the mean±S.E. Significant effects ($P<0.05$) were determined using Student t-test.

2.3. Flow cytometric analysis of TNFα and TRAIL receptors

Untreated or IFNγ-stimulated HT29-D4 cells were cultured in FCS-free DMEM as described above and then incubated for 90 min at 4 °C with Abs (20μg/ml) against TNFR1, TNFR2 (R & D Systems), TRAIL-R1/DR4 or TRAIL-R2/DR5 (Diaclone) or with irrelevant control Ab. Washed cells were incubated with FITC-conjugated Ab (1:150) for 30 min at 4 °C, washed, fixed in 2% paraformaldehyde and subjected to flow cytometry. The relative fluorescence intensity was compared with the fluorescence intensity of the same cells stained with the control Ab. Results were presented as the number of cells (10.000/analysis) versus the log of fluorescence intensity.

2.4. RNA isolation and cDNA expression array

After 6 h incubation in the different conditions described above, total cell RNA extracts were prepared from pelleted cells (washed twice in PBS) using RNAqueous-4PCR kit (Ambion Inc.) according to the manufacturer's recommendations. The concentration and purity of RNA were determined by spectophotometer reading at 260 and 280 nm and by agarose gel electrophoresis.

^{33}P-labeled cDNA probes were synthesized from 2 μg total RNA with the Strip-EZ RT kit (Ambion Inc.) using oligodT primers and according to the manufacturer's recommendations. The specific labeling was evaluated in a scintillation counter after gel chromatography (PD30, BioRad).

The following membranes were purchased from Superarray Bioscience Corporation:

- GEArray Q Series Human Apoptosis Gene Array
- GEArray Q Series Human NF-KappaB Signal Transduction Gene Array
- GEArray Q Series Human Signal Transduction PathwayFinder Gene Array

The lists of genes are available on Superarray's web site: www.superarray.com.

Pre-hybridization, hybridization and washings were carried out at 60 °C. After 3 h of prehybridization, probe normalized quantities were hybridized overnight. Membranes were washed twice with SCC×2+SDS 1% and twice with SCC×0.1+SDS 0.5%. Membranes, sealed in plastic pouches, were exposed 24 h and readed in a FLA2000 phosphoimager (Fugifilm). Spots were quantified using two free downloaded softwares: ScanAlyse 2.35 (Eisen Laboratory, Stanford University) and GEArrayAnalyser 1.2 (Superarray). Membrane stripping was performed at 70 °C using Strip-EZ RT kit protocol and a maximum of 8 re-uses was carried out for each membrane.

Hybridization data standardization was performed using as reference the mean signal of a housekeeping genes pool (GAPDH, Cyclophilin A and RPL13A) strongly expressed in all our experiments and spotted at least two times on each membrane. To statistically identify the genes differentially expressed between two experimental conditions, the non-parametric Mann–Whitney test was used with at least four independent assays. Only values with $P<0.05$ and positive min/max separation were considered. The expression ratios (treated versus untreated cells) and standard error of the selected genes were calculated.

2.5. Comparative RT-PCR

Total RNA (0.5 μg) was reverse-transcripted in the presence of oligodT and the amplification of cDNA was performed in a duplex PCR with specific oligonucleotides for tested genes and for 18S rRNA as internal

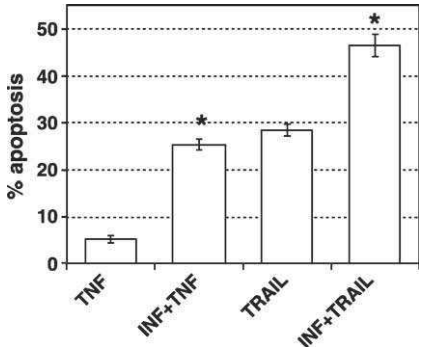

Fig. 1. Percent of apoptotic HT29-D4 cells pretreated or not for 15 min with IFNγ (40 ng/ml) and incubated for 24 h with TNFα (50 ng/ml) or TRAIL (100 ng/ml). Cell death is measured by YO-PRO-1 fluorescence. Values are the mean±S.E. of four independent experiments. *Statistically significant value ($P<0.05$) as compared to apoptosis induced by the same TNSF ligand but without IFNγ-sensitization.

standard (QuantumRNA Classic 18S kit, Ambion Inc.). Primers for Bcl-xL (5′-CCAGAAGGGACTGAATCG-3′ and 5′-CCTTGTCTACGCTTTCCAC-3′; 361 bp), Bax (5′-CAGCTGACATGTTTTCTGAC-3′ and 5′-CCACATCTGATGATCTGAAG-3′; 342 bp), Bak (5′-CTG CCGACCCAGAGATG-3′ and 5′-CCCAGGAAGCCAGTCAAG-3′; 292 bp), ICAM-1 (5′-AGCTTCGTGTCCTGTATGG-3′ and 5′-TGGGCCTGTTGTAGTCTG-3′; 388 bp), IL-8 (5′-AGCCTTCCTGATTTCTGC-3′ and 5′-GCCCTCTTCAAAAACTTCTC-3′; 255 bp) and IKBα (5′-CTGGCTTTCCTCAACTTCC-3′ and 5′-TCAGCCCCACACTTCA-AC-3′; 425 bp), were designed in order to obtain derived products displaying a size similar to the internal standard (489 bp). Different ratios of specific/competimer oligonucleotides of the QuantumRNA Classic 18S kit were used to equalize studied gene and standard signals. RT-PCR was performed (50 °C, annealing temperature) in a Gene Amp PCR System 2400™ (Perkin Elmer) using 25–30 cycles according to the linear part of the amplification curve. PCR products were run on 2% agarose gel and Sybr Green stained (Roche Diagnostics). Bands were visualized in a FLA2000 phosphoimager and quantified with ImageMaster 1D software (Pharmacia Biotech). The intensity of the co-amplified 18S product was taken as normalization reference. Differentially expressed genes were identified by their expression ratios±S.E. (treated versus untreated cells) calculated from at least four independent assays.

2.6. Cytosolic cytochrome c analysis

Assay was done as previously reported [10]. Briefly, cells treated as described above during different times were washed in PBS and incubated for 1 min in permeabilization buffer (10 mM phosphate buffer (pH 7.6), 75 mM NaCl, 1 mM EDTA, and 350 μg/ml digitonin). Permeabilized cells were centrifuged at 12,000×*g* for 10 min (4 °C) and supernatants and pellets (containing mitochondrial membranes) were collected. Equal amounts of protein (30 μg and 10 μg respectively) were separated by 15% SDS-PAGE, transferred onto a nitrocellulose membrane and probed overnight at 4 °C with an appropriate dilution (1:500) of monoclonal Abs anti-cytochrome *c* (BD Biosciences) or anti-Porin 31 HL Human (VDAC; Calbiochem) or of polyclonal Ab against actin (Santa Cruz Biotech.). Signals were visualized with Western Blot Chemiluminescence Reagents (Amersham). Total cell lysate was used as positive immunoblot control. Actin signal was used as normalization reference.

3. Results

To study IFNγ regulation of TNFSF ligand-induced apoptosis, HT29-D4 cells were presensitized or not with IFNγ and then incubated with TNFα or TRAIL. Untreated and IFNγ-pretreated only cells showed a low apoptosis level (lower than 1%, not shown). TNFα-stimulated cells were almost totally resistant to apoptosis (5.4%). In contrast, HT29-D4 cells showed a strong

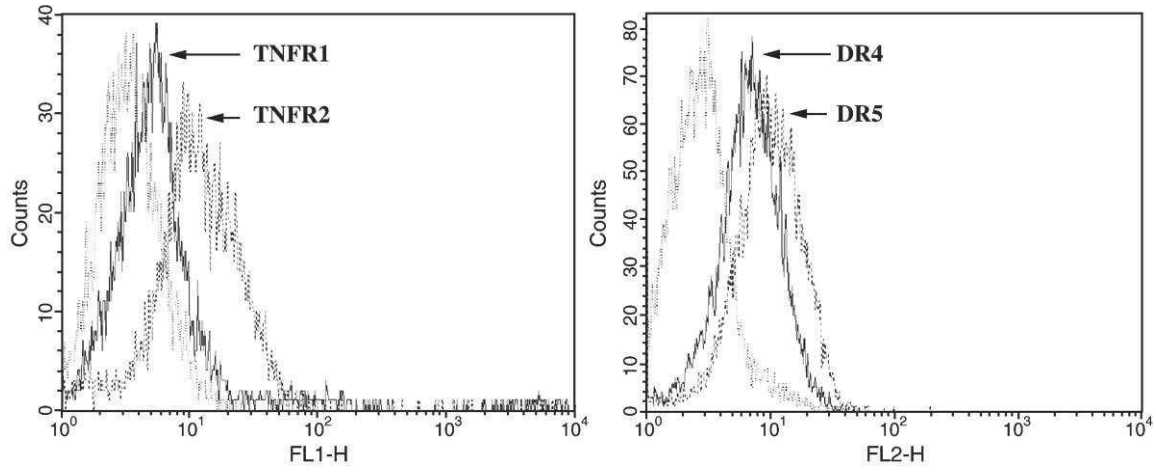

Fig. 2. Flow cytometry analysis of TNFα (left panel) and TRAIL (right panel) receptors in untreated HT29-D4 cells with either an irrelevant control Ab (point line) or specific Abs against TNF (TNFR1 and TNFR2) or TRAIL (TRAIL-R1/DR4 and TRAIL-R2/DR5) receptors.

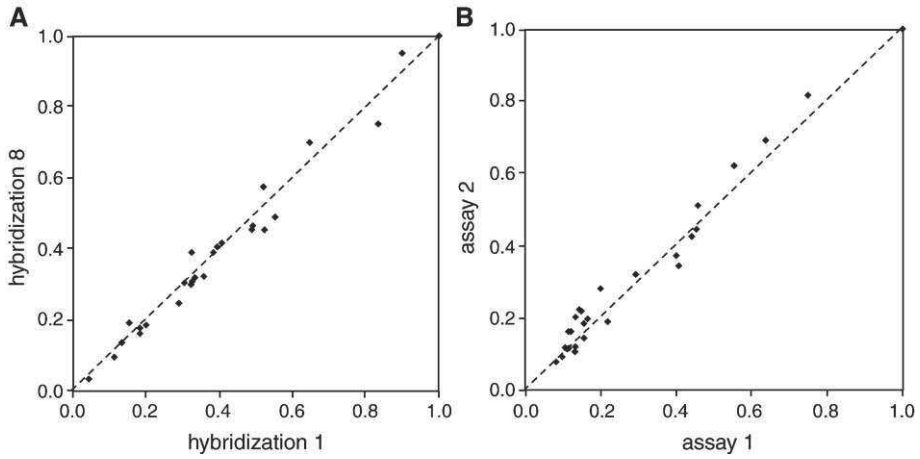

Fig. 3. Typical scatterplots showing the correlation between the normalized data of (A) the first and the eighth hybridization with the same probe on the same membrane and of (B) two independent assays in the same condition (here TNFα-treated cells). Point (1,1) corresponds to a pool of house-keeping genes used as reference for normalization.

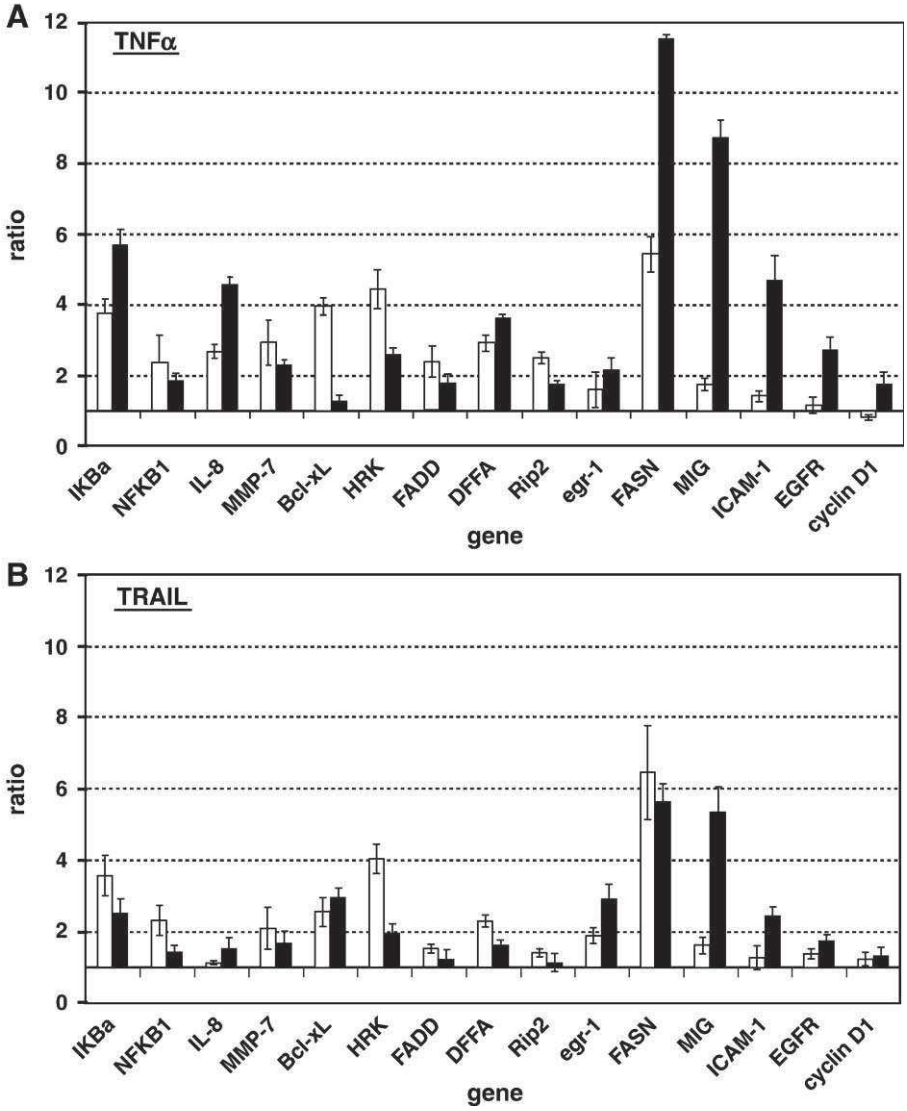

Fig. 4. Gene expression profiles in HT29-D4 cells stimulated by (A) TNFα or (B) TRAIL without (white boxes) or with (black boxes) IFNγ-pretreatment. Data are the mean±S.E. of expression ratios (treated versus untreated cells) of four independent experiments.

TRAIL-induced apoptotic response (28.4%). Cell death was considerably enhanced when cells were pretreated with IFNγ and incubated with TNFα (×5) or, in a lesser extent, with TRAIL (×1.5). Thus, IFNγ is an absolute requirement for TNFα-induced apoptosis and a potentiating factor for TRAIL-induced apoptosis in HT29-D4 cells (Fig. 1).

Flow cytometric analysis indicates that HT29-D4 cells constitutively expressed TNFα (TNFR1 and TNFR2) and TRAIL (DR4 and DR5) specific receptors (Fig. 2). Cell pretreatment by IFNγ did not induce a significant change in the receptor amounts as verified by flow cytometric analysis (not shown).

3.1. Optimization of a procedure to establish gene expression profiling of a targeted signal transduction pathway

Genes profiling with focused cDNA array membranes is an attractive tool to analyze the effects of cell environment on a targeted signaling pathway. In our work, we optimized the cost of DNA array analysis to obtain a sufficient number of experiments in the aim to test statistical significance of gene expression modulations. For instance, we used mild stripping conditions to enhance membrane life spans. In our hands, no difference was observed between the first and the eighth hybridization of the same membrane with the same probe (Fig. 3A). We also verified run-to-run variability: two independent assays in same experimental condition gave very reproducible images (Fig. 3B).

We applied this procedure to clarify how TNFSF ligands and IFNγ signaling pathways interacted to regulate apoptotic responses in human colon carcinoma HT29-D4 cells. As TNFSF ligands are known to activate NF-kappaB factor [4], a cDNA array membrane targeted on this signaling pathway was selected. In addition, two other membranes focused on genes involved in apoptosis and in several signaling pathways were used. These three membranes gathered 249 independent genes but only 24 showed a reproducible hybridization signal (not shown). The genes exhibiting a significant variation ($P<0.05$ and positive min/max separation) of expression in at least one experimental condition were plotted in Fig. 4.

3.2. Gene expression profiles of TNFα- or TRAIL-induced signaling

Among the genes listed in Fig. 4, the expression of only 10 was significantly regulated by TNFα or TRAIL (Table 1). IKBα, NF-kappaB1, IL-8, MMP7 and Bcl-xL genes are reported under NF-kappaB control [4,11]. Bcl-xL, HRK, FADD and DFFA genes are known to be involved in apoptosis regulation [12,13]. A strong up-regulation of FASN gene expression, which codes for an enzyme involved in fatty acid biosynthesis [14], was also observed. Whereas the expression of these 10 genes was regulated by TNFα, the expression of only 7 of them was affected by TRAIL (Table 1, greyed boxes).

A comparison of expression ratios induced by TNFα versus TRAIL showed significant differences for Bcl-xL (×3.94 against ×2.54), IL-8 (×2.66 against ×1.12) and RIP-2 (×2.48 against ×1.40) genes.

3.3. Gene expression profiles of TNFα- and TRAIL-induced signaling in IFNγ-sensitized cells

Among the genes listed in Fig. 4, only 9 showed significant expression differences after IFNγ-pretreatment and TNFα or TRAIL stimulation (Table 2). In addition to the 5 genes already described above, the expressions of 4 other genes (MIG, ICAM1, EGFR and Cyclin D1) were affected. The expression of these 9 genes was regulated by IFNγ/TNFα, whereas IFNγ/TRAIL affected the expression of 3 genes only (Table 2, greyed boxes).

The comparison of gene expression ratios induced by IFNγ/TNFα versus IFNγ/TRAIL showed significant differences for IKBα, IL-8, Bcl-xL, FASN, MIG, ICAM-1, EGFR and Cyclin-D1 genes. It is important to

Table 1
Gene expression ratios of TNFα- or TRAIL-treated versus untreated cells

Gene name	Description	Genebank	TNF / untreated	TRAIL / untreated
IKBα	Nuclear factor of kappa light polypeptide gene enhancer in B-cells inhibitor, alpha	M69043	3.77 ± 0.37	3.58 ± 0.58
NFKB1	Nuclear factor of kappa light polypeptide gene enhancer in B-cells 1 (p105)	M58603	2.35 ± 0.76	2.31 ± 0.41
IL-8	Interleukin 8	M17017	2.66 ± 0.19	1.12 ± 0.05
MMP-7	Matrix metalloproteinase 7	X07819	2.92 ± 0.64	2.08 ± 0.59
BCL-xL	BCL2-like 1	Z23115	3.94 ± 0.24	2.54 ± 0.41
HRK	Harakiri, BCL2-interacting protein	NM_003806	4.42 ± 0.54	4.03 ± 0.42
FADD	Fas associated via death domain	NM_003824	2.39 ± 0.43	1.53 ± 0.21
DFFA	DNA fragment factor-45	NM_004401	2.91 ± 0.23	2.28 ± 0.18
RIP-2	Receptor-interacting serine-threonine kinase 2	AF078530	2.48 ± 0.16	1.40 ± 0.11
FASN	Fatty acid synthase	U26644	5.42 ± 0.50	6.45 ± 1.31

Data are the mean±S.E. of four independent experiments. Greyed boxes highlight the statistically significant differences ($P<0.05$).

Table 2
Gene expression ratios of IFNγ/TNFα- or IFNγ/TRAIL-treated versus TNFα- or TRAIL-treated cells and of IFNγ-treated versus untreated cells

Gene name	Description	Genebank	IFN+TNF / TNF	IFN+TRAIL / TRAIL	IFN / untreated
IKBα	Nuclear factor of kappa light polypeptide gene enhancer in B-cells inhibitor, alpha	M69043	1.51 ± 0.25	0.70 ± 0.41	1.79 ± 0.32
IL-8	Interleukin 8	M17017	1.72 ± 0.18	1.36 ± 0.28	1.98 ± 0.25
BCL-xL	BCL2-like 1	Z23115	0.32 ± 0.19	1.16 ± 0.15	0.99 ± 0.12
HRK	Harakiri, BCL2-interacting protein	NM_003806	0.58 ± 0.20	0.49 ± 042	0.67 ± 0.21
FASN	Fatty acid synthase	U26644	2.12 ± 0.12	0.87 ± 0.20	1.85 ± 0.19
MIG	Monokine induced by gamma interferon	NM_002416	5.00 ± 0.46	3.31 ± 0.72	5.65 ± 0.81
ICAM-1	Intercellular adhesion molecule 1 (CD54) human rhinovirus receptor	NM_000201	3.30 ± 0.71	1.92 ± 0.27	2.87 ± 0.45
Cyclin D1	Epidermal growth factor receptor	X00588	2.35 ± 0.38	1.24 ± 0.18	1.99 ± 0.20
EGFR	Cyclin D1 (PRAD1)	M64349	2.12 ± 0.38	1.09 ± 0.23	2.30 ± 0.41

Data are the mean±S.E. of four independent experiments. Greyed boxes highlight the statistically significant differences ($P<0.05$).

note that IFNγ pretreatment of TNFα-stimulated cells induced an important down-regulation of the Bcl-xL gene expression (×0.32) whereas this latter was not significantly altered in IFNγ/TRAIL-treated cell. The expression of IKBα, IL-8, FASN, EGFR and Cyclin-D1 genes was up-regulated by IFNγ/TNFα (×1.51, ×1.72, ×2.12, ×2.35 and ×2.12 respectively) but not by IFNγ/TRAIL stimulation. Moreover, MIG and ICAM-1 gene expression were increased more strongly by cell incubation with IFNγ/TNFα (×5 and ×3.3 respectively) than with IFNγ/TRAIL (×3.31 and ×1.92 respectively).

IFNγ presensitization of cells without further TNSF ligand stimulation did not change NF-kappaB1, MMP7 and Bcl-xL gene expression (not shown, except for Bcl-xL gene) whereas the IKBα and IL-8 gene were only slightly up-regulated, thus indicating that the NF-KappaB transcriptional pathway was not primary involved in IFNγ signaling. In contrast, FASN, MIG, ICAM-1, EGFR and Cyclin D1 gene expression was specifically modulated by IFNγ (Table 2).

3.4. Control of gene expression levels by comparative RT-PCR

To confirm cDNA array data, a comparative RT-PCR study was performed for IL-8, IKBα and ICAM1 genes between untreated and treated cells. These genes were selected because they had large expression variations in cDNA array analysis and as witness of different biological responses. For instance, IL-8 is a mediator of inflammation [15], IKBα a regulator of NF-KappaB pathway [4] and ICAM-1 is involved in proliferation and cell–cell interactions [16]. The expression of anti-apoptotic Bcl-xL gene and of Bax and Bak genes, two pro-apoptotic members of the Bcl-2 family, was also controlled to understand how 'intrinsic' mitochondrial pathway was involved. Gene expression ratios obtained by RT-PCR were very similar to our cDNA array data (Fig. 5). Moreover, Bax and Bak gene expression, which was not detected by cDNA array analysis, could be analyzed by RT-PCR. After incubation with TNFα or TRAIL, Bax gene expression was strongly up-regulated (×3) whereas Bak gene expression was not affected. Moreover, these transcriptional regulations were not affected by IFNγ presensitization of cells before TNFα or TRAIL stimulation (Fig. 5). In addition, we have observed by RT-PCR that Bcl-xL and Bax

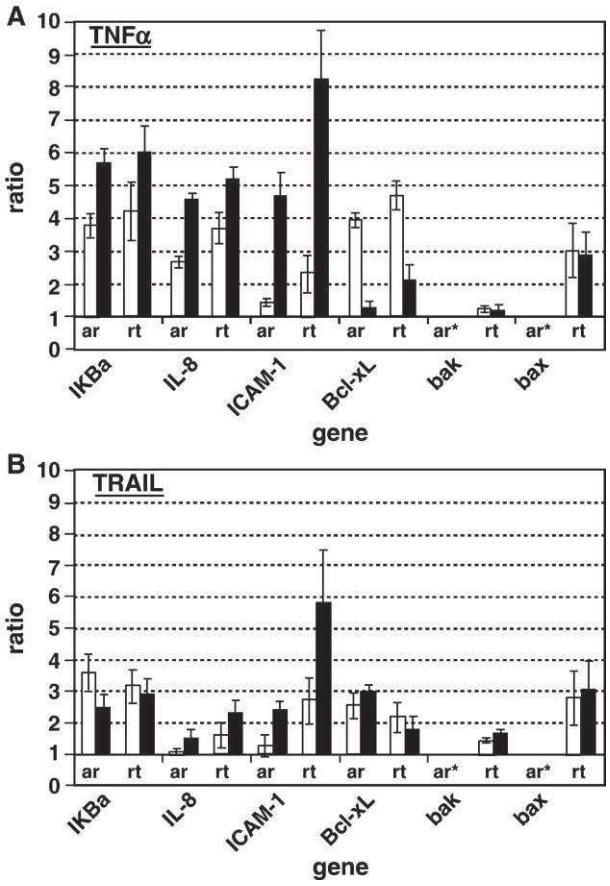

Fig. 5. Comparative gene expression profiles obtained by either (ar) cDNA array or (rt) comparative RT-PCR analysis in HT29-D4 cells stimulated by (A) TNFα or (B) TRAIL without (white boxes) or with (black boxes) IFNγ-pretreatment. Data are the mean±S.E. of expression ratios (treated versus untreated cells) of four independent experiments. (*no data).

gene expression was not regulated by only a pre-incubation with IFNγ (not shown).

3.5. Analysis of cytochrome c release

To assess the mitochondrial pathway involvement in apoptosis induced by the different experimental conditions, kinetic analysis of cytochrome *c* release into cytosol was performed (Fig. 6A). To verify the mitochondrial membrane integrity after lysis, the voltage-dependent anion-selective channel (VDAC), a protein normally inserted into the mitochondrial lipid bilayer, was checked in the cytosol. The cytochrome *c* cytoplasmic release was confirmed also by a parallel kinetic analysis of the cytochrome *c* decrease in mitochondrial membranes (Fig. 6B).

No cytochrome *c* release into cytosol was detected even after 15 h of incubation with TNFα. In contrast, cytochrome *c* was released as early as 6 h following cell stimulation by IFNγ/TNFα, TRAIL or IFNγ/TRAIL (Fig. 6A). The decrease of cytochrome *c* amount in mitochondrial membranes was in agreement with the cytosolic release kinetic (Fig. 6B). Thus, apoptotic mitochondrial pathway was activated in TRAIL- and IFNγ/TRAIL-stimulated cells but triggered by TNFα only when cells were IFNγ-presensitized. We did not observe a higher level of released cytochrome *c* in IFNγ/TRAIL-versus TRAIL-stimulated cells. Thus, pretreatment by IFNγ did not seem to further affect the apoptotic mitochondrial pathway in TRAIL-stimulated cells.

4. Discussion

We used HT29-D4 human colon carcinoma cell line as a model to study the apoptotic response induced by TNFα and TRAIL and its regulation by INFγ. We first performed a cDNA array analysis to identify involved genes and how their expression could regulate the cell death.

4.1. How does TNFα- or TRAIL-modulated gene expression promote apoptosis in HT29-D4 cells?

HT29-D4 cells were resistant to TNFα-induced apoptosis whereas TRAIL induced a strong apoptotic response (Fig. 1). On 249 tested genes, only 10 were significantly regulated by these TNFSF ligands (Table 1). Five of them (IKBα, NF-kappaB1, IL-8, MMP7 and Bcl-xL) were controlled by NF-KappaB factor, highlighting the activation of this transcriptional pathway by TNFSF ligands as previously reported [4]. NF-KappaB is known to be potently and rapidly activated after TNFα binding to TNFRs. Previous studies have shown that cell stimulation by TRAIL can activate NF-KappaB also by a FADD-dependent pathway but with very moderate effect [17]. This seems the case in our work because we observed that IKBα, IL-8, MMP7

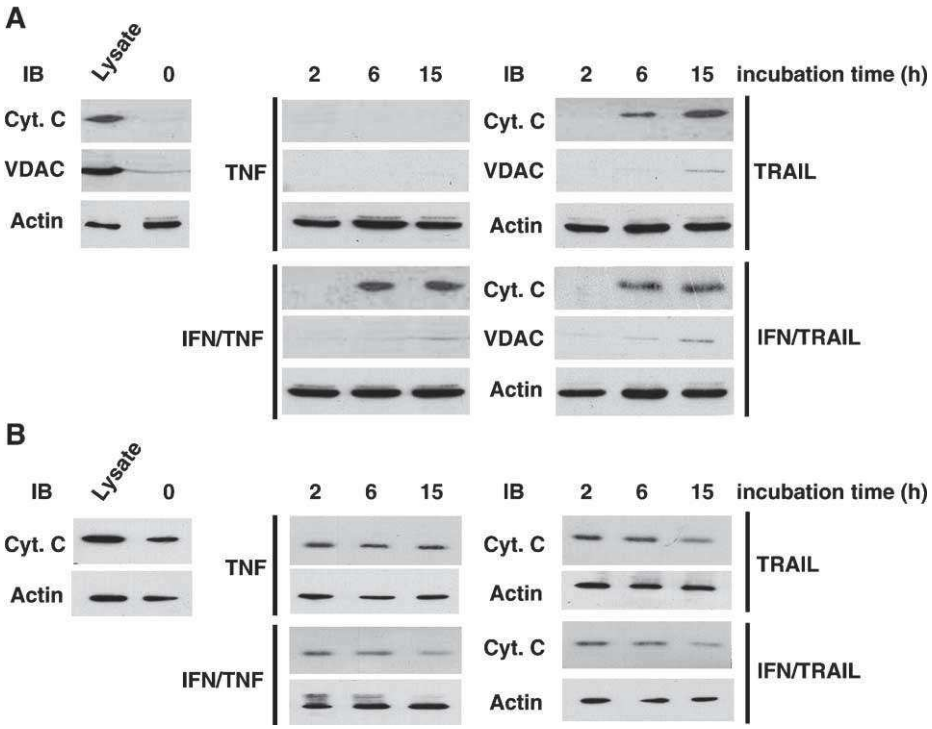

Fig. 6. Kinetic of (A) cytochrome *c* release into cytosol or (B) cytochrome *c* decrease in membrane fraction of TNFα-, TNFα/IFNγ-, TRAIL- or TRAIL/IFNγ-stimulated cells. Total cell lysate is used as positive control and cytosol or membrane fraction of untreated cell as starting reference (time zero). Immunoblots (IB) are analyzed using Abs against actin, VDAC or cytochrome *c*.

and Bcl-xL gene up-expression was significantly lower in TRAIL- than in TNFα-stimulated cells (Table 1 and Fig. 5).

In contrast, while Bcl-xL gene expression was higher in TNFα- than in TRAIL-stimulated cells, RT-PCR showed that Bax gene was equally up-expressed by incubating cells with one or other TNFSF ligands (Fig. 5). It is now well admitted that mitochondrial apoptotic pathway is regulated by a balance between pro- versus anti-apoptotic members of the Bcl-2 family [18,19]. Bcl-xL and Bcl-2, the two major anti-apoptotic protein of the Bcl-2 family, act through a heterodimerization with pro-apoptotic Bcl-2 family proteins such as Bax or Bak. As previously reported [20], we know that Bcl-2 gene is not expressed in HT29 cells. So, we hypothesize that the up-expression of Bcl-xL gene was essential to neutralize the effects of Bax gene up-expression in TNFα-stimulated cells, thus preventing mitochondrial pathway activation. In contrast, Bcl-xL gene expression in TRAIL-stimulated cells was insufficient to block the mitochondrial apoptotic pathway, as confirmed by cytochrome *c* cytosolic release (Fig. 6).

This finding is consistent with a previous report on the crucial regulatory role of Bcl-xL on apoptosis in normal and cancerous colorectal tissues [21]. Moreover, Bcl-xL down-regulation by antisense ODNs was shown to enhance Bax-mediated apoptosis in HCT116 colon cancer cell line [22]. In addition, apoptosis induced by nonsteroidal anti-inflammatory drugs, which is mediated by Bcl-xL gene down-expression, was reported to be completely abolished in colorectal cancer cells without functional Bax gene [23].

The expression of the IL-8 gene was induced by TNFα but not by TRAIL stimulation (Fig. 5). The increase of IL-8 gene expression induced by TNFα was previously reported in HT29-D4 cells [8,24]. IL-8 is a chemokine known to enhance inflammation, survival and proliferation in endothelial cells [15,25]. Another gene, RIP-2, was up-expressed in TNFα- but not in TRAIL-stimulated cells. RIP-2 is known as signaling checkpoint between proliferation and differentiation [13]. The up-expression of these two genes, involved in proliferation control, could reinforce apoptosis resistance in TNFα-stimulated cells.

Finally, our results are in agreement with previous reports, using cDNA or oligonucleotides microarray analysis to study gene expression regulation by TNFα, in which IL-8, IKBα and NF-kappaB1 gene are found frequently up-expressed in epithelial cells [26–29] as in other cellular types [30–33].

4.2. How does IFNγ presensitization act on TNFα- or TRAIL-induced gene expression and on apoptosis?

Except for Bcl-xL, gene expression regulation induced by only IFNγ pretreatment of cells was quite similar to that observed in IFNγ/TNFα- as compared to TNFα-stimulated cells, suggesting these ratios were IFNγ relevant (Table 2). In contrast, gene expression induced by IFNγ pretreatment was largely decreased following TRAIL stimulation. Moreover, stimulation by IFNγ alone did not induce pro-apoptotic Bax gene expression and did not trigger apoptosis.

However, presensitization of HT29-D4 cells by INFγ was necessary to trigger apoptosis with TNFα stimulation and enhanced TRAIL-induced apoptosis (Fig. 1) as previously reported [7,9,34,35]. Interestingly, Bcl-xL gene expression was strongly down-regulated only when the death factor was TNFα whereas the two TNFSF ligands induced similar Bax gene up-expression (Fig. 5). Thus, Bcl-xL, but not Bax gene expression, was down-regulated by a crosstalk between IFNγ and TNFα signaling pathways. This could move the balance between the Bcl-2 family members in favor of cell death, thus triggering the pro-apoptotic mitochondrial pathway and cytochrome *c* release. In contrast, apoptosis increase in IFNγ/TRAIL- versus TRAIL-stimulated cells was independent of the mitochondrial pathway as confirmed by the similar levels of cytochrome *c* release in cytosol (Fig. 6A) and the parallel decrease of cytochrome *c* in the mitochondrial fraction (Fig. 6B). These results suggest that another unidentified pathway could contribute to the increase of IFNγ/TRAIL- versus TRAIL-induced apoptosis without altering the expression of genes tested in this work. Indeed, sensitivity to death receptor-induced apoptosis can be regulated by several factors and expression levels of Bcl-2 family members are only one of them [36]. Thus, the contribution of other IFNγ-induced effects on apoptosis cannot be excluded. IL-8, FASN, EGFR and Cyclin D1 gene expression regulation highlights that the proliferative potential induced by IFNγ is preserved in IFNγ/TNFα- but not in IFNγ/TRAIL-stimulated cells (Table 2). Obviously, the expression modulation of these genes involved in proliferation could not totally prevent cell death, but could play a role in the different apoptosis levels observed after IFNγ presensitization in TNFα- or TRAIL-stimulated cells. For instance, Fatty Acid Synthase (FASN) gene was widely more expressed in IFNγ/TNFα- than in IFNγ/TRAIL-stimulated cells (Fig. 4). It has been reported [14] that FASN overexpression can protect cancer cells from apoptosis. Thus, this difference in FASN gene expression could significantly improve survival in IFNγ/TNFα- as compared to IFNγ/TRAIL-stimulated cells. However, how FASN, that can affect signal transduction by altering membrane phospholipid composition, prevents apoptosis remains a poorly understood phenomenon.

We noticed also a strong up-expression of MIG and ICAM-1 genes in the two experimental conditions, these regulations being known as IFNγ relevant [16,37,38]. Finally, a previous report compared by cDNA microarray analysis the transcriptional responses induced by IFNγ/TNFα versus IFNγ in HT29 cells [39] with results in close agreement with the expression ratios that we obtained for IL-8, MIG and NF-KappaB1 genes.

In this work, tumor environment factors, such as TNFSF ligands and IFNγ, modulate apoptotic response by regulating the expression of genes coding for essential proteins involved in apoptosis, e.g. Bcl-xL and Bax, or in cell

proliferation, e.g. FASN and IL-8. These transcriptional alterations affect the delicate balance between apoptosis and survival/proliferation and highlight the close links between these two opposite mechanisms.

Our findings underline the interest of gene profiling to elaborate hypothesis on targeted signaling pathways. However, they also show DNA array limitations as exemplified by its incapacity to detect Bax gene expression in our experimental conditions. So, a more sensitive method, such as RT-PCR, should be additionally used in order to obtain a complete view of a biological process.

Finally, since IFNγ decreased colon cancer cell resistance to TNFα-induced apoptosis, it will be of interest to test if IFNγ could also subvert the resistance to TRAIL-mediated apoptosis which is observed in some cancer cell lines. In this case, IFNγ association with TRAIL could provide a promising antitumor therapeutic approach to enhance cellular susceptibility to cell death in a more large variety of tumors.

Acknowledgements

We thank Pr. D. Braguer and Dr. M. Lehmann for critical comments on manuscript and Dr. M. Carre for technical assistance on cytochrome *c* release.

This work was supported by grants of "Programme CNRS: Puces à ADN" and of Conseil Général des BdR.

References

[1] U. Gaur, B.B. Aggarwal, Regulation of proliferation, survival and apoptosis by members of the TNF superfamily, Biochem. Pharmacol. 66 (8) (2003) 1403–1408.

[2] A. Ashkenazi, R.C. Pai, S. Fong, S. Leung, D.A. Lawrence, S.A. Marsters, C. Blackie, L. Chang, A.E. McMurtrey, A. Hebert, L. DeForge, I.L. Koumenis, D. Lewis, L. Harris, J. Bussiere, H. Koeppen, Z. Shahrokh, R.H. Schwall, Safety and antitumor activity of recombinant soluble Apo2 ligand, J. Clin. Invest. 104 (2) (1999) 155–162.

[3] P. Vandenabeele, W. Declercq, R. Beyaert, W. Fiers, Two tumour necrosis factor receptors: structure and function, Trends Cell Biol. 5 (10) (1995) 392–399.

[4] R. De Martin, J.A. Schmid, R. Hofer-Warbinek, The NF-kappaB/Rel family of transcription factors in oncogenic transformation and apoptosis, Mutat. Res. 437 (3) (1999) 231–243.

[5] M. Chawla-Sarkar, D.J. Lindner, Y.F. Liu, B.R. Williams, G.C. Sen, R.H. Silverman, E.C. Borden, Apoptosis and interferons: role of interferon-stimulated genes as mediators of apoptosis, Apoptosis 8 (3) (2003) 237–249.

[6] H. Ikeda, L.J. Old, R.D. Schreiber, The roles of IFN gamma in protection against tumor development and cancer immunoediting, Cytokine Growth Factor Rev. 13 (2) (2002) 95–109.

[7] M.M. Remacle-Bonnet, F.L. Garrouste, S. Heller, F. Andre, J.L. Marvaldi, G.J. Pommier, Insulin-like growth factor-I protects colon cancer cells from death factor-induced apoptosis by potentiating tumor necrosis factor alpha-induced mitogen-activated protein kinase and nuclear factor kappaB signaling pathways, Cancer Res. 60 (7) (2000) 2007–2017.

[8] M. Remacle-Bonnet, F. Garrouste, F. El Atiq, M. Roccabianca, J. Marvaldi, G. Pommier, Des-(1-3)-IGF-I, an insulin-like growth factor analog used to mimic a potential IGF-II autocrine loop, promotes the differentiation of human colon-carcinoma cells, Int. J. Cancer 52 (1992) 910–917.

[9] F. Garrouste, M. Remacle-Bonnet, C. Fauriat, J. Marvaldi, J. Luis, G. Pommier, Prevention of cytokine-induced apoptosis by insulin-like growth factor-I is independent of cell adhesion molecules in HT29-D4 colon carcinoma cells—Evidence for a NF-kappaB-dependent survival mechanism, Cell Death Differ. 9 (7) (2002) 768–779.

[10] N. Andre, M. Carre, G. Brasseur, B. Pourroy, H. Kovacic, C. Briand, D. Braguer, Paclitaxel targets mitochondria upstream of caspase activation in intact human neuroblastoma cells, FEBS Lett. 532 (1–2) (2002) 256–260.

[11] M.C. Turco, M.F. Romano, A. Petrella, R. Bisogni, P. Tassone, S. Venuta, NF-kappaB/Rel-mediated regulation of apoptosis in hematologic malignancies and normal hematopoietic progenitors, Leukemia 18 (1) (2004) 11–17.

[12] M.R. Hussein, A.K. Haemel, G.S. Wood, Apoptosis and melanoma: molecular mechanisms, J. Pathol. 199 (3) (2003) 275–288.

[13] B. Munz, E. Hildt, M.L. Springer, H.M. Blau, RIP2, a checkpoint in myogenic differentiation, Mol. Cell. Biol. 22 (16) (2002) 5879–5886.

[14] A. Baron, T. Migita, D. Tang, M. Loda, Fatty acid synthase: a metabolic oncogene in prostate cancer? J. Cell. Biochem. 91 (1) (2004) 47–53.

[15] K. Xie, Interleukin-8 and human cancer biology, Cytokine Growth Factor Rev. 12 (4) (2001) 375–391.

[16] A.K. Hubbard, R. Rothlein, Intercellular adhesion molecule-1 (ICAM-1) expression and cell signaling cascades, Free Radic. Biol. Med. 28 (9) (2000) 1379–1386.

[17] W.H. Hu, H. Johnson, H.B. Shu, Tumor necrosis factor-related apoptosis-inducing ligand receptors signal NF-κB, JNK activation and apoptosis through distinct pathways, J. Biol. Chem. 274 (1999) 30603–30610.

[18] J.C. Sharpe, D. Arnoult, R.J. Youle, Control of mitochondrial permeability by Bcl-2 family members, Biochim. Biophys. Acta 1644 (2–3) (2004) 107–113.

[19] D.M. Finucane, E. Bossy-Wetzel, N.J. Waterhouse, T.G. Cotter, D.R. Green, Bax-induced caspase activation and apoptosis via cytochrome *c* release from mitochondria is inhibitable by Bcl-xL, J. Biol. Chem. 274 (4) (1999) 2225–2233.

[20] S. Violette, L. Poulain, E. Dussaulx, D. Pepin, A.M. Faussat, J. Chambaz, J.M. Lacorte, C. Staedel, T. Lesuffleur, Resistance of colon cancer cells to long-term 5-fluorouracil exposure is correlated to the relative level of Bcl-2 and Bcl-X(L) in addition to Bax and p53 status, Int. J. Cancer 98 (4) (2002) 498–504.

[21] C.A. Maurer, H. Friess, S.S. Buhler, B.R. Wahl, H. Graber, A. Zimmermann, M.W. Buchler, Apoptosis inhibiting factor Bcl-xL might be the crucial member of the Bcl-2 gene family in colorectal cancer, Dig. Dis. Sci. 43 (12) (1998) 2641–2648.

[22] R.L. Hayward, J.S. Macpherson, J. Cummings, B.P. Monia, J.F. Smyth, D.I. Jodrell, Enhanced oxaliplatin-induced apoptosis following antisense Bcl-xl down-regulation is p53 and Bax dependent: genetic evidence for specificity of the antisense effect, Mol. Cancer Ther. 3 (2) (2004) 169–178.

[23] L. Zhang, J. Yu, B.H. Park, K.W. Kinzler, B. Vogelstein, Role of BAX in the apoptotic response to anticancer agents, Science 290 (5493) (2000) 989–992.

[24] S. Vallee, F. Fouchier, P. Bremond, C. Briand, J. Marvaldi, S. Champion, Insulin-like growth factor-1 downregulates nuclear factor kappa B activation and upregulates interleukin-8 gene expression induced by tumor necrosis factor alpha, Biochem. Biophys. Res. Commun. 305 (4) (2003) 831–839.

[25] A. Li, S. Dubey, M.L. Varney, B.J. Dave, R.K. Singh, IL-8 directly enhanced endothelial cell survival, proliferation, and matrix metalloproteinases production and regulated angiogenesis, J. Immunol. 170 (6) (2003) 3369–3376.

[26] B. Zhao, S.A. Stavchansky, R.A. Bowden, P.D. Bowman, Effect of interleukin-1beta and tumor necrosis factor-alpha on gene expression

in human endothelial cells, Am. J. Physiol., Cell Physiol. 284 (6) (2003) 1577–1583.
[27] A. Zhou, S. Scoggin, R.B. Gaynor, N.S. Williams, Identification of NF-kappa B-regulated genes induced by TNFalpha utilizing expression profiling and RNA interference, Oncogene 22 (13) (2003) 2054–2064.
[28] J. Zhou, Y. Jin, Y. Gao, H. Wang, G. Hu, Y. Huang, Q. Chen, M. Feng, C. Wu, Genomic-scale analysis of gene expression profiles in TNF-alpha treated human umbilical vein endothelial cells, Inflamm. Res. 51 (7) (2002) 332–341.
[29] D. Viemann, M. Goebeler, S. Schmid, K. Klimmek, C. Sorg, S. Ludwig, J. Roth, Transcriptional profiling of IKK2/NF-kappa B- and p38 MAP kinase-dependent gene expression in TNF-alpha-stimulated primary human endothelial cells, Blood 103 (9) (2004) 3365–3373.
[30] Q.W. Zhang, N. Ono, Y. Takahara, H. Tanaka, Replicated studentized-deviate detection applied to the identification of differentially expressed genes in TNF-alpha-stimulated cells, Gene 324 (2004) 89–96.
[31] J. Schwamborn, A. Lindecke, M. Elvers, V. Horejschi, M. Kerick, M. Rafigh, J. Pfeiffer, M. Prullage, B. Kaltschmidt, C. Kaltschmidt, Microarray analysis of tumor necrosis factor alpha induced gene expression in U373 human glioblastoma cells, BMC Genomics 4 (1) (2003) 46–57.
[32] Y. Osawa, M. Nagaki, Y. Banno, D.A. Brenner, T. Asano, Y. Nozawa, H. Moriwaki, S. Nakashima, Tumor necrosis factor alpha-induced interleukin-8 production via NF-kappaB and phosphatidylinositol 3-kinase/Akt pathways inhibits cell apoptosis in human hepatocytes, Infect. Immun. 70 (11) (2002) 6294–6301.
[33] J. Gallagher, J. Howlin, C. McCarthy, E.P. Murphy, B. Bresnihan, O. FitzGerald, C. Godson, H.R. Brady, F. Martin, Identification of Naf1/ABIN-1 among TNF-alpha-induced expressed genes in human synoviocytes using oligonucleotide microarrays, FEBS Lett. 551 (1–3) (2003) 8–12.
[34] V. Langaas, S. Shahzidi, J.I. Johnsen, B. Smedsrod, B. Sveinbjornsson, Interferon-gamma modulates TRAIL-mediated apoptosis in human colon carcinoma cells, Anticancer Res. 21 (6A) (2001) 3733–3738.
[35] C. Kumar-Sinha, S. Varambally, A. Sreekumar, A.M. Chinnaiyan, Molecular cross-talk between the TRAIL and interferon signaling pathways, J. Biol. Chem. 277 (1) (2002) 575–585.
[36] M.R. Sprick, H. Walczak, The interplay between the Bcl-2 family and death receptor-mediated apoptosis, Biochim. Biophys. Acta 1644 (2–3) (2004) 125–132.
[37] J. Croitoru-Lamoury, G.J. Guillemin, F.D. Boussin, B. Mognetti, L.I. Gigout, A. Cheret, B. Vaslin, R. Le Grand, B.J. Brew, D. Dormont, Expression of chemokines and their receptors in human and simian astrocytes: evidence for a central role of TNF alpha and IFN gamma in CXCR4 and CCR5 modulation, Glia Mar. 41 (4) (2003) 354–370.
[38] A.D. Santin, P. Hermonat, A. Ravaggi, M. Chiriva-Internati, J.C. Hiserodt, E. Tian, C.A. Carter, S. Pecorelli, G.P. Parham, Effects of retinoic acid combined with interferon-gamma on the expression of major-histocompatibility-complex molecules and intercellular adhesion molecule-1 in human cervical cancer, Int. J. Cancer 75 (2) (1998) 254–258.
[39] E.J. Manos, D.A. Jones, Assessment of tumor necrosis factor receptor and Fas signaling pathways by transcriptional profiling, Cancer Res. 61 (2) (2001) 433–438.

Annexe 4

Biochimica et Biophysica Acta 1783 (2008) 2323–2331

Contents lists available at ScienceDirect

Biochimica et Biophysica Acta

journal homepage: www.elsevier.com/locate/bbamcr

Early adhesion induces interaction of FAK and Fyn in lipid domains and activates raft-dependent Akt signaling in SW480 colon cancer cells

Gilbert Baillat *, Carole Siret, Estelle Delamarre, Jose Luis

INSERM UMR 911, Centre de Recherche en Oncologie biologique et Oncopharmacologie, Aix-Marseille University, Faculté de Pharmacie, 27, bld Jean Moulin, 13285 Marseille cedex 05, France

ARTICLE INFO

Article history:
Received 15 April 2008
Received in revised form 25 July 2008
Accepted 12 August 2008
Available online 5 September 2008

Keywords:
Akt-1
Early adhesion
FAK
Lipid domain
SFK
Signal transduction

ABSTRACT

Integrin-dependent interaction of epithelial tumor cells with extracellular matrix (ECM) is critical for their migration, but also for hematogenous dissemination. Elevated expression and activity of Src family kinases (SFKs) in colon cancer cells is often required in the disease progression. In this work, we highlighted how focal adhesion kinase (FAK) and SFKs interacted and we analyzed how PI3K/Akt and MAPK/Erk1/2 signaling pathways were activated in early stages of colon cancer cell adhesion. During the first hour, integrin engagement triggered FAK-Y397 phosphorylation and a fraction of FAK was located in lipid rafts/caveolae domains where it interacted with Fyn. The FAK-Y861 and/or -Y925 phosphorylations led to a subsequently FAK translocation out of lipid domains. In parallel, a PI3K/Akt pathway dependent of lipid microdomain integrity was activated. In contrast, the MAPK/Erk1/2 signaling triggered by adhesion increased during at least 4 h and was independent of cholesterol disturbing. Thus, FAK/Fyn interaction in lipid microdomains and a Akt-1 activation occurred at the same time during early contact with ECM suggesting a specific signaling dependent of lipid rafts/caveolae domains.

1. Introduction

During cancer progression, tumor cells acquire migrating capability and effective 'homing' in body host environment. Cellular adhesion and migration processes involve cell adhesion molecules such as integrins that link components of the extracellular matrix (ECM) with cytoskeletal proteins.

One of the major tyrosine phosphorylation activities linked to integrin signaling is that of focal adhesion kinase (FAK). High amount of FAK is located in specialized subcellular compartments so-called focal adhesions. The primary function of FAK is to transmit the adhesion signal coming from integrins to the intracellular signaling cascade. Integrin engagement is responsible for FAK autophosphorylation at Y397, activating a binding site that leads to its association with Src family protein tyrosine kinases (SFKs). SFK association with FAK induces other tyrosine phosphorylations of FAK. To date, five sites have been identified, namely tyrosine 407, 576, 577, 861 and 925 [1,2]. These tyrosine phosphorylations generate high affinity binding sites for several intracellular signaling molecules and full activation of FAK. Together with FAK, these signaling molecules recruit and activate regulators of Erk, Jun kinase, and Rho signaling pathways, which modulate multiple genes expression [3,4].

SFKs, consisting of c-Src, Yes, Fyn, Lck, Lyn, Hck, Fgr, Blk and Yrk, are important signaling enzymes that share considerable structural homology and control cell growth, proliferation and migration [5]. Only c-Src, Yes, and Fyn are usually described as 'ubiquitously' expressed [6]. The most characteristic feature of SFKs is that their activities are strictly regulated by two tyrosine phosphorylations. Tyrosine 416 of c-Src is a conserved tyrosine in the kinase domain of SFKs and its phosphorylation leads to full activation, whereas tyrosine phosphorylation in the C-terminal region (Y527 for Src) leads to their inactivation. The SFK signaling is achieved by phosphorylation of specific substrates such as FAK and/or recruitment of specific pools of SFKs within the cell.

SFKs are localized in distinct subcellular compartments, including cholesterol-enriched microdomains [7]. These lipid microdomains are small, heterogeneous, highly dynamic, sterols- and sphingolipids-enriched. Two types of lipid related subdomains have been characterized with structural and functional differences: the lipid rafts and the caveolae [8]. Caveolae are plasma membrane invaginations formed by oligomerization of caveolin-1 that have been implicated in a variety of cellular processes, including signal transduction, endocytosis, transcytosis and cholesterol trafficking. It has been proposed that the function of lipid rafts is the spatial concentration of sets of proteins in specialized membrane areas to increase the efficiency and the specificity of signal transduction and to prevent cross-talk between pathways [9].

* Corresponding author. Tel.: +33 04 91 83 55 84; fax: +33 04 91 83 56 53.
E-mail address: gilbert.baillat@pharmacie.univ-mrs.fr (G. Baillat).

0167-4889/$ – see front matter © 2008 Elsevier B.V. All rights reserved.
doi:10.1016/j.bbamcr.2008.08.008

During tumor progression, primary tumor cells can be disseminated toward distant sites where they form subsequent metastases. Detachment of tumor cells induces a focal adhesion disassembly with mechanisms close to those observed during focal adhesion turnover. Adhesion of these detached cells in a metastasis site has particularly crucial effects on survival and on regulation of kinase signaling for cells of epithelial origin. Integrin engagement with ECM promotes assembly of several molecules, including SFKs and FAK, and initiates focal adhesion reformation [10].

However, surprisingly, FAK and SFKs are not located in the same area since SFKs, in contrast to FAK, are described to be largely associated to lipid microdomains [7]. We hypothesized that FAK could interact with SFKs in lipid rafts/caveolae domains and that this interaction triggered a specific signaling during early attachment of cells. Thus, we studied the time-courses and the spatial compartmentalizations of FAK/SFK interactions and of PI3K and MAPK pathways activation in early adhesion using SW480 cells as model of colon cancer cell.

2. Materials and methods

2.1. Reagents

Unless noted, all reagents were purchased from Sigma-Aldrich. Rabbit polyclonal antibodies (Abs) raised against phospho (p)-Akt (Ser-473), p-FAK (Tyr397), p-FAK (Tyr925), p-Src family (Tyr416), p-Erk 1/2 (Thr-202/Tyr-204) and Akt-1 were purchased from Cell Signaling. P-Src family (Tyr416) is named in reference to the conserved sequence of activation loop in chicken c-Src. Rabbit polyclonal Abs raised against FAK (C 20), p-FAK (Tyr861), SFKs (named c-Src (SCR2)), c-Src (N16), Fyn, Erk1, caveolin-1 (N-20), PI3K-P85α and mouse mAb raised against c-Yes were purchased from Santa Cruz Biotechnology. HRP-conjugated anti-rabbit and anti-mouse IgG secondary Abs and enhanced chemiluminescence reagents (ECL) were from GE Healthcare. Mouse mAb raised against HA tag was from Euromedex. Pharmacological inhibitors SU6656 and PP2 were from Calbiochem.

2.2. Cell culture and adhesion

HT29-D4 cells were cloned by limiting dilution of the HT29 parental cell line [11]. SW480 and SW620 cells were a generous gift of Pr. M. Bracke (Gent University Hospital, Belgium). Each cell line was routinely cultured in high glucose DMEM supplemented with 10% fetal calf serum (FCS) at 37 °C in 5% CO_2.

Cells were starved 4 h in FCS- and calcium-free MEM (SMEM) supplemented with 0.2% BSA and then detached with 5 mM EDTA. Suspended cells were maintained in FCS-free SMEM during 1 h to keep cells isolated and to inactivate outside signals. Then, they were allowed to adhere in low-density condition in six-well plates (2×10^5 cells/well) or 100 mm plates (10^6 cells) at 37 °C in FCS-free DMEM supplemented with 0.2% fatty acid free BSA. Beforehand wells were coated with FCS or type I collagen.

For assays with inhibitors, 20 μM PP2, 60 μM SU6656 or 100 nM actinomycin-D was added in suspended cells and during adhesion.

For cholesterol depletion experiments, 10 mM methyl-β-cyclodextrin (Met-β-CD) was incubated 1 h with suspended cells only before adhesion. To examine the effects of cholesterol repletion, this incubation was carried out in the presence of cholesterol (8 mg/ml). Following either cholesterol depletion or depletion/repletion, the cells were washed three times, and then prepared for adhesion assays as described above.

Adhesion kinetics were performed as previously described [12]. Briefly, treated or untreated cells as described above, in single cell suspension, were added to FCS- or type I collagen-coated wells (96-well plate, 10^4 cells/well) and allowed to adhere at 37 °C for different times in the presence of inhibitors. 100% adhesion was measured with the same number of cells fixed by 1% glutaraldehyde. After several washings, attached cells were stained by 0.1% crystal violet and lysed with 1% SDS. Absorbance was then measured at 600 nm.

In all assays, cell viability was controlled by trypan blue exclusion.

2.3. Membrane raft preparation

Highly purified rafts were isolated by extraction with Brij 98 at 37 °C followed by Optiprep density gradient centrifugation, essentially as previously reported [13], allowing us to specifically analyze interactions present at physiological temperature. In brief, ~30×10^6 cells were sonicated (five 5-s bursts, 5 W) in 1 ml of ice-cold buffer A (25 mM HEPES pH 7.6, 150 mM NaCl, 1 mM EGTA, 10 mM NaF, 5 mM Na_3VO_4, 10 mM NaP-P, and a mixture of protease inhibitors). The post-nuclear supernatant was recovered after centrifugation at 800 ×*g* at 4 °C for 10 min, and then extracted with buffer A containing 1% Brij 98 for 5 min at 37 °C. After dilution with Optiprep 60% containing 5% sucrose (final concentration: Optiprep 43%, sucrose 3.3%, Brij 98 0.3%), lysates were chilled down on ice for 1 h and placed in a centrifuge tube. Samples were then overlaid with 1 ml of 30%, 2 ml of 21%, 3 ml of 20%, 2 ml of 19% and 1 ml of 0% Optiprep in buffer A. The gradients were spun at 175,000 ×*g* in a SW41 rotor (Beckmann Instruments) for 16 h at 4 °C. Fractions were collected from top to bottom of centrifuge tubes and the 19% Optiprep layer was diluted 10-fold with buffer A and concentrated by ultracentrifugation (2 h, 100,000 ×*g*). Resuspended pellet was referred to as buoyant fraction or rafts/caveolae fraction. The last 4 ml of the bottom of centrifuge tube corresponding to layers 30% and 43% Optiprep and containing solubilized membrane and cytosolic extract were referred to as high density fraction or non-raft fraction. Buoyant fraction was separated from non-raft fraction by broad layers of Optiprep 21% and 20% to completely prevent the floating of high density molecules. Under these conditions, known non-raft proteins like clathrin heavy chain or Erk1/2 were totally excluded from rafts/caveolae fraction (Supplementary Fig. S1).

2.4. Transfections

FAK cDNA constructs containing the HA1 triple tag were a generous gift of Pr. Steven K. Hanks (Vanderbilt University School of Medicine, Nashville, TN, USA). Briefly, site-directed mutagenesis was used to change codons for FAK phosphoacceptor tyrosines to phenylalanine codons. Eukaryote expression plasmids encoding FAK variants of the different phosphorylation sites were referred to as wild-type- (wt-), F397Y-, F861Y- and F925Y-FAK [1,14].

Batches of 5×10^6 cells were used in each transfection experiment with the Nucleofector™ (Amaxa Biosystems, Germany). Cells were re-suspended in 100 μl Nucleofector™ solution T at room temperature followed by addition of 5 μg of mutated or non-mutated FAK plasmids. Programs T-20 was used for transfecting the cells. Immediately after transfection, cells were plated in culture medium and incubated 48 h at 37 °C in 5% CO_2. Cell viability and transfection efficiencies, determined with control plasmid pmaxGFP (Amaxa Biosystems), were about 50%. Transfected cells were used for adhesion experiments as described above and HA-tagged proteins expression was specifically monitored by Western blot.

2.5. Immunoprecipitation assay

Fraction related to 19% Optiprep layer was homogenized in a glass-Teflon Potter homogenizer with 2% *N*-octyl β-D-glucopyranoside (OGP) as previously published [15]. After overnight incubation with 1 μg of Ab against FAK, protein G-agarose conjugate beads were added

for 1 h at 4 °C with constant stirring. Then, beads were washed three times with 20 mM Tris–HCl (pH 8.0), 1% OGP, 200 mM NaCl, 1 mM EDTA, 10 mM Na_3VO_4, 10 mM NaP-P, 10 mM NaF and a mixture of protease inhibitors and once with PBS. The non-raft fraction was directly diluted in washing buffer described above and submitted to immunoprecipitation assay as described above. In all cases, immunoprecipitated proteins were analyzed by Western blotting.

2.6. Western blot analysis

After different adhesion times, non-adherent cells were gently washed away and pooled with harvested adherent cells to keep the same amount of cells. Proteins extracted and immunoprecipitated samples were subjected to SDS-PAGE (8 or 10% acrylamide), then electrophoretically transferred onto Hybond-C extra nitrocellulose sheets (Amersham) and probed with the indicated primary Abs or HRP-coupled cholera toxin B chain. Bound Abs were then detected according to the ECL protocol. Blots densitometry was quantified with the ImageMaster software (Amersham).

2.7. Statistical analysis

Data shown are means+/−SEM for at least three separate experiments ($n \geq 3$). Statistical differences were analyzed by use of Student's *t* test for paired data. A *P* value <0.05 was considered significant.

3. Results

3.1. Time-course of SW480 cell adhesion and of FAK-Y397 autophosphorylation

The totality of SW480 cells adhered on complex matrix in 4 h (Fig. 1A). At this time, cells remained round and did not spread. Flattening and generation of protrusions were observed only after an additional period of 4 to 6 h. Actinomycin-D, a inhibitor of transcription, did not disturb adhesion time-course showing that protein synthesis was not implied (data not shown). Although extracellular signalings were drastically reduced after cell starvation and suspension, no cell death was observed in these experiments.

Src expression and its tyrosine kinase activity appear particularly raised in many epithelial cancers, including colon carcinomas [6]. To clarify how SFK activity was implied in cell adhesion, PP2 and SU6656, two specific SFK inhibitors, were used. Both potently inhibited SW480 cell adhesion (Fig. 1A) as well as the adhesion of SW620 and HT29D4 cells, two other human colon cancer lines (data not shown). This inhibition was observed on complex matrix but also on type I collagen-coated surfaces (data not shown).

As significance of SFK localization in lipid domains remains largely unknown, the effect of cholesterol disruption by Met-β-CD on SW480 cell adhesion was also tested (Fig. 1A). This reagent potently inhibited

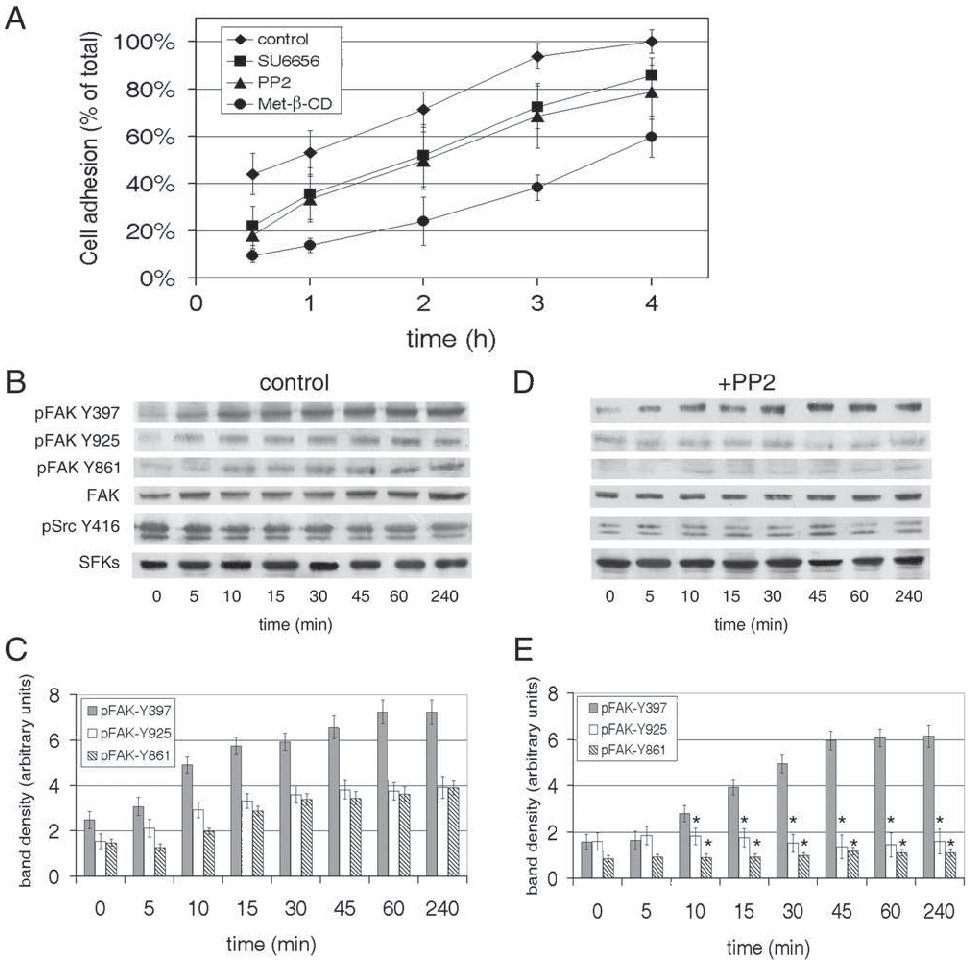

Fig. 1. SW480 cell adhesion kinetics. (A) SW480 cell adhesion kinetics on complex matrix-coated plates were performed in the presence of 20 μM PP2 (▲), 60 μM SU 6656 (■) or after pretreatment with 10 mM Met-β-CD (●) versus untreated control cells (♦). Data were expressed as percent of adherent cells versus total cells. All differences shown between treated versus untreated cells were statistically significant ($P<0.05$). Phosphorylation kinetics of FAK. (B–E) Phosphorylation kinetics of FAK-Y397, -Y861 and -Y925 during SW480 cell adhesion in the absence (B, C) or in the presence of 20 μM PP2 (D, E). (B, D) Western blotting of cell lysates was performed with the indicated antibodies. (C, E) Band densities were quantified and total FAK signal was used as normalization reference to compare the different experiments. In bar graphs, statistically significant differences ($P<0.05$) of FAK-Y397 (grey bars), FAK-Y861 (hatched bars) and FAK-Y925 (white bars) phosphorylations between PP2 treated (E) and control (C) cells were indicated by (*).

SW480 cell attachment, suggesting that early adhesion process needed fully active SFKs and functional lipid domains. In cholesterol depletion, as in SFK inhibition assays, no cell death was observed by trypan blue exclusion assay.

It has been shown that integrin-mediated cell adhesion promotes FAK-Y397 autophosphorylation and FAK/SFK interaction, leading to FAK phosphorylation on Y861 and Y925 [1,2]. Phosphorylation of these residues creates additional protein binding sites named proline-rich region II (Y861 phosphorylation) and Focal Adhesion Targeting (FAT) domain (Y925 phosphorylation).

Therefore, we determined the phosphorylation kinetics of FAK-Y397, -Y861 and -Y925 during SW480 cell adhesion with or without PP2 (Fig. 1B–E). In suspended cells (time 0), FAK was only lightly phosphorylated. FAK-Y397 phosphorylation quickly increased during adhesion, reached a plateau after 1 h and remained maximum during at least 4 h. FAK-Y861 and -Y925 phosphorylation also increased during adhesion with roughly the same time-course (Fig. 1B and C). FAK-Y397 autophosphorylation time-course reflected that cells gradually put down on plate surface during this first hour inducing a quick integrins engagement. However, cells did not firmly adhered at this time since 50% of cells were removed in previous adhesion test with more drastic washings (Fig. 1A).

In the majority of colon tumor cells, Src is constitutively active and an important SFK activity is observed in >80% of colon adenocarcinoma [16]. This appears to be the case in suspended SW480 cells (time 0) and during adhesion (Fig. 1B). However, PP2 potently, but not completely, inhibited SFK activity as confirmed by the strong decrease of Src-Y416 phosphorylation (Fig. 1D). During cell adhesion in the presence of PP2, time-course of FAK-Y397 autophosphorylation did not change drastically, whereas the increase of Y861 and Y925 phosphorylation was completely inhibited (Fig. 1D and E). Thus, during the first hour of adhesion of SW480 cells, integrin engagement quickly induced FAK-Y397 autophosphorylation, independently of SFK activity, but an additional time of 3 h was necessary to reinforce adhesion by downstream mechanisms.

3.2. Lipid domains were enriched in FAK when SFK activity was reduced

Cholesterol disruption strongly inhibited SW480 cell adhesion (Fig. 1A) highlighting the importance of lipid domains. In order to assess how FAK was distributed in raft and non-raft compartments during cell adhesion, lipid domains were extracted on the basis of their resistance to Brij98 solubilization at 37 °C and of their floatation in a low-density layer (Fig. 2). The well established rafts/caveolae-associated protein caveolin-1 and GM1 ganglioside were

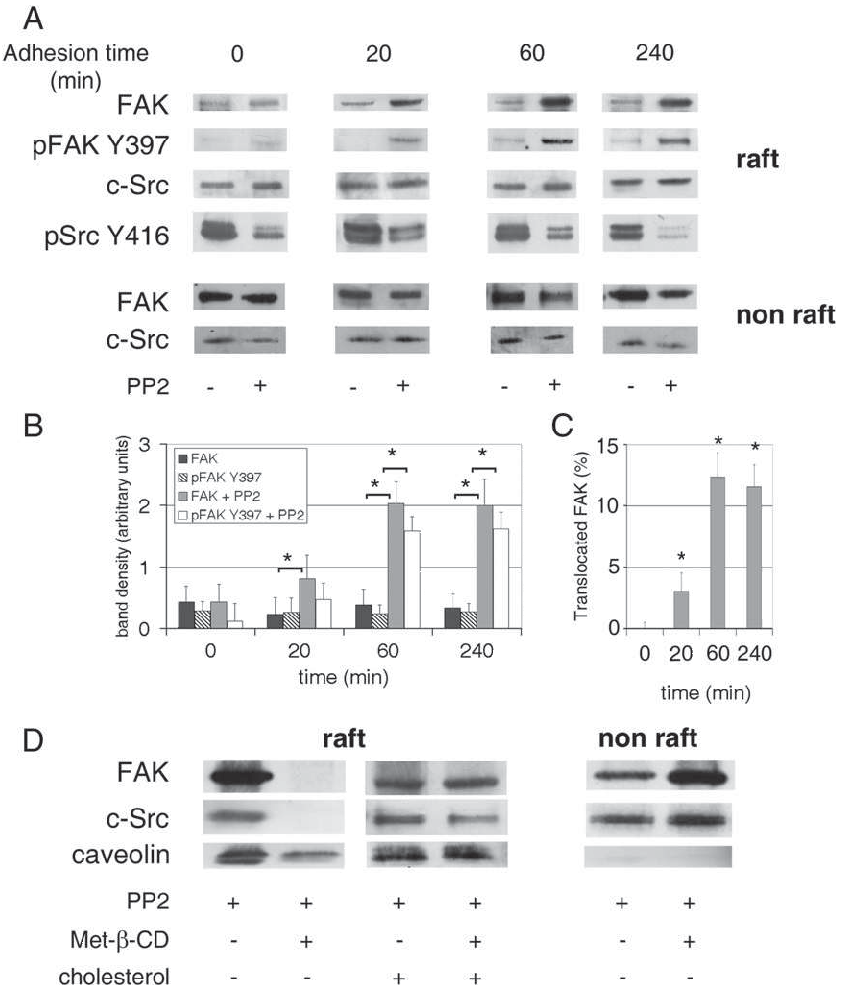

Fig. 2. FAK distribution in raft and non-raft compartments. (A) FAK distribution in raft and non-raft compartments at different times during SW480 cell adhesion in the presence or in the absence of 20 μM PP2. Western blotting of raft and non-raft fractions was performed with the indicated antibodies. (B) Band densities of FAK and p-FAK Y397 were quantified in rafts/caveolae fraction and c-Src signal was used as normalization reference. In bar graphs, statistically significant ($P<0.05$) differences between PP2 treated and untreated cells were indicated by (*). (C) Band density of translocated FAK was quantified and c-Src signal was used as normalization reference. In bar graphs, statistically significant ($P<0.05$) differences in percentage of FAK translocated between PP2-treated and untreated cells were indicated by (*). (D) Effect of cholesterol depletion by 10 mM Met-β-CD or by cholesterol/Me-β-CD complexes on FAK localization in the presence of 20 μM PP2. FAK and caveolin-1 distribution in raft and non-raft compartments was examined by Western blot. C-Src was used as reference to compare the different assays. Shown is a representative assay out of four experiments.

exclusively found in buoyant fraction while the clathrin heavy chain and Erk1/2, two known non-raft proteins, were found only in the heavier fraction Cholesterol depletion and depletion/repletion assays confirmed the correct partitioning of proteins in our purified raft and the non-raft compartment (Supplementary Fig. S1).

Highly purified lipid domains were prepared after various time of adhesion in the presence or in the absence of PP2 (Fig. 2A) and of SU6656 (Supplementary Fig. S2). The amount of FAK observed in rafts/caveolae fraction prepared from suspended cells was very low and did not increase during adhesion. By contrast, a quick increase of FAK concentration was detected in buoyant fraction during adhesion of SFK inhibitors-treated cells, reaching a maximum upon 1 h adhesion (Fig. 2B and Supplementary Fig. S2). In parallel, the amount of FAK phosphorylated on Y397 increased in rafts/caveolae fraction suggesting the importance of activation of SFK binding site for translocation. FAK enrichment in rafts/caveolae fraction was also observed in SW620 and HT29D4 cells treated by PP2 during early stages of adhesion (data not shown).

Synchronously, FAK quantity decreased in non-raft fraction during adhesion only when cells were processed with PP2. Blot quantification showed that the amount of FAK translocated from non-raft to rafts/caveolae fractions reached 12+/−1.9% upon 1 h adhesion (Fig. 2C). However, it is possible that this translocation was minimized because SFK activity was not totally inhibited by PP2 as shown by a residual Src-S416 phosphorylation.

To analyze the effect of cholesterol depletion on FAK localization, SW480 cells in suspension were treated with Met-β-CD before adhesion in the presence of PP2 (Fig. 2D). Treatment induced a drastic shift of FAK and c-Src from the buoyant fraction to high density fraction confirming FAK localization in cholesterol-dependent microdomains. However, Met-β-CD did not efficiently delocalize caveolin-1 compared to drastic shift of FAK and c-Src, suggesting that these two proteins could be associated to lipid rafts rather than caveolae. To ensure that this was a specific effect of cholesterol depletion, cells were treated with Met-β-CD in the presence of cholesterol. The shift in the localization of FAK, c-Src and caveolin-1 was fully reversed with cholesterol/Me-β-CD complexes, indicating that association of these molecules with detergent-resistant membrane microdomains is actually cholesterol-dependent.

Altogether, these data supported the idea that, during early adhesion of colon carcinoma cells, a fraction of FAK is blocked in buoyant fraction when SFK activity was reduced. As FAK is not described as located in lipid domains and has no domain allowing a direct association, we hypothesized that FAK localization in lipid microdomains was dependent on interactions with SFK members and could be transient. This idea was reinforced by the parallel increase of amount of FAK phosphorylated on Y397 in rafts/caveolae fraction.

3.3. FAK accumulation in lipid domains was controlled by Tyr phosphorylation

To clarify whether FAK phosphorylation sites were involved in raft localization, FAK mutants, in which tyrosine phosphorylation sites

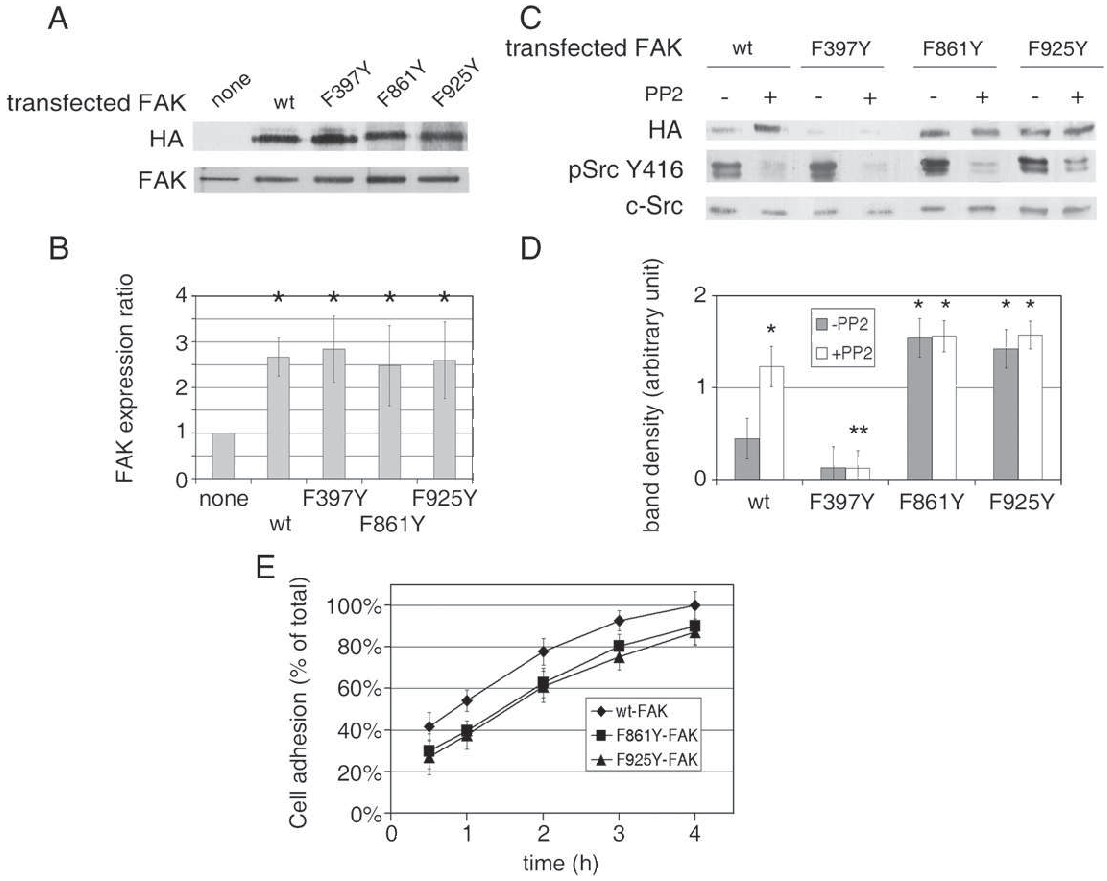

Fig. 3. FAK variant distribution in raft and non-raft compartments. (A, B) Expression of HA-tagged FAK variants in SW480 cells 48 h after transfection. (A) Western blotting of untransfected (none) and transfected cell lysates was performed with the indicated antibodies. (B) FAK amounts were quantified with the ImageMaster software. In bar graph, statistically significant ($P<0.05$) differences of FAK expression ratios between transfected versus untransfected cells were indicated by (*). (C, D) Distribution of HA-tagged FAK variants in raft compartment was examined in SW480 cells after 1 h adhesion in the presence or in the absence of 20 μM PP2. (C) Immunoblots were analyzed using indicated antibodies. (D) Band densities were quantified in rafts/caveolae fraction and c-Src signal was used as normalization reference. In bar graph, statistically significant ($P<0.05$) differences of HA signal were indicated by (*) between the FAK variants versus wt-FAK transfected cells without PP2 or by (**) to compare HA signal in presence of PP2 in transfected cells by F397Y- versus wt-FAK. (E) Adhesion kinetics on complex matrix-coated plates of SW480 cells transfected with wt- (◆), F861Y- (■) or F925Y-FAK (▲) plasmids. Data were expressed as percent of adherent cells versus total cells. All differences shown between FAK mutants versus wild-type transfected cells were statistically significant ($P<0.05$, $n=8$).

were mutated to phenylalanine, were expressed in SW480 cells (Fig. 3). A non-mutated FAK protein (wt) was also expressed as a control. All these proteins carried a HA tag allowing to detect only the expression of transfected FAK. 48 h after the transfection shock, surviving cells recovered a normal morphology. Moreover, transfected cells with wt-FAK vector displayed the same adhesion kinetics compared to non-transfected cells (Fig. 3E versus Fig. 1A). All mutants were expressed at equivalent levels (Fig. 3A) and increased the FAK amount in transfected cells of about 2.5-fold compared to non-transfected cells (Fig. 3B).

Distribution of these FAK mutants was investigated in rafts/caveolae domains after 1 h adhesion (Fig. 3C and D). Wt-FAK concentration was low in untreated cells, but increased when SFK activity was inhibited by PP2 as observed with endogenous FAK. Importantly, almost no F397Y-FAK was detected in lipid microdomains whether or not cells were treated with PP2. Thus, FAK localization in lipid domain was controlled by FAK-Y397 phosphorylation that activates the SFK binding site.

Expressed F861Y- and F925Y-FAK were detected in buoyant domains from untreated cells in concentration equivalent to that observed with wt-FAK in PP2-treated cells. Moreover, PP2 treatment had no effect on their location in buoyant fraction. Thus, FAK delocalization out of lipid rafts/caveolae domains was controlled by Tyr phosphorylations dependent on SFK kinase activity in the FAT and proline-rich regions of FAK. This result was confirmed by co-localization assays of GM1 with F861Y- and F925Y-FAK mutants (Supplementary Fig. S3).

Adhesion assays were performed with cells expressing wt-, F861Y- or F925Y-FAK mutants (Fig. 3E). If wt-FAK had no effect on kinetics, both FAK variants slowed down SW480 adhesion, but the effect was less important than that obtained after treatment with PP2. This result must be largely underestimated because only 50% of cells were transfected and endogenous FAK level remained considerable in transformed cells.

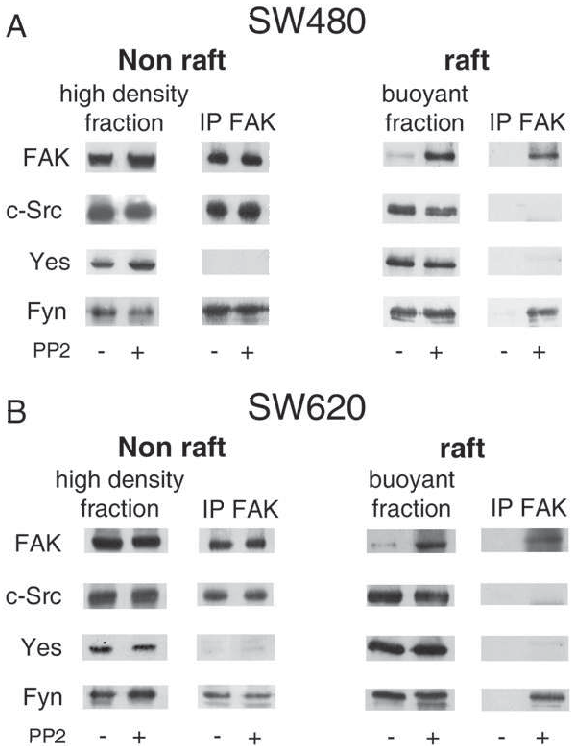

Fig. 4. FAK interactions with c-Src, Yes and Fyn in raft and non-raft compartments. In SW480 (A) and SW620 (B) cells, the distribution of FAK, c-Src, Yes and Fyn was tested in raft and non-raft fractions and in immunoprecipitated samples by antibodies against FAK of each compartments (IP FAK) in the presence or in the absence of 20 μM PP2. Proteins were revealed with the indicated antibodies on separated immunoblots for each SFKs tested. Western immunoblottings shown were representative of three different assays.

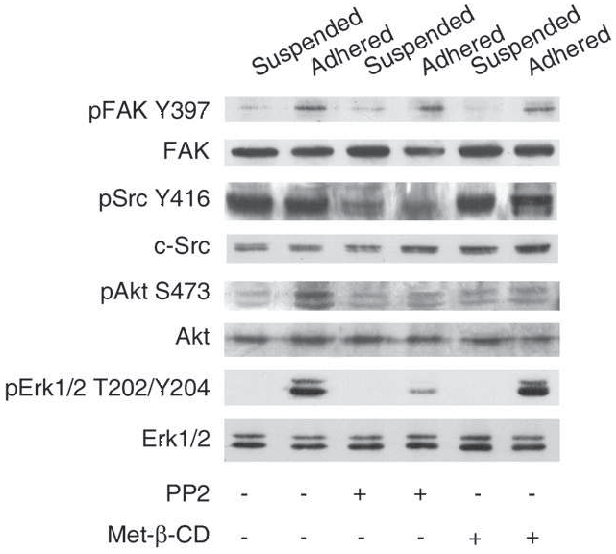

Fig. 5. Phosphorylation levels of FAK, SFKs, Akt and Erk1/2 after 1 h of adhesion. Disturbing action of 20 μM PP2 or of pretreatment with 10 mM Met-β-CD on FAK, SFKs, Akt and Erk1/2 phosphorylation levels was analyzed in suspended and in 1 h adhered cells. Western blotting of cell lysates was performed using indicated antibodies. Shown is a representative experiment out of four individual assays.

Altogether, these data support the idea that FAK is transiently co-located with SFKs in rafts/caveolae domains during early adhesion process. The quick Y397 phosphorylation induced by adhesion (Fig. 1B–E) activated the SFK binding site and subsequently caused the partial localization of FAK in lipid microdomains (Fig. 2A). Delocalization out of these domains was regulated by SFKs-dependent phosphorylation of tyrosine in FAT or proline-rich regions (Fig. 3C). In addition, disturbance in the FAK phosphorylation process induced perturbation of early adhesion.

3.4. FAK was associated with different SFK members in raft and non-raft domains

Widely coexpressed SFK members c-Src, Fyn and Yes are involved in various cellular events, including proliferation, survival, adhesion and migration, and often act downstream of receptor tyrosine kinases. They are absolutely required to mediate specific functions regulated by ECM proteins and tyrosine phosphorylation of focal adhesion proteins, including FAK.

Thus, to analyze the interactions of c-Src, Yes and Fyn with FAK in lipid domains, co-immunoprecipitation studies were performed using raft and non-raft fractions prepared from 1 h adhered SW480 and SW620 cells in the presence or in the absence of PP2 (Fig. 4). The three isoforms were expressed in cells, but only c-Src and Fyn interacted with FAK in non-raft fraction as previously described [17]. These interactions were not disturbed by PP2 treatment. In contrast, although the three isoforms were also detected in rafts/caveolae fraction, only Fyn was co-immunoprecipitated with FAK in buoyant fraction of PP2-treated SW480 and SW620 cells suggesting that Fyn is the specific partner of FAK in lipid domains during the first hour of adhesion.

3.5. MAPK and PI3K/Akt signalings were differently altered by Met-β-CD

In addition to its kinase activity, FAK–SFK complex has been suggested to act as a platform to integrate multiple signaling

pathways in response to extracellular stimuli [18]. MAPK/Erk1/2 and PI3K/Akt pathways were both known to be activated by integrin receptor binding to ECM in different cell types [19,20].

Actions of PP2 and Met-β-CD on phosphorylation levels of FAK, SFKs, Akt and Erk1/2 were compared in suspended and in 1 h adhered cells (Fig. 5). In parallel to FAK-Y397 phosphorylation, Akt-S473 and Erk1/2-T202/Y204 were phosphorylated revealing activation of PI3K and Erk signaling pathways. As previously observed (Fig. 1B–E), PP2 did not change FAK-Y397 phosphorylation, but totally prevented activation of PI3K and Erk pathways. In contrast, Met-β-CD did not change FAK-Y397 phosphorylation, but completely prevented Akt-S473 phosphorylation without affecting Erk1/2 phosphorylation. Thus, raft integrity was crucial for the activation of PI3K/Akt but not of MAPK/Erk pathways during the first hour of adhesion process.

To clarify how these two pathways were regulated during the first 4 h of adhesion, activation kinetics of PI3K/Akt and MAPK/Erk signalings were compared in the absence (Fig. 6A and B) or in the presence of Met-β-CD (Fig. 6C and D). Without Met-β-CD, Akt-1 phosphorylation reached a plateau after 45 min of adhesion and then remained maximum. In contrast, Erk1/2 phosphorylation increased gradually during the 4 h tested.

Met-β-CD totally prevented Akt-S473 but not Erk1/2 phosphorylation (Fig. 6C and D) whereas cholesterol repletion allowed a correct Akt1 activation (Fig. 6E and F), suggesting that lipid raft has an important role in the regulation of PI3K/Akt signaling pathway induced during early cell adhesion. As previously described, this signaling can be triggered by direct targeting of PI3K regulatory subunit p85α [21] or of Akt-1 [22] in raft microdomains. However, Akt-1 was not detected in our rafts/caveolae fraction (data not shown). Moreover, although p85α was detected in our buoyant fraction, we failed to highlight an increased amount of p85α upon PP2 treatment. Thus, the increase of Akt phosphorylation observed in early time of adhesion did not seem related to a direct targeting of p85α subunit or of Akt-1 in lipid rafts.

Kinetics of Akt-S473 phosphorylation, revealing PI3K/Akt pathway activation, was in strong correlation with time-course of FAK-Y397 phosphorylation that was the reflection of integrin engagement. Moreover, Akt phosphorylation was SFK activity-dependent. Thus, PI3K/Akt pathway activation must be connected to the interaction between FAK and members of the SFKs. As this process was also sensitive to Met-β-CD, a cholesterol perturbing reagent, we hypothesize that this interaction takes place in membrane lipid microdomains where Fyn interacts with FAK in early adhesion.

4. Discussion

Signaling pathway during cell adhesion involves a series of sequential phosphorylation events initiated by FAK/SFK interaction. In this work, we analyzed the activation kinetics and timeline localization of FAK/SFK association and of PI3K and MAPK signaling induced by early adhesion of SW480 cells.

Cell starvation and suspension in FCS- and calcium-free medium allowed to inactivate almost completely PI3K/Akt and MAPK/Erk signaling pathways and decreased strongly FAK phosphorylation. In contrast, SFK activation remains unchanged. Indeed, these cells, like a majority of colon cancer lines, are known to own high intrinsic Src activity [23]. In these conditions, plating of these isolated cells on complex matrix in the absence of other stimulating factors was supposed to induce only adhesion pathways related to integrins.

Our results provide evidence that a fraction of FAK was directed toward lipid rafts/caveolae domains during early adhesion. This process was controlled by autophosphorylation of Y397 induced by integrin engagement. This is in agreement with recent data suggesting that FAK can be integrated into lipid microdomains. In adherent B16 melanoma cells, ~10% of total FAK is detected in low-density fraction and is associated with GM3. Rho A (50%), Ras H (95%) and c-Src (90%) are also detected in this fraction [24,25]. In adherent pro-B cells, stimulation by CXL chemokine ligand 12 induces FAK-Y397 phosphorylation and recruitment of FAK and PI3K regulating subunit p85 into lipid membrane domains [26]. In endothelial cells, detachment also induced a rapid decrease in membrane order correlated with cholera toxin subunit B-stained domains internalization. During adhesion, membrane fluidity decreases and phosphorylated FAK and caveolin-1 are located in ordered domains [27]. We excluded from discussion some reports on FAK localization in detergent-resistant membrane (DRM) or detergent-insoluble membrane (DIM) because the extraction procedure uses only one property of lipid domains and rafts/caveolae fractions can be contaminated by unrelated proteins.

In parallel with FAK targeting to buoyant fraction, we observed that FAK was continuously translocated out of lipid rafts/caveolae domains

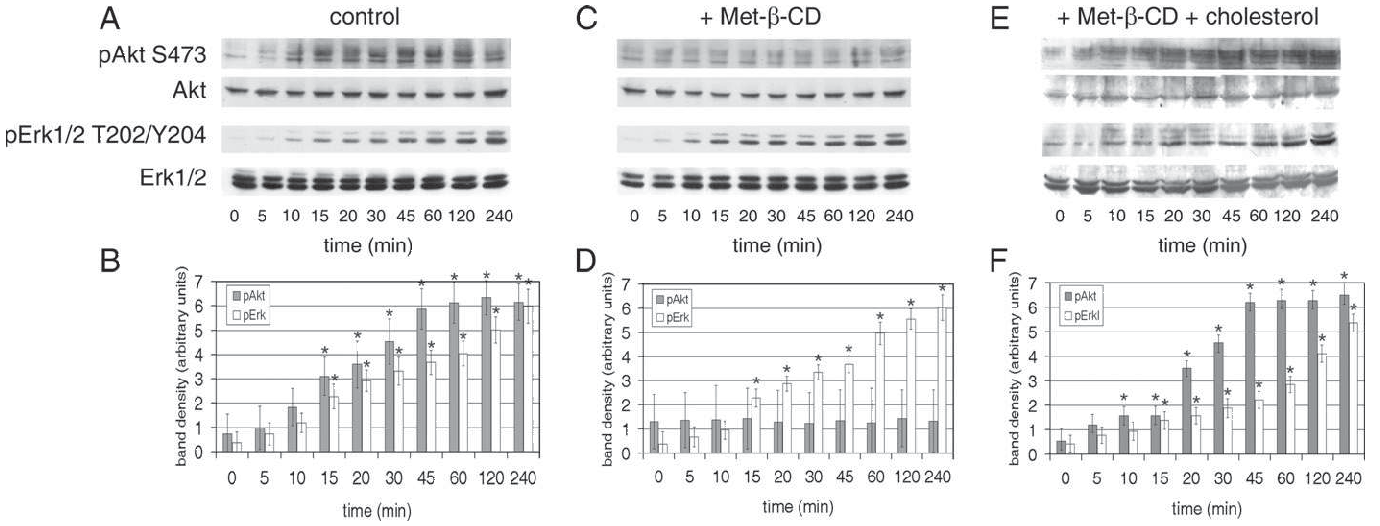

Fig. 6. Phosphorylation kinetics of Akt-S473 and Erk1/2-T202/Y204 during adhesion of untreated SW480 cells (A, B), after pretreatment with 10 mM Met-β-CD (C, D) or after pretreatment with 10 mM Met-β-CD and cholesterol repletion (E, F). (A, C and E) Western blotting of cell lysates was performed using indicated antibodies. (B, D and F) Blot densities were quantified with the ImageMaster software. Total Akt and Erk 1/2 signals were used as normalization reference to compare their respective phosphorylations. In bar graphs, statistically significant ($P<0.05$) differences between Akt-S473 (black bars) and Erk1/2-Erk1/2-T202/Y204 (white bars) phosphorylations of three independent assays at different times versus initial time were indicated by (*).

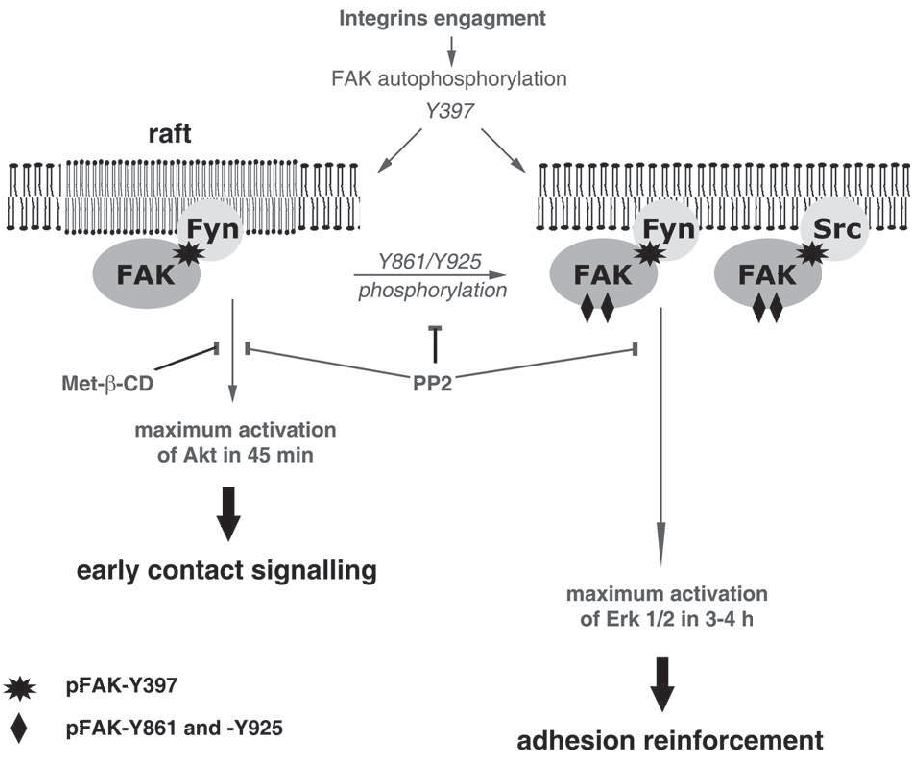

Fig. 7. Schematic summary and working model of data presented in this study. Integrins engagement induces quick FAK-Y397 autophosphorylation and subsequent translocation of a fraction of FAK in raft compartments. In lipid domains, FAK interacts only with Fyn while it interacts with c-Src and Fyn in non-raft fraction. A parallel FAK translocation from raft to non-raft domain occurs and is FAK-Y861 and/or -Y925 phosphorylation-dependent. In parallel, a PI3K/Akt signaling is quickly activated and is dependent on lipid domain integrity. A MAPK/Erk1/2 signaling is activated with longer kinetics and is not dependent on lipid domain integrity. Both signaling pathways contribute to adhesion process of SW480 cells.

likely under control of Y861 and/or Y925 phosphorylation by SFKs. Moreover, transfection by FAK variants of these two tyrosines reduced adhesion kinetics of SW480 cells. Several other reports highlighted the crucial role of FAK C-terminal domains in cell adhesion process. Thus, upon activation, FAK co-localizes at focal adhesions and structural studies have shown that the FAT domain is responsible for this localization [4]. Interestingly, adenoviral transduction of a DNA segment encoding the FAT domain resulted in cellular rounding and loss of adhesion of breast cancer cells [28]. By contrast, overexpression of FAK C-terminal fragment in MDCK cells triggers Erk phosphorylation, which in turn facilitates cells spreading and lipid raft-dependent migration [29]. These results and our contribution suggest that FAK C-terminal domains are important in cell adhesion and consecutive spreading. Therefore, as FAK-Y861 and -Y925 phosphorylation activate protein binding sites, we hypothesize that FAK translocation out of lipid domains could be induced by interactions with other molecules in FAT and/or proline-rich domains. To our knowledge, this is the first time that FAK was reported dynamically localized in lipid raft under control of phosphorylation by SFKs.

In consideration of their dynamic properties, lipid rafts could function as microcompartments for the preassembly of signaling complexes integrating SFKs [30]. In $Src^{(-/-)}$, $Yes^{(-/-)}$ and $Fyn^{(-/-)}$ fibroblasts, expression of palmitoyl-modulated mutants of these SFKs restores specifically FAK tyrosine phosphorylation on Y861, highlighting the importance of the correct subcellular location of SFKs in lipid domains [31]. Thus, in mouse fibroblasts, Fyn, Src, Yes and Lyn are detected in lipid domain, but only Fyn remain permanently present and concentrated in lipid rafts, whereas Src is transiently relocated to non-raft fraction during cell adhesion. In these cells, Fyn localized in rafts is the predominant kinase for Cbp, a C-terminal Src binding protein, which serves as a sensor of adhesion [32]. Moreover, during cell-matrix interaction of fibroblasts, Fyn but not Src is recruited to focal contacts at early times (30 min) and its palmitoylation is required for this recruitment. Fyn and its substrate p130Cas are also involved in the rigidity response and accelerate cell spreading [33]. Indeed, although all SFKs are myristoylated and have the ability to attach the cellular membrane, only Fyn is palmitoylated in its N-terminal domain and strongly associated to rafts, suggesting that Fyn can play a specific role in lipid domain. This is in accordance to our present data showing that Fyn was the specific SFKs that interacted with FAK in lipid rafts/caveolae domain during early stage of adhesion.

MAPK/Erk and PI3K/Akt signaling pathways were activated during SW480 cell adhesion. Both activations were SFKs-dependent, but only Akt phosphorylation was sensitive to cholesterol disturbing. Other reports describe a role for lipid rafts in PI3K/Akt modulation. For instance, in Vero cells stimulated by LPA, p85α is found located in lipid rafts and cholesterol depletion specifically modulates phosphorylation of Akt-1, but not of Erk1/2 [34]. In the same way, in newly formed oligodendrocytes, lipid raft integrity is required for PI3K activation elicited by PDGF [35] and, in LNCaP prostate cancer cells, a subpopulation of Akt-1 is specifically activated in lipid fractions [22]. Moreover, in cells derived from small cell lung cancer, the PI3K/Akt signaling in response to growth factors stimulation is dependent on lipid raft integrity in contrast to Ras activation [36].

If these reports underline the importance of lipid domains in activation of PI3K/Akt pathway, our work shows for the first time that FAK in lipid raft can act as a signaling intermediate regulated by Fyn during early adhesion process. We did not find an increase of p85α quantity or a Akt-1 recruitment in lipid fraction as previously described [21,22]. However p85α was detected in buoyant fraction. Thus, we hypothesize that Akt pathway activation probably resulted from phosphorylations events initiated in raft microdomain by PI3K and was implied in a positive environmental signal induced by ECM contact [37]. Moreover, other isoforms of PI3K could be implied in this activation.

During SW480 cell adhesion, we observed that MAPK/Erk signaling required longer time than PI3K/Akt pathway to be fully activated. Several authors reported differences in MAPK and PI3K pathways

activation during cell adhesion. During adhesion of Caco-2 cells, FAK/Src signaling contributes to the activation of PI3K/Akt and MAPK/Erk pathways in undifferentiated cells, but does not influence PI3K/Akt signal in differentiated ones [38]. In suspended epithelial cells, physical forces, such as shear and pressure, stimulate adhesion by increasing FAK phosphorylation and subsequently by modulating integrins binding affinity. This force-activated adhesiveness involves Src, PI3K and Akt-1 but not Erk [39], indicating that these two pathways seems regulated by different independent processes during cell adhesion. Particularly, the recruitment of several focal adhesion-associated proteins and activation of MAPK/Erk need the clustering of integrins/FAK complexes [40], suggesting that the observed duration of Erk1/2 phosphorylation depends on the time necessary to build these clusters and to obtain a strong adhesion.

A schematic diagram was proposed in Fig. 7 to summarize our results and integrated the effects of inhibitory reagents. No doubt that an exact structural and biochemical definition of how FAK acts in concert with other molecules to reinforce adhesion and initiate spreading will be a fascinating target of future studies.

Acknowledgements

We thank Pr S.K. Hanks (Department of Cell and Developmental Biology, Vanderbilt University School of Medicine, Nashville, Tennessee, USA) for kindly providing variants FAK plasmids and Pr M. Bracke (Department of Radiotherapy and Experimental Cancer, University Hospital Gent, Belgium) for gift of SW480 and SW620 colon cancer lines.

We thank Dr M. Lehmann and Dr F. Andre for their critical comments on manuscript. Our research was supported by the Cancéropôle Provence Alpes Côte d'Azur and Association pour la Recherche sur le Cancer (ARC).

Appendix A. Supplementary data

Supplementary data associated with this article can be found, in the online version, at doi:10.1016/j.bbamcr.2008.08.008.

References

[1] M.B. Calalb, T.R. Polte, S.K. Hanks, Tyrosine phosphorylation of focal adhesion kinase at sites in the catalytic domain regulates kinase activity: a role for Src family kinases, Mol. Cell. Biol. 15 (1995) 954–963.
[2] D.D. Schlaepfer, T. Hunter, Evidence for in vivo phosphorylation of the Grb2 SH2-domain binding site on focal adhesion kinase by Src-family protein-tyrosine kinases, Mol. Cell. Biol. 16 (1996) 5623–5633.
[3] D.D. Schlaepfer, S.K. Mitra, Multiple connections link FAK to cell motility and invasion, Curr. Opin. Genet. Dev. 14 (2004) 92–101.
[4] J.T. Parsons, Focal adhesion kinase: the first ten years, J. Cell Sci. 116 (2003) 1409–1416.
[5] R.A. Klinghoffer, C. Sachsenmaier, J.A. Cooper, P. Soriano, Src family kinases are required for integrin but not PDGFR signal transduction, EMBO J. 18 (1999) 2459–2471.
[6] M.C. Frame, Src in cancer: deregulation and consequences for cell behaviour, Biochim. Biophys. Acta 1602 (2002) 114–130.
[7] X. Liang, A. Nazarian, H. Erdjument-Bromage, W. Bornmann, P. Tempst, M.D. Resh, Heterogeneous fatty acylation of Src family kinases with polyunsaturated fatty acids regulates raft localization and signal transduction, J. Biol. Chem. 276 (2001) 30987–30994.
[8] F. Galbiati, B. Razani, M.P. Lisanti, Emerging themes in lipid rafts and caveolae, Cell 106 (2001) 403–411.
[9] A. Kusumi, K. Suzuki, Toward understanding the dynamics of membrane-raft-based molecular interactions, Biochim. Biophys. Acta 1746 (2005) 234–251.
[10] S.K. Mitra, D.D. Schlaepfer, Integrin-regulated FAK-Src signaling in normal and cancer cells, Curr. Opin. Cell Biol. 18 (2006) 516–523.
[11] J. Fantini, B. Abadie, A. Tirard, L. Remy, J.P. Ripert, A. el Battari, J. Marvaldi, Spontaneous and induced dome formation by two clonal cell populations derived from a human adenocarcinoma cell line, HT29, J. Cell Sci. 83 (1986) 235–249.
[12] A. Kadi, V. Pichard, M. Lehmann, C. Briand, D. Braguer, J. Marvaldi, J.B. Rognoni, J. Luis, Effect of microtubule disruption on cell adhesion and spreading, Biochem. Biophys. Res. Commun. 246 (1998) 690–695.
[13] M. Remacle-Bonnet, F. Garrouste, G. Baillat, F. Andre, J. Marvaldi, G. Pommier, Membrane rafts segregate pro- from anti-apoptotic insulin-like growth factor-I receptor signaling in colon carcinoma cells stimulated by members of the tumor necrosis factor superfamily, Am. J. Pathol. 167 (2005) 761–773.
[14] M.B. Calalb, X. Zhang, T.R. Polte, S.K. Hanks, Focal adhesion kinase tyrosine-861 is a major site of phosphorylation by Src, Biochem. Biophys. Res. Commun. 228 (1996) 662–668.
[15] P. Munoz, M.C. Navarro, E.J. Pavon, J. Salmeron, F. Malavasi, J. Sancho, M. Zubiaur, CD38 signaling in T cells is initiated within a subset of membrane rafts containing Lck and the CD3-{zeta} subunit of the T cell antigen receptor, J. Biol. Chem. 278 (2003) 50791–50802.
[16] M.S. Talamonti, M.S. Roh, S.A. Curley, G.E. Gallick, Increase in activity and level of pp60c-src in progressive stages of human colorectal cancer, Clin. Invest. 91 (1993) 53–60.
[17] B.S. Cobb, M.D. Schaller, T.H. Leu, J.T. Parsons, Stable association of pp60src and pp59fyn with the focal adhesion-associated protein tyrosine kinase, pp125FAK, Mol. Cell. Biol. 14 (1994) 147–155.
[18] D.J. Webb, K. Donais, L.A. Whitmore, S.M. Thomas, C.E. Turner, J.T. Parsons, A.F. Horwitz, FAK-Src signalling through paxillin, ERK and MLCK regulates adhesion disassembly, Nat. Cell Biol. 6 (2004) 154–161.
[19] D.D. Schlaepfer, T. Hunter, Focal adhesion kinase overexpression enhances Ras-dependent integrin signaling to ERK2/mitogen-activated protein kinase through interactions with and activation of c-Src, J. Biol. Chem. 272 (1997) 13189–13195.
[20] D.G. Stupack, D.A. Cheresh, Get a ligand, get a life: integrins, signaling and cell survival, J. Cell Sci. 115 (2002) 3729–3738.
[21] H.C. Chen, P.A. Appeddu, H. Isoda, J.L. Guan, Phosphorylation of tyrosine 397 in focal adhesion kinase is required for binding phosphatidylinositol 3-kinase, J. Biol. Chem. 271 (1996) 26329–26334.
[22] R.M. Adam, N.K. Mukhopadhyay, J. Kim, D. Di Vizio, B. Cinar, K. Boucher, K.R. Solomon, M.R. Freeman, Cholesterol sensitivity of endogenous and myristoylated Akt, Cancer Res. 67 (2007) 6238–6246.
[23] T.C. Windham, N.U. Parikh, D.R. Siwak, J.M. Summy, D.J. McConkey, A.J. Kraker, G.E. Gallick, Src activation regulates anoikis in human colon tumor cell lines, Oncogene 21 (2002) 7797–7807.
[24] S.I. Hakomori, Cell adhesion/recognition and signal transduction through glycosphingolipid microdomain, Glycoconj. J. 17 (2000) 143–151.
[25] K. Iwabuchi, S. Yamamura, A. Prinetti, K. Handa, S.I. Hakomori, GM3-enriched Microdomain involved in cell adhesion and signal transduction through carbohydrate-carbohydrate interaction in mouse melanoma B16 cells, J. Biol. Chem. 273 (1998) 9130–9138.
[26] Y. Le, M. Honczarenko, A.M. Glodek, D.K. Ho, L.E. Silberstein, CXC chemokine ligand 12-induced focal adhesion kinase activation and segregation into membrane domains is modulated by regulator of G protein signaling 1 in Pro-B cells, J. Immunol. 174 (2005) 2582–2590.
[27] K. Gaus, S. Le Lay, N. Balasubramanian, M.A. Schwartz, Integrin-mediated adhesion regulates membrane order, J. Cell Biol. 174 (2006) 725–734.
[28] L.H. Xu, X. Yang, R.J. Craven, W.G. Cance, The COOH-terminal domain of the focal adhesion kinase induces loss of adhesion and cell death in human tumor cells, Cell Growth Differ. 9 (1998) 999–1005.
[29] W.C. Wei, Y.C. Hsu, W.T. Chiu, C.Z. Wang, C.M. Wu, Y.K. Wang, M.R. Shen, M.J. Tang, Low substratum rigidity of collagen gel promotes ERK phosphorylation via lipid raft to augment cell migration, J. Cell. Biochem. 103 (2007) 1111–1124.
[30] P.F. Lenne, L. Wawrezinieck, F. Conchonaud, O. Wurtz, A. Boned, X.J. Guo, H. Rigneault, H.T. He, D. Marguet, Dynamic molecular confinement in the plasma membrane by microdomains and the cytoskeleton meshwork, EMBO J. 25 (2006) 3245–3256.
[31] E. Sandilands, V.G. Brunton, M.C. Frame, The membrane targeting and spatial activation of Src, Yes and Fyn is influenced by palmitoylation and distinct RhoB/RhoD endosome requirements, J. Cell Sci. 120 (2007) 2555–2564.
[32] T. Shima, S. Nada, M. Okada, Transmembrane phosphoprotein Cbp senses cell adhesion signaling mediated by Src family kinase in lipid rafts, Proc. Natl. Acad. Sci. 100 (2003) 14897–14902.
[33] A. Kostic, M.P. Sheetz, Fibronectin rigidity response through Fyn and p130Cas recruitment to the leading edge, Mol. Biol. Cell. 17 (2006) 2684–2695.
[34] C. Peres, A. Yart, B. Perret, J.P. Salles, P. Raynal, Modulation of phosphoinositide 3-kinase activation by cholesterol level suggests a novel positive role for lipid rafts in lysophosphatidic acid signalling, FEBS Lett. 534 (2003) 164–168.
[35] L. Decker, C. Ffrench-Constant, Lipid rafts and integrin activation regulate oligodendrocyte survival, J. Neurosci. 24 (2004) 3816–3825.
[36] A. Arcaro, M. Aubert, M.E. Espinosa del Hierro, U.K. Khanzada, S. Angelidou, T.D. Tetley, A.G. Bittermann, M.C. Frame, M.J. Seckl, Critical role for lipid raft-associated Src kinases in activation of PI3K-Akt signalling, Cell Signal. 19 (2007) 1081–1092.
[37] E.J. Müller, L. Williamson, C. Kolly, M.M. Suter, Outside-in signaling through integrins and cadherins: a central mechanism to control epidermal growth and differentiation? J. Invest. Dermatol. 128 (2008) 501–516.
[38] V. Bouchard, M.J. Demers, S. Thibodeau, V. Laquerre, N. Fujita, T. Tsuruo, J.F. Beaulieu, R. Gauthier, A. Vézina, L. Villeneuve, P.H. Vachon, Fak/Src signaling in human intestinal epithelial cell survival and anoikis: differentiation state-specific uncoupling with the PI3-K/Akt-1 and MEK/Erk pathways, J. Cell. Physiol. 212 (2007) 717–728.
[39] M.D. Basson, An intracellular signal pathway that regulates cancer cell adhesion in response to extracellular forces, Cancer Res. 68 (2008) 2–4.
[40] B.Z. Katz, S. Miyamoto, H. Teramoto, M. Zohar, D. Krylov, C. Vinson, J.S. Gutkind, K. M. Yamada, Direct transmembrane clustering and cytoplasmic dimerization of focal adhesion kinase initiates its tyrosine phosphorylation, Biochim. Biophys. Acta 1592 (2002) 141–152.

Annexe 5

HIV-1 Infected Patients have Antibodies Recognizing Folded Tat

Sonia Mediouni, Gilbert Baillat, Albert Darque, Isabelle Ravaux and Erwann Loret*

Equipe de Recherche Technologique 2011, Faculté de Pharmacie, 27 BD Jean Moulin, 13385 Marseille, France

Abstract: Tat is a regulatory viral protein known as transactivator of HIV-1 genes but Tat is also secreted in the blood from HIV-1 infected cells. Extra cellular Tat can cross cellular membranes to trigger apoptosis and might explain the incapacity of the cellular immunity to eliminate HIV-1 infected cells. There is a controversy regarding Tat structure with studies suggesting that Tat would be a naturally unfolded protein. Here, we show that synthetic Tat variants need to be folded to have a transactivation activity in a cellular assay but this folding is unstable regarding the buffers and/or pH used as solvent. We show also that the recognition of a Tat variant versus peptides, covering its sequence, was different. Using an indirect ELISA method with 40 sera from volunteer HIV-1 infected patients, we show that Tat was recognized by 19 human sera either exclusively (n=8) or with Tat peptides (n=11). Dot Blot showed that unfolded Tat was no longer detectable by sera of the first group (n=8) compared to folded Tat. As a conclusion, this study suggests that Tat could be a naturally folded protein in the blood of HIV infected patients.

Keywords: Antibodies, HIV-1, infected patients, Oyi, Tat, vaccine.

INTRODUCTION

Tat was first described as a HIV-1 cycle regulatory protein [1], but Tat is also the only HIV-1 protein to be functionally secreted by HIV-1 infected CD4 T cells [2]. Tat is secreted very early following HIV-1 infection and Tat appears to play a key role in preventing HIV-1 infected cells to be eliminated by the cellular immune system [3]. The inhibition of the cells involved in the cellular immunity could be related to the amazing capacity of Tat to cross membranes, to bind to cytoskeleton proteins called tubulins, triggering the mitochondrial apoptosis [3]. Therefore, a therapeutic vaccine targeting Tat could restore the cellular immunity against HIV-1 infected cells [4].

Tat is a short protein encoded by two exons with a variable size from 86 to 101 residues. Mutations up to 40 % are observed among Tat variants regarding HIV-1 subtypes (or clades) without loss of transactivation activity [3]. However, these mutations affect the cross clades recognition since a serological survey made on HIV-1 infected patients from Uganda (n=80) showed that the cross-reactivity of anti-Tat IgG in these patients is subtype-specific and that all Tat variants are not recognized [5]. It is interesting to note that only almost half (46%) of these patients had antibodies against Tat [5]. Moreover, the patients who had Tat antibodies progressed to AIDS as the patients from the same cohort who had no Tat antibodies [6]. These studies in Uganda show that regular Tat variants in the blood of HIV-1 infected patients who progress to AIDS can not generate cross clades and neutralizing antibodies against extra cellular Tat variants [3].

A Tat vaccine using the Tat Oyi variant has the capacity to trigger an immune response characterized by a cross clades recognition of Tat variants [3, 7]. Due to specific mutations, Tat Oyi can transform the only highly conserved surface in Tat variants as a conformational (3D) epitope and induce neutralizing antibodies against Tat variants from different HIV-1 clades [3]. Therefore, this vaccine approach is based on the presence of conserved folding in Tat variants. Three 2D NMR studies with Tat variants having the transactivation activity in a cellular assay showed that there is a conserved folding among Tat variants with localized structural variations due to mutations [8-10]. However, a 2D-NMR study of a peptide corresponding to a first exon of Tat (1-72) showed that no structure could be identified in this peptide and concluded that Tat variants were natively unfolded proteins [11]. Recently, the crystal structure of Tat in a complex with different human proteins reveals that Tat can have a structure and adapts its folding regarding its function [12].

The main purpose of this study was to know if antisera from HIV-1 infected patients could recognize a conformational structure of Tat, supporting that this protein is folded *in vivo*. We were authorized to carry out a clinical study to obtain blood samplings from 40 HIV-1 infected patients who were infected with B-clade HIV-1 strains, prevalent in France. ELISA showed that a synthetic Tat HXB2 variant specific of B-clade strains was recognized by antibodies in the sera of 19 patients. Eight patients recognized only Tat HXB2 and did not recognize peptides covering the Tat HXB2 sequence. Tat HXB2 is no longer recognized in Dot Blots when Tat HXB2 was unfolded.

MATERIEL AND METHODS

Transactivation Assay with HeLa Cells

Synthesis in solid phase, purification and characterization of Tat HXB2, peptides and Tat OyiC22 were carried out as previously described [13,14]. Five peptides (1-22, 13-46, 38-72, 57-86 and 72-100) used to cover the full sequence of Tat HXB2 with overlaps were respectively named peptide 1 to 5. The transactivation activity of Tat was analyzed by monitoring the production of β-Galactosidase after activation of *lac Z* expression in HeLa-P4 cells as previously described [14].

*Address correspondence to this author at the Equipe de Recherche Technologique 2011, Faculté de Pharmacie, 27 BD Jean Moulin, 13385 Marseille, France; Tel:/Fax: + 33 04 91 83 55 08;
E-mail: Erwann.loret@univmed.fr.

1871-5265/11 $58.00+.00

Lyophilized Tat was first diluted at 5 µM in phosphate buffer 100mM pH 4.5 (or other buffers described in Table **1**, Sigma-Aldrich). In the other experiments, Tat (5 µM) was supplemented with urea buffer 3M and/or was heated at 90°C during 15min. Before adding to cells, Tat was diluted to 1/10 with Dulbecco's Modified Eagles Medium (DMEM) supplemented with 0.1% Bovine Serum Albumin (BSA, Sigma-Aldrich) and 0.01% protamine, bringing the pH to 7.5 (or other pH described in Table **1**). After 18h at 37°C in 5% CO_2, β-galactosidase production was measured according to manufacturer's recommendations (β-Gal ELISA, Roche Diagnostics) and normalized by the total protein amount. Transactivation ratio was the amount of β-galactosidase in presence of Tat divided by the amount without Tat.

ELISA Test with Human Sera

Blood samplings (n=40) were carried out in the department of infectious diseases of the hospital "La Conception" (Marseille, France) from patients infected by B clade HIV-1 variants. The clinical study was approved from the "Direction Générale de la Santé" (authorization n°DGS2007-0204) and the ethics committee "Comité de Protection des Personnes Sud Med 1" (authorization n°2007-A00302-51). Sera were obtained after centrifugation at 4500 rpm, during 30 min. Antibodies were detected with an Enzyme Linked Immunosorbent Assay (ELISA) as previously described [7]. BSA was used as a control.

Wells were coated with 100 µl of protein or peptides (2 µg/ml) overnight at 4°C. After blocking with PBS supplemented with 2% milk, sera (100 µl) diluted at 1/25 in PBS supplemented with 0.2% milk were tested. Serum of uninfected patient (1/25) was used as a negative control and rabbit sera anti-HXB2 or anti-Oyi (1/500) obtained as previously described [7], as a positive control.

Dot Blot Assay

Tat was heated during 15 min at 90°C in presence of 3M Urea to obtain unfolded protein as done in transactivation assay. Tat HXB2, folded or unfolded, was spotted on nitrocellulose membranes (0.2 or 0.05 µg). Protein amounts were controlled by staining with Ponceau red (Sigma-Aldrich). Membranes were incubated for 1 h with PBS supplemented with 2% milk, then overnight with patient serum at 1/50 in PBS, 0.2% milk. The secondary antibody was peroxidase-labeled anti-human IgG (Sigma) diluted 1/1000 and bands were revealed with H_2O2/0.1%, diaminobenzidine tetra hydrochloride (Sigma) in PBS buffer as substrate.Rabbit sera anti-HXB2 was used as positive control and patient 21 serum, representative of the 21 patients who had no antibodies against Tat HXB2, as a negative control. Sera depletion was carried out during 3 h in ELISA plate using a pool of the five peptides (1 µg each). Then, depleted sera were used in Dot Blot assay as described above.

Table 1. Tat OyiC22 Activity as a Function of Buffers, pH and Molarities

Buffers	Molarity (mM)	pH	Transactivation pH	Transactivation ratio	SD(±)
Phosphate	10	4.5	8.0	5.02	0.07
	100	4.5	7.3	7.48	0.00
	100	7	7.6	2.48	0.12
	1000	4.5	6.3	1.03	0.04
TRIS	10	4.5	8.0	5.16	0.02
	100	4.5	7.7	4.86	0.25
	100	7	7.8	3.66	0.02
	1000	4.5	7.1	1.41	0.14
Hepes	10	4.5	8.0	6.01	0.05
	100	4.5	7.4	5.67	0.25
	100	7	7.7	5.01	0.09
	1000	4.5	6.6	5.76	0.09
Citrate*	10	4.5	7.9	3.83	0.27
	100	4.5	7.0	4.81	0.10
	100	7	8.1	5.50	0.14
	1000	4.5	5.9	1.23	0.04

These results showed the final pH in transactivation assays and the transactivation ratios (±SD).
*Citrate buffer: Citric acid-NaOH, 100mM NaCl.

RESULTS

Tat Needed to be Folded for its Biological Activity

Tat HXB2 and Tat OyiC22 were obtained from solid phase synthesis and a main fraction was purified with the expected mass of 11541 MW or 11577 MW corresponding respectively to the sequences Fig. (**1**). The biological activity of Tat HXB2 was tested with a transactivation assay using HeLa-P4 cells Fig. (**2**). Tat HXB2 highly increased the production of ß-Gal Fig. (**2B**) regarding the basal level without Tat Fig. (**2A**). Amazingly, our purified synthetic Tat HXB2 was still able to maintain its biological activity when it was heated at 90°C and cooled Fig. (**2C**), unlike recombinant Tat produce from *E. coli* that lost its activity after heating [15]. This result could be due to *E. Coli* proteins such as endotoxin that could remain associated to Tat. When Tat was heated in presence of urea, which is a chaotropic agent, transactivation activity drastically decreased Fig. (**2D**). However, the same transactivation level was still observed with urea if Tat was not heated Fig. (**2E**). These results showed that our synthetic Tat had to be folded to have a transactivation activity and suggested the capacity for Tat for a spontaneous re-folding, blocked by urea when Tat was heated.

Tat Folding is Unstable Regarding the Buffers and/or pH Used as Solvent

To evaluate the effect of different buffers on Tat conformation, we used the Tat Oyi variant, which is planed to be used for a vaccine [3]. A cysteine at position 22 (Tat OyiC22) instead of Ser was introduce to restore its transactivation activity [16]. The transactivation ratio of Tat OyiC22 diluted in buffers at different pH and molarities was determined and the final pH in cell culture middle was measured (Table **1**). When Tat Oyi C22 was diluted in phosphate buffer 100 mM pH 4.5, we observed the highest transactivation ratio. Amazingly, when Tat was diluted in phosphate buffer 100 mM pH 7, we observed almost no transactivation activity. In contrast, citrate and HEPES buffers showed a transactivation ratio almost unchanged when Tat was diluted at pH 4.5 or 7 but not TRIS buffer. The transactivation ratio remained almost unchanged in HEPES buffer regarding pH and molarities (Table **1**). These results were also observed with Tat HXB2 (data not shown). Thus, phosphate buffer 100 mM pH 4.5 appeared to be the most appropriate to obtain a biologically active Tat and this experiment suggests that the folding of Tat is facilitated with a preliminary step at pH 4.5.

HIV-1 Infected Patients have Antibodies that Recognized a Folded Tat

ELISA plates were coated with either Tat HXB2 or five peptides covering the full sequences of Tat HXB2 or a pool of these peptides. Sera of 40 HIV-1 infected patients were tested Fig. (**3** and supplemental Figs. **S1** and **S2**) show ELISA results for all patients. Rabbit sera were used as positive control Fig. (**3A**) and an uninfected patient serum as a negative control Fig. (**3B**). Sera from 21 patients (53%) had no Tat antibodies against Tat HXB2 and displayed the same ELISA as shown for patient 21 Fig. (**3C**). From the 19 patients having Tat antibodies, eleven (27%) recognized both Tat HXB2 and peptides as shown with sera from patients 13 and 19 Figs. (**3D** and **E**). It was interesting to observe that eight patients (20%) recognized only Tat HXB2 as shown with the serum from patient 14 Fig. (**3F**). These eight sera appeared to recognize only 3D epitopes at the surface of Tat HXB2, and suggested that Tat should be folded in blood of patients. For the eleven sera that recognized the peptides and Tat HXB2, the recognition of the pool of peptides, in spite of a large excess, was not as high as the recognition of Tat HXB2. We carried out a depletion of sera antibodies against the pool of peptides and we observed that it remained antibodies against Tat HXB2 (data not shown). These results suggested that these sera had also antibodies that recognized folded Tat in their blood.

Dot Blot Showed that Unfolded Tat was no Longer Recognized

To verify if the eight patients sera that recognized only Tat HXB2 recognized effectively a folded protein, Dot Blot experiments were carried out respectively with folded and unfolded Tat HXB2 Fig. (**4** and supplemental Fig. **S3**). Dot blot was used because urea could interfere with the coating in ELISA. Protein amounts were normalized with Ponceau red Fig. (**4A**). Rabbit sera were used as positive control. These rabbit sera recognized folded or unfolded Tat and confirmed spots normalization Fig. (**4B**). As expected, the eight sera recognized only folded Tat Fig. (**4D** and supplemental Fig. **S3**). Folded Tat was recognized up to 0.05 µg for six patients while patient 6 and 15 had a lower recognition. In contrast, patient 21, a negative control serum, did not recognize folded or unfolded Tat Fig. (**4C**). To show the specificity of the recognition, depletion with the pool of peptides was carried out as previously described. No change of signal intensity was observed after the peptide pool depletion Fig. (**4D**). ELISA and Dot Blot experiments showed that a significant number of patients had antibodies that recognized Tat HXB2 as a folded protein supporting that extra cellular Tat variants, in the blood of HIV-1 infected patients, should have a similar folding.

Mutations between Tat HXB2 and Tat OyiC22 Modified Tat Recognition in Human Sera

The recognition of Tat OyiC22 and Tat HXB2 was compared in ELISA Fig. (**5**). Antibodies of patients 1 and 16 had

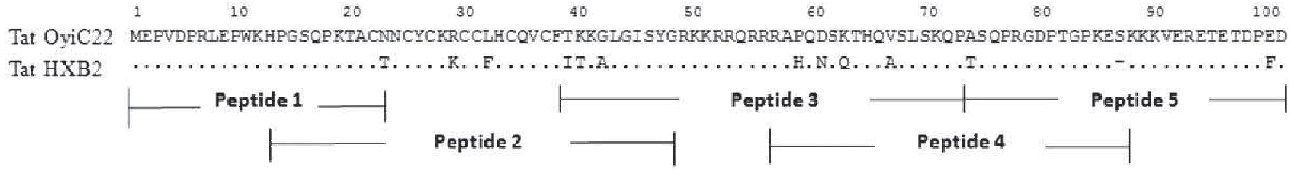

Fig. (1). Sequences of Tat OyiC22, Tat HXB2 and Tat HXB2 peptides (1-22, 13-46, 38-72, 57-86 and 72-100).

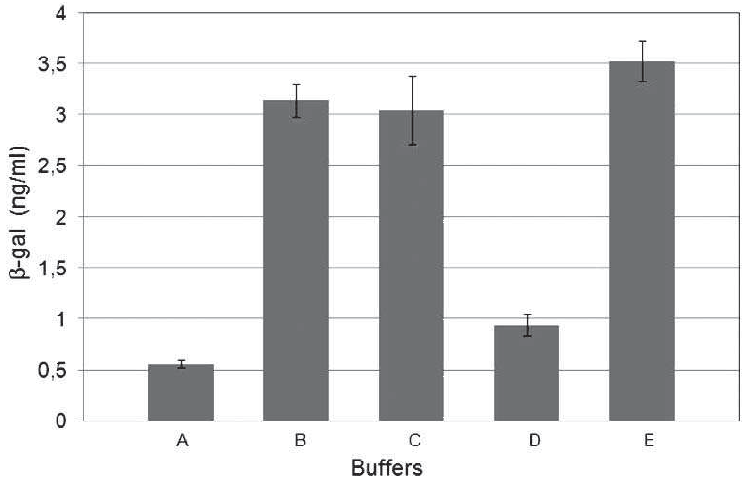

Fig. (2). Transactivation assay with Tat HXB2. (**A**) control without Tat HXB2, (**B**) Tat HXB2, (C) Tat HXB2 heated at 90°C, (**D**) Tat HXB2 heated at 90°C in urea 3M, (**E**) Tat HXB2 in urea 3M but not heated. Transactivation assay was carried out in triplicate assays and the production of β galactosidase is expressed in ng/ml (± SD).

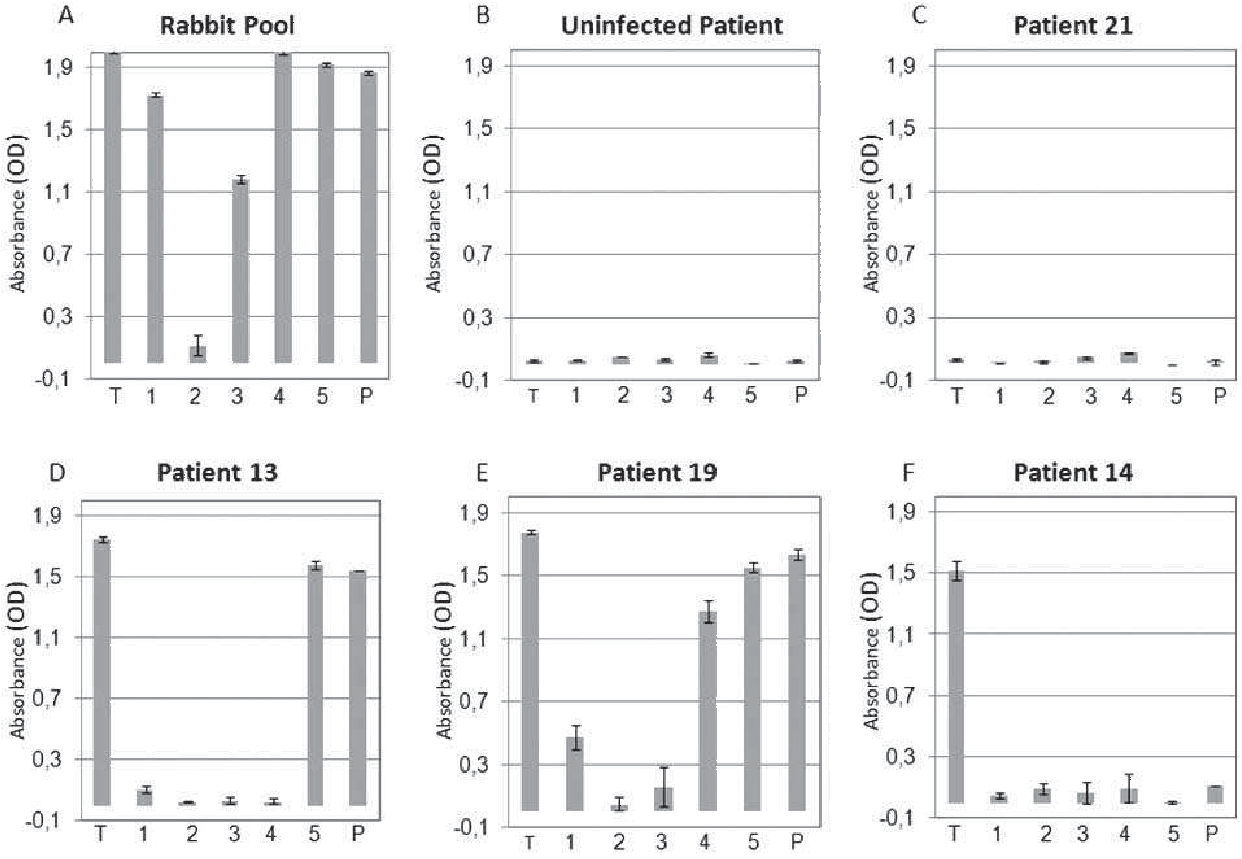

Fig. (3). ELISA recognition of full Tat HXB2 and peptides with patient sera. (**A**) Rabbit sera as a positive control, (**B**) An uninfected patient serum as a negative control, (**C**) Patient 21 serum, representative of patients without Tat HXB2 antibodies, (**D** & **E**) Patients 13 and 19 sera, representatives of the eleven patients who recognized Tat HXB2 and peptides, (**F**) Patient 14 serum, representative of the eight patients who recognized only Tat HXB2. T corresponds to the Tat HXB2, the number 1 to 5 corresponds to Peptide 1 to 5 and P corresponds to the Pool of the five peptides. Data were the average of three independents experiments (±SD).

a better recognition for Tat OyiC22 than Tat HXB2 whereas four patients (5, 6, 15 and 18) recognized equally Tat OyiC22 and Tat HXB2. However, patients 8 and 14 had sera with a lower recognition for Tat OyiC22. This experiment showed that Tat OyiC22 had a folding similar to Tat HXB2 and other Tat variants specific of HIV-1 strains that infected patients in our cohort. However, the few mutations between these two variants were able to modify the recognition from human sera.

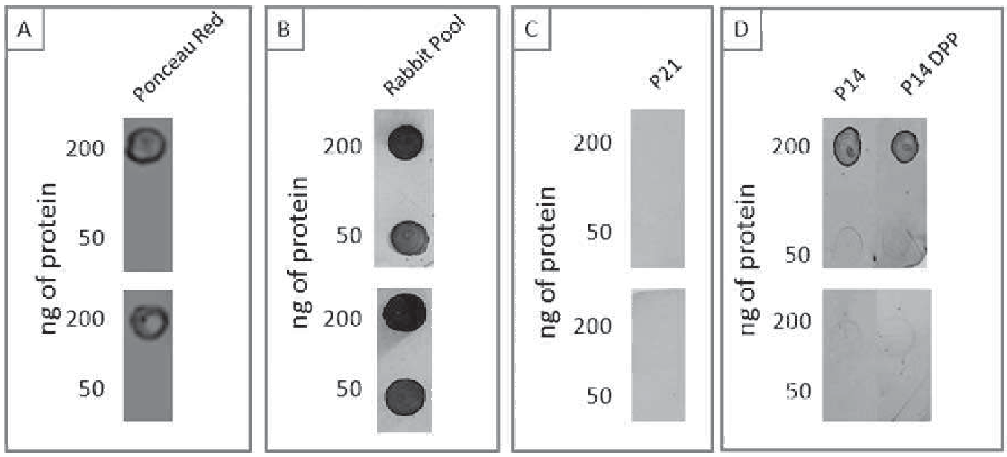

Fig. (4). Dot Blot with Folded (upper panels) and Unfolded (lower panels) Tat HXB2. (**A**) Protein amounts stained with Ponceau red, (**B**) Rabbit sera as a positive control, (**C**) Negative control with the serum of Patient 21 representative of the 21 patients without Tat HXB2 antibodies, (**D**) Serum of Patient 14, representative of the eight patients that recognized only Tat HXB2. To show the specificity of the recognition, a depleted serum of patient 14 was used as a control (14Dpp). This experiment was representative of two independents experiments.

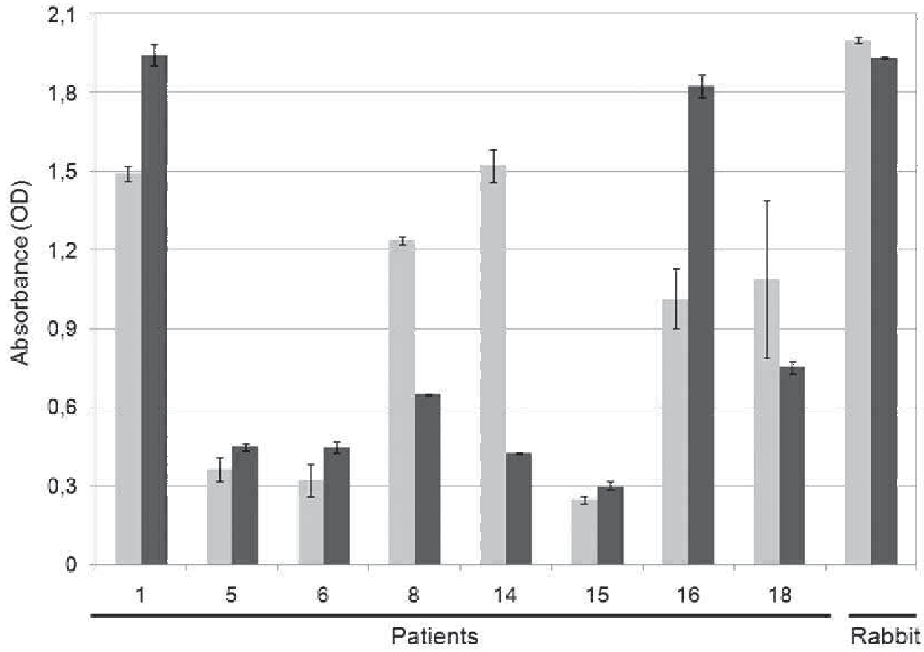

Fig. (5). ELISA recognition of Tat HXB2 and OyiC22 with patient sera that recognized only Tat HXB2 (n=8). Light grey represents Tat HXB2 recognition and dark grey Tat OyiC22 recognition. Data were the average of three independents experiments (±SD).

DISCUSSION

Almost half (47 %) of our HIV-1 infected patients had Tat antibodies recognizing linear or/and 3D epitopes. This result is in accordance with a previous study carried out with patients in Uganda showing that 46 % of HIV-1 infected patients had Tat antibodies [5]. Linear epitopes are more specific of a sequence compared to 3D epitopes, and the uses of peptides can affect the detection of antibodies against Tat variants in blood of patients. This is probably why previous serological studies using only peptides have underestimated or missed the presence of Tat antibodies in HIV-1 infected patients [17].

It is interesting to observe that our positive control with rabbit sera show that peptide 2 is the only one that is not recognized Fig. (**3A**). Peptide 4, which contains the basic region which is highly conserved in Tat variants, is not well recognized by our human sera supplemental Fig. (**S2**). This result was also observed in a similar study [17]. However, structural studies made with biologically active Tat variants show that the basic region is well exposed to the solvent [8-10] and immunization of animals shows that this is one of the major linear epitope [18]. One explanation is that the Tat basic region (^{48}GRKKRRQRRR) has a sequence homology with the basic region of a human protein called protamine (^{24}RSCRRRKRRSCR) suggesting that Tat recognition could be repressed in humans [3]. In contrast, peptide 5 (C-terminus), is well recognized in humans as previously reported [19].

The highest Tat activity is observed at pH 4.5. In acidic pH, Tat which is a basic protein contains mainly positives charges and a presence of well hydrated anions to the protein surface leads to repulsive hydration forces and causes electrostatic repulsion between all Tat proteins in solution. In this monomeric form, Tat can transactivate [15]. Whereas the presence of chaotropic anions (urea) leads to attractive force and caused aggregation of proteins which explains the loss of activity in transactivation assay.

The highest Tat activity is observed with phosphate buffer. This data suggests that phosphate ions could help Tat to be folded following a preliminary step in acidic pH. Tat is a flexible protein and has the capacity to have different folding as demonstrated by the crystal structure of Tat [12]. Phosphate ions could play a role of specific counter ions and remain associated to Tat during these structural changes. However, our data shows that *in vitro* this role seems not possible at neutral pH. This specificity is not unique to Tat since the heat-shock transcription factor 1 [20], prothymosin alpha [21], alpha synuclein [22] adopt a conformation only with an appropriate buffers. This is also confirmed in a recent review that outlines the buffers effects on conformational stability [23]. Table **1** explains also the controversy regarding Tat structure since structural studies suggesting that Tat was a natively unfolded protein were carried out in buffers and pH that was not appropriate to allow the folding [11]. In contrast, the structural studies showing that Tat was folded were carried out in phosphate buffer at pH 4.5 [8-10].

Although Tat Oyi is an African B clade strain [16], which has few sequence differences with Tat HXB2, the eight sera that recognize only folded Tat HXB2, recognize also Tat OyiC22. This result confirms that there is a similar folding in these two proteins. However, the few mutations between these two Tat variants are enough to change the immune properties. Patients 1 and 16 have in their blood Tat variants with mutations and/or localized structural variations similar to Tat OyiC22 while patient 8 and 14 have Tat variants in their blood with mutations and/or localized structural variations differing from Tat OyiC22. Therefore, Tat variants have a conserved folding but the mutations observed in Tat variants induce localized structural variations that can modify the immune response against Tat.

As a conclusion, we show that Tat variants in the blood of HIV-1 infected patients have a folding similar to our synthetic Tat variants. A vaccine is the only therapeutical approach that could end the AIDS pandemic [24]. The fact that Tat is a folded protein in blood of HIV-1 infected patients has to be taken in account for the development of an AIDS vaccine targeting Tat and supports the Tat OyiC22 vaccine approach.

COMPETING INTERESTS

The authors declare that they have no competing interests.

SUPPLEMENTARY MATERIALS

Supplementary material is available on the publishers Web site along with the published article.

ACKNOWLEDGMENTS

We thank Professors Andreas Stein and Philippe Brouqui to have accepted that the clinical study could occur in their hospital departments. We thank Professors Catherine Dhiver, Malika Moktari, Hervé Moreau and Hervé Tissot-Dupond for their participation. We thank the patients and the medical staff for their participation to this study. We thank Professor Catherine Thamalet for providing data regarding patient HIV-1 subtypes. We thank Daniel Laffite and Claude Villars for technical assistance.

REFERENCES

[1] Fisher, A.G.; Feinberg, M. B.; Josephs, S. F.; Harper, M. E.; Marselle, L. M.; Reyes, G.; Gonda, M. A.; Aldovini, A.; Debouk, C.; Gallo, R. C.; Wong-staal, F. The trans-activator gene of HTLV-III is essential for virus replication. *Nature,* **1986**, *320*, 367-371.

[2] Ensoli, B.; Barillari, G.; Salahuddin, S. Z.; Gallo, R. C.; Wong-Staal, F. Tat protein of HIV-1 stimulates growth of cells derived from Kaposi's sarcoma lesions of AIDS patients. *Nature,* **1990**, *345*, 84-86.

[3] Campbell, G. R.; Loret, E. P. What does the structure-function relationship of the HIV-I Tat protein teach us about developing an AIDS vaccine? *Retrovirology,* **2009**, *6*, 50-63.

[4] Gallo, R. C. Tat as one key to HIV-induced immune pathogenesis and Tat toxoid as an important component of a vaccine. *Proc. Natl. Acad. Sci. USA,* **1999**, *96*, 8324-8326.

[5] Campbell, G. R.; Senkaali, D.; Watkins, J.; Esquieu, D.; Opi, S.; Yirrell, D. L.; Kaleebu, P.; Loret, E. P. Tat mutations in an African cohort that do not prevent transactivation but change its immunogenic properties. *Vaccine,* **2007**, *25*, 8441-8447.

[6] Senkaali, D.; Kebba, A.; Shafer, L. A.; Campbell, G. R.; Loret, E. P.; Van Der Paal, L.; Grosskurth, H.; Yirrell, D.; Kaleebu, P. Tat-specific binding IgG and disease progression in HIV type 1-infected Ugandans. *AIDS Res. Hum. Retrovirus.,* **2008**, *24*, 587-594.

[7] Opi, S.; Peloponèse, J. M.; Esquieu, D.; Campbell, G.; Mareuil, J.; Walburgert, A.; Solomiac, M.; Gregoire, C.; Bouveret, E.; Yirrell, D. L.; Loret, E. P. Tat HIV-1 primary and tertiary structures critical to immune response against non-homologous variants. *J. Biol. Chem*., **2002**, *277*, 35915-35919.

[8] Peloponese, J. M.; Gregoire, C.; Opi, S.; Esquieu, D.; Sturgis, J. ; Lebrun, E.; Meurs, E. ; Collette, Y. ; Olive, D. ; Aubertin, A. M.; Witvrow, M.; Pannecouque, C.; De Clercq, E.; Bailly, C.; Lebreton, J.; Loret, E. P. H-13C nuclear magnetic resonance assignment and structural characterization of HIV-1 Tat protein. *C R Acad. Sci. III,* **2000**, *323*, 883-894.

[9] Gregoire, C.; Peloponése, J. M.; Esquieu, D.; Opi, S.; Campbell, G.; Solomiac, M.; Lebrun, E.; Lebreton, J.; Loret, E. P. Homonuclear 1H-NMR assignement and structural characterization of human immunodeficiency virus type 1 Tat Mal protein. *Biopolymers,* **2001**, *62*, 324-335.

[10] Watkins, D. J.; Campbell, R. G.; Halimi, H.; Loret, P. E. Homonuclear H NMR and circular dichroism study of the HIV-1 Tat variant. *Retrovirology,* **2008**, *5*, 83-94.

[11] Shojania, S.; O'Neil, D. J. HIV-Tat is a natively unfolded protein. The solution conformation and dynamics of reduced Hiv-1 (1-72) by NMR spectroscopy. *J. Biol. Chem.,* **2006**, *281*, 8347-8356.

[12] Tahirov, T. H.; Babayeva, N. D.; Varzavand, K.; Cooper, J. J.; Sedore, S. C.; Price, D. H. Crystal structure of HIV-1 Tat complexed with human P-TEFb. *Nature*, **2010**, *465*, 747-752.

[13] Barany, G.; Merrifield, R. B. Solid phase peptide synthesis. In: *The Peptide: Analysis, Synthesis*, *Biology*. Gross, E.; Meinhofer, J., Eds.; New York, NY: Academic Press, **1980**, *vol 2,* pp.1-284.

[14] Péloponèse, J. M.; Collette, Y.; Gregoire, C.; Bailly, C.; Campese, D.; Meurs, E. F; Olive, D.; Loret, E. P. Full peptide synthesis, purification, and characterization of six Tat variants. *J. Biol. Chem.,* **1999**, *274*, 11473-11478.

[15] Koken, S. E.; Greijer, A. E.; Verhoef, K.; Wamel, J. V.; Bukrinskaya, A. G.; Berkhout, B. Intracellular analysis of *in vitro* modified HIV Tat protein. *J. Biol. Chem.*, **1994,** *269*, 8366-8375.

[16] Huet, T.; D'azza, M. C.; Brun-Vezinet, F.; Roelants, G. E.; Wain-Hobson, S. A highly HIV-1 strain isolated from a healthy Gabonese individual presenting an atypical western blot. *AIDS*, **1989**, *3*, 707-715.

[17] Butto, S.; Fiorelli, V.; Tripiciano, A.; Ruiz-Alvarez, M. J.; Scoglio, A.; Ensoli, F.; Ciccozzi, M.; Collacchi, B.; Sabbatucci, M.; Cadaro, A.; Guzman, C.A.; Borsetti, A.; Caputo, A.; Vardas, E.; Colvin, M.; Lukwiya, M.; Rezza, G.; Ensoli, B.; Tat multicentric study group. Sequence conservation and antibody cross-recognition of clade B human immunodefisciency virus (HIV) type 1 Tat protein in HIV-1-infected Italians, Ugandans, and South Africans. *J. Infect. Dis.,* **2003**, *188*, 1171-1180.

[18] Tikhonov, I.; Ruckwardt, T. J.; S.Hatfield, G.; Pauza, C. D. Tat neutralizing in vaccinated macaques. *J. Virol.,* **2003**, *77*, 3157-3166.

[19] Mc Phee, D. A.; Kemp, B. E.; Cumming, S.; Stapleton, D.; Gus, I. D.; Doherty, R. R. Recognition of envelope and Tat protein synthetic peptide analogs by HIV positive sera or plasma. *FEBS J.*, **1988**, *233*, 393-396.

[20] Pattaramanon, N.; Sangha, N.; Gafni, A. The carboxy-terminal domain of Heat-Shock Factor 1 is largely unfolded but can be induced to collapse into a compact, partially structured state. *J. Biol. Chem.,* **2007**, *46*, 3405-3415.

[21] Uversky, V. N.; Gillespie, J. R.; Millett, I. S.; Khodyakova, A.V.; Vasilenko, R. N.; Vasiliev, A. M.; Rodionov, I. L.; Kozlovskaya, G. D.; Dolgikh, D. A.; Fink, A. L.; Doniach, S.; Permyakov, E. A.; Abramov, V. M. Zn^{2+}-Mediated Structure formation and compaction of the "Natively Unfolded" Human Prothymosin α. *Biochem. Biophys. Res. Commun.,* **2000**, *267*, 663-668.

[22] Uversky, V.N.; Li, J.; Fink, A.L. Evidence for a partially folded intermediate in α-synuclein fibril formation. *J. Biol. Chem.,* **2001**, *276*, 10737-10744.

[23] Ugwu, S.O.; Apte, S. P. The effect of buffers on protein conformational stability. *Pharma. Technol.,* **2004**, *28,* 1543-2521.

[24] Virgin, H.W.; Walker, B. D. Immunology and the elusive AIDS vaccine. *Nature,* **2010**, *464*, 224-231.

Received: February 2, 2009 **Accepted: July 15, 2009**

Annexe 6

Immunology:

A Monoclonal Antibody Directed against a Conformational Epitope of the HIV-1 Trans-activator (Tat) Protein Neutralizes Cross-clade

Sonia Mediouni, Jennifer D. Watkins, Michel Pierres, Angélique Bole, Erwann P. Loret and Gilbert Baillat

J. Biol. Chem. 2012, 287:11942-11950.
doi: 10.1074/jbc.M111.319863 originally published online February 23, 2012

THE JOURNAL OF BIOLOGICAL CHEMISTRY VOL. 287, NO. 15, pp. 11942–11950, April 6, 2012

A Monoclonal Antibody Directed against a Conformational Epitope of the HIV-1 Trans-activator (Tat) Protein Neutralizes Cross-clade[S]

Received for publication, November 2, 2011, and in revised form, February 13, 2012 Published, JBC Papers in Press, February 23, 2012, DOI 10.1074/jbc.M111.319863

Sonia Mediouni[‡], Jennifer D. Watkins[§], Michel Pierres[¶], Angélique Bole[¶], Erwann P. Loret[‡1], and Gilbert Baillat[‡2]

From the [‡]Equipe de Recherche Technologique 2011, Université de la Méditerranée, Faculté de Pharmacie, 27 BD Jean Moulin, 13385 Marseille Cedex 5, France, the [§]Dana-Farber Cancer Institute, Harvard Medical School, Boston, Massachusetts 02215, and the [¶]Centre d'Immunologie de Marseille Luminy INSERM (UMR-S613)/CNRS (UMR 6102), Université de la Méditerranée (UNIVMED UM631), Parc Scientifique de Luminy, Case 906, 13288 Marseille Cedex 9, France

Background: Tat, an essential HIV-1 replication factor and extracellular toxin acting on immune cells, is an interesting target to develop therapeutic antibodies.
Results: mAb 7G12 recognizes a conformational epitope of Tat, cross-neutralizes different Tat variants, and blocks Tat uptake.
Conclusion: mAb 7G12 could be used in immunotherapy to restore the immunity of patients.
Significance: Development of alternatives to antiretroviral therapy is crucial.

The identification of a neutralizing mAb against extracellular HIV-1 transactivator of transcription (Tat) is important for the development of an efficient HIV-1 treatment. Tat plays an essential role in HIV-1 pathogenesis, not only for HIV-1 replication but also as an extracellular toxin able to disrupt the immune system. We showed previously that immunization of rabbits with Tat Oyi, a variant cloned from an African woman who did not develop AIDS following HIV-1 infection, raised antibodies able to recognize different Tat variants. We carried out mice immunization with Tat Oyi and selected a mAb named 7G12, which had the capacity to cross-recognize heterologous Tat variants by a common three-dimensional epitope. These results highlighted that Tat variants were able to acquire a structure, in contrast to a number of studies showing Tat as an unfolded protein. mAb 7G12 also had the capacity to neutralize the biological activities of these Tat variants by blocking the cellular uptake of extracellular Tat. This is the first study using Tat Oyi to produce a mAb able to neutralize effectively activities of extracellular Tats from different HIV-1 subtypes. This mAb has an important potential in therapeutic passive immunization and could help HIV-1 infected patients to restore their immunity.

Developing an effective vaccine against HIV-1 remains an important task because of the high genetic variability of HIV-1. In addition, the virus capability to evade immune responses, particularly in immunologically weakened infected patients, highlights the challenge to find a target that induces broadly reactive antibodies. Besides, an efficient vaccine must elicit potent HIV-1 neutralizing antibodies. Conserved epitopes are generally considered to be the key approach to obtain such broadly neutralizing antibodies. Passive immunization studies with mAb targeting the Env protein in simian-human immunodeficiency virus challenge showed promising results (1). However, other potential HIV-1 protein targets such as transactivator of transcription (Tat)[3] should be considered because of its extracellular functions. Tat is one of the first proteins produced by infected cells (2). It is essential for initiation (3) and elongation (4) of HIV-1 gene expression. Moreover, Tat is secreted from HIV-1 infected cells and can cross membranes, inducing apoptosis in different immune cells and protecting HIV-1-infected cells and reservoir cells against the cellular immune system (5). Extracellular Tat also plays a role in spreading the infection by inducing the expression of chemokine receptors CCR5 and CXCR4, which are CD4 coreceptors for HIV-1 (6).

A clade B Tat variant, named Tat Oyi, has been cloned in the 1980s from a seropositive patient who did not develop AIDS in a remote area of Gabon. HIV-1 Oyi genes were similar to genes of usual HIV-1 strains except the *tat* gene, which had mutations never found in other Tat variants (7). We showed previously that rabbit immunization with the Tat Oyi variant rose antibodies able to recognize different Tat variants (8). A heterologous simian-human immunodeficiency virus-BX08 challenge carried out on macaques vaccinated with Tat Oyi showed a reduced viremia in vaccinated monkeys. Furthermore, reservoir cells were no longer detectable (9). Thus, Tat Oyi has specific immunogenic features to generate neutralizing mAbs against Tat variants (8).

In this study, we immunized mice with Tat Oyi and screened mAbs for their cross-clade recognition. We selected one IgG1 mAb, named 7G12, showing an efficient cross-recognition against various HIV-1 subtypes. mAb 7G12 was able to neutral-

[S] This article contains a supplemental figure.

[1] To whom correspondence may be addressed: Equipe de Recherche Technologique 2011, Université de la Méditerranée, Faculté de Pharmacie, 27 BD Jean Moulin, 13385 Marseille Cedex 5, France. Tel.: 33-04-91-83-55-08 or 33-04-91-83-56-65; E-mail: erwann.loret@univmed.fr.
[2] To whom correspondence may be addressed: Equipe de Recherche Technologique 2011, Université de la Méditerranée, Faculté de Pharmacie, 27 BD Jean Moulin, 13385 Marseille Cedex 5, France. Tel.: 33-04-91-83-55-08 or 33-04-91-83-56-65; E-mail: gilbert.baillat@univmed.fr.

[3] The abbreviations used are: Tat, transactivator of transcription; β-Gal, β-galactosidase; 3D, three-dimensional; ART, antiretroviral therapy.

ize the biological activities of Tat variants from the five main HIV-1 subtypes and to block Tat uptake. This is the first report of a broadly neutralizing mAb against Tat with a therapeutic potential.

EXPERIMENTAL PROCEDURES

Tat Variants and Peptide Synthesis—Tat Oyi was assembled in solid phase synthesis as described previously (10). A Ser → Cys substitution at position 22 in Tat Oyi sequence (Fig. 1) allowed recovering biological activity of Tat Oyi and its use in neutralization assays with antibodies. Five peptides covering the full sequence with overlaps (1–22, 13–46, 38–72, 57–86, and 72–101) and, respectively, named peptide 1 to 5 were synthesized. Other synthesized Tats correspond to clade A (Ug11RP), clade D (Eli), circulating recombinant form AE (CM240), clade C (96Bw), and clade B, predominant in Europe and the Americas (HxB2) (Fig. 1). Purification and analysis were performed as described previously (10). Purity and mass were controlled by mass spectrometry. After lyophilization, biological activity of Tat variants were checked by transactivation assays with HeLa P4 cells as described previously (11).

Immunization and Monoclonal Antibody Production—Four BALB/c mice were immunized with 10 μg of synthetic Tat Oyi in 100 μl of phosphate calcium gel adjuvant (Brenntag Biosector) by the subcutaneous route. Two weeks later, mice were boosted with the same preparation. Five weeks later, mice were boosted again with the same preparation by the intramuscular route. Three control mice were also immunized with the same adjuvant and protocol but without Tat protein. On day 45, mice were euthanized and bled terminally. The spleenocytes were immediately separated to hybridize with myeloma cells as described (12). Supernatants of isolated hybridoma were screened by ELISA against Tat Oyi variant to identify producing clones. Then, they were subcloned by limiting dilutions (< 1.0 cell/well) twice, and antibody positive clones were screened by ELISA against firstly Tat Oyi and then against Tats Ug11RP, ELI, CM240, 96BW and HxB2. Previously, a similar immunization with Tat Oyi of four rats has been performed and a mAb (IgG1), named 27A8, had been selected on its high recognition of Tat Oyi and was used as a control. Selected hybridomas were cultured, and mAbs were purified by protein G chromatography (Roche) according to the manufacturer's instructions. After purification, antibodies were dialyzed against Hepes buffer 20 mM, NaCl 120 mM (pH 7.3) and concentrated at 1 mg/ml.

Detection of Purified mAbs Responses by ELISA—96-well plates were coated with 100 ng of folded or denatured Tats or peptides 1 to 5 (1 μg/ml in phosphate buffer 100 mM (pH 4.5)) or peptides pool (each peptide, 1 μg/ml in phosphate buffer 100 mM (pH 4.5)). Tats (10 μg/ml) were denatured by heating at 90 °C during 20 min in presence of urea 3 M and then diluted 10-fold with cold phosphate buffer 100 mM (pH 4.5). To control urea effect, folded Tats were coated in the presence of 0.3 M urea. The nonspecific signal was controlled in coating 100 ng of BSA by well.

Following blocking with 5% skim milk and washing steps, plates were incubated with 100 μl of diluted purified mAb for 1 h at 37 °C. After the washing steps, 100 μl of HRP-conjugated anti-mouse or anti-rat IgG (GE Healthcare) were added, and the plates were incubated for 1 h at 37 °C. After washing steps, 100 μl of 2.2′-azino-di (3-ethylbenzothiazoline-6-sulfonate) (ABTS) substrate (Roche) was added. The absorbance was measured at a wavelength of 405 nm 1 h later.

Measurement Association Rate Constants of mAb 7G12 with Tats in Solution—An ELISA-based method was used for measuring antigen/antibody association rate constants in solution (13). Briefly, 96-well plates were coated with 100 ng of Tat Oyi in 100 mM phosphate buffer (pH 4.5) overnight at 4 °C. One well of four was left uncoated. Following washing steps, the plates were blocked with 5% skim milk in PBS for 1 h. The antibody (1 μg/ml) and the Tat variants (0 to 0.4 μg/ml) solutions were prepared in 20 mM Hepes buffer, 120 mM NaCl (pH 7.3) at twice the final concentration. At time zero, similar volumes of antibody and antigen solutions were mixed, and 100 μl were immediately (time zero of the kinetic analysis) transferred to three coated wells and one uncoated well. Each 5 min, the wells were filled with a sample of mAb/Tat mixture. Each sample was incubated in the wells for 4.5 min and removed. At the end of the kinetic analysis, plates were washed and incubated with HRP-conjugated anti-mouse IgG. After washing steps, 100 μl of ABTS substrate was added. The absorbance was measured at a wavelength of 405 nm 1 h later. Association and dissociation rate constants (k_{on} and k_{off}) were then determined, allowing the calculation of the equilibrium dissociation constant (K_D).

Western Blot Analysis—Tats (100 ng) were subjected to SDS-PAGE (15%) under reducing conditions (DTT 100 mM and urea 6 M in Laemmli sample buffer at 96 °C for 10 min). Tats were then electrotransferred to nitrocellulose membrane (Schleicher and Schuell). After blocking with 5% skim milk, strips of the membrane were incubated for 1 h with mAbs 7G12 or 27A8 at 1:2500. The secondary antibody was HRP-conjugated anti-mouse or anti-rat IgG (GE Healthcare) diluted 1:1000, and bands were revealed with H_2O_2 0.1%, diaminobenzidine tetra hydrochloride (Sigma) as substrate.

Neutralization of Tat Transactivation—Neutralization of Tat transactivation was performed with HIV long-terminal repeat (LTR) promoter transfected HeLa cells (HeLa-P4) and analyzed by monitoring the production of β-galactosidase (β-Gal) as described previously (11). Briefly, HeLa-P4 cells were incubated in DMEM with glutamine supplemented with 10% (v/v) heat-inactivated fetal calf serum and 50 units/ml neomycin. 2×10^5 cells/well were incubated in 400 μl of DMEM supplemented with 0.01% (w/v) protamine (Sigma-Aldrich) and 0.1% (w/v) BSA (Sigma) in 24-well plates (Falcon). Lyophilized or denatured Tats were diluted at 5 μM (or 10 μM) in phosphate buffer 100 mM (pH 4.5). Tat (0.5 μM final) and described concentrations of antibodies were added to cells. Volumes were completed to 500 μl with 20 mM Hepes buffer, 120 mM NaCl (pH7.3). When added together, denatured, and folded, Tat had a final concentration of 0.5 μM each.

After 18 h at 37 °C, β-Gal production was measured with a β-Gal ELISA kit (Roche) according to manufacturer's recommendations. The background against BSA was removed. The transactivation ratio was the amount of β-Gal in the presence of Tat divided by the amount without Tat.

Methyl Thiazolyl Tetrazolium Assay—The Jurkat T-cell quantity remaining after incubation with Tat, reflection of induced apoptosis, was measured with an MTT-based method as previously described (14). Jurkat T-cells were cultivated in RPMI 1640 medium with glutamine supplemented with 10% (v/v) heat-inactivated fetal calf serum, 100 μg/ml streptomycin, and 100 units/ml penicillin. 10^5cells in 100 μl of RPMI with 0.1% BSA and 0.01% protamine A were transferred in wells of 96-wells plates. Lyophilized Tats were diluted at 65 μM in 100 mM phosphate buffer (pH 4.5). Cells were incubated for 48 h at 37 °C with 10 μl of Tats and 20 μl of mAbs or 20 mM Hepes buffer, 120 mM NaCl (pH7.3). Control wells were adjusted with 10 μl of 100 mM phosphate buffer (pH 4.5) and 20 μl of 20 mM Hepes buffer, 120 mM NaCl (pH7.3) to verify cell viability. 0.5 mg of MTT (InterChim) was added and incubated for 5 h. Formazan crystals were dissolved in 200 μl dimethyl sulfoxide, and absorbance was measured at 510 nm.

Tat Uptake—Translocated Tat localization in the nucleus and cytosol was evaluated by immunoblot analysis in Jurkat and HeLa cells. Jurkat T-cells (or HeLa cells) were incubated as described above. 10^6 cells by well (24-well plate) were incubated in 400 μl of RPMI (or DMEM) supplemented with 0.01% (w/v) protamine (Sigma) and 0.1% (w/v) BSA (Sigma). Lyophilized Tats were diluted at 50 μM in 100 mM phosphate buffer (pH 4.5). 50 μl of Tat (5 μM final) and 50 μl of purified antibodies (50 μg) or 50 μl of 20 mM Hepes buffer, 120 mM NaCl (pH7.3) were added, and cells were incubated for 2 h at 37 °C. Cells were washed with 1 ml PBS and potterized in lysis buffer (50 mM Tris-HCl buffer (pH 7.5), 150 mM NaCl, and protease inhibitors (Roche)). Complete lysis was controlled by microscopy. A pellet corresponding to the nuclear extract was obtained by centrifuging the lysate at 600 × *g* for 15 min at 4 °C. Supernatant was centrifuged at 100,000 × *g* for 1 h at 4 °C, and the membrane pellet was retrieved. The cytoplasmic fraction (supernatant 2) was Trichloroacetic acid precipitated overnight at −20 °C. The final pellet was washed by 1 ml of cold acetone. Nuclear, membrane, and cytoplasmic pellets were subjected to SDS-PAGE (15%) under reducing conditions (100 mM DTT and urea 6 M in Laemmli sample buffer at 96 °C for 10 min) and electrotransferred to a nitrocellulose membrane (Schleicher and Schuell). Protein amounts were controlled by staining with Ponceau red (Sigma). After blocking with 5% skim milk, membrane was incubated overnight with an anti-Tat rabbit sera (1:1000) described previously (11). The secondary HRP-conjugated anti-rabbit antibody (GE Healthcare) was diluted to 1:5000, and bands were revealed with Immobilon Western chemiluminescent HRP substrate (Millipore). The intensity of the bands was analyzed by densitometric imaging using the freely available ImageJ program (National Institutes of Health). Densitometries in the nucleus and cytosol were added to evaluate total translocated Tat without antibody (100%). Densitometries of each compartment in the presence of antibodies were compared and expressed as a percentage. Annexin 1, P-AC-histone H3, and Fusin (Santa Cruz Biotechnology) antibodies were used as cytoplasmic, nuclear, and membrane fractions control, respectively.

```
        1--------10--------20--------30--------40--------50--------
OyiC22  MEPVDPRLEPWKHPGSQPKTACNNCYCKRCCLHCQVCFTKKGLGISYGRKKRRQRRRAP
HxB2    MEPVDPRLEPWKHPGSQPKTACTNCYCKKCCFHCQVCFITKALGISYGRKKRRQRRRAH
UgllRP  MDPVDPNIEPWNHPGSQPTTPCNKCYCKVCCYHCLVCFQSKGLGISYGRKKRKQRRGPT
ELI     MDPVDPNLEPWNHPGSQPRTPCNKCHCKKCCYHCPVCFLNKGLGISYGRKKRRQRRGPP
CM240   MELVDPNLEPWNHPGSQPTTACSKCYCKKCCWHCQLCFLKKGLGISYGRKKRRHRRGTP
96BW    MEPVDPNLEPWNHPGSQPRTACTKCYCKYCCYHCLVCFQTKGLGISYGRKKRRQRRSTP

        60--------70--------80--------90--------100
OyiC22  QDSKTHQVSLSKQPASQPRGDPTGPKESKKKVERETETDPED 101
HxB2    QNSQTHQASLSKQPTSQPRGDPTGPKE-KKKVERETETDPFD 100
UgllRP  QSNKQHQNPIPKQPIPRTQGISTGPEESKKKVEDKTETDRRD 101
ELI     QGGQAHQVPIPKQPSSQPRGDPTGPKEQKKKVESEAETDP--  99
CM240   QSSKDHQNPIPKQPLPIIRRNPTDPKESKKEVASKAETDQCD 101
96BW    PSSESHQNLISEQPLPRTQGNPTGSEESKKKVESKTEADPFA 101
```

Statistical Analysis—Statistical differences were analyzed by use of a Mann-Whitney test. $p < 0.05$ was considered significant.

RESULTS

mAb 7G12 Cross-recognizes Tat Variants from the Five Main HIV-1 subtypes—Mice were immunized with Tat Oyi, and one IgG1 mAb, named 7G12, was selected among 132 prescreened clones for its broadly reactive immune response against a panel of Tat variants representative of main HIV-1 clades (Fig. 1). To characterize the cross-recognition, the affinities of mAb 7G12 for the different Tat variants were evaluated in ELISA (Fig. 2*A*). mAb 7G12 bound all Tats with a similar high affinity. Only one mAb, named 6E7, also showed a broadly reactive immune response but with 10 times lower affinities (Fig. 2*B*). All other clones did not recognize all tats, showed very low affinities, or were IgM subtype. The control mAb named 27A8 bound only Tats Oyi and HxB2 with high affinities but not the others (Fig. 2*C*).

To quantify mAb 7G12 affinities for Tat variants, an ELISA-based method (13) was used to measure antigen/antibody association rate constants in solution. Antigen and antibody were mixed, and aliquots were withdrawn at different time intervals to determine the amount of free antibodies. The disappearance of free antibodies reflected the time course of the association reaction. Affinity constant obtained for Tat Oyi was high (K_D = 7 ± 0.4 nM). K_D for Tats UG11RP (12 ± 0.5 nM), Eli (5.7 ± 0.1 nM), CM240 (3.2 ± 0.1 nM), and 96BW (7.4 ± 0.3 nM) were very similar. These results confirmed ELISA affinity curves (Fig. 2*A*) and suggested that mAb 7G12 recognized a common site on the surface of all Tat variants tested. Interestingly, sequence comparison shows only a small percentage of potential continuous epitopes (> 5 amino acids) between the different Tats (Fig. 1).

mAb 7G12 Recognizes a 3D Epitope—To map the epitopes recognized by mAbs 7G12, 6E7, and 27A8, ELISA was carried out as described previously (15), using 100 ng of different overlapping peptides spanning the entire sequence of Tat Oyi (Fig. 3*A*). mAb 7G12 did not recognize peptides, whereas mAb 27A8 recognized peptide 5 covering the C-terminal sequence (72 to 100). Thus, mAb 27A8 recognized a linear epitope in the C-terminal domain, conserved only between Tats Oyi and HxB2 (identity 87.1%) but not in other Tat variants. In contrast, mAb 6E7 recognized peptides 1 and 2, indicating that its epitope matched, at least partly, with the overlapping sequence (residue 13 to residue 22). Thus, mAb 6E7 showed a broad immune response against the panel of Tat variants because this linear

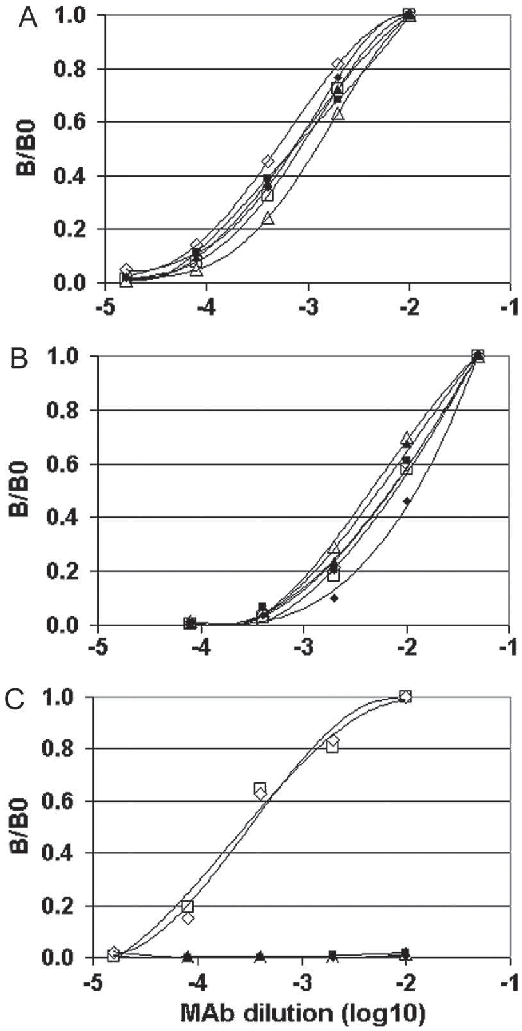

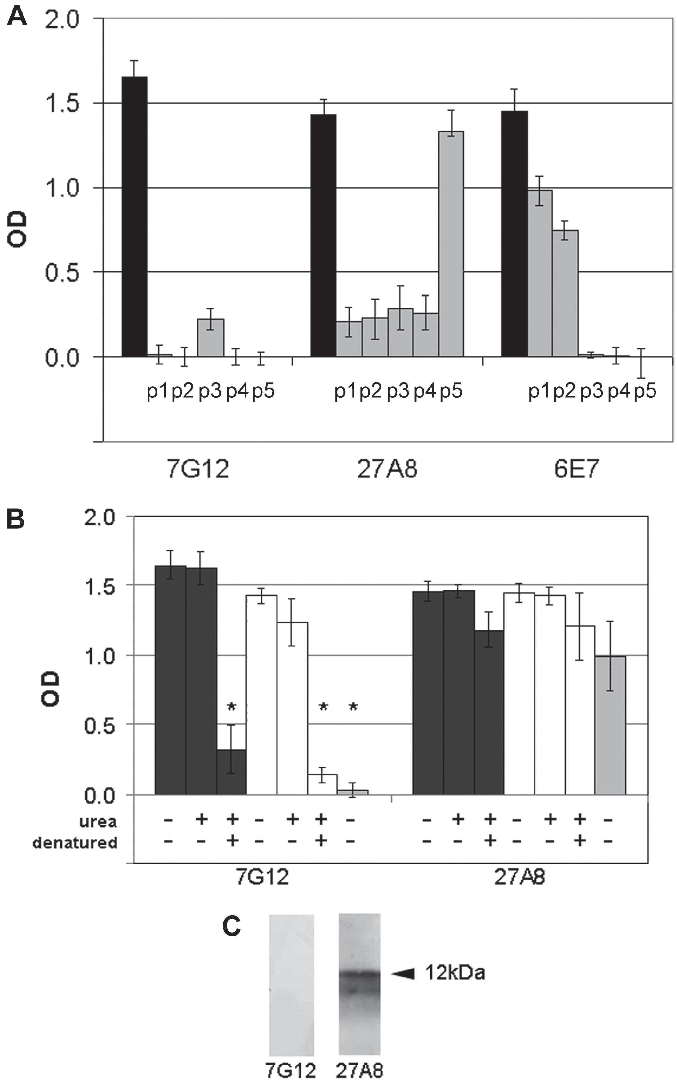

epitope is highly conserved in the N-terminal domain of these proteins (Fig. 1). These data suggested that mAb 7G12 did not recognize a linear epitope but a 3D epitope on the surface of Tat Oyi that corresponds to a particular folding highly conserved in Tat variants.

To test this hypothesis, ELISA with mAbs 7G12 and 27A8 were performed against folded and denatured Tats Oyi and HxB2 (Fig. 3*B*). Urea alone, used for complete denaturation, did not modify the ELISA responses for both mAbs, whereas high temperature drastically decreased mAb 7G12 binding to Tat without modifying 27A8 binding. mAb 7G12 did not recognize Tat variants following denaturation or a peptide pool, highlighting that this antibody recognized a 3D epitope and not a linear epitope. In contrast, mAb 27A8 recognized denatured Tat variants and a peptide pool, confirming that this mAb was directed against a linear epitope. Moreover, mAb 7G12 was also unable to recognize Tat Oyi in Western blot analysis (Fig. 3*C*). In contrast, mAb 27A8 in the same dilution strongly recognized Tat Oyi.

mAb 7G12 Neutralizes Tat Oyi Transactivation Activity—We studied the effects of mAb 7G12 (3D epitope) and of mAbs 6E7 or 27A8 (linear epitopes) on the Tat Oyi biological activities. The neutralizing effect of mAb 7G12 on transactivation activity of Tat Oyi was monitored with HeLa P4 cells (Fig. 4*A*). 50 μg of mAb 7G12 neutralized almost completely Tat Oyi (0.5 μM) transactivation activity. The neutralization potency of mAb 7G12 correlated with the concentration of antibody. In our assays, the maximal neutralization was reached with 0.33 nmoles (50 μg) of mAb against 0.25 nmoles of Tat, suggesting a molar-molar association. In contrast, mAb 27A8 only had a very low effect on transactivation activity of Tat Oyi (Fig. 6*A*).

To determine whether the neutralizing effect of mAb 7G12 was due to recognition of a 3D epitope, transactivation activity was examined using 0.5 μM of folded and denatured Tat Oyi (Fig. 4*B*). Denatured Tat Oyi had lost the transactivation activ-

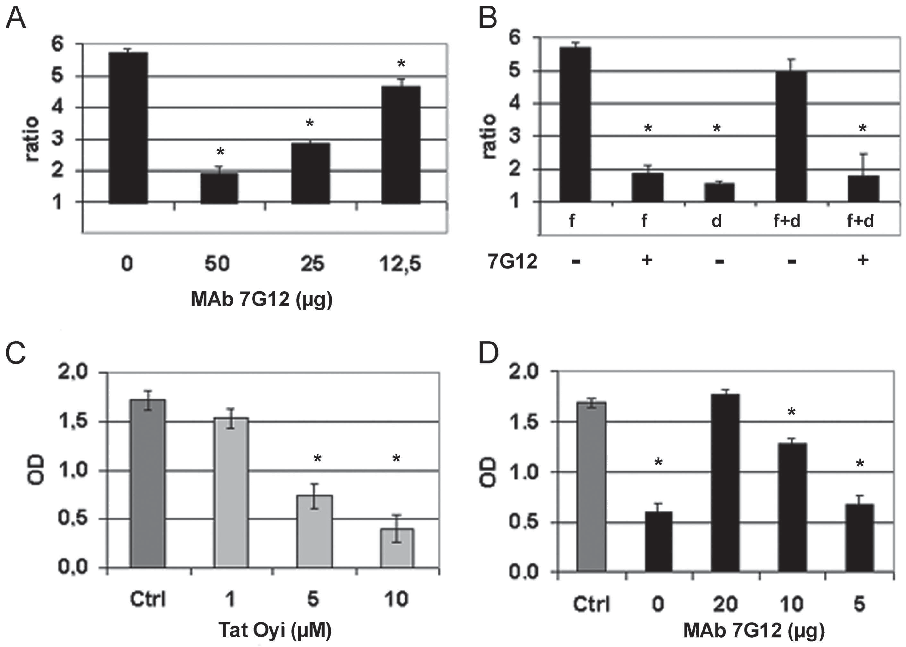

ity but did not prevent the biological effect of folded Tat when both were added together. Interestingly, unfolded Tat did not decrease the neutralizing effect of 50 μg of mAb 7G12 when folded and denatured Tats were in competition. This demonstrated that the activity of Tat Oyi in solution was conformation-dependent and blocked by the mAb 7G12, which recognized a 3D epitope.

mAb 7G12 Inhibits Tat Oyi-induced Apoptosis in Lymphocytes—Discordance between the transactivation and other Tat functions was observed previously (16). Thus, to confirm the mAb 7G12 neutralizing effect, an inhibition assay was performed on Tat-induced apoptosis (17). Viability of Jurkat lymphocytes cells was monitored in presence of Tat Oyi, using a tetrazolium salts-based colorimetric assay (Fig. 4*C*). 10 μM of Tat Oyi almost completely inhibited formazan production in Jurkat cells. This inhibition was correlated with the concentration of Tat Oyi up to 1 μM. The neutralizing effect of mAb 7G12 was evaluated (Fig. 4*D*). 20 μg (1 μM) of mAb 7G12 completely blocked the apoptosis of lymphocytes induced by Tat Oyi (5 μM). Partial neutralization was observed up to 5 μg (0.25 μM) of mAb 7G12 but not with 1 μM of mAb 27A8 (Fig. 6*B*).

mAb 7G12 Blocks Extracellular Tat Uptake—Exogenous Tat is able to enter cells, inducing apoptosis or activating transcription. We evaluated the ability of mAb 7G12 to neutralize Tat Oyi uptake using Jurkat cells (Fig. 5). mAb 27A8, which recognized a linear epitope of Tat Oyi, was used as mAb control. As described previously (18, 19), most internalized Tat was located in the nucleus (78%), and only a small part was in the cytosol (22%). mAb 27A8 only showed a non-significant decrease in cytosolic fraction. In contrast, mAb 7G12 almost totally blocked Tat translocation, as shown by the significant drop in the nuclear (-75.6%) and cytosolic (-98.5%) fractions. Very similar results were observed with HeLa cells (data not shown). Thus, mAb 7G12 was able to block Tat uptake, preventing apoptosis and transcription more effectively than a mAb that recognized only a linear epitope.

mAb 7G12 Cross-neutralizes Biological Activities of Other Heterologous Tat Variants—Cross-neutralizing activity of 50 μg (0.66 μM) of mAb 7G12 was evaluated using the transactivation assay with HeLa P4 cells and 0.5 μM of Tat variants representative of the various HIV-1 subtypes including A, B, C, D, and the circulating recombinant form AE (Fig. 6*A*). MAbs 27A8 and 6E7 were used as control at the same concentration. mAb 7G12 inhibited the transactivation activity of all Tat variants as well as with Tat Oyi. Precisely, mAb 7G12 inhibited 61.9%, 66.3%, 57.1%, 53.2% and 50.8% of transactivation activities of Tats UG11RP, HxB2, 96Bw Eli, and CM240 respectively, compared with 63.7% observed with Tat Oyi. In contrast, mAb 27A8 showed a low inhibitory effect only for Tat Oyi and Tat HxB2 (12% and 19.4%, respectively) and no significant inhibition with others Tats. mAb 6E7 had no inhibitory effect on all Tat variants. We also examined the neutralizing effects of mAbs 7G12, 27A8, and 6E7 on inhibition of lymphocytes proliferation induced by 5 μM of Tat variants (Fig. 6*B*). Unlike mAbs 27A8 and 6E7, mAb 7G12 completely reversed the proliferation inhibition induced by the Tat variants.

Thus, mAb 7G12 neutralized the biological activities of the different Tat variants tested with a similar efficiency, suggesting that the epitope recognized by this antibody was conserved on the surface of the variants and that their folding play an important role for Tat activity.

DISCUSSION

Up to now, the main targets to obtain therapeutic antibodies to HIV-1 were the surface envelope glycoprotein gp120 and the transmembrane glycoprotein gp41 (20–28). These antibodies

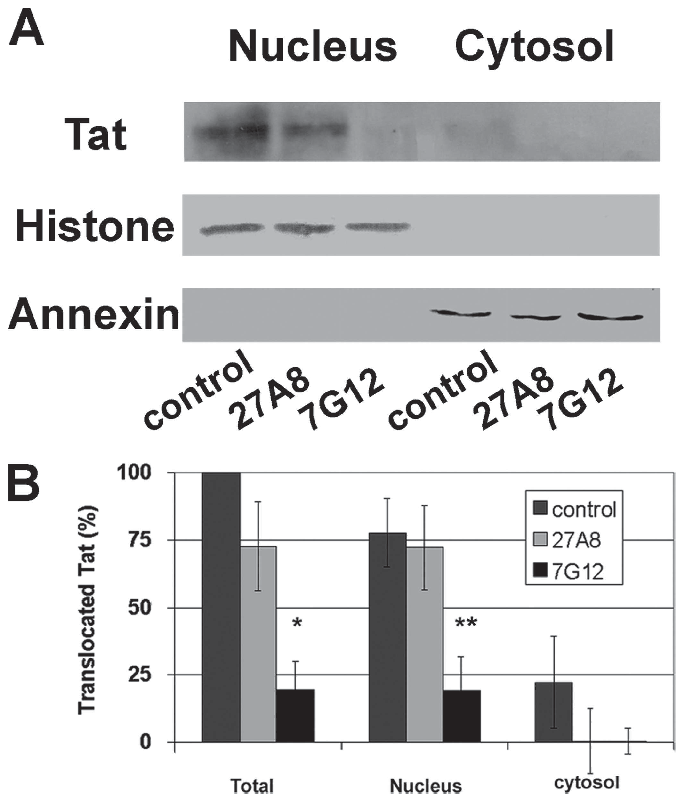

were designed to block virus uptake in cells, but resistances emerged by selection of escape mutants. Most of these antibodies recognize linear epitopes that can mutate easily or be modified after transcription (29–31). Recently, screening strategies in infected patients using new technologies have selected neutralizing antibodies efficient against a large number of variants of HIV-1 (32–34). These studies highlight that only a very limited number of antibodies in a few patients are broadly neutralizing. Some mAbs against Tat were developed on mice (35–37) and tested on humans (38, 39), but none of them had the capacity to cross-recognize Tat variants.

In this study, we used the immunogenic property of Tat Oyi to obtain a mAb, named 7G12, selected for its high recognition of several genetically heterologous Tat variants. This specific feature of Tat Oyi has been described previously (8). Among these variants, the Tat HxB2 sequence has the highest sequence identity (87.1%) with Tat Oyi, whereas Tat variants CM240, UG11RP, 96Bw, and Eli have identities of 67.3%, 65.3%, 67.3%, and 73.3%, respectively. Moreover, identical amino acids among the six variants are gathered in sequence between residues 13 to 18 and residues 43 to 52 (Fig. 1). The sequence 13–18 corresponds to the core region of Tat, and the sequence 43 to 52 appears to lack immunogenicity, although exposed to solvent (40). mAb 6E7, used as a control, recognized a linear epitope located in the common sequence (residues 13 to 22) of the N-Terminus of Tat. mAb 6E7 also showed a broad immune response but with lower affinities than mAb 7G12. Moreover, mAb 6E7 was unable to block the biological activities of the different Tat variants, suggesting that this region was not reachable in active Tats.

MAb7G12 did not recognize any peptides covering the Tat Oyi sequence, and the affinities were comparable for all these heterologous Tats. Thus, we concluded that this antibody recognized sites on a common surface in all Tat variants. This common surface required a conserved folding of Tat variants that plays an important role for Tat activity. This conclusion is in disagreement with studies showing that Tat is an unfolded protein (41). The absence of recognition of all Tat variants after urea/heat degradation in ELISA and on Western blot analysis (data not shown) confirms the existence of a common 3D structure. The presence of a conserved folding in Tat variants is also supported by previous structural studies on three Tat variants with a biological activity (42). Accordingly, mAb 7G12 could be used to map the 3D epitope able to induce broadly cross-reactive antibodies. Preliminary recognition experiments with different Tat Oyi domains combinations have shown that the sequences 1–22, 38–53, and 93–101 were involved in proper folding conditions to be recognized by mAb 7G12 (data not shown). A protection assay against acetylation on lysine residues could be an appropriate means to precisely map the discontinuous epitope but needs further development.

We showed that mAb 7G12 neutralized two biological activities for all Tat variants tested. We used a higher Tat concentration in the Jurkat cells apoptosis assay (5 μM) compared with the transactivation assay with HeLa cells (0.5 μM) because these two cell lines are differently sensitive to the extracellular Tat. For instance, Jurkat T-cells do not express caveolin and cannot internalize Tat by this pathway (43). Moreover, the full-length form of Tat is less efficient for apoptosis than the short form, whereas no difference is observed for the transactivation assay (44). In contrast, the quantity of antibodies used to obtain a high neutralization seemed less important in the apoptosis assay (20 μg) than in the transactivation assay (50 μg), but the final antibody concentrations were similar (0.2 μg/μl and 0.1 μg/μl, respectively). The lower Tat/antibody ratio needed to obtain complete neutralization in the transactivation assay arises from the efficiency of the LTR promoter. Thus, a molar:molar ratio (0.25 nmoles of Tat and 0.33 nmoles of mAb) is crucial to block all Tats able to trigger β-Gal expression. In contrast, trigger apoptosis pathways are more difficult, especially in a stable cell line, and the neutralization is easier, needing a higher Tat:antibody ratio (0.65 nmoles of Tat and 0.14 nmoles of mAb). We observed a low neutralization of Tats Oyi and HxB2 transactivation activities with mAb 27A8 (Fig. 6*A*). This antibody recognized a common linear epitope in the C-terminal domain of these two clade B variants. mAb 27A8 could interfere with their transactivation activities but with a very low efficiency com-

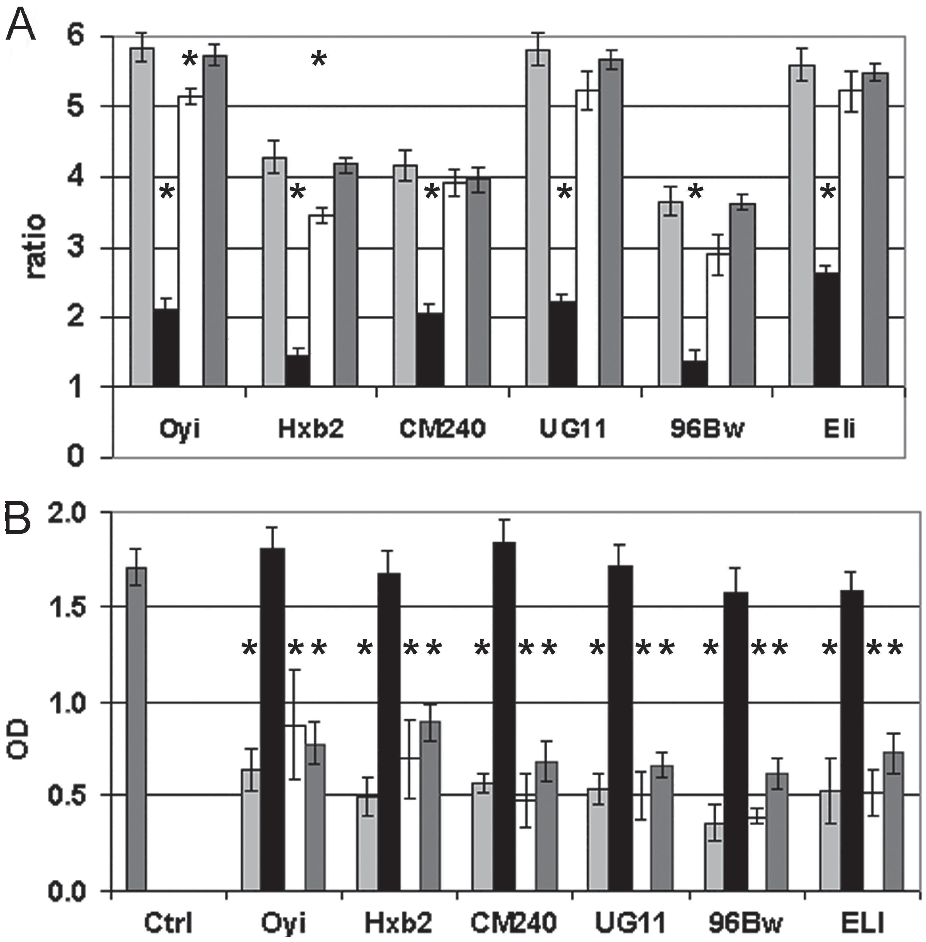

pared with mAb 7G12. Moreover, mAb 27A8 was unable to prevent apoptosis activities of these Tats.

Intracellular pathways leading to Tat induced transactivation and apoptosis were probably distinct but both dependent on Tat uptake. We observed that mAb 7G12 was able to block Tat uptake in both cell lines. Kinetic conditions used resulted from data published previously (44), highlighting that internalization was almost completed after 2 h. Experimental conditions were close to those of the transactivation assay but with 5 μM (and not 0.5 μM) of Tat. A highest Tat concentration was used to obtain a good signal in nuclear and cytosolic fractions on immunoblot analysis. However, because of experimental limitations, a molar:molar ratio between Tat and mAb was not reached in these conditions, explaining why 19% of Tat was still observed in the nucleus (Fig. 5). We assume that, with a molar: molar ratio, mAb 7G12 could completely block Tat uptake. mAb 27A8 had a low effect on Tat Oyi uptake, it was not significant in the assay. In molar:molar conditions, this effect could become significant, as observed in figure 6*A*, on transactivation activities of the Oyi and HXB2 Tat variants. However, mAb 27A8 was inefficient compared with mAb 7G12 and did not inhibit the other variants without the specific C-terminal linear epitope.

Up to now, only antiretroviral therapy (ART) is an efficient treatment against HIV-1 but does not eradicate the virus (45). Stopping treatment triggers the viral production because of the existence of reservoir cells (46). Passive immunization with a neutralizing antibody targeting other pathways would complement ART. Thus, mAb 7G12 properties are interesting for this purpose after humanization. We showed that Tat is a naturally folded protein in the blood of HIV-infected patients and can generate antibodies against 3D epitopes (15). Thus, therapeutic antibodies recognizing 3D epitopes of Tat could be selected by competitive ELISA with mAb 7G12 on isolated B-cells from long-term non-progressor patients. Studies also suggested that mAbs combination might protect more effectively against HIV-1 (47). Thus, passive immunization, using broadly neutralizing antibodies against different targets, such as Tat and gp120, should be evaluated for therapeutic potential.

REFERENCES

1. Kramer, V. G., Siddappa, N. B., and Ruprecht, R. M. (2007) Passive immunization as tool to identify protective HIV-1 Env epitopes. *Curr. HIV Res.* **5,** 642–655
2. Wu, Y., and Marsh, J. W. (2001) Selective transcription and modulation of resting T-cell activity by preintegrated HIV DNA. *Science* **293,** 1503–1506
3. Wong-Staal, F., and Gallo, R. C. (1985) Human T-lymphotropic retrovi-

ruses. *Nature* **317,** 395–403
4. Cullen, B. R. (1990) The HIV-1 Tat protein. An RNA sequence-specific processivity factor? *Cell* **63,** 655–657
5. Gougeon, M. L. (2003) Apoptosis as an HIV strategy to escape immune attack. *Nat. Rev. Immunol.* **3,** 392–404
6. Huang, L., Bosch, I., Hofmann, W., Sodroski, J., and Pardee, A. B. (1998) Tat protein induces human immunodeficiency virus type 1 (HIV-1) coreceptors and promotes infection with both macrophage-tropic and T-lymphotropic HIV-1 strains. *J. Virol.* **72,** 8952–8960
7. Huet, T., Dazza, M. C., Brun-Vézinet, F., Roelants, G. E., and Wain-Hobson, S. (1989) A highly defective HIV-1 strain isolated from a healthy Gabonese individual presenting an atypical Western blot. *AIDS* **3,** 707–715
8. Opi, S., Péloponèse, J. M., Jr., Esquieu, D., Campbell, G., de Mareuil, J., Walburger, A., Solomiac, M., Grégoire, C., Bouveret, E., Yirrell, D. L., and Loret, E. P. (2002) Tat HIV-1 primary and tertiary structures critical to immune response against non-homologous variants. *J. Biol. Chem.* **277,** 35915–35919
9. Watkins, J. D., Lancelot, S., Campbell, G. R., Esquieu, D., de Mareuil, J., Opi, S., Annappa, S., Salles, J. P., and Loret, E. P. (2006) Reservoir cells no longer detectable after a heterologous SHIV challenge with the synthetic HIV-1 Tat Oyi vaccine. *Retrovirology* **3,** 8–17
10. Péloponèse, J. M., Jr., Collette, Y., Grégoire, C., Bailly, C., Campèse, D., Meurs, E. F., Olive, D., and Loret, E. P. (1999) Full peptide synthesis, purification, and characterization of six Tat variants. Differences observed between HIV-1 isolates from Africa and other continents. *J. Biol. Chem.* **274,** 11473–11478
11. Campbell, G. R., Watkins, J. D., Esquieu, D., Pasquier, E., Loret, E. P., and Spector, S. A. (2005) The C terminus of HIV-1 Tat modulates the extent of CD178-mediated apoptosis of T cells. *J. Biol. Chem.* **280,** 38376–38382
12. Fuller, S. A., Takahashi, M., and Hurrell, J. G. R. (1991) in *Current Protocols in Molecular Biology*, pp. 11.01–11.11.5, John Wiley and Sons, New York
13. Hardy, F., Djavadi-Ohaniance, L., and Goldberg, M. E. (1997) Measurement of antibody/antigen association rate constants in solution by a method based on the enzyme-linked immunosorbent assay. *J. Immunol. Methods* **200,** 155–159
14. Harakeh, S., Diab-Assaf, M., Niedzwiecki, A., Khalife, J., Abu-El-Ardat, K., and Rath, M. (2006) Apoptosis induction by Epican Forte in HTLV-1 positive and negative malignant T-cells. *Leuk. Res.* **30,** 869–881
15. Mediouni, S., Baillat, G., Darque, A., Ravaux, I., and Loret, E. (2011) HIV-1 infected patients have antibodies recognizing folded Tat. *Infect. Disord. Drug Targets* **11,** 57–63
16. Siddappa, N. B., Venkatramanan, M., Venkatesh, P., Janki, M. V., Jayasuryan, N., Desai, A., Ravi, V., and Ranga, U. (2006) Transactivation and signaling functions of Tat are not correlated. Biological and immunological characterization of HIV-1 subtype-C Tat protein. *Retrovirology* **3,** 53–73
17. de Mareuil, J., Carre, M., Barbier, P., Campbell, G. R., Lancelot, S., Opi, S., Esquieu, D., Watkins, J. D., Prevot, C., Braguer, D., Peyrot, V., and Loret, E. P. (2005) HIV-1 Tat protein enhances microtubule polymerization. *Retrovirology* **2,** 5–15
18. Ensoli, B., Buonaguro, L., Barillari, G., Fiorelli, V., Gendelman, R., Morgan, R. A., Wingfield, P., and Gallo, R. C. (1993) Release, uptake, and effects of extracellular human immunodeficiency virus type 1 Tat protein on cell growth and viral transactivation. *J. Virol.* **67,** 277–287
19. Ma, M., and Nath, A. (1997) Molecular determinants for cellular uptake of Tat protein of human immunodeficiency virus type 1 in brain cells. *J. Virol.* **71,** 2495–2499
20. Trkola, A., Purtscher, M., Muster, T., Ballaun, C., Buchacher, A., Sullivan, N., Srinivasan, K., Sodroski, J., Moore, J. P., and Katinger, H. (1996) Human monoclonal antibody 2G12 defines a distinctive neutralization epitope on the gp120 glycoprotein of human immunodeficiency virus type 1. *J. Virol.* **70,** 1100–1108
21. Zwick, M. B., Parren, P. W., Saphire, E. O., Church, S., Wang, M., Scott, J. K., Dawson, P. E., Wilson, I. A., and Burton, D. R. (2003) Molecular features of the broadly neutralizing immunoglobulin G1 b12 required for recognition of human immunodeficiency virus type 1 gp120. *J. Virol.* **77,** 5863–5876
22. Conley, A. J., Gorny, M. K., Kessler, J. A., 2nd, Boots, L. J., Ossorio-Castro, M., Koenig, S., Lineberger, D. W., Emini, E. A., Williams, C., and Zolla-Pazner, S. (1994) Neutralization of primary human immunodeficiency virus type 1 isolates by the broadly reactive anti-V3 monoclonal antibody, 447–452D. *J. Virol.* **68,** 6994–7000
23. Moulard, M., Phogat, S. K., Shu, Y., Labrijn, A. F., Xiao, X., Binley, J. M., Zhang, M. Y., Sidorov, I. A., Broder, C. C., Robinson, J., Parren, P. W., Burton, D. R., and Dimitrov, D. S. (2002) Broadly cross-reactive HIV-1-neutralizing human monoclonal Fab selected for binding to gp120-CD4-CCR5 complexes. *Proc. Natl. Acad. Sci. U.S.A.* **99,** 6913–6918
24. Zhang, M. Y., Shu, Y., Phogat, S., Xiao, X., Cham, F., Bouma, P., Choudhary, A., Feng, Y. R., Sanz, I., Rybak, S., Broder, C. C., Quinnan, G. V., Evans, T., and Dimitrov, D. S. (2003) Broadly cross-reactive HIV neutralizing human monoclonal antibody Fab selected by sequential antigen panning of a phage display library. *J. Immunol. Methods* **283,** 17–25
25. Zhang, M. Y., Xiao, X., Sidorov, I. A., Choudhry, V., Cham, F., Zhang, P. F., Bouma, P., Zwick, M., Choudhary, A., Montefiori, D. C., Broder, C. C., Burton, D. R., Quinnan, G. V., Jr., and Dimitrov, D. S. (2004) Identification and characterization of a new cross-reactive human immunodeficiency virus type 1-neutralizing human monoclonal antibody. *J. Virol.* **78,** 9233–9242
26. Tudor, D., and Bomsel, M. (2011) The broadly neutralizing HIV-1 IgG 2F5 elicits gp41-specific antibody-dependent cell cytotoxicity in a FcγRI-dependent manner. *AIDS* **25,** 751–759
27. Stiegler, G., Kunert, R., Purtscher, M., Wolbank, S., Voglauer, R., Steindl, F., and Katinger, H. (2001) A potent cross-clade neutralizing human monoclonal antibody against a novel epitope on gp41 of human immunodeficiency virus type 1. *AIDS Res. Hum. Retroviruses* **17,** 1757–1765
28. Zwick, M. B., Labrijn, A. F., Wang, M., Spenlehauer, C., Saphire, E. O., Binley, J. M., Moore, J. P., Stiegler, G., Katinger, H., Burton, D. R., and Parren, P. W. (2001) Broadly neutralizing antibodies targeted to the membrane-proximal external region of human immunodeficiency virus type 1 glycoprotein gp41. *J. Virol.* **75,** 10892–10905
29. Manrique, A., Rusert, P., Joos, B., Fischer, M., Kuster, H., Leemann, C., Niederöst, B., Weber, R., Stiegler, G., Katinger, H., Günthard, H. F., and Trkola, A. (2007) *In vivo* and *in vitro* escape from neutralizing antibodies 2G12, 2F5, and 4E10. *J. Virol.* **81,** 8793–8808
30. Trkola, A., Kuster, H., Rusert, P., Joos, B., Fischer, M., Leemann, C., Manrique, A., Huber, M., Rehr, M., Oxenius, A., Weber, R., Stiegler, G., Vcelar, B., Katinger, H., Aceto, L., and Günthard, H. F. (2005) Delay of HIV-1 rebound after cessation of antiretroviral therapy through passive transfer of human neutralizing antibodies. *Nat. Med* **11,** 615–622
31. Chen, W., and Dimitrov, D. S. (2011) Monoclonal antibody-based candidate therapeutics against HIV Type 1. *AIDS Res. Hum. Retroviruses.* 10.1089/aid.2011.0226
32. Wu, X., Yang, Z. Y., Li, Y., Hogerkorp, C. M., Schief, W. R., Seaman, M. S., Zhou, T., Schmidt, S. D., Wu, L., Xu, L., Longo, N. S., McKee, K., O'Dell, S., Louder, M. K., Wycuff, D. L., Feng, Y., Nason, M., Doria-Rose, N., Connors, M., Kwong, P. D., Roederer, M., Wyatt, R. T., Nabel, G. J., and Mascola, J. R. (2010) Rational design of envelope identifies broadly neutralizing human monoclonal antibodies to HIV-1. *Science* **329,** 856–861
33. Corti, D., Langedijk, J. P., Hinz, A., Seaman, M. S., Vanzetta, F., Fernandez-Rodriguez, B. M., Silacci, C., Pinna, D., Jarrossay, D., Balla-Jhagjhoorsingh, S., Willems, B., Zekveld, M. J., Dreja, H., O'Sullivan, E., Pade, C., Orkin, C., Jeffs, S. A., Montefiori, D. C., Davis, D., Weissenhorn, W., McKnight, A., Heeney, J. L., Sallusto, F., Sattentau, Q. J., Weiss, R. A., and Lanzavecchia, A. (2010) Analysis of memory B cell responses and isolation of novel monoclonal antibodies with neutralizing breadth from HIV-1-infected individuals. *PLoSONE* **5,** e08805
34. Walker, L. M., Simek, M. D., Priddy, F., Gach, J. S., Wagner, D., Zwick, M. B., Phogat, S. K., Poignard, P., and Burton, D. R. (2010) A limited number of antibody specificities mediate broad and potent serum neutralization in selected HIV-1 infected individuals. *PLoSPathog.* **6,** e1001028
35. Steinaa, L., Sørensen, A. M., Nielsen, J. O., and Hansen, J. E. (1994) Antibody to HIV-1 Tat protein inhibits the replication of virus in culture. *Arch. Virol.* **139,** 263–271
36. Re, M. C., Furlini, G., Vignoli, M., Ramazzotti, E., Roderigo, G., De Rosa, V., Zauli, G., Lolli, S., Capitani, S., and La Placa, M. (1995) Effect of anti-

body to HIV-1 Tat protein on viral replication *in vitro* and progression of HIV-1 disease *in vivo*. *J. Acquir. Immune Defic. Syndr. Hum. Retrovirol.* **10,** 408–416
37. Valvatne, H., Szilvay, A. M., and Helland, D. E. (1996) A monoclonal antibody defines a novel HIV type 1 Tat domain involved in trans-cellular trans-activation. *AIDS Res. Hum. Retroviruses* **12,** 611–619
38. Rodman, T. C., Lutton, J. D., Jiang, S., Al-Kouatly, H. B., and Winston, R. (2001) Circulating natural IgM antibodies and their corresponding human cord blood cell-derived Mabs specifically combat the Tat protein of HIV. *Exp. Hematol.* **29,** 1004–1009
39. Moreau, E., Hoebeke, J., Zagury, D., Muller, S., and Desgranges, C. (2004) Generation and characterization of neutralizing human monoclonal antibodies against human immunodeficiency virus type 1 Tat antigen. *J. Virol.* **78,** 3792–3796
40. Watkins, J. D., Campbell, G. R., Halimi, H., and Loret, E. P. (2008) Homonuclear 1H NMR and circular dichroism study of the HIV-1 Tat Eli variant. *Retrovirology* **5,** 83–93
41. Shojania, S., and O'Neil, J. D. (2006) HIV-1 Tat is a natively unfolded protein. The solution conformation and dynamics of reduced HIV-1 Tat-(1–72) by NMR spectroscopy. *J. Biol. Chem.* **281,** 8347–8356
42. Campbell, G. R., and Loret, E. P. (2009) What does the structure-function relationship of the HIV-1 Tat protein teach us about developing an AIDS vaccine? *Retrovirology* **6,** 50–63
43. Lamaze, C., Dujeancourt, A., Baba, T., Lo, C. G., Benmerah, A., and Dautry-Varsat, A. (2001) Interleukin 2 receptors and detergent-resistant membrane domains define a clathrin-independent endocytic pathway. *Mol. Cell* **7,** 661–671
44. Mann, D. A., and Frankel, A. D. (1991) Endocytosis and targeting of exogenous HIV-1 Tat protein. *EMBO J.* **10,** 1733–1739
45. Saitoh, A., Hsia, K., Fenton, T., Powell, C. A., Christopherson, C., Fletcher, C. V., Starr, S. E., and Spector, S. A. (2002) Persistence of human immunodeficiency virus (HIV) type 1 DNA in peripheral blood despite prolonged suppression of plasma HIV-1 RNA in children. *J. Infect. Dis.* **185,** 1409–1416
46. Finzi, D., Blankson, J., Siliciano, J. D., Margolick, J. B., Chadwick, K., Pierson, T., Smith, K., Lisziewicz, J., Lori, F., Flexner, C., Quinn, T. C., Chaisson, R. E., Rosenberg, E., Walker, B., Gange, S., Gallant, J., and Siliciano, R. F. (1999) Latent infection of CD4+ T cells provides a mechanism for lifelong persistence of HIV-1, even in patients on effective combination therapy. *Nat. Med* **5,** 512–517
47. Kitabwalla, M., Ferrantelli, F., Wang, T., Chalmers, A., Katinger, H., Stiegler, G., Cavacini, L. A., Chou, T. C., and Ruprecht, R. M. (2003) Primary African HIV clade A and D isolates. Effective cross-clade neutralization with a quadruple combination of human monoclonal antibodies raised against clade B. *AIDS Res. Hum. Retroviruses* **19,** 125–131

Annexe 7

HMG Advance Access published July 2, 2014

Human Molecular Genetics, 2014 **1–15**
doi:10.1093/hmg/ddu320

Golgi fragmentation in *pmn* mice is due to a defective ARF1/TBCE cross-talk that coordinates COPI vesicle formation and tubulin polymerization

Sarah Bellouze[1], Michael K Schäfer[2], Dorothée Buttigieg[1], Gilbert Baillat[1], Catherine Rabouille[3,4] and Georg Haase[1,*]

[1]Institut de Neurosciences de la Timone, Centre National de la Recherche Scientifique (CNRS) and Aix-Marseille Université UMR7289, Marseille, France, [2]Klinik für Anästhesiologie, Universitätsmedizin Mainz, Mainz, Germany, [3]Hubrecht Institute-KNAW and [4]Department of Cell Biology, University Medical Center Utrecht, Utrecht, The Netherlands

Received May 9, 2014; Revised and Accepted June 17, 2014

Golgi fragmentation is an early hallmark of many neurodegenerative diseases but its pathophysiological relevance and molecular mechanisms are unclear. We here demonstrate severe and progressive Golgi fragmentation in motor neurons of progressive motor neuronopathy *(pmn)* mice due to loss of the Golgi-localized tubulin-binding cofactor E (TBCE). Loss of TBCE in mutant *pmn* and TBCE-depleted motor neuron cultures causes defects in Golgi-derived microtubules, as expected, but surprisingly also reduced levels of COPI subunits, decreased recruitment of tethering factors p115/GM130 and impaired Golgi SNARE-mediated vesicle fusion. Conversely, ARF1, which stimulates COPI vesicle formation, enhances the recruitment of TBCE to the Golgi, increases polymerization of Golgi-derived microtubules and rescues TBCE-linked Golgi fragmentation. These data indicate an ARF1/TBCE-mediated cross-talk that coordinates COPI formation and tubulin polymerization at the Golgi. We conclude that interruption of this cross-talk causes Golgi fragmentation in *pmn* mice and hypothesize that similar mechanisms operate in human amyotrophic lateral sclerosis and spinal muscular atrophy.

INTRODUCTION

The mammalian Golgi apparatus is a single copy membrane-bound organelle that comprises stacked flattened cisternae. It lays at the heart of the secretory pathway where it controls the processing and dispatching of proteins *en route* from their site of synthesis in the endoplasmic reticulum to their final subcellular destination (1). Remarkably, structural and functional alterations of the Golgi apparatus are a common hallmark of many neurodegenerative diseases including Parkinson, Alzheimer and prion disease (2). They are best characterized in amyotrophic lateral sclerosis (ALS) where Golgi fragmentation and atrophy are among the earliest pathological features of degenerating motor neurons (3,4).

Two main hypotheses have been proposed to explain pathological Golgi fragmentation in ALS. The first hypothesis focuses on microtubule defects. Indeed, Golgi fragmentation observed in degenerating motor neurons of transgenic mutant SOD1 mice (4), the most widely used familial ALS model, bears similarities with the change in the Golgi organization induced by microtubule-depolymerizing agents in cell culture (5–7). In addition, the microtubule-destabilizing protein Stathmin is strongly up-regulated in the spinal cord of these mice (8). The second hypothesis incriminates protein misfolding or mislocalization. Aggregation-prone mutant SOD1 proteins have been shown to mislocalize in the lumen of the Golgi apparatus (9) but see (10), to inhibit anterograde protein transport and to cause Golgi fragmentation *in vitro* (11,12).

To investigate whether microtubule defects or protein misfolding/mislocalization are the primary cause of Golgi fragmentation in degenerating motor neurons *in vivo*, we took advantage of the unique features of *progressive motor neuronopathy* (*pmn*) mice (13). These mice bear a mutation in the tubulin-binding cofactor E (TBCE) gene (14,15) which encodes one of at least five tubulin-specific chaperones (TBCA–TBCE) known to promote tubulin folding and microtubule polymerization (16,17). TBCE is prominently expressed in motor neurons (14) where it localizes to the Golgi and shuttles as a peripheral membrane-associated protein

*To whom correspondence should be addressed at: Institut de Neurosciences de la Timone, UMR 7289 CNRS Aix-Marseille University 27, boulevard Jean Moulin, 13385 Marseille cx 5, France. Tel: +33 673238113; Fax: +33 491324056; Email: georg.haase@univ-amu.fr

between the Golgi membrane and the cytosol (18). The importance of TBCE function in human disease is underscored by autosomal recessive TBCE mutations in patients with Sanjad–Sakati/Kenny–Caffey syndrome suffering from severe growth and mental retardation, facial dysmorphism and congenital hypoparathyroidism (19).

The *pmn* mutation, a homozygous Trp–Gly exchange at the C-terminus of TBCE, destabilizes the protein (14) which decreases the level of polymerized microtubules but increases the level of soluble tubulin (18), allowing to test the two above mentioned hypotheses on the molecular mechanism of Golgi fragmentation. Furthermore, microtubule loss in *pmn* mice starts in distal axons leading to axonal dying back (18) but leaves motor neuron cell bodies in spinal cord intact (20) enabling to investigate Golgi structure during the entire disease course.

Here, we show that in *pmn* mice as in human ALS, Golgi fragmentation is one of the earliest features of degenerating motor neurons. Loss of TBCE in *pmn* spinal motor neurons and in TBCE-depleted NSC34 motor neuron cultures impairs the polymerization of Golgi-derived microtubules, as expected, but surprisingly also results in the loss of COPI vesicle subunits, defective localization of Golgi tethering factors and increased levels of ER-Golgi v-SNAREs, yet impaired SNARE pair formation, all features sustaining the observed changes in Golgi architecture and leading to extensive Golgi vesiculation. Conversely, ARF1 that drives COPI vesicle formation recruits TBCE to the Golgi membrane, enhances polymerization of Golgi-derived microtubules and rescues TBCE-linked Golgi fragmentation. These data unravel an unprecedented ARF1/TBCE-mediated cross-talk that coordinates COPI formation and tubulin polymerization at the Golgi. We conclude that defective TBCE function in the cross-talk causes Golgi fragmentation in *pmn* motor neurons and hypothesize that similar mechanisms operate in other motor neuron diseases such as SOD1-linked ALS and SMA.

RESULTS

Golgi fragmentation and atrophy in *pmn* motor neurons involves severe progressive Golgi vesiculation

To investigate whether Golgi structure is altered in motor neurons of *pmn* mice, we first used a microscopy approach. When examined in lumbar spinal cord cryosections of 25-day-old mice by immunofluorescence for the Golgi transmembrane protein MG160, the Golgi of *pmn* motor neurons is fragmented and atrophied when compared with wild-type littermates (Fig. 1A–E and Supplementary Material, Fig. S1A–B), whereas ER (KDEL) and early endosomes (EEA1) appear normal (Supplementary Material, Fig. S1C–D).

When examined by electron microscopy, the Golgi in the cell body of wild-type motor neurons exhibits the typical morphology of stacked cisternae (Fig. 1F). In *pmn* motor neurons, however, three prominent types of Golgi alterations are observed (Fig. 1F). In the first, some Golgi cisternae are disrupted and replaced by tubules and vesicles whereas others remain intact ('partially vesicular'). In the second, Golgi cisternae are completely transformed into dense clusters of numerous tubules and small vesicles of ∼40–50 nm in diameter ('completely vesicular'). In the third, only small remnants of fragmented Golgi are observed ('remnant'). Between Day 15 when the first symptoms appear and Day 35 just before the animal's death, the frequency of completely vesiculated Golgi increases four fold (Fig. 1G), suggesting that Golgi fragmentation and atrophy in *pmn* motor neurons is due to progressive Golgi vesiculation.

Loss of TBCE results in COPI degradation and dispersion of the tethers p115/GM130

To start addressing the mechanisms of Golgi vesiculation in *pmn* motor neurons, we asked whether the formation and trafficking of COPI, COPII and clathrin-coated vesicles that mediate transport to, through and from the Golgi (1) is affected. To do so, we assessed the expression of specific coat proteins. The immunoreactivity of the COPI coat subunit β-COP is almost undetectable in *pmn* motor neurons (Fig. 2A) and the protein levels of β-COP and ε-COP in *pmn* spinal cords are strongly reduced when assessed by western blot (Fig. 2B), whereas the levels of clathrin, the COPII coat subunit Sec23 and also the intraluminal Golgi-resident enzymes Mannosidase II (MannII) and Galactosyltransferase (GalT) are similar in *pmn* and wild-type tissues (Fig. 2B). To investigate this further, we used NSC34 motor neuron cultures where endogenous TBCE was completely depleted (Fig. 2C–E). Similar to *pmn* motor neurons *in vivo*, TBCE-depleted NSC34 cells exhibit extensive Golgi fragmentation observed by the pattern of MannII-green fluorescent protein (GFP) (Fig. 2C), as well as strongly decreased β-COP levels observed by immunofluorescence (Fig. 2C), western blot (Fig. 2D) and flow cytometry (Fig. 2E).

Since β-COP directly interacts with a number of vesicle tethering proteins including p115 (22), we then tested whether the reduction of β-COP impacts on p115 and indirectly on GM130, a known p115 interactor (23). p115 and GM130 show reduced immunofluorescence signals at the Golgi of *pmn* motor neurons (Fig. 2F) but unaltered protein levels in *pmn* spinal cords (Fig. 2G), suggesting that the loss of the COPI coat affects the membrane recruitment of these tethering proteins but not their stability. Cell fractionation (Fig. 2H) confirmed that a significant pool of p115 and GM130 is cytosolic in *pmn* spinal cord contrasting with their exclusive association with membranes in wild-type. Similarly, TBCE-depleted motor neurons in culture display more hazy GM130 immunofluorescence (Fig. 2I) and decreased membrane-bound p115 (Fig. 2J).

To characterize these changes quantitatively, we fractionated cell compartments on sucrose gradients (Fig. 2K). In control cells, TBCE, MannII and GM130 are confined to light fractions containing Golgi membranes whereas β-COP is expressed in membranes of increasing densities, including fractions of 1.14–1.36 M sucrose known to contain COPI vesicles (21). Conversely, in TBCE-depleted cells, β-COP expression is specifically lost in the vesicle fractions and GM130 is no longer associated to Golgi membrane (Fig. 2K), confirming that loss of TBCE function leads to β-COP redistribution and degradation as well as reduced membrane recruitment of tethers. Since β-COP degradation is sufficient to cause vesicle accumulation and GM130 redistribution in HeLa cells (24), it most likely

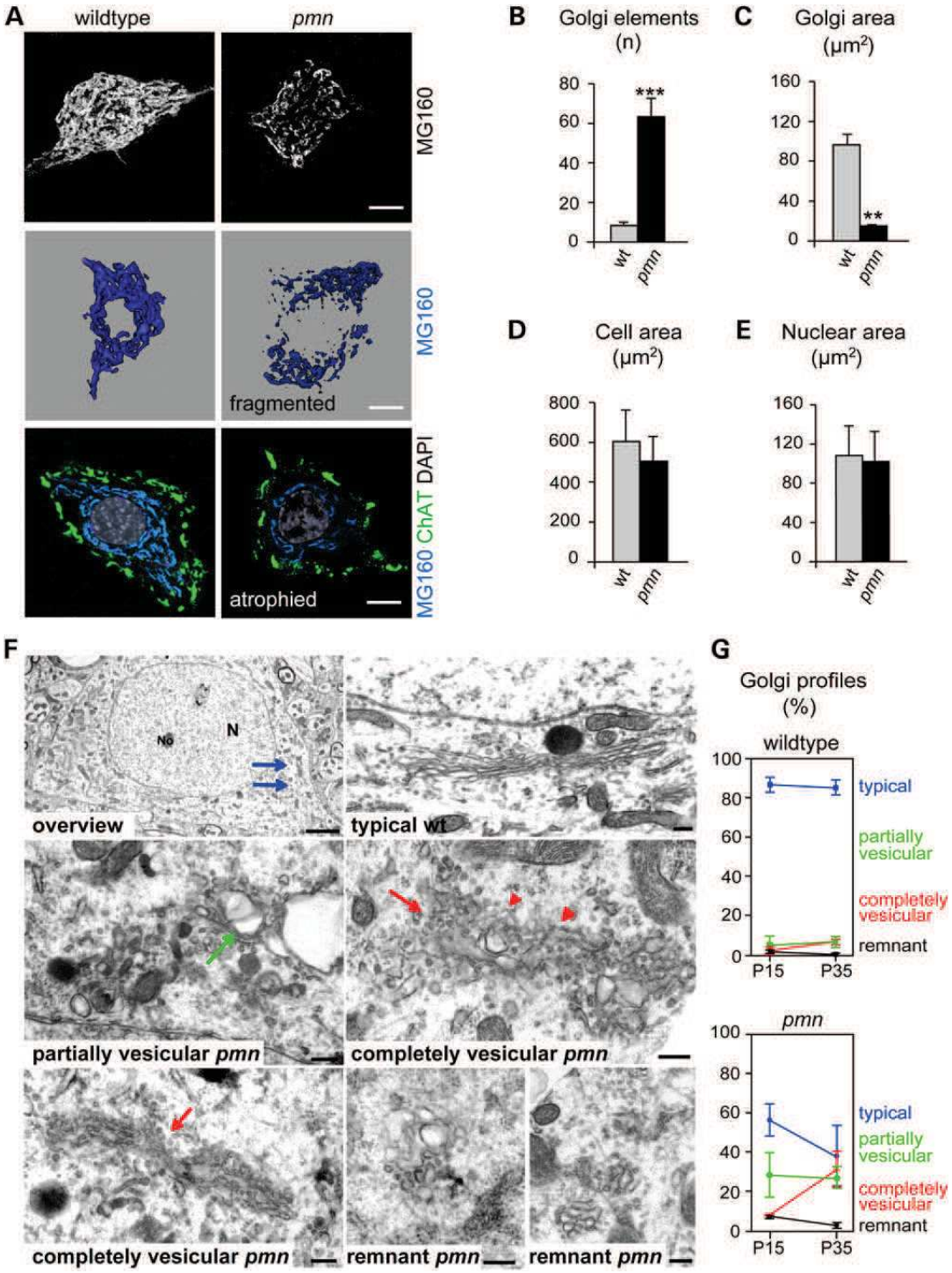

Figure 1. Golgi pathology in motor neurons of *pmn* mice. (**A**) Golgi architecture assessed by immunofluorescence using MG160 in wild-type and *pmn* motor neurons. The middle row shows a 3D surface modeling illustrating Golgi fragmentation and the lower row demonstrates the strong reduction in Golgi area (atrophy) in *pmn* motor neurons. (**B**) Increased number of Golgi elements labeled with MG160 in *pmn* motor neurons after 3D modeling (mean ± SD, $n = 12$ motor neurons per genotype, $^{***}P < 0.0001$ by Student's *t*-test). (**C**) Reduced cross-sectional area of MG160-labeled Golgi elements in *pmn* motor neurons as assessed by immunofluorescence (mean ± SD, $n = 50$ motor neurons per genotype, $^{**}P < 0.001$ by Student's *t*-test, unpaired, unequal variance). (**D**–**E**). Sizes of cell area and nuclear area measured, respectively, by VAChT immunofluorescence and DAPI staining are not statistically different between wt and *pmn*. (**F**) Electron microscopy showing an overview of a wild-type motor neuron (Day 35) with nucleus (N), nucleolus (No) and numerous Golgi profiles (arrows). Typical Golgi profiles in wild-type can be distinguished from partially vesicular, completely vesicular and remnant Golgi profiles in *pmn* motor neurons. (**G**) Quantification of Golgi profiles from the indicated categories in wild-type and *pmn* motor neurons at Day 15 and Day 35. Golgi profiles analyzed per time point: $n = 287$ (Day 15), $n = 372$ (Day 35). For each category and time point the difference between wt and *pmn* was statistically different, $P < 0.05$, Student's *t*-test, unpaired. Scale bar 10 µm (A), 200 nm (C).

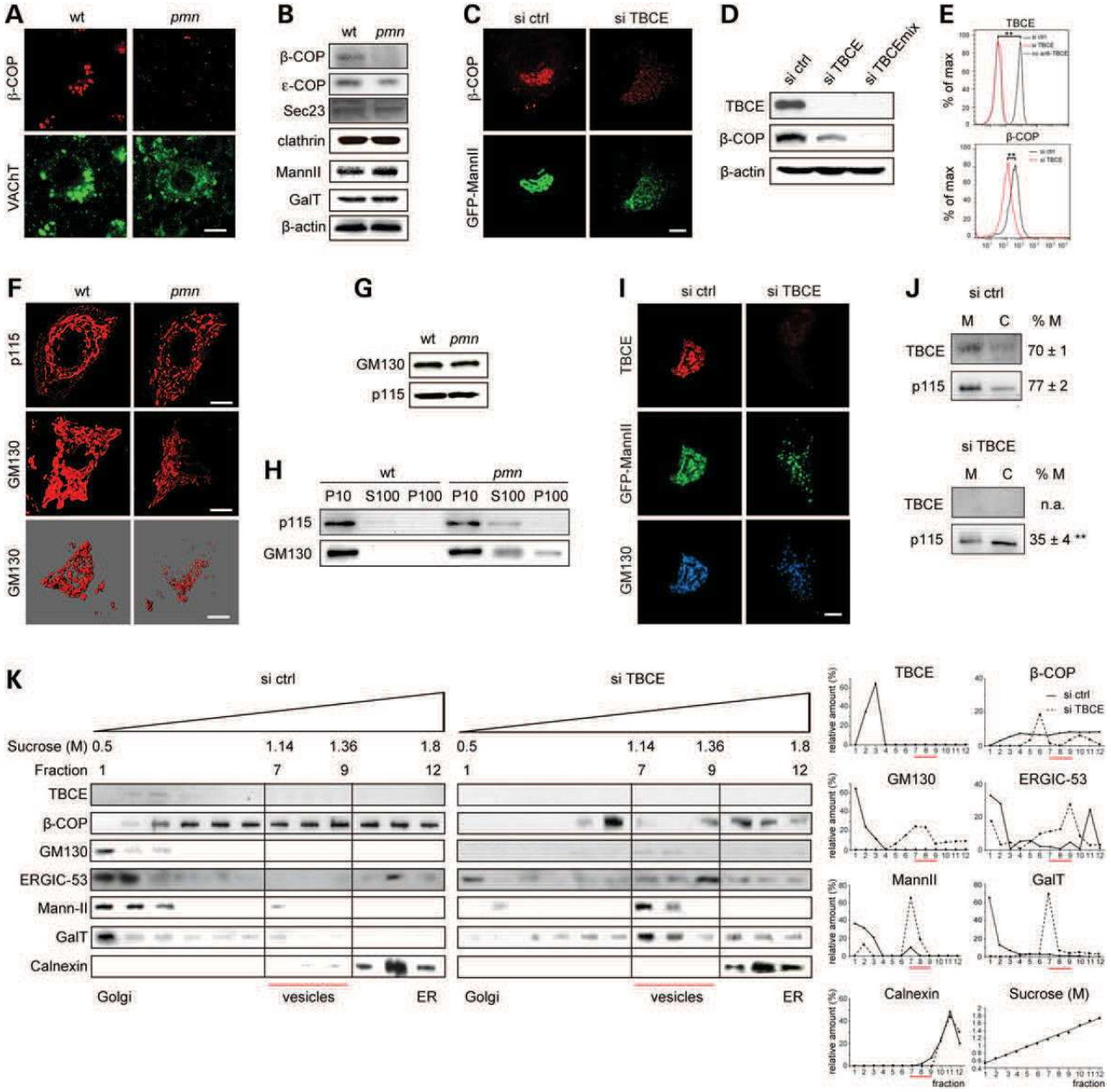

Figure 2. Defective COPI vesicle formation and tethering in mutant *pmn* and TBCE-depleted NSC34 motor neurons. (**A**) Confocal microscopy showing decreased β-COP immunoreactivity in a *pmn* motor neuron identified by vesicular acetylcholine transporter (VAchT) expression, as compared with a wild-type motor neuron at age 25 days. At least 100 motor neurons were analyzed from each lumbar spinal cord ($n = 3$ mice per genotype). (**B**) Western blot analysis of *pmn* lumbar spinal cords at age 25 days showing reduced levels of β-COP and ε-COP but normal levels of Sec23 and clathrin as compared with wild-type. Levels of MannII and GalT are also similar between *pmn* and wild-type. Western blots were performed using samples from three pairs of *pmn* and wt litter mice. Repeating the experiment twice gave similar results. (**C**) Confocal microscopy demonstrating decreased β-COP immunoreactivity in a TBCE-depleted NSC34 motor neuron with GFP-MannII-labeled Golgi fragmentation, as compared with a control neuron at 4 days in vitro (DIV) after transfection. (**D**) Western blot analysis of NSC34 motor neuron cultures showing decreased levels of β-COP after efficient TBCE depletion with si TBCE or si TBCE mix as compared with control. (**E**) Flow cytometry showing complete TBCE depletion in NSC34 motor neurons (upper panel), as compared with control cells incubated without primary antibody, and significant reduction of cellular β-COP levels (lower panel). $T(x) > 4$, $^{**}P < 0.01$ by χ^2 test. (**F**) Decreased p115 and GM130 immunoreactivity at Golgi membranes of *pmn* motor neurons as compared with wild-type siblings (upper rows). 3D-modeling of GM130 membranes (lower rows) confirms Golgi fragmentation in *pmn*. (**G**) Western blots demonstrating similar total levels of GM130 and p115 in *pmn* and wild-type spinal cords. (**H**) Subcellular fractionation showing pathological redistribution of GM130 and p115 from P10 fraction (membranes) to S100 (cytosol) and for GM130 also to P100 (membrane fragments, vesicles) in *pmn* spinal cord extracts, $n = 3$ independent experiments. (**I**) Confocal microscopy showing decreased GM130 immunoreactivity at fragmented Golgi (GFP-MannII) in TBCE-depleted NSC34 cell as compared with control cell. (**J**) Cell fractionation showing lower p115 recruitment to membranes in TBCE-depleted cells, as compared with controls. Protein expression in membrane (M) and cytosol (C) is quantified relative to total, $\%M = M/(M + C)$, mean ± SD, $^{**}P < 0.001$ by Student's *t*-test. na, not applicable, $n = 3$ independent experiments. (**K**) Sucrose density fractionation. In control cells, Golgi membranes are identified in fractions 1–4 by TBCE, MannII and GM130, vesicles in fractions 7–9 according to their sucrose density of 1.14–1.36 M (21) and ER membranes in fractions 10–12 by Calnexin. In TBCE-depleted cells, GM130 is completely lost from Golgi membranes, β-COP is specifically lost from vesicle fractions and ERGIC-53, MannII as well as GalT peak in vesicle fractions. Plots showing relative protein content per fraction (right panels) are representative of ≥2 independent experiments. Sucrose concentration in each fraction was measured by enzymatic assay. Scale bars 10 μm.

mediates Golgi vesiculation in *pmn* and TBCE-depleted motor neurons.

In the early secretory pathway, COPII vesicles normally fuse with themselves (25) and the ER/Golgi intermediate compartment (ERGIC) (26). β-COP-depletion is known to cause fragmentation of the ERGIC into vesicular structures containing ERGIC-53 (27) and Golgi-resident enzymes, such as GalT (22). In line with this, we found that ERGIC-53 and GalT are completely shifted to vesicle fractions in TBCE-depleted cells (Fig. 2K), suggesting that the accumulating vesicles represent ERGIC fragments and COPII vesicles unable to fuse.

Loss of TBCE leads to increased levels of Golgi v-SNAREs but impaired vesicle fusion

The fusion of COPI and COPII vesicles with their target membranes is mediated by the pairing of ER/Golgi v-SNAREs with cognate t-SNAREs (28). The vesicle accumulation in *pmn* and TBCE-depleted motor neurons might therefore suggest an impaired SNARE pairing. To test this, we assessed the formation of the two known ER/Golgi SNARE pairs GS28/Syntaxin 5a (29) and GS15/Ykt6 (30). By western blot, the total levels of the t-SNAREs Syntaxin 5a and Ykt6 (Fig. 3A) remain unchanged in *pmn* spinal cords whereas the levels of the v-SNAREs GS15 and GS28 are increased by >10-fold in *pmn* when compared with wild-type spinal cords (Fig. 3A). The level of the endosomal v-/t-SNAREs Vti1a/Syntaxin 6 remains unaffected demonstrating specificity (Fig. 3A). The increase in GS28 and GS15 levels in *pmn* versus wild-type motor neurons is also documented by immunofluorescence (Fig. 3B, upper rows). Quantitative polymerase chain reaction analyses showed no increase in GS15 and GS28 mRNA levels in *pmn* spinal cords at various time points (Supplementary Material, Fig. S2), suggesting that the increase in v-SNARE protein levels is due to enhanced protein stability or reduced protein degradation rather than to transcriptional up-regulation.

ER/Golgi v-SNAREs are recycled back to the ER by COPI vesicles (31,32) and loss of β-COP in *pmn* and TBCE-depleted cells might impede this recycling. To assess v-SNARE recycling, we examined the distribution of GS15 and GS 28 that accumulate in small dispersed puncta, as shown by 3D modeling (Fig. 3B, lower rows). These puncta likely correspond to Golgi vesicles or groups of Golgi vesicles as both v-SNAREs are shifted to vesicle fractions in TBCE-depleted fractionated cells (Fig. 3C), suggesting that loss of TBCE function impairs v-SNARE recycling to the ER.

To investigate why the v-SNARE-loaded Golgi vesicles accumulate instead of fusing, we assessed v-/t-SNARE pairing by immunoprecipitation and found that in TBCE-depleted cells GS15/Syntaxin 5a and GS28/Syntaxin 5a complexes are less abundant than in control cells (Fig. 3D upper rows), whereas unpaired GS15, GS28 and Syntaxin 5a are more abundant (Fig. 3D, lower rows). High resolution confocal imaging and pixel per pixel analysis supported that GS28/Syntaxin 5a signals are dissociated in TBCE-depleted cells but overlapping in control cells (Fig. 3E). Taken together, these data suggest that ER/Golgi SNARE pairing and recycling is strongly impaired in the absence of TBCE despite the increased protein levels of GS15 and GS28.

Golgi vesiculation in *pmn* motor neurons is caused by loss of TBCE and not a consequence of neuronal damage

Since Golgi fragmentation is one of the earliest pathological features of degenerating motor neurons in ALS (4), we thought to determine the onset and kinetics of Golgi vesiculation in *pmn* mice. Motor neuron disease in *pmn* mice first manifests at Day 15 with skeletal muscle paresis and atrophy and leads to the animal's death 3 weeks later (13). We here demonstrate that the loss of myelinated fibers in the phrenic motor nerve starts at Day 15 and then continues progressively (Supplementary Material, Fig. S3), in line with our earlier studies (20,33). We therefore monitored Golgi vesiculation in *pmn* and control litter mice at two presymptomatic stages (Days 5 and 10), disease onset (Day 15), midstage (Day 25) and endstage (Day 35). Altered GM130 and GS28 immunofluorescence in motor neurons is first detected at Day 10 (Fig. 4A–B), 5 days before first clinical and histopathological alterations. GM130 and GS28-labeled Golgi vesiculation then progressively affects the majority of motor neurons (Fig. 4A–B), matching a continuous rise of the v-SNARE levels in *pmn* spinal cords (Fig. 4C).

The presymptomatic onset of Golgi vesiculation in *pmn* mice suggests that this phenomenon is not a simple consequence of motor neuron damage. We tested this by unilateral transection of the sciatic nerve in wild-type mice and analysis of the retrogradely labeled lesioned motor neurons (Fig. 4D–F). Both p115 labeling (Fig. 4D–E) as well as β-COP, GS15 and GS28 protein levels (Fig. 4F) are unaffected in the lesioned motor neurons when compared with unlesioned ones, indicating that Golgi vesiculation in *pmn* motor neurons is not a consequence of motor neuron damage but may be a contributor to the disease.

To demonstrate that Golgi vesiculation in *pmn* motor neurons is due to loss of TBCE function, we complemented *pmn* mice with wild-type TBCE transgenes (18), which partially or completely restore TBCE expression at the Golgi apparatus (Fig. 4G–I). Transgenic TBCE complementation restores normal p115 labeling in individual motor neurons (Fig. 4G–H) and rescues the pathological spinal cord levels of β-COP, GS15 and GS28 (Fig. 4I). Transgenic TBCE complementation also normalizes the pathologically increased number of GS28-labeled Golgi elements in motor neurons of *pmn* mice, as shown by quantitation of 3D Golgi modelings (Fig. 4J–K). Whereas the number of small GS28-labeled Golgi elements increases in *pmn* motor neurons, it goes down to wild-type levels upon TBCE transgene expression in both lines of transgenic TBCE *pmn* mice, indicating full rescue of Golgi vesiculation. Taken together, these data indicate that loss of TBCE function in *pmn* motor neurons is responsible for Golgi vesiculation.

TBCE is instrumental for the nucleation and growth of Golgi-derived microtubules

How may loss of TBCE function cause Golgi vesiculation? According to previous studies (16), TBCE is essential for the folding of α-tubulin and its polymerization into microtubules. Tubulin polymerization in differentiated neurons mainly takes place at non-centrosomal sites (34) such as the Golgi (35,36) where TBCE is localized (18). We therefore searched for defects in Golgi-associated microtubules containing detyrosinated (Δ-Tyr) tubulin (37) and found that these are greatly diminished

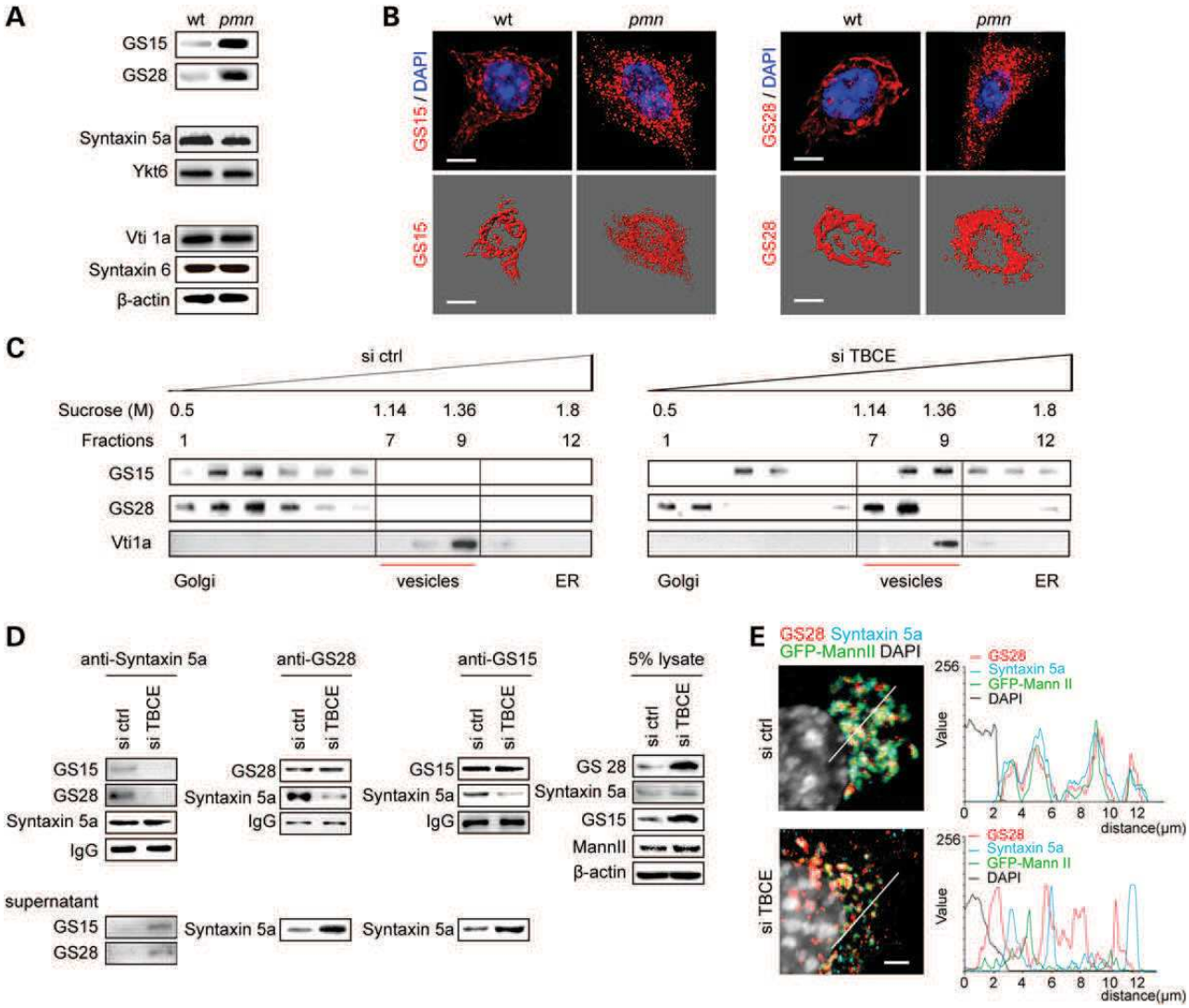

Figure 3. TBCE-linked Golgi vesiculation is associated with defective SNARE pairing and recycling. (**A**) Western blots showing a drastic increase in Golgi v-SNAREs GS15 and GS28 in *pmn* spinal cord but normal expression of the corresponding t-SNAREs Syntaxin 5a and Ykt6 as compared with wild-type siblings. Expression of endosomal SNARE pairs Vti1a/Syntaxin 6 and also of MannII and GalT is unaltered in *pmn*. (**B**) Confocal imaging (upper rows) and 3D modeling (lower rows) reveal accumulation of GS15 and GS28 in small vesicle-like puncta of *pmn* motor neurons. (**C**) Sucrose gradient fractionation showing a shift of GS15 and GS28 to vesicle fractions in TBCE-depleted cells. The control protein Vt1a is not shifted. Data are representative of ≥2 independent experiments. (**D**) Immunoprecipitation analysis of v-/t-SNARE complexes. Reduced levels of GS15/Syntaxin 5a and GS28/Syntaxin 5a complexes (upper panels) but increased amounts of unpaired SNAREs (lower panels) in TBCE-depleted cells as compared with control cells. Controls: MannII and β-actin in cell lysates, IgG in immunoprecipitates. Two independent experiments gave similar results. (**E**) High resolution confocal imaging and fluorescent line profiles showing dissociated GS28/Syntaxin 5a signals in TBCE-depleted cells as compared with overlapping signals in control cells, $n = 20$ cells analyzed per condition. Scale bars 10 μm (B), 5 μm (E).

in mutant *pmn* (Fig. 5A) and TBCE-depleted motor neurons (Fig. 5B–C). To confirm that TBCE is required for the nucleation and growth of Golgi-derived microtubules, we performed washout experiments after treatment with the microtubule-disrupting drug nocodazole (10 μM, 5 h). Nocodazole causes Golgi fragmentation into ministacks (5,6) but does not displace TBCE from the Golgi membrane (Fig. 5D). In control cells, small microtubule asters begin to form immediately after nocodazole washout at dispersed Golgi profiles (Fig. 5E). These microtubules then grow rapidly (Fig. 5F) and reach neighboring Golgi profiles (Fig. 5E, G), leading to re-formation of a compact Golgi ribbon within 200 min (Supplementary Material, Fig. S4). In TBCE-depleted cells however, Golgi-derived microtubules are rare (Fig. 5E), grow much slower than in control cells (Fig. 5F) and only rarely reach neighboring Golgi profiles (Fig. 5E, G) leaving the Golgi disrupted at all time points (Supplementary Material, Fig. S4). These data indicate that TBCE is required for the nucleation and growth of Golgi-derived microtubules.

Accumulation of soluble α-tubulin is not sufficient to trigger Golgi vesiculation

During tubulin folding, α- and β-tubulins first interact with the chaperone proteins prefoldin (38) and cytosolic chaperonin

(39), thus generating tubulin folding intermediates (16). α-tubulin folding intermediates interact with tubulin chaperones TBCB and TBCE and β-tubulin folding intermediates with TBCA and TBCD (16,17). Finally, TBCE/α-tubulin, TBCD/β-tubulin and TBCC form a supercomplex that releases native α/β-tubulin heterodimers competent for polymerization into microtubules (40). In line with the function of TBCE in this pathway, we found that TBCE-depleted NSC34 cells contain more soluble α-tubulin (Fig. 6A), less polymerized α-tubulin (Fig. 6A), and alterations of cellular microtubules (Fig. 6C–D). These changes are closely associated with the molecular and structural stigmata of Golgi vesiculation (Fig. 6B–D).

To determine whether an increase in soluble α-tubulin can trigger Golgi vesiculation, we expressed the folding-defective α-tubulin mutant TUBA1 R264C which is unable to stably interact with TBCB (41). In contrast to its wild-type counterpart, flag-tagged mutant TUBA1 is not efficiently polymerized into cellular microtubules (Fig. 6E, H) and accumulates in a soluble form (Fig. 6E). Mutant TUBA1 significantly increases the cellular levels of soluble α-tubulin (Fig. 6F), similarly to TBCE depletion (Fig. 6A), but without affecting the polymerization of endogenous α-tubulin (Fig. 6F) or the structure of the residual microtubule network (Fig. 6H–I). Strikingly, expression of mutant TUBA1 does not alter β-COP, GS15 and GS28 levels (Fig. 6G) or Golgi structure (Fig. 6H–I), indicating that mutant TUBA1 expression is not sufficient to drive Golgi vesiculation. The differential effects of mutant TUBA1 expression and TBCE depletion strongly suggest that Golgi vesiculation is caused by loss of microtubules rather than by accumulation of soluble α-tubulin.

Golgi maintenance depends on an ARF1/TBCE-mediated cross-talk that coordinates COPI vesicle formation and tubulin polymerization at the Golgi

Our data raise the hypothesis that TBCE maintains Golgi structure by adjusting the polymerization of Golgi-derived microtubules to the formation of COPI vesicles. To begin to test this, we modulated the activity of ARF1, the small GTPase that controls COPI vesicle formation (1). Inhibiting ARF1 activity with brefeldin A not only reduces the levels of β-COP at the Golgi, but also shifts TBCE into the cytosol and decreases the number of Golgi-derived microtubules (Supplementary Material, Fig. S5A–B), suggesting that ARF1 regulates TBCE activity.

We next enhanced ARF1 function by (over)expressing wild-type ARF1 or the constitutively active ARF1 mutant Q71L. Both forms of ARF1 accumulate at the Golgi and recruit β-COP (Fig. 7A), as expected. Remarkably, they also lead to an increased recruitment of TBCE to the Golgi membrane, as observed by immunolabeling (Fig. 7A, arrows on right panels), cell fractionation (Fig. 7B) and flow cytometry (Fig. 7C) and to increased polymerization of Golgi-derived microtubules (Fig. 7A and C). Overall, ARF1 Q71L is significantly more effective than ARF1 wt (Fig. 7C). Taken together, these data suggest a cross-talk between ARF1 and TBCE that coordinates tubulin polymerization and COPI formation at the Golgi.

To test whether this cross-talk is involved in Golgi maintenance, we attempted to rescue TBCE-linked Golgi alterations with ARF1. Remarkably, overexpression of ARF1 Q71L after TBCE knockdown strongly prevents alterations of Golgi-derived microtubules (Fig. 7D–E) and rescues defective Golgi architecture labeled by β-COP and GM130 (Fig. 7D–E and data not shown). Flow cytometry suggests that this occurs through ARF1-mediated stabilization of membrane-bound TBCE (Fig. 7F). These data show that defective ARF1/TBCE cross-talk causes Golgi fragmentation in motor neurons.

DISCUSSION

We here report a novel ARF1/TBCE-mediated cross-talk (Fig. 7G) in which membrane-bound active ARF1 catalyzes COPI coat assembly and recruits TBCE to the Golgi membrane where TBCE drives the nucleation and polymerization of Golgi-derived microtubules. We hypothesize that these microtubules then stabilize the COPI coat through their reported interaction with the β-COP subunit (7). The ARF1/TBCE cross-talk is reminiscent of the regulation of the tubulin-binding co-factor TBCD by the ARF1-related GTPase ARL2 (42). It also mirrors interactions between COPII and the microtubule-dependent motor protein dynein at ER exit sites (43), and between clathrin and actin at the trans Golgi network (44,45), illustrating emerging signaling pathways between vesicular coats, cytoskeleton and motor proteins that ensure efficient coordination of carrier formation and transport in the secretory pathway.

How does an interrupted cross-talk between ARF1 and TBCE cause Golgi fragmentation? We show that absence of TBCE causes loss of Golgi-derived microtubules, β-COP degradation and diminished membrane-recruitment of tethering factors p115/GM130. The degradation of β-COP, ε-COP and possibly other COPI subunits impedes the function of the ER/Golgi intermediate compartment as the target for COPII-derived vesicles (25,26), resulting in accumulation of the latter. This scenario of Golgi fragmentation (Fig. 7G) is recapitulated by β-COP depletion, causing accumulation of small vesicles containing Golgi enzymes at the cell center (22) and redistribution of GM130 (24).

How does loss of TBCE function cause the increased level of Golgi v-SNAREs GS15 and GS28? There are two possibilities. First, GS28 is known to be recycled by COPI vesicles (46) and to be degraded by the proteasome after interaction with the ubiquitin-like (UBL) protein GATE-16 and its regulator ORP7 (47,48). The *pmn* mutation results in the incorporation of the v-SNAREs in COPII vesicles, possibly away from GATE-16 and its function in proteasomal degradation, hence leading to their accumulation. Second, TBCE itself contains a C-terminal UBL domain which is structurally similar to GATE-16 (T. Levine, personal communication) and might thus directly participate in the v-SNARE degradation. The Trp524>Gly mutation in *pmn* would destabilize the UBL domain inhibiting its interaction with the proteasome (49) leading to the v-SNARE increase.

Does altered COPI vesicle formation or trafficking cause Golgi fragmentation in other neurodegenerative diseases than *pmn*? It may be the case in mice mutated in the COPI subunit δ-COP/Archain with Purkinje cell degeneration (50) and in mice mutated in the β-COP-interacting protein Scyl1 such as *muscle deficient* (51,52) or Scyl1 KO (53) with motor neuron degeneration which, however, need to be investigated for potential Golgi alterations. It is likely the case in motor neurons of mutant

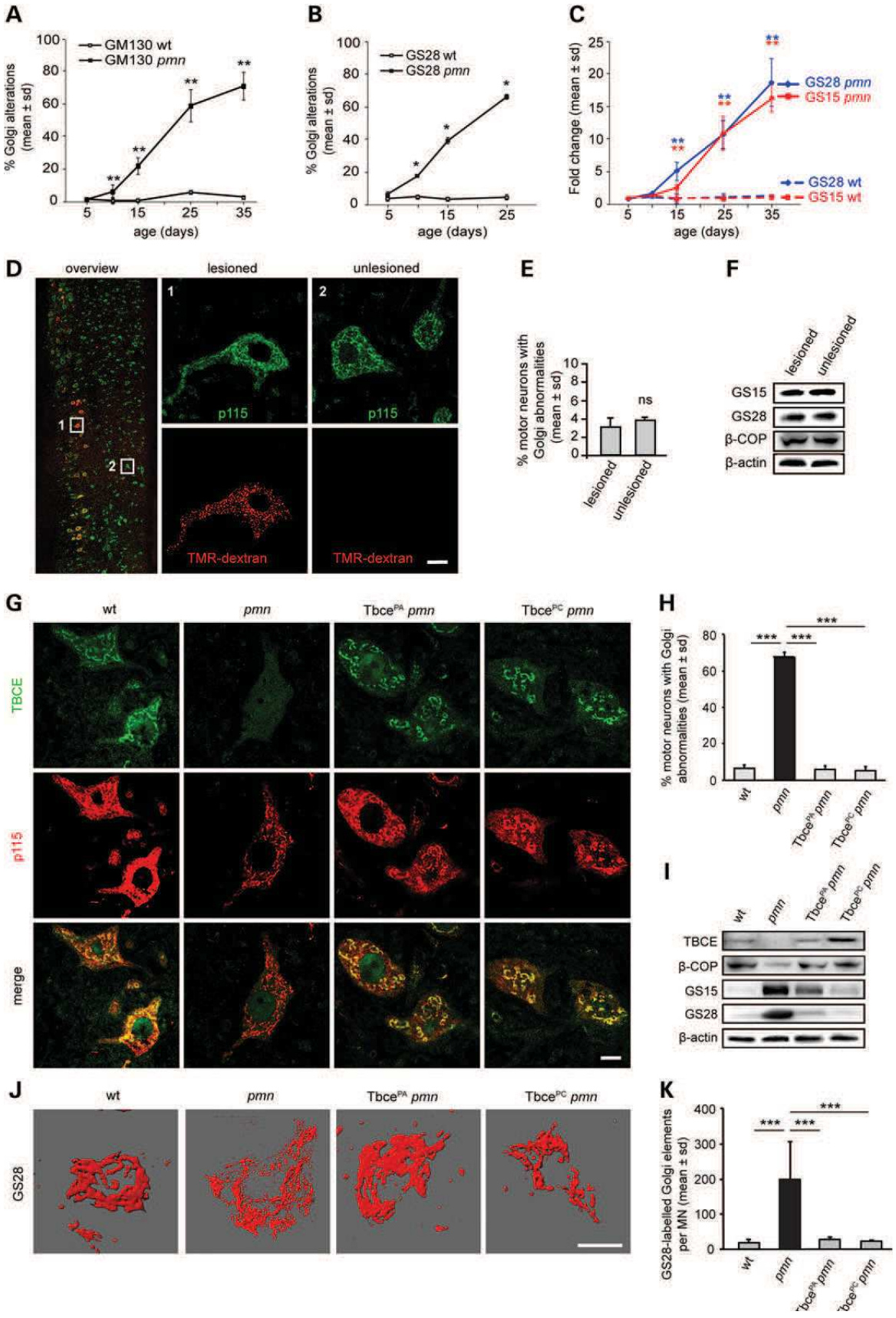

SOD1 mice since these display Golgi fragmentation and up-regulation of the microtubule-depolymerizing protein stathmin (8) together with similar dysregulation of β-COP, GS15 and GS28 (Supplementary Material, Fig. S6A-D) and similar GS15- and GS28-labeled Golgi vesiculation (Supplementary Material, Fig. S6E–F) as *pmn* mice. Defective coordination of vesicle formation and trafficking may thus cause Golgi fragmentation in human SOD-linked ALS and other neurodegenerative disorders.

What may be the contribution of altered COPI vesicle trafficking to motor neuron degeneration and dysfunction? Blocking COPI formation in neuronal cultures by inhibiting ARF1 causes collapse of growing axons (54), suggesting a critical role of COPI vesicles in axon growth or maintenance. The COPI subunit α-COP has been shown to interact with survival motor neuron (SMN), the protein deficient in spinal muscular atrophy, and to co-traffic with SMN in motor axons (55). Interrupting α-COP–SMN interactions leads to SMN accumulation at the Golgi (56), reduced neurite outgrowth (57) and growth cone defects similar to those observed after pharmacological Golgi fragmentation (56). Furthermore, the COPI subunits α-, β- and γ-COP bind numerous mRNAs (58,59) at least some of which require microtubules for their axonal transport (58). The Golgi apparatus is also responsible for packaging precursors of synaptic vesicles which are lost at an early disease stage in mutant SOD1 (60), SMN (61) and *pmn* mice (B.S., G.H., unpublished data). Defective coordination between the polymerization of microtubules and the formation of COPI vesicles may thus compromise the transport of critical axon and synapse constituents and thereby contribute to motor neuron degeneration and dysfunction.

MATERIALS AND METHODS

Antibodies and reagents

Primary antibodies were as follows [supplier, dilution in immunofluorescence (IF), western blot (WB) and cytometry (Cyt)]: TBCE [rabbit SA53 (18)], IF 1:300, WB 1:500, Cyt 1:50), TBCE (Abnova, IF 1:200), FLAG (Sigma, IF 1:1000, WB 1:2000), GFP (Roche, WB 1:2000), HA (Roche, WB 1:1000, cytometry 1:750), VAChT (Sigma, IF 1:2000), ChAT (Chemicon, IF 1:100), GM130 (Becton Dickinson, IF 1:300, WB 1:500), p115, GS15, GS28, Rab5, Syntaxin 6, Calnexin, Clathrin, Vti1a, (Becton Dickinson; IF 1:300, WB 1:1000), Syntaxin 5a (Abcam, WB1:1000), Sec23 (Abcam 50672, WB 1:1000), β-COP (Abcam, WB 1:2000, IF 1:500, Cyt 1:1000), β-COP (Dr R. Duden, University of Lübeck, WB 1:1000), MG160 (Abcam, IF: 1:500), ARF1 (Dr R.A. Kahn, Emory University, WB 1:1000), Ykt6 (Dr J.C. Hay, University of Michigan, WB 1:2000), MannII (Covance, WB 1:1000), GalT (PTG, WB 1:1000), KDEL (StressGen, IF 1:500), α-tubulin (Sigma, IF 1:2000, WB 1:5000), acetylated-tubulin (Sigma, WB 1:2000), β-actin (Sigma, WB 1:5000), α-tubulin-fluorescein isothiocyanate (FITC) (Sigma, Cyt 1:2000), β_{III}-tubulin (TuJ1, Babco, IF 1:2000, WB 1:10000), Δ-Tyr-tubulin (Dr A. Andrieux, IF 1:5000, WB 1:10000, Cyt 1:1000), Tyr-tubulin (Dr A. Andrieux, WB 1:2000). Fluorochrome-conjugated secondary antibodies were from Molecular Probes (Carlsbad, CA) and horse radish peroxidase-conjugated secondary antibodies from Jackson Immuno Research (West Grove, PA).

Small interfering (si) RNA duplexes against mouse TBCE (NM_178337, refs D-057655-00 and M-057655-01) or luciferase control (ref P-002099-01-20) were purchased from Dharmacon (Chicago, IL).

si TBCE 5′-GUAGAAGAGUUGAAGUUAA
si TBCE mix 5′-GUAGAAGAGUUGAAGUUAA,
5′-CCACGAAGGUACUAUGUAU,
5′-UACCUCAAGUCUAACAAUA,
5′-CUAGAAACCCUUUGAGCAA
si luciferase 5′-CAUUCUAUCCUCUAGAGGAUG

Plasmid expression vectors contained the following cDNAs: GFP-MannII (Dr M. Bornens, Institut Curie, Paris), TUBA1A wt or TUBA1A R264C (Dr J. Chelly, Institut Cochin, Paris), ARF1 wt, Q71L and T31N (Dr J. Donaldson, NIH, Bethesda).

Additional reagents were from the following suppliers: phosphate buffered saline (PBS), Hank's balanced salt solution, trypsin, culture media and supplements (Invitrogen, Carlsbad,

Figure 4. Kinetics, specificity and TBCE-mediated rescue of Golgi vesiculation in *pmn* motor neurons. (**A–B**) Kinetics of Golgi alterations labeled by immunofluorescence for GM130 (A) or GS28 (B) in *pmn* and wild-type motor neurons, $n > 200$ motor neurons from at least two mice per genotype and time-point, $^{**}P < 0.01$ by Student's *t*-test. (**C**) Kinetics of GS15 and GS28 levels in *pmn* and wild-type spinal cord extracts analyzed by western blot. Fold changes are expressed relative to levels at Day 5. Each time point represents $n = 3$ spinal cords per genotype analyzed each by two independent densitometric scans. $^{*}P < 0.05$ by Student's *t*-test., $^{**}P < 0.01$ by Student's *t*-test. (**D**) Confocal imaging showing the absence of Golgi alterations after axotomy. Sciatic nerves of 35-day-old normal mice were unilaterally transected, motor neurons retrogradely labeled with Tetramethylrhodamin (TMR)–dextran and lumbar spinal cord sections immunolabeled for p115. The overview in the frontal plane shows motor neurons on the lesioned and unlesioned side. The zooms demonstrate absence of Golgi pathology in lesioned motor neurons, as compared with unlesioned motor neurons. (**E**) No significant Golgi alterations in lesioned motor neurons. $P = 0.34$ (ns, non-significant by Student's *t*-test), $n = 251$ (lesioned), $n = 275$ (unlesioned) motor neurons from a total of three animals. (**F**) Western blots showing similar levels of β-COP, GS15 and GS28 in lumbar spinal cord hemisegments from the lesioned and unlesioned side. (**G**) Confocal imaging showing rescue of Golgi alterations in *pmn* mice by transgenic complementation with wild-type TBCE. Lumbar spinal cord cross sections from 35-day-old wild-type, *pmn*, transgenic $Tbce^{PA}$ *pmn* and $Tbce^{PC}$ *pmn* mice were immunolabeled for TBCE and p115. Loss of TBCE expression in *pmn* motor neurons is associated with reduced p115 immunolabeling at Golgi membranes. Transgenic TBCE expression in motor neurons of $Tbce^{PA}$ *pmn* and $Tbce^{PC}$ *pmn* mice restores normal p115 immunolabeling. (**H**) Rescue of p115-labeled Golgi alterations in motor neurons of transgenic $Tbce^{PA}$ *pmn* and $Tbce^{PC}$ *pmn* mice. Number of motor neurons and mice analyzed per genotype: wt $n = 390$ (four mice), *pmn* 397 (four mice), $Tbce^{PA}$ *pmn* $n = 275$ (3 mice), $Tbce^{PC}$ *pmn* $n = 321$ (three mice). Statistical significance $^{***}P < 0.001$ by one-way ANOVA and Tukey's *post hoc* test: significant for *pmn* versus wt, $Tbce^{PA}$ *pmn* versus *pmn*, and $Tbce^{PC}$ *pmn* versus *pmn*, $Tbce^{PA}$ *pmn* versus wt, not significant for $Tbce^{PC}$ *pmn* versus wt, $Tbce^{PA}$ *pmn* versus *pmn* and $Tbce^{PC}$ *pmn* versus $Tbce^{PA}$ *pmn*. (**I**) Transgenic rescue of pathological β-COP, GS15 and GS28 expression analyzed by western blot in lumbar spinal cord of $Tbce^{PA}$ *pmn* and $Tbce^{PC}$ *pmn* mice as compared with wild-type and *pmn* mice. Data are representative of three independent tissue samples per genotype. Two independent experiments gave similar results. (**J**) Rescue of Golgi vesiculation by transgenic TBCE complementation. 3D modelings show GS28-labeled Golgi elements in lumbar motor neurons of the indicated genotypes. (**K**) Rescue of the number (mean ± SD) of GS28-labeled Golgi elements determined by 3D-modeling. Number of motor neurons counted by an observer blinded to the genotypes: wt $n = 12$, *pmn* $n = 12$, $Tbce^{PA}$ *pmn* $n = 13$, $Tbce^{PC}$ *pmn* $n = 12$, each from two mice per genotype. Statistical significance $P < 0.0001$ between groups by Kruskal–Wallis test and Dunn's *post hoc* test for *pmn* versus wt, $Tbce^{PA}$ *pmn* versus *pmn* and $Tbce^{PC}$ *pmn* versus *pmn*; not significant for $Tbce^{PA}$ *pmn* versus wt, $Tbce^{PC}$ *pmn* versus wt, and $Tbce^{PA}$ *pmn* versus $Tbce^{PC}$ *pmn*. Scale bars 10 μm.

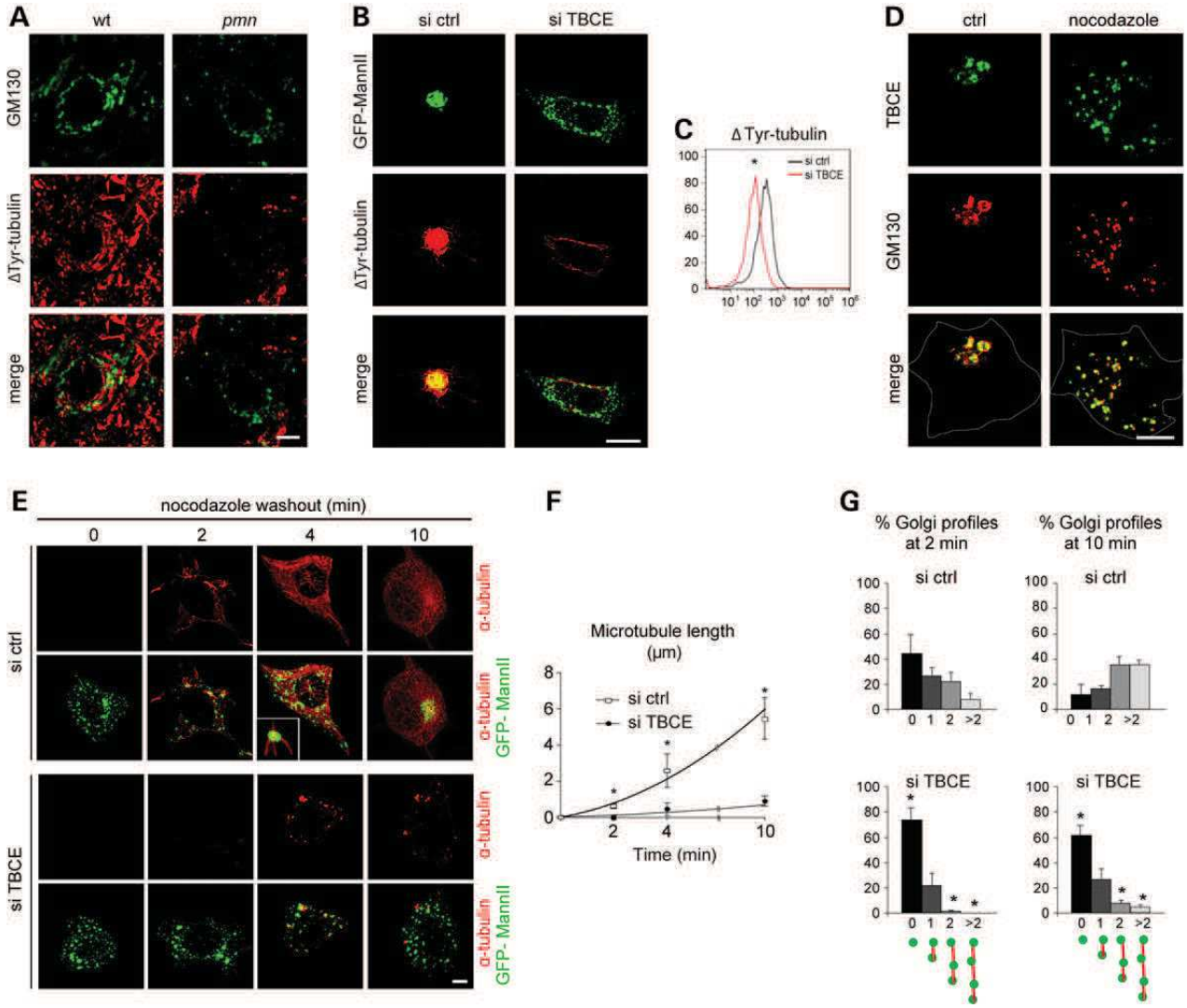

Figure 5. Defective polymerization of Golgi-derived microtubules in *pmn* and TBCE-depleted motor neurons. (**A**) Immunofluorescence showing that fragmentation of the GM130-labeled Golgi apparatus in motor neurons of 25-day-old *pmn* mice is associated with loss of Golgi-associated microtubules labeled for ΔTyr-tubulin, as compared with wild-type. (**B**) Loss of ΔTyr-tubulin-labeled microtubules in TBCE-depleted NSC34 motor neurons co-labeled with GFP-MannII, as compared with control. (**C**) Flow cytometry showing reduced levels of ΔTyr-tubulin-labeled microtubules after TBCE-depletion. (**D**) Immunofluroescence showing that TBCE remains associated with GM130-labeled Golgi profiles in nocodazole-treated NSC34 cells. (**E**) Immunofluroescence showing regrowth of microtubules from GFP-MannII-labeled Golgi profiles in control and TBCE-depleted NSC34 motor neurons after nocodazole treatment and washout. (**F**) Reduced growth rate of Golgi-derived microtubules in TBCE-depleted cells. Each point (means of mean ± SD) represents $n = 10$ cells per condition/time point and 10 randomly chosen microtubules per cell, $^{*}P < 0.05$ by Student's *t*-test. (**G**) Increased percentage of Golgi elements unlinked to microtubules in TBCE-depleted cells as compared with control cells after nocodazole washout. Golgi elements are classified into four categories. Mean ± SD, $n \approx 500$ profiles analyzed per time point and condition, $^{*}P < 0.05$ by Student's *t*-test.

CA), polyornithin, taxol, nocodazole (Sigma), Vectashield (Vector laboratories, Burlingame, CA), Complete protease inhibitors (Roche, Basel, Switzerland), Ketamine (Bayer, Leverkusen, Germany) and Xylazine (Mérial, Lyon, France), coverslips and Superfrost Plus glass slides (Menzel, Schwerte, Germany).

Mouse lines

Mutant *pmn* mice, $TBCE^{PA/+}$ *pmn* and $TBCE^{PC/+}$ *pmn* mice were maintained on a mixed background (C57/BL6; 129/SvJ) using intercrosses (>F8) and genotyped by PCR (18).

Axotomy and retrograde labeling of motor neurons

Mice were anesthetized by intraperitoneal injection of Ketamine (50 mg/kg) and Xylazine (10 mg/kg). Under a stereomicroscope, a skin incision was made, the sciatic nerve identified and cut at the hip level. A piece of hemostatic sponge (Spongostan, Ferrosan, Denmark) 2 × 2 × 2 mm in size was soaked in tetramethylrhodamine–dextran (Molecular Probes, 10% w/v in PBS) and applied to the proximal stump. The wound was closed with metal clips and an antibiotic prophylaxis with ampicillin administered. All experiments with animals were performed in strict compliance with French and European legislation.

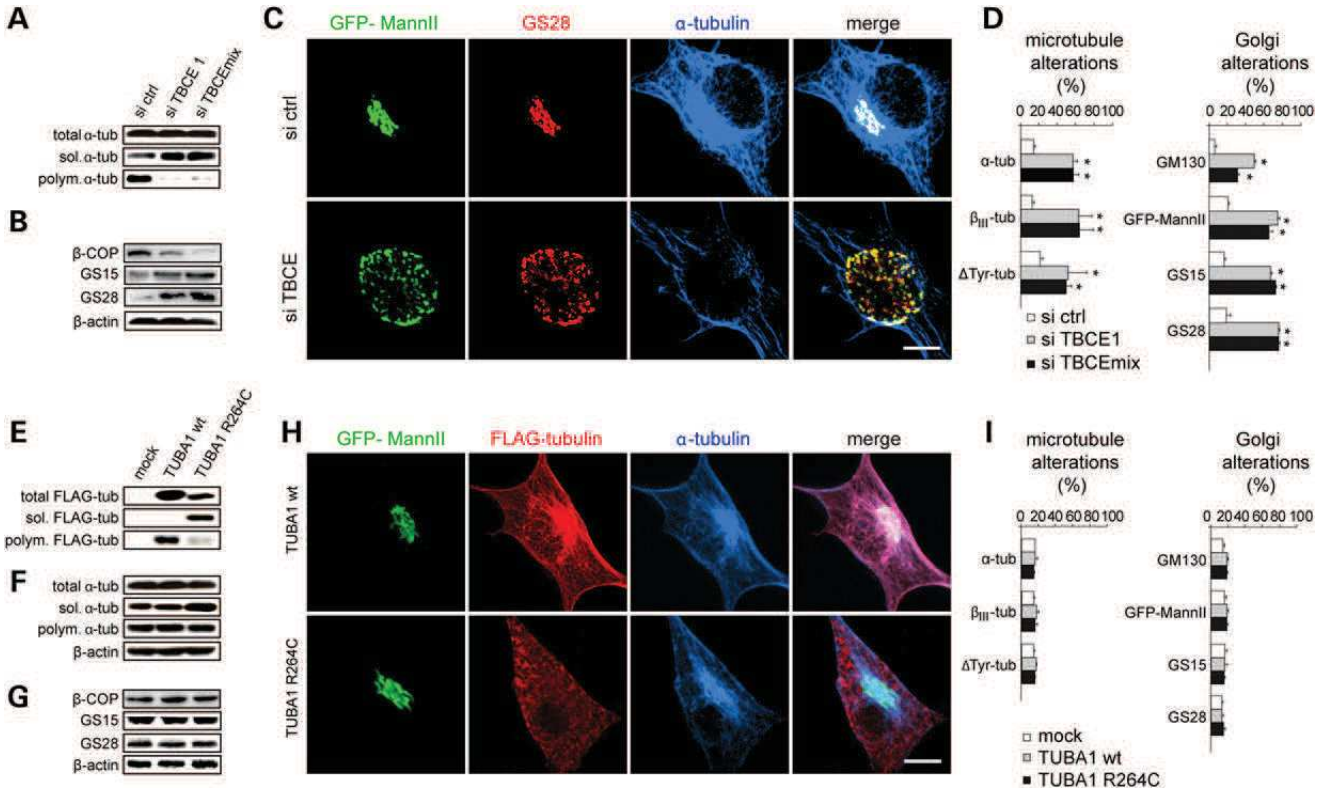

Figure 6. Tubulin polymerization, Golgi structure and vesicle markers after TBCE depletion or mutant α-tubulin expression. (**A**) Western blot showing that TBCE-depletion does not affect the total levels of α-tubulin but leads to a drastic decrease in the levels of polymerized α-tubulin and a significant increase in the levels of soluble α-tubulin (siTBCE 1: 1.6 ± 0.3-fold, siTBCE mix: 1.9 ± 0.1-fold, mean ± SD, Mann–Whitney test, paired). Soluble α-tubulin levels were quantified by densitometric analysis of six blots from three independent transfections. β-actin loading control is shown in panel B. (**B**) Decreased levels of β-COP in TBCE-depleted cells in comparison to control cells. Levels of GS15 and GS28 are increased in comparison to control by 7.4 ± 0.6 and 6.2 ± 0.3-fold (mean ± SD) respectively, as quantified by densitometric analysis of four independent experiments. (**C**) Confocal imaging showing that the α-tubulin-labeled microtubule alterations in TBCE-depleted cells are associated with Golgi alterations labeled with GFP-MannII and GS28, as compared with control. (**D**) Increased percentage of microtubule alterations labeled with α-, β_{III}- or ΔTyr-tubulin and Golgi alterations labeled with GM130, GFP-MannII, GS15, and GS28 in TBCE-depleted cells, as compared with control cells, mean ± SD, $n \geq 100$ cells per condition. Asterisks indicate statistical significance, $P < 0.05$ as measured by Student's *t*-test, unpaired, unequal variance. (**E**) Western blot analysis with anti-FLAG antibodies showing that expression of FLAG-tagged mutant α-tubulin (TUBA1 R264C) leads to increased levels of soluble mutant α-tubulin and decreased levels of polymerized mutant α-tubulin, in comparison to expression of FLAG-tagged wild-type α-tubulin (TUB1A wt). (**F**) Western blot with anti-α-tubulin antibodies showing a 1.6 ± 0.2-fold increase (mean ± SD) in the levels of soluble α-tubulin after TUBA1 R264C expression, as quantified by densitometric analysis of six independent blots; $P < 0.026$, Mann–Whitney test, paired, unequal variance. (**G**) Unaltered expression of β-COP, GS15 and GS28 in mutant TUBA1 R264C expressing cells. (**H**) Confocal imaging demonstrating that FLAG-tagged α-tubulin mutant TUBA1 R264C does not affect Golgi or microtubule structure. (**I**) Absence of microtubule or Golgi alterations in cells expressing mutant TUBA1 R264C α-tubulin, mean ± SD, $n \geq 100$ cells per condition. Scale bars 5 μm.

Confocal imaging, morphometry and 3D modeling

Images were obtained with an LSM 510 confocal microscope (Zeiss, Oberkochen, Germany). Motor neurons on spinal cord tissue cryosections were identified by staining for the motor neuron markers VAChT (vesicular acetylcholine transferase) or ChAT (choline acetyltransferase). Cells were imaged by confocal microscopy using a ×40 water immersion objective, an *xy*-resolution of 1024 × 1024 pixel, a *z*-interval of 0.3 μm and a mean scan depth of 30 μm.

Morphometric analyses were done with Metamorph software (Molecular Dynamics) using single confocal cross sections taken at the nuclear midplane. The boundaries of the ChAT-labeled cell soma and the DAPI-stained nucleus were manually delineated with the Metamorph drawing tool. Golgi surface area was automatically determined with the Metamorph morphometry tool by applying a fixed threshold to the MG160 signal.

Three-dimensional (3D) modelings of the Golgi apparatus were done with Imaris software (Bitplane, Zurich, Switzerland). Images were processed and Golgi membranes visualized using the IsoSurface mode of the Surpass module. The number of individual Golgi elements per motor neuron was determined in a blinded manner. Fluorescent line intensity profiles were determined with the linescan module of Zen software (Zeiss) on confocal *z*-stacks of NSC34 cells (*z*-interval 0.3 μm, scan depth 10 μm).

Electron microscopy

Deeply anesthetized mice were transcardially perfused with Sorensen's phosphate buffer (pH 7.4) followed by glutaraldehyde (2% v/v in cacodylate). Spinal cords were dissected out, post-fixed for 24 h and cut into small segments comprising the

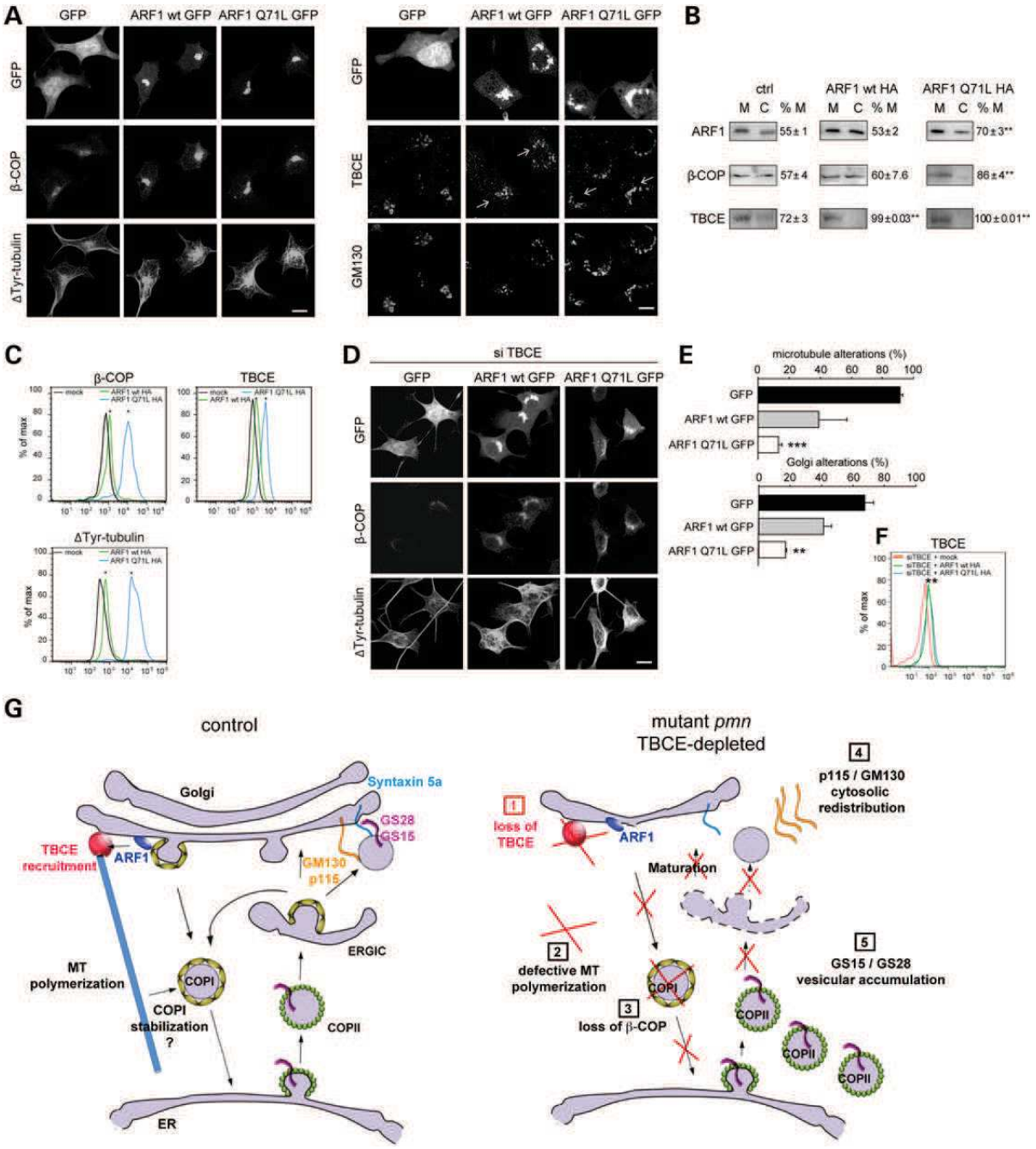

Figure 7. Role of an ARF1/TBCE-mediated cross-talk in Golgi maintenance. (**A**) Confocal imaging showing that expression of GFP-tagged ARF1 wt or ARF1 Q71L in NSC34 cells triggers a stronger β-COP signal and polymerization of more ΔTyr-tubulin-containing microtubules around the Golgi apparatus than GFP expression (left panels). GFP-tagged ARF1 wt and GFP-tagged ARF1 Q71L recruit TBCE to Golgi membranes labeled with GM130 (arrow, right panels). (**B**) Cellular fractionation. Expression of HA-tagged ARF1 wt or ARF1 Q71L stimulates recruitment of β-COP and TBCE from cytosolic (C) to membrane fractions (M). Relative protein expression is indicated as %M: M/(M + C), mean ± SD, $n = 3$ experiments, $^{**}P < 0.001$, by Student's t-test. (**C**) Flow cytometry showing increased levels of β-COP, TBCE and ΔTyr-tubulin-containing microtubules after expression of ARF1 Q71L HA, in comparison to ARF1 wt HA or mock. Statistical significance *ARF1 wt HA versus mock $T(x) > 4$, $P < 0.01$; ARF1 Q71L HA versus ARF1 wt $T(x) > 28$, $P < 0.01$, by χ^2 test. (**D**) Confocal imaging reveals rescue of the pathologically decreased β-COP expression in siTBCE transfected cells by expression of GFP-tagged ARF1 wt or ARF1 Q71L, as compared with expression of GFP (upper and middle rows). Note also enhanced polymerization of ΔTyr-tubulin by expression of GFP-tagged ARF1 wt or GFP-tagged ARF1 Q71L (lower rows). (**E**) Rescue of microtubule or GM130-labeled Golgi alterations by ARF1 Q71L GFP in siTBCE-transfected cells (mean ± SD). Each experiment was done in triplicate conditions with $n > 50$ cells per condition. Statistical significance: $^{***}P < 0.0002$ (microtubule alterations) and $^{**}P < 0.0036$ (Golgi alterations) by Kruskal–Wallis test and Dunn *post hoc* test for ARF1 Q71L GFP/siTBCE versus GFP/siTBCE. (**F**) Flow cytometry showing increased levels of TBCE by (over)expression of ARF1 wt HA or ARF1 Q71L HA. Statistical significance **ARF1 wt HA-siTBCE wt versus mock siTBCE $T(x) > 26$, $P < 0.01$; ARF1 Q71L HA/si TBCE versus mock/si TBCE $T(x) > 26$, $P < 0.01$, by $\chi 2$ test. (**G**) Model showing the ARF1/TBCE cross-talk which coordinates polymerization of Golgi-derived microtubules and COPI vesicle formation and the consequences of its disruption in mutant *pmn* and TBCE-depleted motor neurons. Scale bars 10 μm.

ventral spinal cord before processing for resin embedding (epon) following standard protocols. Sixty nanometer ultrathin cross sections were contrasted with uranyl acetate and visualized under a JEOL electron microscope. At least two lumbar spinal cords from each genotype were analyzed and three sections (each containing up to 30 motor neurons) were analyzed per time point. Motor neurons were recognized on the basis of their frequency (1:20), large size and pale nucleus. Within individual motor neurons, all Golgi profiles were categorized.

Cell culture

NSC34 motor neurons were cultured in DMEM supplemented with 10% (v/v) fetal calf serum at 37°C and 7.5% CO_2 and transfected with siRNAs and/or DNA plasmids using Lipofectamine 2000 (Invitrogen) as described (18).

Immunoblots and subcellular fractionation

Lumbar spinal cords from deeply anesthetized mice and NSC34 cells were homogenized in lysis buffer containing 50 mM Tris–HCl pH 7.5, 150 mM NaCl, 2 mM ethylenediaminetetraacetic acid (EDTA), 1% Triton X-100, Complete antiproteases and, for GM130, also 0.25% sodium dodecyl sulfate (SDS). 30 or 50 μg protein were subjected to SDS-polyacrylamide gel electrophoresis and blotted on Immobilon membranes (Millipore) which were processed by standard methods, reacted with ECL or ECL plus kits (Amersham) and revealed with XAR films (Kodak) or a Biorad imager. Band intensities were quantified by TotalLabQuant software.

Crude fractionation of membranes from lumbar spinal cord was done after tissue freezing (−80°C), thawing and homogenization in 50 mM 4-(2-hydroxyethyl)-1-piperazineethanesulfonic acid (HEPES), pH 7.4, 250 mM sucrose, 1 mM Mg acetate and protease inhibitors (Complete, EDTA-free). Lysates were homogenized using a Dounce homogenizer (15 passes) and centrifuged at 1 000 g for 10 min. The postnuclear supernatant was centrifuged at 10 000 g for 30 min at 4°C yielding a P10 pellet and the supernatant was centrifuged at 100 000 g (Beckman TLA-110) for 1 h at 4°C yielding an S100 supernatant and a P100 pellet.

For membrane fractionation on sucrose density gradients, cells were homogenized in an isotonic sucrose solution by 10 passages through a Dounce homogenizer and centrifuged at 1 000 g for 10 min. The postnuclear supernatants were centrifuged at 190 000 g (43 000 rpm) for 1 h in a Beckman SW60 Ti rotor; 12 fractions of 330 μl each were collected from top to bottom and equal volumes analyzed by immunoblot. Sucrose concentrations in fractions and standards were determined by an enzymatic assay (Sigma, ref. SCA-20) using a Biochrom WPA spectrophotometer. Subcellular fractionation of NSC34 cells into membrane and cytosolic fractions was done as described (21).

Microtubule re-growth assay

Growth dynamics of Golgi-derived microtubule were studied by modifying an earlier reported procedure (18). NSC34 cells transfected with siRNAs and a GFP-MannII plasmid were treated at 5 days in vitro (DIV) with nocodazole (10 μM, 5 h, 37°C). Nocodazole was then washed out with warm culture medium, and neurons further incubated at 37°C. At time intervals ranging from 0 to 200 min, cultures were rinsed with PHEM 60 mM piperazine-N,N'-bis(2-ethanesulfonic acid), 25 mM HEPES, 10 mM ethylene glycol tetraacetic acid, 2 mM $MgCl_2$, 1% formaldehyde (pH 6.9) and then treated for 3 min with PHEM containing 0.2% Triton X-100 and 20 μM taxol to extract soluble proteins and stabilize microtubules. Cells were fixed, blocked and counterstained for α-tubulin. After confocal imaging of entire cells, number and length of Golgi-derived microtubules were determined using Metamorph and ImageJ software respectively.

Immunoprecipitation

Transfected NSC34 cells from 6-well plates were harvested in PBS using a cell scraper and lysed on ice for 10 min in 50 mM Tris pH 7.5, 150 mM NaCl, 5 mM EDTA, 1% Triton X-100 and Complete protease inhibitors. After removal of cell debris, 300 μl of cell lysates were incubated with 3 μg antibodies and 30 μl protein G-magnetic beads (Millipore) on a tube rotator for 4 h. Supernatants and immune complexes were then collected using a magnetic stand holder.

Flow cytometry

Transfected cells were harvested at 3 DIV (ARF1) or 5 DIV (siTBCE), rinsed with PBS, centrifuged at 250*g*, washed with PHEM and treated for 3 min with PHEM containing 0.1% Triton X-100 and 20 μM taxol to extract soluble proteins and to stabilize microtubules. Cells were fixed for 15 min at RT by adding an equal volume of 8% (v/v) FA in PBS, rinsed in PBS, centrifuged and blocked for 30 min in 5% goat serum, 1% (w/v) BSA and 0.1% (v/v) Triton X-100. Cells were incubated for 1 h with primary antibodies and for 1 h with secondary antibodies or biotin/streptavidin reagents coupled to Alexa-594 (HA) or Alexa-488 (β-COP, TBCE and ΔTyr-tubulin). One thousand five hundred cells per duplicate sample and condition were analyzed with a FACS ARIA SORP (Becton Dickinson) and signals plotted with FlowJo software.

Statistical analyses

Each experiment was performed with several biological replicates, i.e. usually three pairs of wild-type and *pmn* mice and duplicate or triplicate cultures of control and siTBCE-transfected cells. All experiments were repeated once or twice. Data were analyzed with Microsoft Excel, SigmaStat 3.1 (Systat, Evanston, IL) or GraphPad Prism (GraphPad). Data from two groups showing Gaussian distribution were analyzed with Student's *t*-test; otherwise the Mann–Whitney *U* test was used. Data from more than two groups showing Gaussian distribution and equal variance were analyzed with one-way ANOVA test and Tukey's *post hoc* test; otherwise the Kruskal–Wallis test and Dunn *post hoc* test were used. Cytometry data were tested for significance with the $\chi 2$ test using FlowJo software.

SUPPLEMENTARY MATERIAL

Supplementary Material is available at *HMG* online.

ACKNOWLEDGEMENTS

We gratefully acknowledge the expert help of D. Xanthakis (Department of Cell Biology, UMC Utrecht, NL) in processing, sectioning and electron microscopic analysis of tissue samples, the expert help of P. Weber (IBDML, Marseille, France) and A. Bernadac (CNRS, Marseille, France) in confocal microscopy and imaging software and the contribution of Dr H. Schmalbruch (University of Copenhagen) to earlier stages of the work. We are grateful to Dr A. Spang for critical reading of the manuscript and to Drs A. Andrieux, M. Bornens, J. Chelly, J. Donaldson, R. Duden, J.C. Hay and R.A. Kahn for providing essential reagents.

Conflict of Interest Statement. None declared.

FUNDING

Work in G. Haase's laboratory is supported by grants from Association Française contre les Myopathies (AFM), Agence Nationale pour la Recherche and ERANET Neuron. Work in C. Rabouille's laboratory is supported by NWO. S.B. was supported by student fellowships from Fondation pour la Recherche Médicale (FRM) and AFM. M.S. was supported by postdoctoral fellowships from Deutsche Forschungsgemeinschaft and INSERM.

REFERENCES

1. Bonifacino, J.S. and Glick, B.S. (2004) The mechanisms of vesicle budding and fusion. *Cell*, **116**, 153–166.
2. Fan, J., Hu, Z., Zeng, L., Lu, W., Tang, X., Zhang, J. and Li, T. (2008) Golgi apparatus and neurodegenerative diseases. *Int. J. Dev. Neurosci.*, **26**, 523–534.
3. Gonatas, N.K., Stieber, A., Mourelatos, Z., Chen, Y., Gonatas, J.O., Appel, S.H., Hays, A.P., Hickey, W.F. and Hauw, J.J. (1992) Fragmentation of the Golgi apparatus of motor neurons in amyotrophic lateral sclerosis. *Am. J. Pathol.*, **140**, 731–737.
4. Mourelatos, Z., Gonatas, N.K., Stieber, A., Gurney, M.E. and Dal Canto, M.C. (1996) The Golgi apparatus of spinal cord motor neurons in transgenic mice expressing mutant Cu,Zn superoxide dismutase becomes fragmented in early, preclinical stages of the disease. *Proc. Natl. Acad. Sci. U.S.A.*, **93**, 5472–5477.
5. Thyberg, J. and Moskalewski, S. (1985) Microtubules and the organization of the Golgi complex. *Exp. Cell Res.*, **159**, 1–16.
6. Cole, N.B., Sciaky, N., Marotta, A., Song, J. and Lippincott-Schwartz, J. (1996) Golgi dispersal during microtubule disruption: regeneration of Golgi stacks at peripheral endoplasmic reticulum exit sites. *Mol. Biol. Cell*, **7**, 631–650.
7. Allan, V.J. and Kreis, T.E. (1986) A microtubule-binding protein associated with membranes of the Golgi apparatus. *J. Cell Biol.*, **103**, 2229–2239.
8. Strey, C.W., Spellman, D., Stieber, A., Gonatas, J.O., Wang, X., Lambris, J.D. and Gonatas, N.K. (2004) Dysregulation of stathmin, a microtubule-destabilizing protein, and up-regulation of Hsp25, Hsp27, and the antioxidant peroxiredoxin 6 in a mouse model of familial amyotrophic lateral sclerosis. *Am. J. Pathol.*, **165**, 1701–1718.
9. Urushitani, M., Sik, A., Sakurai, T., Nukina, N., Takahashi, R. and Julien, J.P. (2006) Chromogranin-mediated secretion of mutant superoxide dismutase proteins linked to amyotrophic lateral sclerosis. *Nat. Neurosci.*, **9**, 108–118.
10. Atkin, J.D., Farg, M.A., Soo, K.Y., Walker, A.K., Halloran, M., Turner, B.J., Nagley, P. and Horne, M.K. (2014) Mutant SOD1 inhibits ER-Golgi transport in amyotrophic lateral sclerosis. *J. Neurochem.*, **129**, 190–204.
11. Stieber, A., Gonatas, J.O., Moore, J.S., Bantly, A., Yim, H.S., Yim, M.B. and Gonatas, N.K. (2004) Disruption of the structure of the Golgi apparatus and the function of the secretory pathway by mutants G93A and G85R of Cu, Zn superoxide dismutase (SOD1) of familial amyotrophic lateral sclerosis. *J. Neurol. Sci.*, **219**, 45–53.
12. Sundaramoorthy, V., Walker, A.K., Yerbury, J., Soo, K.Y., Farg, M.A., Hoang, V., Zeineddine, R., Spencer, D. and Atkin, J.D. (2013) Extracellular wildtype and mutant SOD1 induces ER–Golgi pathology characteristic of amyotrophic lateral sclerosis in neuronal cells. *Cell. Mol. Life Sci.*, **70**, 4181–4195.
13. Schmalbruch, H., Jensen, H.S., Bjaerg, M., Kamieniecka, Z. and Kurland, L. (1991) A new mouse mutant with progressive motor neuronopathy. *J. Neuropathol. Exp. Neurol.*, **50**, 192–204.
14. Martin, N., Jaubert, J., Gounon, P., Salido, E., Haase, G., Szatanik, M. and Guenet, J.L. (2002) A missense mutation in Tbce causes progressive motor neuronopathy in mice. *Nat. Genet.*, **32**, 443–447.
15. Bömmel, H., Xie, G., Rossoll, W., Wiese, S., Jablonka, S., Boehm, T. and Sendtner, M. (2002) Missense mutation in the tubulin-specific chaperone E (Tbce) gene in the mouse mutant progressive motor neuronopathy, a model of human motoneuron disease. *J. Cell Biol.*, **159**, 563–569.
16. Tian, G., Huang, Y., Rommelaere, H., Vandekerckhove, J., Ampe, C. and Cowan, N.J. (1996) Pathway leading to correctly folded beta-tubulin. *Cell*, **86**, 287–296.
17. Tian, G., Lewis, S.A., Feierbach, B., Stearns, T., Rommelaere, H., Ampe, C. and Cowan, N.J. (1997) Tubulin subunits exist in an activated conformational state generated and maintained by protein cofactors. *J. Cell Biol.*, **138**, 821–832.
18. Schaefer, M.K., Schmalbruch, H., Buhler, E., Lopez, C., Martin, N., Guenet, J.L. and Haase, G. (2007) Progressive motor neuronopathy: a critical role of the tubulin chaperone TBCE in axonal tubulin routing from the Golgi apparatus. *J. Neurosci.*, **27**, 8779–8789.
19. Parvari, R., Hershkovitz, E., Grossman, N., Gorodischer, R., Loeys, B., Zecic, A., Mortier, G., Gregory, S., Sharony, R., Kambouris, M. *et al.* (2002) Mutation of TBCE causes hypoparathyroidism–retardation–dysmorphism and autosomal recessive Kenny–Caffey syndrome. *Nat. Genet.*, **32**, 448–452.
20. Haase, G., Kennel, P., Pettmann, B., Vigne, E., Akli, S., Revah, F., Schmalbruch, H. and Kahn, A. (1997) Gene therapy of murine motor neuron disease using adenoviral vectors for neurotrophic factors. *Nat. Med.*, **3**, 429–436.
21. Xiang, Y., Seemann, J., Bisel, B., Punthambaker, S. and Wang, Y. (2007) Active ADP-ribosylation factor-1 (ARF1) is required for mitotic Golgi fragmentation. *J. Biol. Chem.*, **282**, 21829–21837.
22. Guo, Y., Punj, V., Sengupta, D. and Linstedt, A.D. (2008) Coat-tether interaction in Golgi organization. *Mol. Biol. Cell*, **19**, 2830–2843.
23. Nakamura, N., Lowe, M., Levine, T.P., Rabouille, C. and Warren, G. (1997) The vesicle docking protein p115 binds GM130, a *cis*-Golgi matrix protein, in a mitotically regulated manner. *Cell*, **89**, 445–455.
24. Razi, M., Chan, E.Y. and Tooze, S.A. (2009) Early endosomes and endosomal coatomer are required for autophagy. *J. Cell Biol.*, **185**, 305–321.
25. Xu, D. and Hay, J.C. (2004) Reconstitution of COPII vesicle fusion to generate a pre-Golgi intermediate compartment. *J. Cell. Biol.*, **167**, 997–1003.
26. Horstmann, H., Ng, C.P., Tang, B.L. and Hong, W. (2002) Ultrastructural characterization of endoplasmic reticulum–Golgi transport containers (EGTC). *J. Cell. Sci.*, **115**, 4263–4273.
27. Styers, M.L., O'Connor, A.K., Grabski, R., Cormet-Boyaka, E. and Sztul, E. (2008) Depletion of beta-COP reveals a role for COP-I in compartmentalization of secretory compartments and in biosynthetic transport of caveolin-1. *Am. J. Physiol. Cell. Physiol.*, **294**, C1485–C1498.
28. Bentley, M., Liang, Y., Mullen, K., Xu, D., Sztul, E. and Hay, J.C. (2006) SNARE status regulates tether recruitment and function in homotypic COPII vesicle fusion. *J. Biol. Chem.*, **281**, 38825–38833.
29. Subramaniam, V.N., Peter, F., Philp, R., Wong, S.H. and Hong, W. (1996) GS28, a 28-kilodalton Golgi SNARE that participates in ER-Golgi transport. *Science*, **272**, 1161–1163.
30. Xu, Y., Wong, S.H., Zhang, T., Subramaniam, V.N. and Hong, W. (1997) GS15, a 15-kilodalton Golgi soluble *N*-ethylmaleimide-sensitive factor attachment protein receptor (SNARE) homologous to rbet1. *J. Biol. Chem.*, **272**, 20162–20166.
31. Ballensiefen, W., Ossipov, D. and Schmitt, H.D. (1998) Recycling of the yeast v-SNARE Sec22p involves COPI-proteins and the ER transmembrane proteins Ufe1p and Sec20p. *J. Cell. Sci.*, **111**, 1507–1520.
32. Rein, U., Andag, U., Duden, R., Schmitt, H.D. and Spang, A. (2002) ARF-GAP-mediated interaction between the ER-Golgi v-SNAREs and the COPI coat. *J. Cell Biol.*, **157**, 395–404.

33. Haase, G., Pettmann, B., Bordet, T., Villa, P., Vigne, E., Schmalbruch, H. and Kahn, A. (1999) Therapeutic benefit of ciliary neurotrophic factor in progressive motor neuronopathy depends on the route of delivery. *Ann. Neurol.*, **45**, 296–304.
34. Stiess, M., Maghelli, N., Kapitein, L.C., Gomis-Ruth, S., Wilsch-Brauninger, M., Hoogenraad, C.C., Tolic-Norrelykke, I.M. and Bradke, F. (2010) Axon extension occurs independently of centrosomal microtubule nucleation. *Science*, **327**, 704–707.
35. Chabin-Brion, K., Marceiller, J., Perez, F., Settegrana, C., Drechou, A., Durand, G. and Pous, C. (2001) The Golgi complex is a microtubule-organizing organelle. *Mol. Biol. Cell*, **12**, 2047–2060.
36. Miller, P.M., Folkmann, A.W., Maia, A.R., Efimova, N., Efimov, A. and Kaverina, I. (2009) Golgi-derived CLASP-dependent microtubules control Golgi organization and polarized trafficking in motile cells. *Nat. Cell Biol.*, **11**, 1069–1080.
37. Skoufias, D.A., Burgess, T.L. and Wilson, L. (1990) Spatial and temporal colocalization of the Golgi apparatus and microtubules rich in detyrosinated tubulin. *J. Cell Biol.*, **111**, 1929–1937.
38. Vainberg, I.E., Lewis, S.A., Rommelaere, H., Ampe, C., Vandekerckhove, J., Klein, H.L. and Cowan, N.J. (1998) Prefoldin, a chaperone that delivers unfolded proteins to cytosolic chaperonin. *Cell*, **93**, 863–873.
39. Gao, Y., Thomas, J.O., Chow, R.L., Lee, G.H. and Cowan, N.J. (1992) A cytoplasmic chaperonin that catalyzes beta-actin folding. *Cell*, **69**, 1043–1050.
40. Tian, G., Bhamidipati, A., Cowan, N.J. and Lewis, S.A. (1999) Tubulin folding cofactors as GTPase-activating proteins. GTP hydrolysis and the assembly of the alpha/beta-tubulin heterodimer. *J. Biol. Chem.*, **274**, 24054–24058.
41. Tian, G., Kong, X.P., Jaglin, X.H., Chelly, J., Keays, D. and Cowan, N.J. (2008) A pachygyria-causing alpha-tubulin mutation results in inefficient cycling with CCT and a deficient interaction with TBCB. *Mol. Biol. Cell.*, **19**, 1152–1161.
42. Bhamidipati, A., Lewis, S.A. and Cowan, N.J. (2000) ADP ribosylation factor-like protein 2 (Arl2) regulates the interaction of tubulin-folding cofactor D with native tubulin. *J. Cell Biol.*, **149**, 1087–1096.
43. Watson, P., Forster, R., Palmer, K.J., Pepperkok, R. and Stephens, D.J. (2005) Coupling of ER exit to microtubules through direct interaction of COPII with dynactin. *Nat. Cell Biol.*, **7**, 48–55.
44. Carreno, S., Engqvist-Goldstein, A.E., Zhang, C.X., McDonald, K.L. and Drubin, D.G. (2004) Actin dynamics coupled to clathrin-coated vesicle formation at the trans-Golgi network. *J. Cell Biol.*, **165**, 781–788.
45. Anitei, M., Stange, C., Parshina, I., Baust, T., Schenck, A., Raposo, G., Kirchhausen, T. and Hoflack, B. (2010) Protein complexes containing CYFIP/Sra/PIR121 coordinate Arf1 and Rac1 signalling during clathrin-AP-1-coated carrier biogenesis at the TGN. *Nat. Cell Biol.*, **12**, 330–340.
46. Orci, L., Ravazzola, M., Volchuk, A., Engel, T., Gmachl, M., Amherdt, M., Perrelet, A., Sollner, T.H. and Rothman, J.E. (2000) Anterograde flow of cargo across the Golgi stack potentially mediated via bidirectional 'percolating' COPI vesicles. *Proc. Natl. Acad. Sci. U.S.A.*, **97**, 10400–10405.
47. Sagiv, Y., Legesse-Miller, A., Porat, A. and Elazar, Z. (2000) GATE-16, a membrane transport modulator, interacts with NSF and the Golgi v-SNARE GOS-28. *EMBO J.*, **19**, 1494–1504.
48. Zhong, W., Zhou, Y., Li, S., Zhou, T., Ma, H., Wei, K., Li, H., Olkkonen, V.M. and Yan, D. (2011) OSBP-related protein 7 interacts with GATE-16 and negatively regulates GS28 protein stability. *Exp. Cell Res.*, **317**, 2353–2363.
49. Voloshin, O., Gocheva, Y., Gutnick, M., Movshovich, N., Bakhrat, A., Baranes-Bachar, K., Bar-Zvi, D., Parvari, R., Gheber, L. and Raveh, D. (2010) Tubulin chaperone E binds microtubules and proteasomes and protects against misfolded protein stress. *Cell. Mol. Life Sci.*, **67**, 2025–2038.
50. Xu, X., Kedlaya, R., Higuchi, H., Ikeda, S., Justice, M.J., Setaluri, V. and Ikeda, A. (2010) Mutation in archain 1, a subunit of COPI coatomer complex, causes diluted coat color and Purkinje cell degeneration. *PLoS Genet.*, **6**, e1000956.
51. Blot, S., Poirier, C. and Dreyfus, P.A. (1995) The mouse mutation muscle deficient (mdf) is characterized by a progressive motoneuron disease. *J. Neuropathol. Exp. Neurol.*, **54**, 812–825.
52. Schmidt, W.M., Kraus, C., Hoger, H., Hochmeister, S., Oberndorfer, F., Branka, M., Bingemann, S., Lassmann, H., Muller, M., Macedo-Souza, L.I. *et al.* (2007) Mutation in the Scyl1 gene encoding amino-terminal kinase-like protein causes a recessive form of spinocerebellar neurodegeneration. *EMBO Rep.*, **8**, 691–697.
53. Pelletier, S., Gingras, S., Howell, S., Vogel, P. and Ihle, J.N. (2012) An early onset progressive motor neuron disorder in Scyl1-deficient mice is associated with mislocalization of TDP-43. *J. Neurosci*, **32**, 16560–16573.
54. Jareb, M. and Banker, G. (1997) Inhibition of axonal growth by brefeldin A in hippocampal neurons in culture. *J. Neurosci.*, **17**, 8955–8963.
55. Peter, C.J., Evans, M., Thayanithy, V., Taniguchi-Ishigaki, N., Bach, I., Kolpak, A., Bassell, G.J., Rossoll, W., Lorson, C.L., Bao, Z.Z. *et al.* (2011) The COPI vesicle complex binds and moves with survival motor neuron within axons. *Hum. Mol. Genet.*, **20**, 1701–1711.
56. Ting, C.H., Wen, H.L., Liu, H.C., Hsieh-Li, H.M., Li, H. and Lin-Chao, S. (2012) The spinal muscular atrophy disease protein SMN is linked to the Golgi network. *PLoS One*, **7**, e51826.
57. Custer, S.K., Todd, A.G., Singh, N.N. and Androphy, E.J. (2013) Dilysine motifs in exon 2b of SMN protein mediate binding to the COPI vesicle protein alpha-COP and neurite outgrowth in a cell culture model of spinal muscular atrophy. *Hum. Mol. Genet.*, **22**, 4043–4052.
58. Bi, J., Tsai, N.P., Lu, H.Y., Loh, H.H. and Wei, L.N. (2007) Copb1-facilitated axonal transport and translation of kappa opioid-receptor mRNA. *Proc. Natl. Acad. Sci. U.S.A.*, **104**, 13810–13815.
59. Todd, A.G., Lin, H., Ebert, A.D., Liu, Y. and Androphy, E.J. (2013) COPI transport complexes bind to specific RNAs in neuronal cells. *Hum. Mol. Genet.*, **22**, 729–736.
60. Pun, S., Santos, A.F., Saxena, S., Xu, L. and Caroni, P. (2006) Selective vulnerability and pruning of phasic motoneuron axons in motoneuron disease alleviated by CNTF. *Nat. Neurosci.*, **9**, 408–419.
61. Torres-Benito, L., Neher, M.F., Cano, R., Ruiz, R. and Tabares, L. (2011) SMN requirement for synaptic vesicle, active zone and microtubule postnatal organization in motor nerve terminals. *PLoS One*, **6**, e26164.